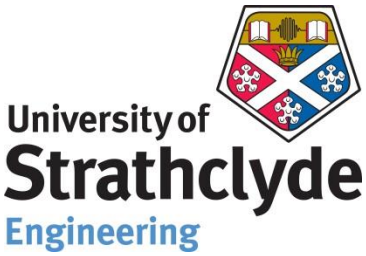

Department of Biomedical Engineering

Towards non-invasive characterisation of re-endothelialisation and restenosis following coronary stenting: an in vitro investigation using impedance spectroscopy

Ian Holland

A thesis presented in the fulfilment of the requirements for the degree of Doctor of Engineering

June 2017

Declaration

This thesis is the result of the author's original research. It has been composed by the author and has not been previously submitted for examination which has led to the award of a degree.

Signed:

Date:

Abstract

Following the permanent implantation of a coronary stent, optimal arterial wall healing is characterised by re-endothelialisation, the regrowth of a functional Endothelial Cell (EC) monolayer over the exposed stent surface. However incomplete re-endothelialisation, increases the risk of stent thrombosis which can cause vessel narrowing to reoccur. Previous research has suggested that the stent itself could be used as an electrode and when combined with non-invasive impedance spectroscopy techniques monitor post stenting healing. This could then inform clinicians on cell regrowth without the need for invasive imaging techniques. This study investigated the feasibility of the concept using 3 in vitro models representing potential cellular regrowth scenarios: re-endothelialisation (ECs), smooth muscle cell (SMCs) proliferation and co-culture (ECs and SMCs).

Primary porcine ECs and SMCs were seeded onto platinum black electrodes and a bespoke impedance spectroscopy system used to carry out automated measurements for time periods of up to 10 days. Endothelium function was assessed through the measurement of the impedance response of confluent EC monolayers to the addition of either a gap junction enhancer, dipyridamole, or an inhibitor (heptanol or carbenoxolone).

The results show that confluent, stent surface comparable populations of SMCs, ECs and co-culture of both cell types gives rise to distinct impedance signatures, most evident in the reactance component of impedance. This provides a potential method of non-invasively characterising the two cell types. Gap junction inhibition of EC monolayers dose dependently reduced total impedance. Conversely dipyridamole's enhancing effect on gap junction formation caused an increase in total impedance. These novel findings show the importance of intercellular gap junction communication in the maintenance of the endothelial barrier function. Overall, the results demonstrate the potential of impedance spectroscopy in characterising vascular healing and endothelium function and could, in the future, provide clinically useful information in the development of new stents.

Acknowledgements

My first acknowledgement must go to my project supervisor Chris McCormick. His guidance and assistance have been invaluable during the duration of this project. Thanks too to Trish Connolly for her assistance with the project and also for setting up the doctoral training centre without which none of this would be possible.

For her help and assistance with cell work, thanks go to Katie Henderson and also for making level 4 such an enjoyable laboratory environment to work in. Thanks too, to Suky Kaloya for his help with cell isolation and maintenance.

I have thoroughly enjoyed my EngD studies and this is thanks to my friends who have cheered me throughout my time Glasgow. Many thanks to Shiny Puthenkalam, Olivia Macneill, Heather Black, Lindsay Millar and Sarah Morgan.

Finally I would like to thank my Mum and Dad, for their encouragement, support and assistance throughout my extended education.

Contents

List of figures

List of Tables

1 Introduction

Coronary artery disease is a leading cause of morbidity amongst the United Kingdom population (British Heart Foundation, 2017). Understanding of the disease has progressed significantly over the previous decades and has aided in the development of an array of amelioratory treatments, of which coronary stents can be considered one of the most successful. Since their introduction stents themselves have experienced their own research led development process, primarily aimed at preventing the incidences of restenosis and thrombosis, both of which pose a major danger to the patients' health. Despite significant success in this regard these problems have not been completely resolved and clinicians still lack a suitable monitoring technology that can provide an early indication as to when the aforementioned problems arise. In parallel to the progress that has been made in cardiovascular disease research, an understanding of the electrical properties of cells has also evolved. In particular there is interest in how this understanding can be exploited to provide insights into cell behaviour. Impedance spectroscopy is one such technique that has greatly contributed to these findings and is now accepted as a potent research tool for monitoring cells. The research contained within this thesis aims to contribute towards a solution to the aforementioned clinical need by combining these disparate strands of science and engineering.

1.1 Atherosclerosis

Atherosclerosis is the leading cause of death in Europe (Nichols *et al.*, 2012). A number of risk factors have been identified that increase the likelihood of atherosclerotic plaque initiation and progression, with smoking, diet and sedentary lifestyles highlighted in the literature (Perk *et al.*, 2012). These traits and behaviours are associated with modern human behaviour and led to the conclusion that the disease is a relatively new concern for societies. However the discovery of atherosclerotic plaques on human specimens tracing back to 4000 years ago has revealed a much longer history, prompting a much wider question as to whether

atherosclerosis is a symptom of aging rather than just lifestyle factors (Thompson *et al.*, 2013).

The progression of the disease begins with the development of an atherosclerotic lesion on an arterial wall through an inflammatory process and the expansion of the lesion occludes the flow of blood through the artery. When present within the coronary vasculature this can subsequently cause coronary heart disease, increasing the risk of thrombosis and ultimately myocardial infarction and stroke. Research aimed at identifying factors contributing to the initiation of an atherosclerotic lesion has focused on sites of disrupted blood flow and the resulting behaviour of endothelial cells. Adhesion molecules, expressed by endothelial cells, bind with leukocytes that under healthy circumstances would otherwise continue circulating. At the same time the permeability of the endothelium increases allowing Low Density Lipoproteins (LDLs) present in the blood to permeate into the arterial wall (Libby, Ridker and Hansson, 2011). The concurrent build-up of the Macrophages, a type of leukocyte, alongside LDLs within the intima is the dangerous scenario that initiates the disease. Macrophages then begin to scavenge the LDL and mature into foam cells. The steady accumulation of these foam cells and the detritus arising from their rupture on death causes the expansion of the Atherosclerotic lesion (Hansson, 2014). Additional stages of lesion development follow with the migration of smooth muscle cells from the media to form a fibrotic cap. Studies have also suggested that SMC vascular progenitor cells are attracted to the lesion and differentiate, contributing to the growth of the lesion, and are responsible for 20% to 66% of the cells present (Marx, Totary-Jain and Marks, 2011).

It is often only in the final stages of the disease that patients present to clinicians with indicatory symptoms. These symptoms can be angina or in more severe cases myocardial infarction and identification of atherosclerosis is then typically achieved via an angiogram. Following diagnosis, symptoms can be treated with the use of drugs and recommendations for modifying the patient's lifestyle. However in more acute cases direct intervention procedures are necessary. The surgical procedure of coronary artery bypass grafting is one option available to clinicians but carries all of the risks that accompany major invasive surgery. A less invasive procedure is the

insertion of a stent into the diseased artery, an intervention that has become increasingly common since their first use in humans in 1986 (Sigwart *et al.*, 1987). A stent is a tubular structure comprising wire struts that when expanded onto the affected region braces itself against the arterial wall, expanding it and allowing blood flow to resume. Stents are designed to resist the hoop stresses induced by the radial pressure of the compressed lesion and artery. The delivery of the stent to the affected artery is achieved using a catheter insertion method. The pre expansion of the artery with a balloon – known as balloon angioplasty - compresses the lesion. Prior to the development of stents this was as far as the intervention went and the catheter was then removed. However elastic recoil and re-narrowing of the artery necessitated the development of stents, a more permanent method of maintaining the artery diameter (Lowe, Oesterle and Khachigian, 2002). Immediately after balloon angioplasty the stent is expanded and the procedure completed by catheter removal. Elastic recoil of the artery is reduced by the stent struts bracing against the arterial wall, opening up the artery diameter and permitting an increased blood flow in comparison to pre-procedure rates (Bennett, 2003). The principle advantage of stent implantation, when compared to coronary bypass grafting is the avoidance of major surgery, which for some patients is not feasible due to co-morbidity conditions. They are intended to be implanted for the duration of the patient's life with stent removal being a high risk and rarely used procedure (Triantafyllou, Frangoulis and Kolettis, 2006).

1.2 In stent restenosis

In stent restenosis is considered as a distinct process to restenosis which is used to refer to arterial narrowing after balloon angioplasty (Lowe, Oesterle and Khachigian, 2002). The mechanisms of in stent restenosis have been extensively studied in both in vitro and in vivo animal models however there remains debate surrounding specific aspects. The following outline is based upon the review by Mitra and Agrawal, 2006. Upon stent expansion the endothelial layer is stretched causing rupture at multiple sites and the struts themselves penetrate the internal elastic laminar and continue on into the media. The principle cause of in stent restenosis is an inflammatory response to this vascular injury. Studies have also identified stent material, stent polymer coating and embedded drugs as additional potential causes of

the inflammatory response (Inoue *et al.*, 2011). However it is vascular injury and the subsequent initiation of a complex cascade mechanism involving platelets, leukocytes and macrophages that has attracted the most research and will be described here. The early phase of in stent restenosis is characterised by platelet adherence to the site of injury and the stent itself, encouraging the recruitment of leukocytes via a variety of chemoattractants and adhesion molecules. The chemoattractants and adhesion molecules are released and expressed by not only the platelets themselves but also local endothelial cells and smooth muscle cells too. There exist interdependent relationships between these, with one example being the release of the monocyte chemoattractant protein MCP-1 by platelets causing a corresponding expression of the same protein in endothelial and smooth muscle cells resulting in the attraction of monocytes (Joner *et al.*, 2007). Additional mechanisms of adhesion and migration exist although monocyte derived macrophages represent the majority of leukocyte movement into the arterial wall and this early stage happens in the first days and weeks following stent insertion. The next stage of in stent restenosis is characterised by the behaviour of smooth muscle cells, migrating and switching in phenotype from the contractile-quiescent to the synthetic-proliferative. Experimentation has linked these two stages by correlating the magnitude of vascular injury to the amount of subsequent smooth muscle cell proliferation (Curcio, Torella and Indolfi, 2011). The production of cytokines from the aforementioned monocytes and platelets, alongside a lowering in proliferation inhibitors from endothelial cells begin a number of signalling cascades within the smooth muscle cells. Identified cytokines are TNF-α, IL1, IL6 and PDGF. These act in concert to push the smooth muscle cells from the quiescent G0 phase and into G1, where they are able to migrate. From this point onwards no additional growth factors are need to move the cell through the S, G2 and M phases and ultimately resulting in cell division (Marx, Totary-Jain and Marks, 2011). The migration and proliferation of smooth muscle cells along with the accompanying output of extra cellular matrix accounts for the neo intimal growth that reduces the lumen diameter. As the disease progresses the proportion of the extra cellular matrix increases in relation to the smooth muscle cells (Chung *et al.*, 2002) and it has been found that in late stage lesions, 11% of this growth comprises smooth muscle cells whilst the remaining

proportion is composed of the extra cellular matrix (Bennett, 2003). However it is the cells that secrete the matrix and thus are of critical importance to the in stent restenosis mechanism. The stent struts therefore become surrounded by this neo-intimal growth decreasing the diameter of the artery and occluding blood flow.

A number of risk factors have been found to increase to likelihood of in stent restenosis occurrence. Studies of cardiovascular intervention patient populations that have gone on to develop in stent restenosis have highlighted clinical risk factors such as diabetes mellitus and the presence of high serum concentrations of interleukin 6, 10 or c-reactive protein (Garg and Serruys, 2010; Kim and Dean, 2011). Clinical presentation of in stent restenosis is often recurrent angina, however patients can also develop the more the severe symptoms of coronary heart disease, myocardial infarction and ultimately death (Manoharan, Davidavicius and Wijns, 2007). Patients can show the elevation of cardiac markers associated with myocardial infarction (Dangas *et al.*, 2010; Alfonso *et al.*, 2014), all symptoms that the stent was originally inserted to ameliorate.

Clinicians have several options when considering how to treat in stent restenosis. The insertion of another stent over the neo-intimal growth known as repeat stenting reuses the original principle of artery expansion and creates a tubular sandwich. The use of a 2nd or 3rd generation drug-eluting stent helps to inhibit further neo-intimal growth. Besides repeat stenting one of the other therapeutic intervention options is balloon angioplasty using a balloon coated with an antiproliferative drug. It is a simple procedure that re-expands the artery, restoring blood flow and inhibiting further smooth muscle cell proliferation (Piraino *et al.*, 2017). Variants of balloon angioplasty use a cutting or scoring balloon that expands and slices through the neo-intimal growth, making its compression easier and lowering the forces required. Techniques that remove the unwanted tissue before balloon expansion have also proven to be less susceptible to reoccurring in stent restenosis with laser ablation and rotational atherectomy used in this manner (Alfonso *et al.*, 2014). Although requiring the patient to undergo major surgery, bypass grafting is also carried out on patients with in stent restenosis (Triantafyllou, Frangoulis and Kolettis, 2006). All treatment options are made easier by the early identification of the disease.

The time progression of the disease has proven difficult to study in humans due to the difficulty in achieving high resolution images at multiple time points, as discussed later in this section. Presentation of myocardial infarction caused by in stent restenosis has been identified in bare metal stents at an average time of 5.5 months following implantation (Nayak *et al.*, 2006). There are less data available for drug-eluting stents with one study indicating 12 months until in stent restenosis detection (Dangas *et al.*, 2010). A published example of a 72 year old patient implanted with a drug-eluting stent identified in stent restenosis with angiography a very short time after implantation time, within a window of 33 to 91 days. The authors suggested that the disease developed after the drug-eluting stent had completed release of the anti-proliferative drug (Contractor, Mamas and Fraser, 2008). Late stage in stent restenosis is also possible with development being observed beyond 2 years from the procedure. It should be noted that for all studies the point of disease identification will be either once when the patient has developed symptoms or the point of neo-intimal growth has become large enough to become visible with the available imaging techniques. Initiation and early progression of the disease will have occurred at some unknown previous point in time. More recent research has revaluated late stage in stent restenosis as a potentially different disease pathology, neoatherosclerosis.

1.3 Neoatherosclerosis

The observation of lipid-laden foamy macrophages and fibrous caps in thrombi from patients who suffered late stage thrombosis 4 years after stent implantation has led to a new assessment of late stage neo-intimal growth. The similarities between the lesions found in this phase and the atherosclerotic plaques in native arteries has led to the term neoatherosclerosis. In a similar fashion to atherosclerosis, the disruption of the plaque can lead to thrombosis. Indeed a high incidence of late stage thrombosis has been identified as an issue with stent implants (Finn and Otsuka, 2012). Evidence also suggests that the progression of neoatherosclerosis begins earlier in drug-eluting stents when compared to bare metal stents (Park *et al.*, 2012). The evidence for neoatherosclerosis developing 4 years after implantation further emphasises the need for long term regular monitoring of cellular behaviour around the stent struts.

1.4 Re-endothelialisation

Re-endothelialisation refers to the process of endothelial cells growing over the exposed stent struts, recreating the pre-implantation arterial wall scenario whereby only the endothelium is in contact with the circulating blood. A complete, healthy endothelium provides an antithrombotic surface and modulates the vasomotor tone through the release of modulators such as the platelet adherence inhibitor thrombomodulin and the vasodilator nitric oxide (Tesfamariam, 2016). Re-endothelialisation prevents the initiation and progression of the coagulation cascade that leads to stent thrombosis. Incomplete re-endothelialisation is therefore a strong risk factor for the development of in-stent thrombosis, furthermore the re-establishment of the endothelium reduces the possibility of in stent restenosis (Inoue *et al.*, 2011). The consensus within the literature is that rapid re-endothelialisation over the stent struts is the gold standard for post implantation arterial healing.

In animal models the process of re-endothelialisation after stent implantation has indeed been shown to happen rapidly. In vivo studies with bare metal stents have demonstrated complete re-endothelialisation, post implantation, occurring after 7 days in porcine models (Pérez de Prado *et al.*, 2011) and 28 days in rabbits (Finn, Nakazawa, *et al.*, 2007). There is however a notable gap between re-endothelialisation rates in studies of animals and in humans. The later generation of drug-eluting stents have shown partial 90% re-endothelialisation after 9 months (Barlis *et al.*, 2010), there also are observed cases of patients lacking re-endothelialisation after time periods of up to a year (Joner *et al.*, 2008). One potential reason - besides the species - is the considerable age gap between the animal models - pigs at 2 months - and the average ages of humans who undergo a stent implantation procedure – 62 years (Holmes *et al.*, 2004). The following overview of the mechanism of re-endothelialisation is derived from the aforementioned animal models as they can provide an insight into the entire length of the process, whilst human studies are undertaken on examples following patient death. Consequently it potentially may differ from that in humans, particularly in the time domain as previously indicated. Furthermore it should also be noted that drug-eluting stents can alter the course of re-endothelialisation, and this will be discussed in later sections.

In the immediate aftermath of implantation the stent is covered in a layer of platelets and fibrin onto which then reside a large number of the inflammatory cells, lymphocytes and neutrophils. Endothelial cells are also present as they begin to migrate from the intact endothelium adjacent to the stent struts. Progressively the migration and proliferation of endothelial cells continues over the stent struts with the areas covered in inflammatory cells encroached upon. Re-endothelialisation is considered complete when stent struts are fully coated with a monolayer of endothelial cells. More recent research has identified additional mechanisms of endothelial repair through cells types present in the circulating blood. Circulating endothelial cells are fully mature cells that have been removed from the vascular endothelium either as part of the normal replenishment process or from being dislodged by injury events, like stent implantation. They are believed to play a role in re-endothelialisation through the expression of surface adhesion molecules that allow attachment to the region needing repair (Tesfamariam, 2016).

The other mechanism deemed important to endothelium repair is the homing of endothelial progenitor cells to the site of injury. Originating in the bone marrow and differentiating from haemopoietic stem cells the levels of these cells are thought to be elevated as a response to inflammatory cytokines arising from vascular injury. Once at the site of injury, continued differentiation into endothelial cells promotes the re-endothelialisation process. Smooth muscle progenitor cells are also attracted to site of injury differentiating from the same CD34+ haemopoietic stem cells as endothelial progenitor cells and there is thought to be a healthy balance between the two cell types that promotes re-endothelialisation over the aforementioned in stent restenosis (Inoue *et al.*, 2011). The identification of this mechanism of vascular endothelial repair prompted the development of the Genous stent by Orbusneich (www.orbusneich.com). The stent surface has adhered to its surface the antihuman-CD34 monoclonal antibody which the manufacturers claim recruits circulating endothelial progenitor cells, promoting re-endothelisation (Larsen *et al.*, 2012). This concept has now been included alongside luminal drug elution in the COMBO stent (Jaguszewski *et al.*, 2017).

Even if the endothelium is fully reformed over the struts, studies have demonstrated that it and immediate surrounding endothelial cells may not have the full functionality of a normal healthy monolayer, this is termed endothelial dysfunction. Endothelial dysfunction has been linked with increased expression of inflammatory mediators and prothrombotic molecules (Tesfamariam, 2016) and variation in gap junction communication (Ebong and Depaola, 2013).

1.5 Drug-eluting stents

The development of drug-eluting stents was driven by the clinical need to reduce the prevalence of in stent restenosis occurring in cases where bare metal stents have been implanted. The first instance of drug-eluting stent implantation into humans is recorded as happening in 1999 (Morice *et al.*, 2002). Examples of drugs in the first generation of drug-eluting stents are rapamycin and paclitaxel. These drugs have been replaced by everolimus, biolimus and zotarolimus in later second and third generation drug-eluting stents that are in current clinical use (O'Brien *et al.*, 2016). These drugs have an inhibitory effect on the migration and proliferation of smooth muscle cells, an important factor in the development of neo-intimal tissue formation in in stent restenosis (Lüscher *et al.*, 2007; Marx, Totary-Jain and Marks, 2011). Research has continued to identify other drugs that intentionally target specific aspects of the mechanism of in stent restenosis. An example is Pioglitazone which targets the aforementioned MCP-1 monocyte chemoattractant (Joner *et al.*, 2007).

The drug selected by the stent manufacturer is either contained within a polymer coated onto the stent or adsorbed into purposefully created surface features (Acharya and Park, 2006; O'Brien *et al.*, 2016). Following insertion the drug is eluted into the injured tissue surrounding the struts with the clinical intention being to repress the inflammatory response previously detailed as the cause of in stent restenosis. The time period of the drug release profile varies depending on the stent type and drug combination used but the majority of drug release normally occurs over the first 30 days following stent implantation (Venkatraman and Boey, 2007; Joner *et al.*, 2008).

The use of drug-eluting stents in preference to bare metal stents achieved a demonstrable reduction in in stent restenosis cases. As a result the popularity of drug-eluting stents increased dramatically within a short space of time and by 2005

accounted for 80-90% of all revascularisation procedures (Curcio, Torella and Indolfi, 2011). Patients implanted with the first generation of drug-eluting stents did however present with in stent restenosis with the range of rates cited in the literature being between 5 and 20% (Dangas *et al.*, 2010; Farooq, Gogas and Serruys, 2011; Alfonso *et al.*, 2014; Looser, Kim and Feldman, 2016; Piraino *et al.*, 2017). Later generations of drug-eluting stents have further reduced the occurrence of in stent restenosis. With 2 year follow up results from the SCAAR trial showing an improved 4% in-stent stenosis rate for the now extensively used Xscience (everolimus), Endeavour Resolute (zotarolimus) and promus (everolimus) stents (Sarno *et al.*, 2012). These percentages should be considered alongside the large number of procedures performed using drug-eluting stents with an estimated 100,000 procedures performed in the United Kingdom alone (Ludman and Gavalova, 2014). It can be stated that even a low occurrence of in stent restenosis in the worldwide drug-eluting stent population represents a large number of a patients and a significant clinical concern (Alfonso *et al.*, 2015; Piraino *et al.*, 2017). It should also be noted that bare metal stents are still used where the cost of drug-eluting stents is considered prohibitive. The prolonged risk of stent thrombosis seen with the use of drug-eluting stents requires the use of extended durations of anti-platelet therapy, discussed further in the next section. This may be unsuitable for patients with additional conditions where bleeding is a problem and a non-drug-eluting stent may be prescribed that requires less anti-platelet therapy (Alfonso *et al.*, 2014). In stent restenosis remains an ongoing problem for those clinicians who use bare metal stents and also those who use drug-eluting stents.

1.6 Stent thrombosis

An additional risk following stent implantation is the development of stent thrombosis. The growth of a thrombus in the region of the stent has dire consequences for the patient, potentially leading to myocardial infarction and death. As with in stent restenosis the thrombus formation involves the initiation and continuation of a series of complex cascades. In the beginning the mechanical impact of the stent struts into the arterial wall compresses and then fractures the endothelium exposing the sub-endothelial layer. Endothelial cells in the injured region become

activated, a state that causes them to reduce the expression of antithrombotic molecules with thrombomodulin and heparin being two identified examples (Tesfamariam, 2016). It should always be borne in mind that the thrombotic and inflammatory pathways share common cascades and that one scenario does not preclude the occurrence of the other.

Stent thrombosis is typically defined by the time stage of occurrence. Acute and early stage thrombosis are defined as being within 24 and 30 days of the stent implantation respectively, late less than 1 year and very late greater than 1 year. It is the late and very late stages that are linked to the lack of re-endothelialisation and vascular repair around the stent struts (Inoue *et al.*, 2011). The first generation of drug-eluting stents were shown to reduce the risk of in stent restenosis but were also found to be more susceptible to late or very late stage stent thrombosis when compared to the previous generation of bare metal stents (Garg and Serruys, 2010). A debate in the literature persisted for several years when attempting to assign a cause for stent thrombosis. The task is further complicated when considering additional influencing factors such as stent design and procedural variations that are also common to all stent type interventions. However when combining the patient data analysis with research into the effect of the drugs on the proliferative capacity of endothelial cells the case became compelling. Both rapamycin and paclitaxel have been demonstrated to cause a delay in the re-endothelialisation process (Finn, Joner, *et al.*, 2007; Lüscher *et al.*, 2007) and has been confirmed with in vivo animal studies (Pérez de Prado *et al.*, 2011). Like their inhibitory effects on smooth muscle cells the mode of action in their delaying of re-endothelialisation of these two drugs is also different. Rapamycin inhibits endothelial proliferation by suppressing a kinase pathway in the cell cycle whereas paclitaxel inhibits microtubules, essential in the mitosis phase of the cell cycle (Finn, Nakazawa, *et al.*, 2007). A further indentified cause for stent thrombosis, and also in stent restenosis, was hypersensitivity arising from the polymer used to incorporate the drug into the stent (Azarbal and Currier, 2006). This finding drove the development of polymer free drug-eluting stents and polymers with improved biocompatibility (Stefanini and Holmes, 2013). Even more recent stent generations with biodegradable polymer coatings have been shown to increase apoptosis limiting re-endothelialisation (Tesfamariam, 2007).

To help prevent thrombus formation on areas of stents not covered by endothelial cells clinicians extend the prescription of dual anti-platelet therapy. This course of therapy was previously only thought essential in the early stages after the procedure, however for patients with drug-eluting stents a standard prescription of 6 months is used with ongoing trials investigating shorter 3 month drug regimens (Wilson *et al.*, 2017). In some cases a prescription can be extended up and beyond 12 months after stenting is used (Stefanini and Holmes, 2013). Such dual anti-platelet therapy influences the thrombotic properties across the whole of the patient's circulation. There is a desire to avoid – where possible - long term drug treatment regimens, particularly if the patient has additional conditions that are worsened by bleeding (Urban *et al.*, 2015). The ability to confirm that re-endothelialisation has been completed - reducing the risk of thrombosis - would allow clinicians to make a judgement on the continuation of anti-platelet therapy for this at risk cohort of patients.

1.7 Re-endothelialisation and in stent restenosis diagnosis - non-invasive techniques

When attempting to assess the progress of cellular regrowth around the struts of implanted stents clinicians have a range of options.

1.7.1 Magnetic Resonance Imaging

As a non-irradiative imaging technique Magnetic Resonance Imaging (MRI) has become the leading method of diagnosis for a wide range of diseases. Its use in the case of in stent restenosis is however complicated by a number of factors. Stainless steel is used as a material for stent struts in many devices even in drug-eluting stents where it is only the surface which is modified to encapsulate the drugs. This material selection leads to a safety concern in MRI whereby the inducement of current causes heating to occur in the stainless steel stent, a phenomenon seen in other implanted devices (Busch *et al.*, 2005). A further concern is that MRI - as the name implies - will apply a magnetic force to the stent that could cause movement of the device during imaging. However the magnitude of the forces is considered lower than those imparted by normal heart contraction and flow induced shear stress (van Geuns and Baks, 2007). Despite these concerns clinicians and researchers safely use MRI on

patients with implanted stents. The primary technical challenge in using MRI as a diagnostic tool for in stent restenosis is the presence of artefacts in the imaging and a local signal void in the stent region all caused by the metallic arrangement of the stent struts. These issues have led to the development of specific stents constructed from alloys that are magnetic resonance transparent thus allowing visualisation of the lumen (Spuentrup *et al.*, 2005), although no device has yet progressed beyond animal trials. Currently direct imaging of the lumen in the stented region in clinical use is not possible and the best method of in stent restenosis diagnosis using MRI is through the measurement of flow patterns in the regions around the stent where artefacts and are reduced. The advantages of using MRI in this fashion are the non-invasive nature of the procedure and its inherent safety when compared to irradiative imaging techniques. However MRI is only able to provide data on occluded flow caused by late stage in stent restenosis and cannot characterise cellular regrowth such as re-endothelialisation around the stent struts.

1.7.2 Computed Tomography

Computed Tomography (CT) scanning is a powerful non-invasive medical imaging technique that involves the assembling of 2 dimensional cross-sectional X-ray images into a 3 dimensional model. The addition of contrast agents to the area of concern can highlight the tissues that they are incorporated into. CT scanning of implanted stents is hindered by similar problems to MRI, such as blurring arising from motion of the artery and artefacts induced by the metallic stent struts. Despite these challenges improvements in resolution has resulted in the successful use of CT scanning to non-invasively diagnose late state in stent restenosis through a reduction in artefacts caused by beam hardening effects (Andreini *et al.*, 2012). Further improvements in CT angiography are anticipated and the technology is likely to be the main competitor for any novel non-invasive device or technique that seeks to identify in stent restenosis. However should developments continue to improve to the point whereby early stages of cellular regrowth can be determined the irradiative basis of the technique curtails the number of times a patient can undergo the imaging procedure and this in turn limits the temporal resolution and subsequent assessment of the progression of the disease.

Although all of the imaging techniques described here are able to provide clinicians with a non-invasive option of in stent restenosis diagnosis they are severely limited in their ability to characterise the nature of cellular regrowth. Consequently the available imaging techniques are only able to provide later stage in stent restenosis diagnosis once blood flow has been occluded. No non-invasive technique is able to determine re-endothelialisation or assess the level of functionality of the new endothelium. To provide more information clinicians can use invasive methods of diagnosing in stent restenosis.

1.8 Re-endothelialisation and in stent restenosis diagnosis - invasive techniques

Patients are not typically subjected to invasive diagnostic procedures unless the progression of in stent restenosis is strongly suspected and more information before intervention is sought. The methods described here use catheterisation as a means of deploying contrast agents, or measurement and visualisation devices into the region of interest. Whilst catheterisation is an extremely common procedure it is still a surgical intervention procedure and may not even be possible at a given point in time for some patients due to development of coexisting conditions since the original stenting procedure. If a patient is considered at too high a risk for invasive in stent restenosis then they are also considered to be unsuitable for intervention procedure such as angioplasty or repeat stenting.

1.8.1 Angiography

The most common method of in stent restenosis diagnosis is angiography, using the same principles and procedures as those used to diagnose atherosclerosis. The technique involves the percutaneous delivery of a radiopaque contrast medium to the coronary circulation, permitting vessel visualisation with X-ray imaging. The stented section is then imaged and a 50% artery diameter reduction threshold is used to indicate the presence of in stent restenosis. Inevitably this diagnosis is only able to be accomplished once the level of neo-intimal growth has become large enough to be visible, by which time the patient may already be experiencing symptoms. There have also been shown to be limitations in the use of angiography to identify in stent restenosis with image interpretation and diagnosis known to vary from clinician to

clinician (Klauss and Pijls, 2007). Furthermore it is an irradiative technique and regular imaging is not considered safe. Angiography is only capable of assessing the extent of late stage in stent restenosis and is not sensitive enough to diagnose rendothelialistion of the stent struts.

1.8.2 Pressure wire gauge

Amongst the most commonly used invasive technique is the insertion of a pressure gauge wire into the region of interest. By measuring the pressure of the blood flow at points adjacent to the stent an indication can be gained on the level of blood flow occlusion, quantified by the calculation of the parameter Fractional Flow Reserve. In common with other diagnostic techniques the flow of blood must have been already been occluded to the point where it is measurable and therefore the size of the in stent restenosis lesion must be at a later stage of development. The ability to directly measure the effect that in stent restenosis has on blood flow can inform clinicians how serious the danger is to the patients' health and a judgment on intervention can be made. An additional advantage of this diagnostic technique is its reliance on the measurement of quantifiable variables reducing variation that arises from a qualitative assessment by clinicians (Klauss and Pijls, 2007).

1.8.3 Intravascular ultrasound

An invasive imaging technique that enables clinicians to visualise the interior of the stented vessel is intravascular ultrasound. The procedure involves the introduction of an ultrasonic probe that is positioned near to the suspected region of in stent restenosis via catheterisation. As a tool for the assessment of in stent restenosis the images provided can give an indication to clinicians on the progression of the disease, although the lesion must have grown to a visible size. The resolution of intravascular ultrasound is not high enough to provide information on the re-endothelialisation of the stent struts (Mintz, 2007).

1.8.4 Optical coherence tomography

Optical coherence tomography is procedurally similar to intravascular ultrasound imaging but is able to provide a 10 times higher axial resolution of 15μm. Consequently the technology is able to visualise in stent restenosis at earlier stages of

development than any of the other currently available techniques and has been used as a research tool for investigating the aforementioned neoatherosclerosis (Alfonso *et al.*, 2014). It has been claimed that the resolution of optical coherence tomography is sufficiently high enough to identify re-endothelialisation of the stent struts (Kauffmann, Motreff and Sarry, 2010). However the cited study assumes that the initial cellular regrowth seen is comprised of endothelial cells as the resolution is not high enough to provide information on cell morphology. Should the assumption be correct such a visual based assessment still cannot provide an indication on the functionality of the new endothelium. In addition the invasiveness of the procedure restricts how often imaging can carried out, limiting its use in following the progression of cellular regrowth at multiple points in time.

1.8.5 Impedance spectroscopy

The use of impedance spectroscopy to analyse coronary artery lesions has been pioneered by a research group led by Süselbeck who first published results from animal studies in 2005. The method remains in the research domain but is discussed here due to its relevance to the research reported in this thesis. The underlying principle behind these studies is to adhere flexible, micro-electrodes to the outer surface of a standard catheter balloon and then press them directly onto the suspected diseased region. Positioning of the balloon adjacent to the lesion and subsequent inflation pushes the electrodes into contact with the tissue of interest. It is then possible to apply impedance sweeps across the lesion permitting analysis and classification of the tissue (Süselbeck, Thielecke, Köchlin, *et al.*, 2005). The advantage of this method of identification is that it can provide information on the cellular constitution of the lesion beyond the capability of other diagnostic techniques. The first published study investigated if the technology was capable of determining neointimal growth following arterial wall injury by stent implantation. Rabbit iliac arteries were stented and then the electrode catheter arrangement used to compare the total impedance of the stented and unstented regions at time points of 14, 28 and 56 days. The increase in stenosis across the three time points was correlated with a rise in total impedance of the stented regions when compared to the adjacent unstented arterial wall. The greatest impedance differences between the two wall sections were discovered when using a frequency range of 1 *kHz* to 10 *kHz*.

Amongst the study's limitations - beyond the animal-human comparison - are the use of the iliac artery rather than the coronary artery owing to size constraints and that the ballooning procedure itself may cause damage to tissue that will affect the impedance measurements. Since this initial study the research group's direction has moved away from the investigation of in stent restenosis and the method has been applied to investigate the impedance properties of ex-vivo atherosclerotic plaques in humans, with total impedance increases correlated with inflammatory cellular behaviour (Streitner *et al.*, 2012). Other research groups have contributed incremental advances with improvements in electrode configuration (Packard *et al.*, 2016) and comparison with theoretical models (Yu *et al.*, 2011), however all on atherosclerotic plaques not in stent restenosis lesions. In relation to the research contained within this thesis the importance of these invasive electrode studies lies in the fact that lesions in arteries can be characterised using impedance spectroscopy and that this has been proven with in vivo results from both animals and humans.

1.9 Clinical and research needs

It can be concluded that there is a clinical need for technologies that can identify the course of cellular regrowth over the struts of a coronary stent summarised in the following quote.

"Early detection tools, ideally noninvasively, are required to identify those who develop restenosis, although preventing or halting the process is preferred." (Manoharan, Davidavicius and Wijns, 2007)

None of the described diagnostic methods are able to fulfil this need. Non-invasive imaging techniques are hindered by low resolutions and artefacts caused by the presence of the stent and as such can only identify late stages of in stent restenosis. Invasive methods can identify in stent restenosis at an earlier stage and provide a more accurate assessment of lesion development but are severely limited by the need to deliver the measurement device through catheterisation. Most importantly, neither class, invasive or non-invasive, can conclusively inform clinicians that re-endothelialisation has occurred or the level of re-endothelialisation over the stent struts. Partially re-endothelialised stent struts place the patient at an increased risk of developing in-stent thrombosis. A technology that can characterise between a full

and partial re-endothelialised stent would be of benefit to clinicians, with such information on enabling an informed to be made in the duration of a patient's anti-platelet therapy.

It can also be stated that there exists a need for a research tool to investigate the time progression of re-endothelialisation and restenosis. Animal studies are themselves limited by the available diagnostic technologies and the development of a technology that can provide real time data on the development of in stent restenosis and re-endothelialisation would be a valuable tool in research. In particular there is a dearth of experimental data on the time progression of in vivo cellular regrowth and the importance of new endothelium functionality. Further research into this area would help to inform stent designs that aim to promote re-endothelialisation and suppress in stent restenosis.

1.10 Self-reporting stents

A proposed concept that aims to address the clinical need and could also fulfil the research need is the self-reporting stent. The notion that a stent itself could provide feedback information on the progression of in stent restenosis was first proposed in the Stentenna concept by Takahata et al 2003. This device comprised a modified coil stent with an integrated pressure sensor and was shown, in vitro, to be able to measure pressure fluctuations that are indicative of in stent restenosis but did not progress beyond the research phase. The use of non-invasive cell characterisation as a method of detecting in stent restenosis was proposed in the published literature by Shedden et al 2010. The concepts basis is that the electrical conductivity of the stent struts can be exploited, using them as electrodes to carry out impedance spectroscopy measurements to characterise cellular regrowth. The method by which this could be achieved remotely - and thus non-invasively - has been investigated in a thesis by Shedden, 2008. The study derived recommendations on the future direction of such a device from a review of the literature and experimentation using in vitro remote and direct impedance measurements of stented coronary artery sections and the perceived technological embodiment of this research is captured in a patent (Shedden *et al.*, 2009). It was concluded that a self-reporting stent would need to be a passive device with no implanted power source, primarily due to space requirements. Inductive

coupling was highlighted as a method through which electrical current could be induced from an external device to the internal device comprising the stent itself or micro-circuitry integrated into the stent design. Inductive coupling is a phenomenon whereby electrical current creates an electric field that induces a current in a second remotely placed coil. The separation distance between the external device and the implanted stent of 5cm used by Shedden, although in clinical practice this is likely to be much larger particularly for obese patients. This method of power transfer mimics that used in other implanted medical devices, the most renowned of which was the now discontinued AbioCor replacement heart (Fox *et al.*, 2015). In the intervening years progress has continued on the development of implantable bioimpedance sensors and the current zenith of development is represented in a published device developed by Rodriguez et al, 2016 which fulfils many of Sheddens predictions. Through a 4 electrode setup the prototype was found to be capable of measuring impedance parameters across a frequency range of 2*kHz* to 2M*Hz*. The device is also battery free, using inductive coupling both as its power source and as a means for data transmission, and was shown to be effective at a distance of 4cm. The size of the device at 13mm x 1.2mm is still currently too large to be considered for implantation into coronary arteries.

In concluding her research Shedden predicted that the difficulties in designing a self-reporting stent reside in miniaturisation and being able to apply the range of frequencies required to characterise any neointimal growth or re-endothelialisation. The wider the frequency range required the greater the problems that the design of the self-reporting stent will encounter. Accompanying data from the Shedden thesis and published studies - including the previously described invasive balloon electrode techniques - indicate that the *kHz* region is of the most interest. A further crucial consideration for a self-reporting stent is that it's design should not compromise the therapeutic performance of the stent. Such a design will need to maintain aspects such as thin strut thickness that have been shown to reduce the occurrence of in stent restenosis.

There also exists the commercial development of a self-reporting stent by the French company Sensome (https://www.sensome.com). This company have a patent which

claims that their unique stent device also aims to use a perceived variation in cellular impedance to diagnose disease states (Barakat *et al.*, 2016). Although no specific details are provided the patent cites the need to use more than one frequency to characterise cell types, and it can be surmised that these are the same types as those investigated by Shedden. There are no known published studies relating to this commercial development and consequently more precise details on how disease states are characterised or the effectiveness of their device in monitoring cellular regrowth are not currently known.

1.11 Stent cell regrowth areas

Part of the process towards developing a self-reporting stent would be a series of in vitro studies that aimed to determine both the feasibility of non-invasively characterising cellular regrowth and also identify key parameters that can inform any future design phase. The area of the stent over which cells proliferate requires defining before any investigation can begin. This information can then be used to determine the area over which any in vitro cell testing must take place to ensure that the cell population is clinically relevant. Coronary artery stents are supplied by manufacturers in a variety of sizes to enable clinicians to size match both the lesion and the patient's own anatomy. Of relevance to the detection of in stent restenosis and re-endothelialisation is the exposed area of the stent over which cells regrow following the insertion procedure. It should be noted that this is not the same as the total surface area of the stent but the inner diameter area that is exposed to the blood flow. Stent manufacturers do not generally publish the stent percentage area or release enough dimensional data on their devices to enable an accurate calculation of this area. However in a limited number of cases the United States Food and Drug Administration (FDA) have published enough information within the various Summary and Effectiveness data sheets that manufacturers are required to provide. The data sheets provide dimensions of the largest and smallest stents in the product range as well as the percent surface area which is defined as the percentage of the artery area in contact with the stent. It can be assumed that the outer area of the stent in contact with the artery wall closely approximates to the inner area exposed to the blood flow. With known stent dimensions and the percentage stent area the range of

exposed areas for that particular stent can be calculated. Table 1.1 shows these calculated areas for 4 clinically relevant stents, ranging from first generation through to current state of the art devices. These areas provide a guide on the areas over which in vitro experimentation using cells should be performed to ensure a clinically relevant population.

Stent	TAXUS Liberte	ION	XIENCE V	XIENCE nano
Manufacturer	Boston Scientific Corporation	Boston Scientific Corporation	Abbott Vascular	Abbott Vascular
Stent percentage area	25.6%	23.9%	14.9%	15.0%
Maximum available length (mm)	32.0	32.0	28.0	28.0
Minimum available length (mm)	8.0	8.0	8.0	8.0
Maximum available diameter (mm)	4.0	4.0	4.0	4.0
Minimum available diameter (mm)	2.5	2.3	2.5	2.3
Max exposed stent area (mm^2)	102.9	96.1	52.4	52.8
Min exposed stent area (mm^2)	16.1	13.5	9.4	8.5
Source	http://www.accessdata.fda.gov/cdrh_docs/pdf6/P060008b.pdf	http://www.accessdata.fda.gov/cdrh_docs/pdf10/P100023b.pdf	http://www.accessdata.fda.gov/cdrh_docs/pdf7/P070015b.pdf	http://www.accessdata.fda.gov/cdrh_docs/pdf7/p070015s054b.pdf

Table 1.1 - Exposed areas for 4 stents calculated from data published in FDA Summary and Effectiveness data sheets.

1.12 Electrical properties of cells

The impedance spectroscopy methods that have been investigated for characterising vascular tissue and the response to stenting, all make use of the electrical properties of cells and tissues. All cells are surrounded by a membrane comprising a lipid bilayer approximately 7nm thick, in which protein complexes are interspersed that regulate the cells interaction with its immediate external environment with examples including cell to cell junctions, ion gates and anchorage points. Besides the crucial biochemical functions it performs, the membrane also maintains the physical integrity of the cell, with internal links to cytoskeletal features. In combination with

the aforementioned protein complexes the membrane acts as a selectively permeable barrier to its immediate external environment. Electrically the membrane is considered non-conductive or dielectric and will store charge, with the two opposing lipid layers effectively acting as a capacitor of two plates opposing one another. The capacitance of the membrane has been calculated to be $1\mu F/cm^2$ and is considered a constant for all cells (Hobbie and Roth, 2007). It was the capacitance of the cell membrane that Fricke, 1925, exploited to derive his value for its thickness of 3.3nm. This pioneering research hinted at the potential of utilising the electrical properties of cells to analyse their morphology as microscopy advances later proved Fricke's prediction to be remarkably close to the true value (Pethig and Kell, 1987).

Cells actively control the potential between themselves and their environment through the acceptance and ejection of various ions, with the principle ones being calcium (Ca^{2+}), sodium (Na^{+}), chloride (Cl^{-}) and potassium (K^{+}), and such a process is used as a signalling mechanism between cells. The resting membrane potential of a cell is typically -70mV. In an excitable cell ion pumps can rapidly depolarise a cell to +30mV before repolarisation back to -70mV. This is known as the action potential and a cascade of this mechanism across an array of cells enables physiological events such as communication along nerve cells and coordinated contraction in a collection of muscle cells. Variations in membrane potential have also been recorded during the different stages of cell division (Voets, Droogmans and Nilius, 1996). It is known that the electrical properties of cells varies considerably depending on the cell type and is closely related to the function it is performing. The focus of the research in this thesis is targeted on the two cell types that have a key role in restenosis and re-endothelialisation, specifically endothelial and smooth muscle cells and it these cells electrical properties that will now be discussed.

Endothelial cells are considered a non-excitable cell type so therefore do not actively control the ingress and egress of ions to create action potentials. However their potential is still important to their function and is actively controlled. A wide range of membrane potentials have been measured to range from +5mV to -88mV with bimodal peaks at -81mV and -15mV (Voets, Droogmans and Nilius, 1996). It is Ca^{2+} that is crucial to the signalling between endothelial cells and smooth muscle cells.

Receptors on the cell membrane that respond to external influences such as the shear stress caused by blood flow mediate the influx of calcium into the cell through the control of ion channels, hyperpolarising the cell. Additional signalling mechanisms then control the release of Nitric Oxide which acts upon receptors on Smooth Muscle Cells causing vasodilation. This is one example of a number of agonists related to the membrane potential that control the vasomotor tone and these mechanisms are exploited by the vasodilator class of drugs used in the treatment of coronary heart disease. Physiological changes can also be associated with membrane potential, a reduction in membrane potential has been found also coincide with a reduction in cell stiffness via the reorganisation of the cytoskeleton (Callies *et al.*, 2011).

Smooth muscle cells are one of the three types of muscle cells, the others being skeletal and cardiac. They are an example of an excitable cell type that act in coordinated groups to spread an action potential from cell to cell. Smooth muscle cells can also undergo a change in membrane potential depolarisation from the opening of stretch dependent ion channels. The stretching of smooth muscle cells can be generated by a rise in arterial pressure (Ji *et al.*, 2002). Regardless of how the rise in membrane potential is initiated the result is an increase in calcium via influx from the external environment through the opening of voltage operated Ca^{2+} channels and the release of intracellular calcium stored in the sarcoplasmic reticulum organelle. Calcium interaction with the acidic protein calmodulin, subsequent additional mechanisms involving ATP and myosin contract the cell and thus initiate constriction of the artery (Webb, 2003). The opening of voltage dependent K^+ channels begins the repolarisation of the membrane potential to the resting potential. Additional K^+ entry into the cell from ATP sensitive K^+ ion channels induces hyperpolarisation relaxing the cell and when acting across large groups causes artery dilation and increases the area available for blood flow.

1.13 Electrical cell stimulation

The hypothetical and practical use of external electrical stimuli to influence the behaviour of biological tissues has a long history (Shelley, 1818). In the domain of cellular biology the option exists to electrically stimulate cells that can mimic the in vivo environment and also to apply controlled stimuli that are atypical. This type of

research has produced results that has enabled researchers to actively control aspects of cellular behaviour - an important asset when attempting tissue engineering – and also provided insights into their in vivo reactions. How a potential difference or voltage across a cell can influence its behaviour is highly dependent on a number of variables, particularly the cell type and the nature of the electrical field. Methods of delivering an electrical stimulus to cells can be directly through adhesion onto electrodes, capacitive with the field generated between two plates not in contact with the cells and inductive the use of coils around the cell culture (Balint and Cartmell, 2013). An example of electrical stimulation that is beyond those experienced in vivo is the application of high electrical fields. Using the application of high voltage a phenomenon known as electroporation can be induced, where the cells membrane splits open, an event that is reversible on removal of the electrical field. This brief exposure can allow the selective ingress of marker compounds, drugs or other cell modifying substances into the cell. Higher electrical fields will cause an irreversible fissure of the membrane compromising the integrity of the cell and causing its death. The application of electrical fields has been demonstrated to cause cell alignment (Zhao *et al.*, 2000), differentiation pathway selection (Yamada *et al.*, 2007), division rate, neurite growth (Liu *et al.*, 2009). Smooth muscle cells have been induced into phenotype changes through the application of sinusoidal current causing differentiation into a contractile phenotype (Rowlands and Cooper-White, 2008). It should be noted that the application of the same electrical parameters to a different cell type – or even the same cell in a different environment – may not necessarily have the same effect. At lower voltages there will be little or no discernible physiological effect on the cell, however low voltages can still be used as a diagnostic tool. Impedance spectroscopy is an example of such a cellular analysis technique of which applies voltages directly to cells adhered to electrodes. The voltages applied (typically <100mV) are considered small enough to be non-invasive and therefore not stimulatory (Wegener, Keese and Giaever, 2000).

1.14 Introduction to impedance spectroscopy

Impedance spectroscopy can be defined as the analysis of the resistance of a system to the flow of an applied alternating current across a range of frequencies. It has been

used to analyse and interpret biological systems since the early 20th century (Fricke, 1925). The technique has continued to be used to the present day with selected examples including the measurement of epithelial barrier properties (Benson, Cramer and Galla, 2013), endothelial cell reactions to shear stress (Seebach *et al.*, 2000) and applications beyond life sciences such as diagnosing the performance of proton exchange membranes in fuel cells (Rezaei Niya and Hoorfar, 2013). For cellular analysis the technique and the supporting equipment have matured sufficiently to the point whereby several cell monitoring commercial systems are available.

1.15 Commercially available impedance spectroscopy systems

Multiple companies have developed a range of products that enable researchers to culture cells directly on electrodes and perform impedance spectroscopy experiments. The two most prevalent in the literature are Applied BioPhysics – Electric Cell product and ACEA biosciences xCelligence range, with other companies such as CellSine also marketing similar products. Applied BioPhysics was founded by Charles Keese and Ivar Giaever who initially demonstrated the merits of their impedance spectroscopy system in a number of papers published in the early 1990s (Giaever and Keese, 1991, 1993; Lo, Keese and Giaever, 1995). Each system is similar in terms of equipment and procedural approach. All use gold electrodes arrayed on the base of circular cell culture wells, which interface with a base connected to a multiplexed impedance analyser specific to the system. A number of electrode types and well configurations are available and can be circular or interdigitated in configuration. The final arrangement is coated onto a plate array containing up to 96 wells, which cells are seeded into and cultured inside an incubator, with measured impedance parameters then averaged across wells. A total electrode area of 0.25mm^2 per well is typical and will measure between 100 and 200 cells depending on the type seeded. These systems are utilised as a research tool to monitor the electrical properties of cells and variations caused by the addition of agonists and have each featured in excess of 200 published papers. These automated arrangements are popular with researchers due to their low set up time, repeatability from well plate to well plate, ease of use and ability to generate large amounts of data quickly. The burgeoning amount of published data also permits more reliable

comparisons between studies using the same equipment. Disadvantages of the systems include a lack of control over the parameters of the frequency sweeps, predefined electrode configurations, high impedance gold electrodes and the inevitable high financial cost. The simplistic nature in which the accompanying software presents the results also increases the chance that key findings are inadvertently missed by researchers (Bischoff *et al.*, 2016a).

1.16 Cellular Impedance spectroscopy

Impedance measurement has been applied to analyse biological tissue for several decades. The application of the technique to biological tissue has expanded to the point whereby it is now considered a scientific discipline in its own right, known as bioimpedance. The techniques and equipment used vary considerably with selected examples being the use of multiple electrodes arrays attached to the skin to measure the cardiac cycle (Van Eijnatten *et al.*, 2014) and to provide spatial diagnosis of lung tidal volume (Meier *et al.*, 2008). It is however the use of impedance measurement over a wide range of frequencies on cellular culture that is of relevance to this thesis and will be discussed further. The culture of cells on electrodes and the corresponding measurement of impedance across a frequency range was pioneered by Giaever and Keese, 1986, and named Electric Cell substrate Impedance Sensing (ECIS). In principle the method comprises planar electrodes on a non-conducting surface onto which cells are introduced, and the growth of the cells directly over the electrodes introduces variations in the impedance measurements made between them. The use of a much smaller working electrode in comparison the reference electrode biases the impedance measurement to the events happening at that electrode (Macdonald, 1992). A size ratio of at least 100 to 1 is the standard used in commercial systems and published research. Inevitably space requirements mean that only a small number of cells are able to fit onto the electrode of interest, a constraint negated by the use of multiple wells to increase sample sizes with well numbers up to 384 reported (Wegener and Seebach, 2014). If the working electrode is sufficiently transparent enough to observe the behaviour of the cells then microscopy correlations can be made between the images and the data. The previously described 2 electrode setup is the most commonly employed configuration however more recently

researchers have begun to experiment with more complicated electrode setups comprising 3 and 4 electrode systems and advocate their increased stability (Asfour *et al.*, 2010; Sarró *et al.*, 2012; Ianeselli *et al.*, 2013). Schematics of different electrode configurations are depicted in Figure 1.1.

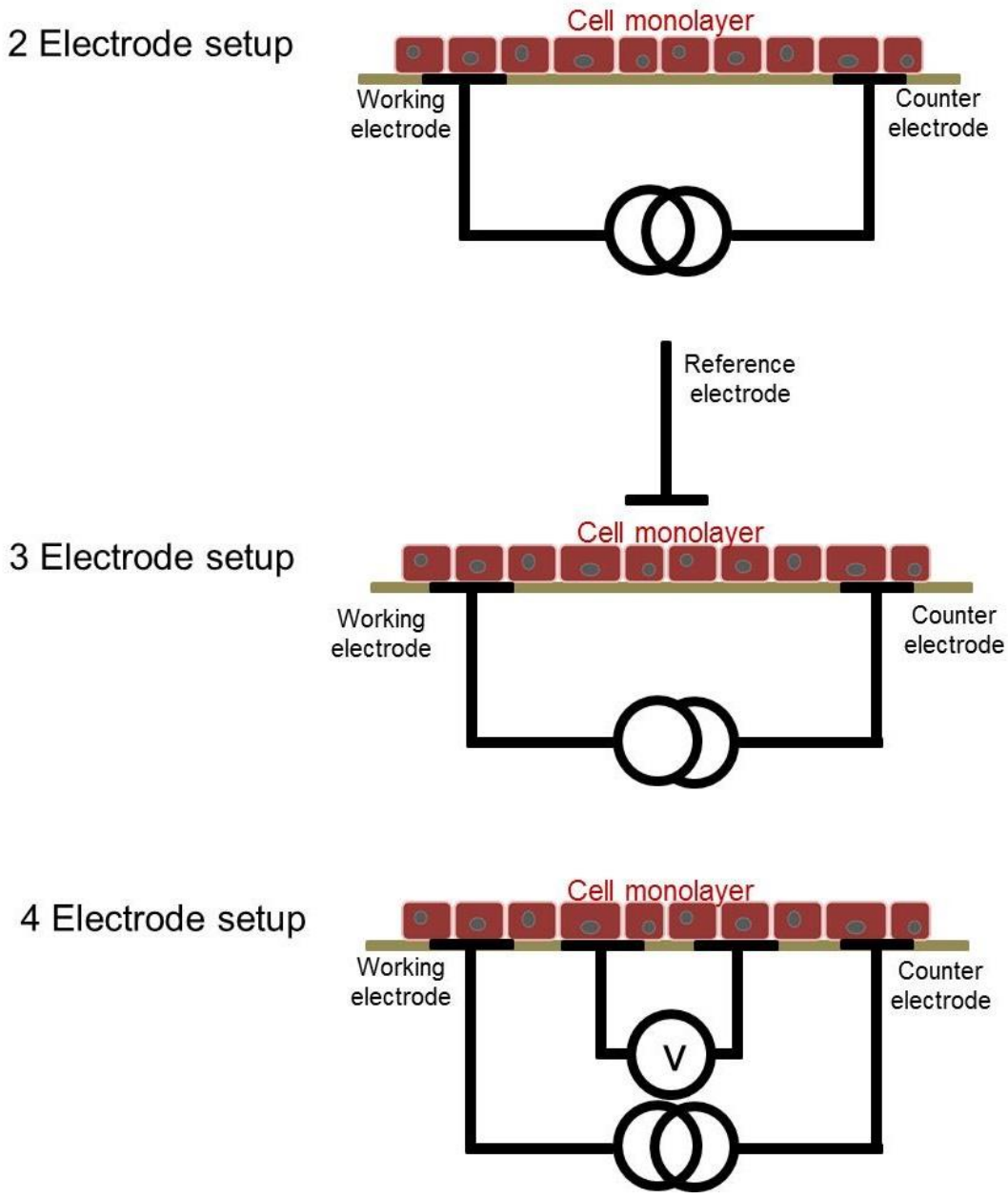

Figure 1.1 - Electrode configurations in cell monolayers impedance spectroscopy experimentation.

As a technique impedance spectroscopy has been proven sensitive enough to measure morphological changes in the cells beyond the capability of standard light microscopy (Bischoff *et al.*, 2016a). Impedance spectroscopy and microfluidic devices have also been integrated in a number of studies with analysis of single cells attained on a number of occasions (Song *et al.*, 2013; Zhu *et al.*, 2015). The aim of such devices is to provide a miniaturised diagnostic tool. An important drawback of single cell analysis is that cells originating from the same line can be at differing points in the division cycle or apoptosis and this can produce dissimilar impedance profiles, making characterisation difficult. Measurement of a multitude of cells has the potential to negate these effects (Qiao *et al.*, 2012).

The electrode substrate used can vary between studies. The most common materials are gold and indium tin oxide; however these materials have no history as a substrate for an implanted device, an important consideration for a substrate in a self-reporting stent. A material that has been used to stimulate cells and record electrical signals in implanted neural microelectrode arrays is platinum black (Franks *et al.*, 2005). The impedance of platinum black electrodes is reduced when compared to materials such as bright platinum or gold due to an increase in surface area cause by the roughness of the surface (Malleo *et al.*, 2010). This roughness means that light is absorbed by the surface creating a black appearance (Desai *et al.*, 2010). A low impedance electrode is desirable as it is more sensitive to changes arising from cellular behaviour than a high impedance electrode (Cote and Gill, 1987). The electro-deposition procedure used to create a platinum black surface means that it can be coated onto any conductive surface. Included in this are materials commonly used in stents such as stainless steel and the later generation devices manufactured from cobalt-chromium alloys.

The typical course of a cellular impedance spectroscopy experiment first involves the seeding of the cells onto the electrodes. As cells first settle after seeding and proliferate the overall impedance of the monolayer increases, contributed to by increases in the resistive and reactance components. The inverse scenario cell death is correlated with falls in impedance and has been proposed as an alternative to more traditional cytotoxicity measurements (Ceriotti *et al.*, 2007). The application of a

drug, mechanical stimulation, virus or additional cells to the monolayer can then induce a change in the cells impedance profile. There are a plethora of examples in the literature ranging from cells undergoing phenotype changes (Haas *et al.*, 2010), cell detachment from the electrodes (Angstmann *et al.*, 2011; Bagnaninchi and Drummond, 2011), cytotoxicity of substances (Opp *et al.*, 2009; Peper *et al.*, 2014), viral infection (Campbell *et al.*, 2007) and flow induced shear force (DePaola *et al.*, 2001; Seebach *et al.*, 2007). The following sections will focus on studies that use impedance spectroscopy measurements to investigate those cells that that play a role in restenosis and atherosclerosis.

1.17 Impedance spectroscopy and endothelial cells

The main research interest in investigating endothelial cells using impedance spectroscopy resides in the effect that drugs have on their barrier function. Endothelial cells form monolayers that compartmentalise regions of tissue from blood and thus control the ingress of drugs targeted at these tissues, the blood brain barrier is one such example. As their in vivo structure is as a monolayer impedance spectroscopy using co-planar electrodes is good method for analysing their behaviour. The key feature in the formation and maintenance of the barrier function are tight junctions that bind adjacent endothelial cells to one another. One of the first uses Giaever and Keese had for their ECIS technology was to investigate the barrier properties of endothelial cells (Giaever and Keese, 1991). They used impedance measurements in combination with mathematical modelling to elucidate three parameters of the endothelial monolayer.

- The barrier function, (termed R_b) a measure of the resistance to current flow in the gap between adjacent cells. The formation of tight junctions increases the barrier function of the cells and thus a corresponding rise in R_b.
- Alpha (α), a measure of the distance between the lower membrane the electrode surface.
- Cell membrane capacitance (C_m) of the basolateral and apical membranes connected in series.

In deriving the formulae for these parameters Giaever and Keese and others acknowledge the limitation that a regular shape must be assumed for the cells, either as circular disks or rectangular slabs depending on the model (Giaever and Keese, 1991; Urdapilleta, Bellotti and Bonetto, 2006). Modelling software to automatically extract the 3 aforementioned parameters forms part of the Applied Biophysics commercial system.

Many other studies have since used impedance spectroscopy as a tool for examining the effects of various agonists and antagonists on the formation of tight junctions in endothelial cells. Experimentation is accompanied by antibody labelling techniques that visualise the presence or absence of proteins that are associated with tight junction formation, such as zonula occludens. Examples of agonists that have been shown to inhibit their formation in a monolayer and thus precipitate a drop in impedance are thrombin (Szulcek, Bogaard and van Nieuw Amerongen, 2014), Vascular Endothelial Growth Factor (Becker *et al.*, 2001), Histamine (Stolwijk *et al.*, 2015) and even ionising radiation (Young and Smilenov, 2011). The technique has also been used as a quality control mechanism to confirm that endothelial cells differentiated from human pluripotent stem cells have a comparable barrier function to established endothelial cell lines (Patsch *et al.*, 2015). These studies utilise a key advantage of impedance spectroscopy when compared to standard labelling techniques in that it can provide a temporal resolution to the addition of the agonist and also any recovery of barrier function on removal of the agonist.

1.18 Transendothelial resistance

Measurement of the barrier function of endothelial cell monolayers is not restricted to direct impedance spectroscopy measurements of cells adhered to electrodes. A widely used method of assessing the endothelial layers permeability to ions is to conduct an experiment to determine the transendothelial resistance (TER). A typical experiment to determine the TER of an endothelial monolayer involves the immersion of a confluent cell sheet on a porous membrane in an electrolyte containing an upper and lower electrode. The application of alternating current between the electrodes causes the cell monolayer to provide a resistance that is then recorded. By standardising protocols researchers can make comparisons between

different endothelial cell layers and commercial systems are available (Benson, Cramer and Galla, 2013). A schematic of a typical TER experiment is displayed below in Figure 1.2. The simplicity and standardisation of the setup make TER experimentation a powerful tool in the analysis of endothelial monolayers. The technology does have limitations in that it is susceptible to gaps in the monolayer allowing a path for current to flow distorting the TER measurement. Additionally the porous membranes are not transparent enough to permit microscopy visualisation (Wegener and Seebach, 2014).

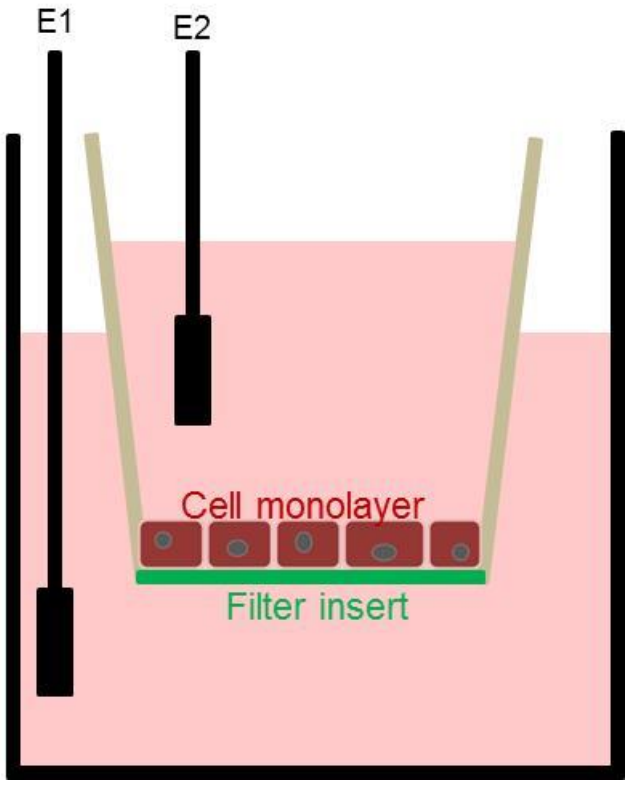

Figure 1.2 - Transendothelial resistance experimental setup schematic.

1.19 Impedance spectroscopy and smooth muscle cells

Impedance spectroscopy as a technique to analyse smooth muscle cells has been used more sparingly in research in comparison to endothelial cells. Smooth muscle cells do not exist in vivo as monolayers but as collective units that contract and relax in reaction to stimuli to maintain the vasomotor tone, as previously detailed in section

1.12 (Electrical properties of cells). As a result a smooth muscle cell monolayer cultured over electrodes is not as representative on the in vivo scenario as a monolayer of endothelial cells. Despite this, experimentation using impedance spectroscopy on smooth muscle cells can still be a useful tool in probing their behaviour. Balasubramanian et al 2008, derived a smooth muscle variant of Giaever and Keese's mathematical model by representing the cells as elongated rectangles. Using the model in combination with in vitro experimentation the study was able to investigate the effect of the application of various proteins onto the electrodes prior to renal vascular smooth muscle cells seeding. Fibronectin was identified as the most effective protein for encouraging cell adhesion and growth. In an extensive study using primary rat aortic smooth muscle cells Haas et al, 2010, were able to discern a reduced impedance magnitude when comparing the synthetic with the contractile phenotype. This finding is of importance when considering using the technique to characterise in stent restenosis where the smooth muscle cells involved are thought to be of the synthetic phenotype (Marx, Totary-Jain and Marks, 2011). Acetylcholine induced smooth muscle cell contraction also reduced impedance magnitude followed by a relaxation associated increase. Finally the group reported lower impedance drops owing to contraction as the passage count of the cells increased, providing impedance based evidence for the commonly observed phenomenon of aging and senescence in cell culture. These experiments were performed in a frequency range of 1*kHz* to 1M*Hz*, as this was the region were greatest impedance variations were observed due to cellular changes.

1.20 Cell characterisation with impedance spectroscopy

Impedance spectroscopy has been used to analyse cells typically with a specific clinical need identified, with numerous examples existing in the literature. Differences between cells of the same type are prevalent, such as the previously discussed smooth muscle cell phenotype study (Haas et al., 2010). Examples where impedance spectroscopy is used to characterise cells of different types are limited to stem cells studies where the differentiation process of transitioning into a functional cell type is monitored. This research is in part driven by the need for the non-invasive technologies to characterise the expansion of stem cell populations

(Ratcliffe, Thomas and Williams, 2011). The general course of these experiments involves the proliferation of stem cells over electrodes whilst carrying out impedance sweeps prior to the introduction of transcription factors to induce differentiation. Bagnaninchi and Drummond, 2011, showed a divergence of all impedance parameters in adipose derived human mesenchymal stem cells during differentiation into osteogenic or an adipogenic linage. These results were repeated separately by Reitinger et al, 2012, and Angstmann et al, 2011, using different stem cell sources. Öz et al, 2013, used changes in the total impedance profiles to characterise the differentiation of different cancerous cell types. All of the cited studies elected only a single frequency to compare cell types but were able to capture measurements at high temporal resolutions.

Part of the Intelligent stent thesis by Shedden, 2008, previously discussed in section 1.10 (Self-reporting stents) was the in vitro investigation of the impedance profiles of porcine endothelial cell, porcine smooth muscle cells and Madine-Darby Canine Kidney epithelial cells (MDCK). The data gathered by Shedden showed that by deriving a ratio of total impedance of the bare electrode and the confluent electrode a frequency dependent peak could be determined that was unique to the aforementioned cell type. In characterising the cells in this manner the study demonstrated the benefits of carrying out impedance sweeps across a wide 1*Hz* to 1M*Hz* frequency range. However the time resolution of measurements was every 24 hours, and cell cultures required removal from an incubator to collect the data, thereby potentially impacting on the results obtained. The results were also obtained on gold electrodes, in a similar fashion to many published studies, and so the extent to which this technique can be used to characterise cell growth, function and type on electrode materials of more relevance to medical implants remains to be determined.

Collectively the described cohort of published studies demonstrates the capability of impedance spectroscopy for characterising cells. In addition they are able to provide guidance that a wide frequency range and a high temporal resolution are desirable attributes for an impedance spectroscopy based cell characterisation system.

1.21 Cell junctions and endothelium functionality

As previously discussed in section 1.4 (Re-endothelialisation), a critical function of the endothelial monolayer is in the prevention of disease states such as atherosclerosis. In the case of an implanted stent the formation of an endothelial layer over the struts and surrounding intimal tissue is the preferred clinical outcome. The functionality of the endothelium is also important in the prevention of in stent restenosis. A dysfunctional endothelium has been linked to in stent restenosis in several studies (Caramori *et al.*, 1999; Thanyasiri *et al.*, 2007; Kubo *et al.*, 2015) and a connection with neoatherosclerosis has also been suggested (Celik *et al.*, 2008). A self-reporting stent that could provide data that allowed clinicians to assess the functionality of the new endothelium would enable a prediction on the likelihood of in stent restenosis developing in the future. Such information would also be of use to stent manufacturers in industry as they seek to optimise and develop future stent technology.

It is widely accepted that the establishment of junctions between endothelial cells is important for forming a healthy monolayer (Bazzoni and Dejana, 2004). Junctions can only form between cells that are in contact with one another and in the case of in vitro experimentation should be studied on confluent cell layers. Junctions are categorised by their type which approximates to their known functions. There are additional sub types within each category and the prevalence of each junction type varies extensively between different cells types. Those junctions that pertain to the research within this thesis will be focussed on with a particular emphasis on, gap junctions.

1.22 Tight junctions

Tight junctions are a firm bond between adjacent cells that form towards the apical edge and in the intercellular cleft between them. They mechanically link the cells together and in the case of endothelial or epithelial cells, provide a means to form a united barrier between the apical and basolateral sides of the cells. Below them in the cleft between cells are the adherens junctions and then the desmosomes, although the latter are not present in endothelial cells (Clark, 2009). Tight junctions are the principle cellular structure that controls the movement of water and solutes through

the cleft, referred to as the paracellular transport route. Like all cell junction types they require transmembrane proteins that cross the lipid membrane boundary forming a link between the internal and external cellular environment. There are 3 types of transmembrane proteins that constitute tight junctions, occludin, claudins and junctional adhesion molecule. By linking with opposing proteins from the adjacent cell a network of fibrils is formed creating the junction. Immediately inside the cell there is a region known as the cytoplasmic plaque that contains additional proteins that bind to - and thus exert an influence over - the transmembrane proteins. One such protein is zonula occludens-1 which binds to the transmembrane proteins and then links into the cytoskeletal features of the cell providing a firm structural link between the cells (Shen *et al.*, 2011). Fluorescent labelling techniques exist for zonula occludens-1 and these are often used in studies to identify the existence of tight junctions. The link zonula occludens-1 provides with the cytoskeleton is thought to provide one mechanism through which the cells can exert control over permeability of the junction, with force arising from contraction of the cytoskeleton transmitted to the transmembrane proteins (Fanning, Mitic and Anderson, 1999; Wang *et al.*, 2015). An additional identified mechanism controlling vascular permeability is a transcellular method of transport that links the opposing sides of the cell through interconnecting vesicles linked to small pits in the membrane known as caveolae (Clark, 2009).

1.23 Gap junctions

Gap junctions are narrow channels between adjacent cells that allow diffusion of small aqueous molecules and ions of a size below 1K Da. The term gap junction originates from the observation of the 2 to 4 nm distance bridged between the cell membranes by the junction rather than the internal pore gap. These structures can only form between cells whose membranes are in contact with one another thus meaning during in vitro culture those cells that have attained confluency. By connecting cells they permit the transfer of metabolites, messenger molecules and ions (Brisset, Isakson and Kwak, 2009). There is also evidence that long chain molecules such as short interfering RNA may be able to squeeze through the central pore providing a role in regulating gene expression (Spray, Ye and Ransom, 2006).

Cells can form gap junctions between cells of the same type and different types with those known to form between endothelial cells and smooth muscle cells the most relevant to the research presented here. Gap junctions are composed of 2 inter-joined hemi channels, known as connexons that cross the cell membrane, with each cell providing a hemi channel to complete the gap junction. More recent research has shown that connexon hemi-channels also have a functional role when not connected as part of a gap junction by providing a selective channel between the internal cellular space and the extra-cellular environment (Spray, Ye and Ransom, 2006). The connexons are themselves comprised of 6 transmembrane proteins known as connexins. A wide range of connexins exist and to date 21 have been discovered in humans and are designated with the prefix Cx followed by a number. A hemi channel may be composed of the same connexins and connect with another of the same composition, forming a homotypic gap junction or hemi-channels made from different connexins can also bind together creating a heterotypic gap junction. There is even further variation added when hemi channels are themselves assembled from different connexins, inevitably this leads to a large range of gap junction types. In endothelial cells gap junctions typically form together in arrays, known as gap junction plaques, however these plaques are not observed in smooth muscle cells (Figueroa, Isakson and Duling, 2004).

The current knowledge of gap junctions has been further enhanced and also complicated by the discovery in 2000 of an additional type of membrane channel constructed from a family of proteins known as pannexins. Three pannexin isoforms have been discerned in mammalian cells and are identified as Panx1, Panx2 and Panx3, with evidence to suggest a variation in expression ratios between cell types (Penuela, Gehi and Laird, 2013). Pannexins share similarities with connexins in that they are transmembrane proteins that form together in groups of 6 to form hemi channels, although the sequence homologies differ between connexins and pannexins. Pannexin hemi channels on their own have been shown to play a role in the release signalling of molecules into the extracellular space, with adenosine triphosphate (ATP) and calcium being the most commonly studied (Lohman and Isakson, 2014). Ambiguity exists in the academic community as to whether pannexin hemi channels in the membrane can join with other similar hemi channels on

adjacent cells to create a gap junction. One study claims to have measured the selectivity of pannexin gap junctions (Sahu, Sukumaran and Bera, 2014), whilst other publications find no evidence for their existence at all (Beckmann *et al.*, 2015). Studying pannexin and connexin hemi channels is made more difficult by the pharmacological nature of the available inhibitors, with many demonstrating effects on both protein types (D'hondt *et al.*, 2009).

Previously gap junctions were considered to be non-selective pores freely allowing diffusion of molecules below the 1 kDa threshold, however studies have indicated that this is not the case with different junctions shown to have selective permeability to certain metabolites (Goldberg, Valiunas and Brink, 2004; Weber *et al.*, 2004). The permeabilities of gap junctions are unique for each isoform and given the aforementioned large number of potential combinations this creates a wide range of gap junction mediated cellular communication (Brisset, Isakson and Kwak, 2009). Mediation of gap junction permeability is achieved via ions (H+, Ca++), phosphorylation and Nitric Oxide (Figueroa, Isakson and Duling, 2004). Whilst cell membranes must be in contact with one another to form junctions, motion between the surfaces has not been found to play a part with no correlation between motility and junction formation discerned (Guo *et al.*, 2007). An explanation for this may be that the half-life of a connexin is 1 to 5 hours indicating that formation and degradation is a perpetual process with cells not needing to be in contact for a long time to create gap junctions (LaFlamme and Kowalczyk, 2008).

The type of connexin involved in forming the gap junctions has been demonstrated to vary between different cell types and in the case of endothelial cells the responsible connexins have been identified as Cx37, Cx40 and Cx43 (Dejana, Corada and Lampugnani, 1995). The balance of their expression has a key role in the healthy functioning of the endothelium and regulation has been linked to different flow conditions. Over expression of Cx43 has been discovered in locations where the normal vascular laminar flow is disturbed, with elevated levels at artery branch points measured (Brisset, Isakson and Kwak, 2009). This phenomenon may be linked to the inhibition of gap junctions at sites which are more prone to the formation of atherosclerotic lesions (Ebong and Depaola, 2013). The use of gene knockout mouse

studies has enabled the correlation of individual connexin deficiencies with clinical disease states. Cx40 deficiency caused hypertension whilst Cx43 deficient mice displayed hypotension (Begandt *et al.*, 2010). It should be noted that a limitation of these studies is that compensatory reactions to the deletion of the gene may mask or create new disease conditions (Figueroa, Isakson and Duling, 2004). The expression of the three connexins has been found to vary in different parts of the vascular tree (Hill *et al.*, 2002) and contributes to the phenotypic heterogeneity known to exist in endothelial cells (Aird, 2007b). The role that gap junctions play in the maintenance of the endothelial barrier function has been highlighted in a study by Nagasawa et al, 2006. This research group found that the blocking of gap junctions in porcine blood brain barrier cells had a detrimental effect on the cells barrier function. As the blockers were found not to alter the expression of proteins associated with tight junction formation the group concluded that gap junctions have a role in maintaining the barrier properties of the endothelium. In a separate study by Ebong and DePaola, 2013, intercellular communication through gap junctions was found to be altered in regions of disturbed flow that are associated with atherosclerotic plaque formation. Yeh et al, 2006, observed a down regulation in the gap junction connexin Cx43 in Human Umbilical Vein Endothelial Cells cultured on a range of coronary stent material surfaces. This in vitro study suggests that endothelium formed over stent surfaces is deficient in gap junction formation, contributing towards a dysfunctional endothelium. Collectively the published research demonstrates the importance of gap junctions in maintaining the vasomotor tone and a healthy endothelium and therefore the study of gap junctions and their role in vascular disease remains a pertinent research topic.

1.24 Myoendothelial junctions

Heterocellular gap junctions can form between cells of different types. Of relevance to research in cardiovascular studies where endothelial and smooth muscle cells are co-cultured together are myoendothelial junctions. Myoendothelial junctions are protrusions that extend principally from endothelial cells through the extracellular matrix to the smooth muscle cells allowing direct contact between their membranes and it is at these points gap junctions form. These protrusions, with their associated

gap junctions are not seen between other cell types and are unique to the vasculature. A single endothelial cell can form myoendothelial junctions with approximately 20 separate smooth muscle cells (Behringer *et al.*, 2012). Within the vascular tree the prevalence of myoendothelial junctions is inversely proportional to diameter the diameter of the vessel and their morphology also varies (Straub, Zeigler and Isakson, 2014). The small size of myoendothelial junctions (approximately 0.5μm) hinders the analysis of the composition of these intercellular gap junctions. However the aforementioned Cx37, Cx40 and Cx43 have all been detected in a range of vascular locations in a variety of species (Brisset, Isakson and Kwak, 2009). Myoendothelial junctions and the associated heterocellular gap junctions should be considered in any experimentation where the two cell types are grown together.

1.25 Gap junction assessment

There are a variety of different methods for both visualising and quantifying gap junctions, non-electrical methods will be discussed first. The simplest technique is the scrape loading assay first published in 1987 by El-Fouly, et al. Cells are grown until they are observed to have attained confluency and are thus likely candidates for gap junction formation. A fluorescing dye of a size below 1K Da is selected and added to the surrounding media. A sharp implement - typically a scalpel or needle - is used to create a scratch across the surface, rupturing the membranes of cells immediately adjacent to the cut. The dye then enters the ruptured cells and, if gap junctions are present, will diffuse from cell to cell through the monolayer. The implementation of constant dye concentrations between samples and the fixation of the cells after a set period of time allows for a level of standardisation between experiments. Subsequent fluorescent imaging can reveal the extent of dye transfer through the monolayer and thus be associated with the number of gap junctions present. Image analysis software can also be used to quantify the level of dye transfer. Care must be taken to select the correct dye due to the known selectivity of some gap junction types. As an example, the dye Lucifer yellow will not transfer through Cx45 channels and should therefore not be used in cells were that connexin is expressed. The method remains a common technique to assess the existence of gap junction formation and is useful in that a large number population of cells can be

assessed at any one time (Abbaci et al, 2008). Deficiencies of the technique are the difficulty in creating a constant cut through the cells by hand, potentially causing a variation in cell rupturing. The method provides a simple way of providing an assessment of gap junctions without the need for specialist equipment.

A method that is of particular relevance to cells grown on conductive electrodes is gap junction assessment via electroporation. With the cells residing in a solution containing one of the aforementioned dyes a potential difference is applied between the cell electrode and an electrode directly above the cells, causing electroporation. Electroporation results in the temporary opening of the cell membrane allowing the dye ingress into the cytoplasm. If gap junctions are present then the dye will permeate from cells on the electrode into the adjacent cells that have not undergone electroporation (Anagnostopoulou *et al.*, 2007). The technique requires a period of testing to determine the optimum voltage parameters to ensure cells next to the electrode are not damaged (Abbaci *et al.*, 2008).

1.26 Electrical assessment of gap junctions

A plethora of techniques have been used to examine the electrical properties of gap junctions and their overall impact on the electrical properties of cells. Studies can be divided into one of two distinct categories experimental and theoretical, with no study as yet combining the two approaches. Both will be discussed in turn here.

An experimental method that has enabled insights into hyperpolarisation and the role that gap junctions play in this, is the use of isolated sections of mouse endothelium from arteries. Application of the gap junction inhibitor Carbenoxolone caused a dramatic reduction in electrical conduction as assessed through microelectrode insertion into distanced endothelial cells. Gap junction inhibition was also confirmed through dye transfer experimentation (Behringer *et al.*, 2012).

The dual patch clamp technique has been employed in several studies to analyse gap junctions. The method comprises the attachment of a patch clamp electrode to 2 joined cells. The generation of a potential difference between the cells allows for the measurement of junctional currents. Through the addition of agonists known to effect gap junctions inferences can be made on their behaviour. This technique was used to

determine the existence of gap junctions formed from pannexin hemi-channels, although this finding remains contested by other published studies (Sahu, Sukumaran and Bera, 2014; Beckmann *et al.*, 2015).

Theoretical studies involve the assembling of a circuit model that includes electronic components that represent cellular features including the gap junctions. An advantage of these studies is that they can consider the closure of gap junctions in isolation to other experimental effects that the cells maybe undergoing. A key disadvantage of these studies is that they are by their very nature lacking experimental validation. Gheorghiu et al, 2002, used their model to predict that the blocking of gap junctions would cause a rise in impedance in connected cells in suspension. A conclusion agreed with by Asami, 2007, when modelling cuboid, 3 dimensional, gap junction connected cell arrays.

Only one study has been published that utilised impedance spectroscopy to investigate the effect of gap junctions blockers on cell monolayers. Asfour et al, 2010, added the gap junction inhibitor heptanol to fibroblast cultures and observed an elevation in total impedance, in the 0.5Hz to 100Hz range and little variation at higher frequencies up to 10kHz. These variations were associated by the authors with a decrease in cell coupling. Gap junction inhibition was not confirmed using a separate staining or visualisation method. It should be noted that there are significant differences between fibroblasts and endothelial cells, the most pertinent being that fibroblasts have a minimal level of tight junction formation in comparison to endothelial cells and do not exist in barrier forming monolayers (Fanning, Mitic and Anderson, 1999).

1.27 Endothelial and smooth muscle cell culture

A large body of the previously cited research studies have derived their findings from in vitro experimentation on cell cultures of endothelial and smooth muscle cells. The key decision researchers must first make in their studies is whether to use primary cells - isolated from an animal or human source - or an established, immortalised cell line.

The main benefit of using a primary cell line is that the cells are considered to be closer in phenotype and behaviour to the in vivo scenario and therefore any findings will carry more clinical relevance. As the majority of research is directed towards human diseases the use of human cells is preferable in this regard, however ethical considerations and availability restrict their use. Consequently primary mammalian cell lines are often created, with murine, bovine and porcine amongst the most common. However researchers using primary cell lines will experience variations between their lines attributable to different donor origin and this also makes comparison between different studies more difficult (Bouiss *et al.*, 2001). Additionally primary cells are subject to a phenomenon known as phenotypic drift whereby successive passaging induces a de-differentiation of the cells, attributed the effects of aging and senescence. Experimentally this process has the effect of progressively moving them further away from a clinically relevant model with each passage. De-differentiation has been demonstrated in both endothelial and smooth muscle cell primary lines and although recommendations vary, a maximum passage number of 5 should be set (Lacorre *et al.*, 2004; Haas *et al.*, 2010). Immortalised cell lines have the advantage that they are readily available from commercial sources and do not de-differentiate. A range of primary endothelial cell lines have been isolated experimentally and many are also available from commercial sources. The most commonly used primary endothelial cell line are Human Umbilical Vein Endothelial Cells (HUVECs) (Bouiss *et al.*, 2001). Benefits of experimenting with HUVECs are they are derived from a human source and their ubiquity throughout the literature permits comparison between studies. They are often used in studies to provide a comparative cell line against other primary endothelial cell types (Patsch *et al.*, 2015). A key disadvantage of HUVECs in investigating atherosclerosis and restenosis is that they are from a venous source and owing to the known phenotypic heterogeneity of the vascular bed, are not wholly representative of coronary endothelial cells where the disease occurs.

During in vitro culture under light microscopy observation, confluent endothelial cells are described as having a cobblestone appearance (Bachetti and Morbidelli, 2000). Smooth muscle cells by comparison are larger and more elongated and are

visually likened to a hill and valley structure when confluent (Heydarkhan-Hagvall *et al.*, 2003).

1.28 Co-culture experimentation

The majority of published research on in vitro studies that relate to re-endothelialisation and in stent restenosis is carried out on cell monolayers of endothelial cell or smooth muscle cells cultured in isolation. In an in vivo environment these cells do not exist in isolation with smooth muscle and endothelial cells residing adjacent to one another in the arterial wall. As previously indicated the time course progression of in stent restenosis in its early phases has not been precisely established. It is not known if the endothelial monolayer is established first and then smooth muscle cell proliferation takes place underneath or if no endothelial layer is formed and smooth muscle cells proliferate first. Therefore an in vitro study aiming to characterise in stent restenosis growth must consider the scenario of an endothelium with a layer of smooth muscle cells underneath. The in vitro growth of endothelial cells and smooth muscle cells types together is referred to as a co-culture model and has been studied and optimised by various research groups (Kinard *et al.*, 1997; Heydarkhan-Hagvall *et al.*, 2003; Lavender *et al.*, 2005; Wallace, Strike and Truskey, 2007; Sakamoto, Kiuchi and Sato, 2011). The interaction between endothelial cells and smooth muscle cells involves an array of signalling molecules that control aspects of the arteries behaviour such as the maintenance of the vasomotor tone, cell proliferation, response to injury. Gene expression of angiogenic factors has been found to be altered in co-cultured endothelial cells and smooth muscle cells (Heydarkhan-Hagvall *et al.*, 2003). The formation of gap junctions between the cell types is also known to occur at the myoendothelial junction, a protrusion from the endothelial cell across the extracellular matrix, to the smooth muscle cell. Consequently co-culture is considered as a more accurate in vitro model of the in vivo arterial wall than single cell type culture and is a powerful tool for investigating both normal and diseased conditions (Truskey, 2011). Examples of endothelial cell - smooth muscle cells co-culture studies include the investigation into the effect of Tumour Necrosis Factor α on endothelial cells (Wallace and Truskey, 2010), shear stress on smooth muscle cell phenotype (Sakamoto, Kiuchi

and Sato, 2011) and endothelial barrier function following virus infection (Taylor *et al.*, 2013).

To achieve a successful in vitro co-culture model it has been found that a number of parameters must be adhered to. The principle challenges are to control the growth rates of two cell types as they differ in cell culture conditions. Furthermore in models where the endothelial cell layer is on top of the smooth muscle cells it must be ensured that the cells underneath receive sufficient access to nutrients contained within the media. In a review paper Truskey, 2011, identified 3 distinct paths that have been adopted by researchers aiming to use a co-culture system.

1. The growth of the two cells separated by a porous membrane.

    By growing the two cell types on opposite sides of a porous membrane researchers can obtain a close model of the in vivo scenario and also exercise a level of control over the variable cell growth rates (Chiu, 2003; Evensen *et al.*, 2009). Whilst cultured separately, and therefore not in direct contact, the endothelial cells and smooth muscle cells are in close enough proximity to one another to be able to exchange the aforementioned signalling molecules through the pores. However the formation of myoendthelial gap junctions is limited. An advantage of this system is that following completion of the co-culture experiment is it easy to remove the cell types separately for later analysis or culture elsewhere.

2. Culture of endothelial cells on a smooth muscle cell-gel layer.

    A method used to create a model of the intima uses the growth of smooth muscle cells within a collagen gel (Imberti *et al.*, 2002). The gel is included to mimic the extra cellular matrix which constitutes a large component of the intima. This technique is used by researchers aiming to create tissue engineered vessels.

3. Direct culture of endothelial cells on top of a layer of smooth muscle cells.

    By seeding endothelial cells directly over smooth muscle cells the aim is to recreate a dual culture layer that closely resembles the in vivo scenario.

Before the addition of endothelial cells the layer of smooth muscle cells must be induced into quiescence to prevent them from becoming over confluent and detaching as the endothelial cells grow on top of them. This action is achieved through serum starvation for a period of 12 to 72 hours. In common with co-culture methods using other cell types a mixture of endothelial cell and smooth muscle cell media is used for the co-culture scenario (Truskey, 2011).

For the purposes of experimenting on stent cell regrowth models using impedance spectroscopy several of the co-culture options can be dismissed. This process results in the selection of the direct culture of endothelial cells onto smooth muscle cells. The growth of cells on membranes would contribute an additional impedance profile that could potentially mask the contributions from the two cell types. The same can also be said for any substance that mimics the extra cellular matrix around the smooth muscle cells. Therefore direct co-culture is the best model for impedance spectroscopy investigating the early phases of in stent restenosis.

There is variation in the literature regarding the optimum parameters and procedures to attain an in vitro direct co-culture model although general best practices can be elucidated. Initially smooth muscle cells are grown to near confluence using standard proliferative media containing 10 to 20% serum. The media is then changed to a low percentage or serum free media to arrest proliferation and push the cells into a quiescent state. Cells are quiesced in this manner for time periods of 12 to 72 hours. Endothelial cells can then be seeded onto the top of the quiesced smooth muscle cell layer. Endothelial cells are seeded at a higher density than smooth muscle cells owing to their smaller size, with more required in order to cover the same area. Culture of both cell types is done using a mixture of mainly quiescent media and endothelial cell proliferative media, with a ratio of 6:1 typically used. The reason for including endothelial cell media is due to their requirement for serum, even in small amounts to maintain their normal cobblestone morphology (Heydarkhan-Hagvall *et al.*, 2003). It should be noted that to date there are no published studies using impedance spectroscopy as a method for analysing the co-culture of smooth muscle and endothelial cells.

1.29 Conducting polymers

The advent of drug-eluting stents coated with a non-conducting polymer, replacing wholly conductive, bare metal stents would have appeared to have obviated the development of a self-reporting stent relying upon impedance spectroscopy as its method of detection. However conducting polymers are a class of polymers that potentially could be used as a coating for stents and for the elution of anti-proliferative drugs. Any study that has as its long term objective the development of a self-reporting stent should consider conducting polymers as part of its clinical translation strategy.

1.29.1 History

The synthesis of conducting polymers was first achieved in the mid-1970s (Shirakawa *et al.*, 1977), a momentous discovery for which the researchers received the Noble prize for chemistry in 2000. A wide range of electro-active polymers have since been developed and conducting polymers are but one class of this growing field. Conducting polymers are of particular interest for use for medical devices due to their biocompatibility, ease of fabrication and charge carrying properties.

1.29.2 Chemical structure and conductivity

The conductivity of a conducting polymer arises from their chemical structure of an alternating single bond, double bond pattern between the carbon atoms along the organic chain, known as the conjugated backbone. Sigma bonds form the continuous chain whilst the alternating extra double bond is a π bond. The π bond attracts electrons from above and below the plane of the polymer chain which forms a delocalised orbital. A schematic of this arrangement is depicted in Figure 1.3. Charge can then be conducted through the polymer via the motion of dissociated electrons with an additional route provided through electron hopping between nearby polymer chains (Inzelt, 2008). However some polymers require the addition of dopant ions to provide the charge necessary to balance the conjugated backbone, the polyheterocycles such as polypyrrole and poly 3,4-Ethylenedioxythiophene (PEDOT) are such materials. The chemical structure of polpyrrole is shown in Figure 1.4. The dopant ions need to be deliberately incorporated during the synthesis of the conducting polymer. In the case of ions, such as chloride in polypyrrole the ion is

sufficiently small to be expulsed and included during oxidation and reduction. Where the dopant is too large to move a cation can be incorporated from the aqueous media (Wallace and Spinks, 2007).

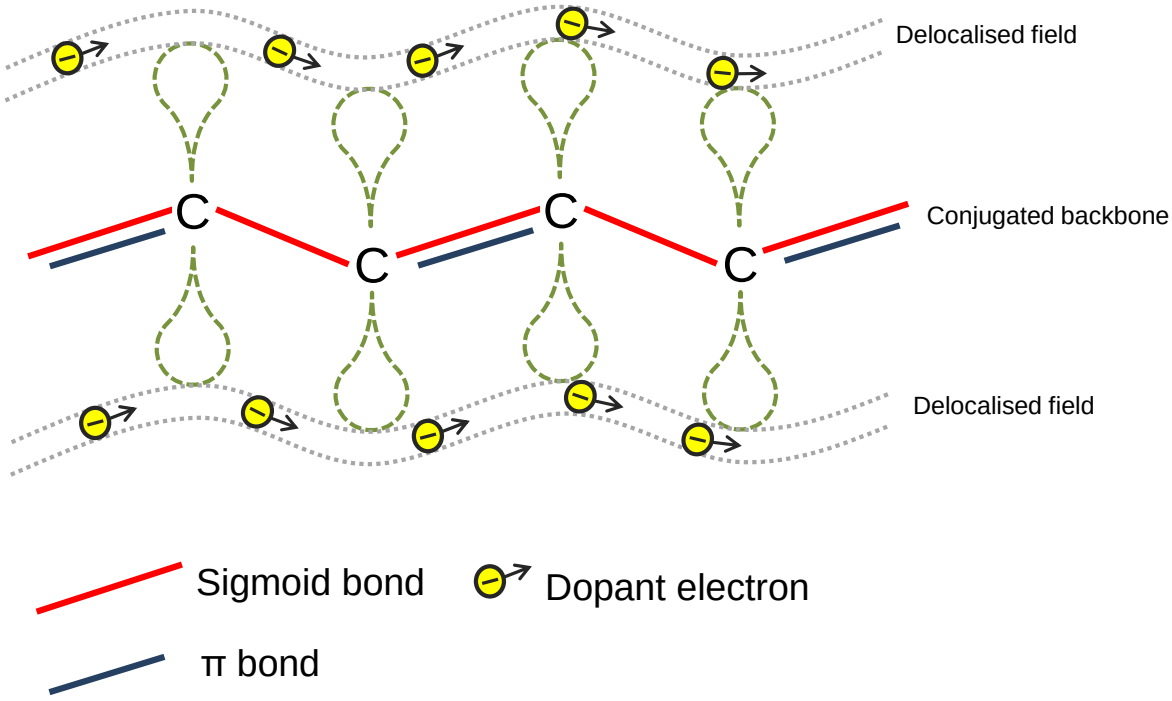

Figure 1.3- Conjugated structure of conducting polymers.

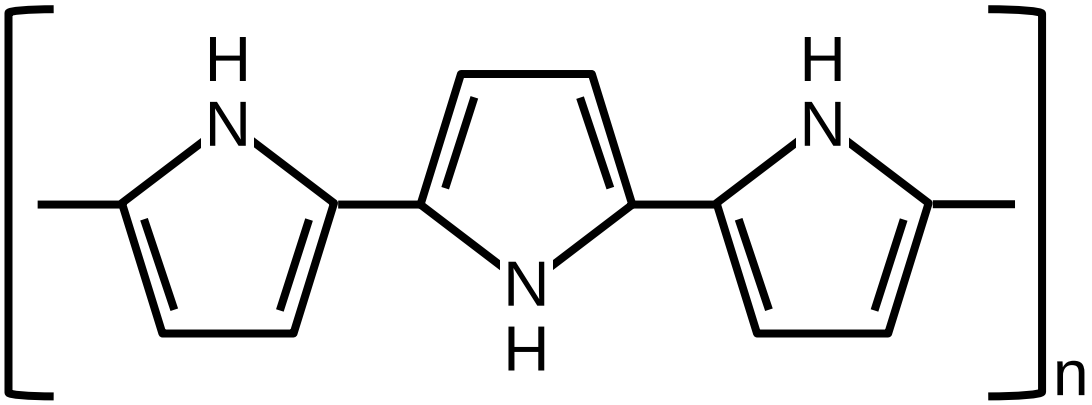

Figure 1.4 – Chemical structure of Polypyrrole.

1.29.3 Methods of synthesis

Two methods of conducting polymer synthesis are possible, chemical and electropolymerisation. The latter process involves immersing a conductor as an anode in a solution of the polymer monomer. The inclusion of a highly conductive cathode, a reference electrode and subsequent current flow initiates polymerisation of the monomer onto the surface of the anode. The conducting polymer begins as a thin film coating and progressively becomes thicker. As an example polypyrrole polymerises onto the surface of the anode in 2 phases. Initiation, where the monomer becomes a dimer and propagation, where oligomers act as a conducting phase to further polymerise monomers (Álvarez-Romero *et al.*, 2006). Included in the solution is the dopant which is included into the newly formed polymer layer as part of the process. The topography and electrical properties of the polymer surface is highly dependent on a variety of synthesis parameters. These include the substrate material, substrate topography, current density, dopant compositions, solution concentrations and the monomer structure. It has been demonstrated that controlling these variables can allow researchers to create specific surface morphologies and conductivities for their needs (Fakhry, Cachet and Debiemme-Chouvy, 2013). Especially relevant for medical devices are the control of topographies for polypyrrole (Ashrafi, Golozar and Mallakpour, 2006) and PEDOT (Patra, Barai and Munichandraiah, 2008). Surfaces created for use in medical devices applications range from the smooth, electropolished to those that with intentionally created micro and nano scale topographical features. The use of such features has been investigated as a method of promoting cell growth and increasing the surface area for enhancing the incorporation of drug coatings. As an example the Yukon, Choice stent has a roughened microporous surface finish that the manufacturers, Translumina, claim enhances re-endothelialisation (http://www.translumina.de/products7.pml). Surface area increase is of importance when using conducting polymers as an electrode material in electrochemical measurement as the impedance is lowered considerably, increasing its sensitivity (Xiao *et al.*, 2004).

The advantage of the electropolymerisation technique is that any conducting surface can potentially be coated with a conducting polymer. In comparison to chemical synthesis, electropolymerisation creates conducting polymers of greater conductivity

(Balint, Cassidy and Cartmell, 2014). The interdependency of the variables in the electropolymerisation process can lead to significant variation in the properties of the resulting conducting polymer film besides its thickness (Zhou and Heinze, 1999). Disadvantages of the electropolymerisation specific to polypyrrole are a low surface roughness and poor mechanical strength when compared to chemical methods (Forciniti *et al.*, 2010). Chemical methods of manufacture are usually used to produce large volumes that are not often required for medical devices (Inzelt, 2008), however chemical polymerisation has been used to create thin films for cell culture experiments (Castano *et al.*, 2004). Whilst all conducting polymers can be synthesised using chemical methods, electropolymerisation is restricted to those whose monomers can be oxidised through the application of potential (Guimard, Gomez and Schmidt, 2007). Electropolymerisation can also allow the incorporation of additional materials such as drugs or biocompatible compounds that become encapsulated during synthesis.

1.29.4 Conducting polymers and drug elution

Conducting polymers with encapsulated drugs have been proposed as a coating for implanted medical devices that fulfil a dual functionality of biocompatibility and drug elution. Of particular relevance to the research contained in this thesis is their suitability as a coating for coronary stents (Weiss *et al.*, 2003; Arbizzani *et al.*, 2007; Okner *et al.*, 2009). The addition of the drug can also serve a dual purpose acting as a dopant ion conferring conductivity on the conducting polymer whilst also being able to elute from the surface, influencing the surrounding biological environment.

1.29.5 Cell culture on conducting polymers

Examples of using conducting polymers to exert a degree of control over the aforementioned desirable factors for cell culture can be found in efforts to match the dopant with the cell type being cultured. A notable example is the inclusion of heparin to promote endothelial cell growth (Garner *et al.*, 1999). The electroactive nature of conducting polymers can be exploited to activate, release or inhibit the availability of incorporated dopants to influence the behaviour of cells in the materials immediate environment.

A wide variety of cell types have been shown to grow and maintain their viability on conducting polymer surfaces (Fonner *et al.*, 2008). Many of these studies have emphasised the need to maintain control of the electrochemical and mechanical surface properties of the polymer during the fabrication stage. Furthermore an understanding of the changes that the conducting polymer can undergo throughout the duration of the experiment is also crucial (Lundin *et al.*, 2011). Amongst those cells successfully cultured in vitro on conducting polymers are mesenchymal stem cells. Scaffolds containing conducting polymers capable of inducing osteogenic differentiation are being explored as a method to create implantable devices for clinical bone tissue engineering (Pelto *et al.*, 2013).

1.29.6 Impedance spectroscopy and conducting polymers

Impedance spectroscopy has been utilised to probe the properties of conducting polymer films. Conducting polymers are a category of materials whereby ionic conduction dominates (Macdonald, 1992). Rubinson and Kayinamura, 2009, summarised the contributing factors towards conducting polymer film impedance as the resistance to ionic charge transport, the resistance to electronic charge transport and the capacitance associated with charge separation. However the authors state that there is no clear understanding of charge transport in conducting polymers.

Studies have exploited the conductive nature of conducting polymers to perform impedance spectroscopy of cells. Two separate investigations have cultured the Madin-Darby Canine Kidney Epithelial Cell line on PEDOT electrodes. Löffler et al, 2015, were able to monitor the loss of barrier function caused by the addition of ionomycin whilst Karimullah et al, 2013, showed the benefits of PEDOT as an electrode substrate over gold. Indeed a key consideration for researchers when selecting a conducting polymer for cell culture experimentation is the whether the optical properties of the material in its final form on the electrode permit observation using light microscopy.

1.30 Experimental rationale

A review of the literature has identified a clinical need to non-invasively characterise re-endothelialisation and in stent restenosis cellular regrowth over implanted coronary stent struts. With regards to re-endothelialisation, current imaging techniques are unable to discern the reformation of the endothelial layer, the level of the endothelial cell coverage or it's functionality. A self-reporting stent using impedance spectroscopy has been identified as a potential technology for addressing this need (Shedden *et al.*, 2010). Non-invasively acquired, real time data would add a temporal aspect to the knowledge of re-endothelialisation and enable clinicians to make a more informed judgement on the continuation of anti-platelet drug therapy. This is an important issue when considering the treatment of patients with additional conditions that can be exacerbated by bleeding. In the same manner non-invasive real time data showing the onset and progression on in stent restenosis would enable clinicians to monitor the progression of the disease up to the point where blood flow is severely occluded. Such temporal data would also enable stent manufacturers and researchers to investigate how the design of a stent could be improved to encourage the re-endothelialisation process and further reduce the rate of in stent restenosis. This is of particular importance in drug-eluting stents where the release of anti-proliferative drugs is aimed at reducing the occurrence of in stent restenosis but conversely inhibits re-endothelialisation. It is possible that data collected from large populations could identify new risk factors and ultimately enable the development of stents with drugs that are tailored specifically to the individual patient. In addition, the development of an in vitro system and model for post stent healing has the potential to be a powerful tool for researchers investigating re-endothelialisation / in stent restenosis and methods of preventing or reducing its occurrence. The use of drugs or surface material variations are two examples. An aspect revealed in a review of the literature is that information on the time progression of re-endothelialisation derived from animal models differs from those observed in humans. Furthermore experimentation involving animal models are costly and time consuming, an in vitro model of post stent arterial healing could negate the need for some animal studies or help reduce the number of parameters that require testing.

Such a device would only be feasible if impedance spectroscopy is capable of identifying re-endothelialisation and restenosis, two post stenting scenarios that are characterised by the regrowth of different cell types over the stent struts. As highlighted in 1.20 (Cell characterisation with impedance spectroscopy) Shedden has previously investigated characterising these cell types, with results indicating that a wide frequency range is preferable. However the system used by Shedden was limited in its capability to capture data at regular intervals in a physiologically relevant environment. This study will attempt to capture in-incubator impedance data at a higher temporal resolution, comparable to those used in commercially available systems but with greater control over the frequency range and cell population being measured. The development of an in vitro system that can capture wide frequency range impedance data at regular intervals for the purposes of vascular cell characterisation in clinically relevant populations is the rationale that underpins the experimental design in this thesis.

In order to mimic the in vivo post-stenting cell regrowth scenarios an in vitro experimental model is proposed. The progress of re-endothelialisation can be represented by the growth of endothelial cells alone over the electrode, with variations in coverage concurrently monitored using light microscopy techniques. An alternative cell type that is known to proliferate over stent struts are smooth muscle cells. Any device that seeks to non-invasively monitor re-endothelialistion should also be able to characterise smooth muscle cell proliferation. This can be modelled in a similar fashion in-vitro by measuring the proliferation of smooth muscle cells over the electrodes. It should be noted that attaining a thicker layer of smooth muscle cells that would represent a clinically relevant in stent restenosis model is not attainable in in-vitro culture as the cells in the lower layers are unable to gain access to sufficient nutrients from the media. A further refinement of the re-endothelialisation model would be the growth of smooth muscle cells with an accompanying layer of endothelial cells, referred to as a co-culture model. These scenarios are schematically depicted in Figure 1.5.

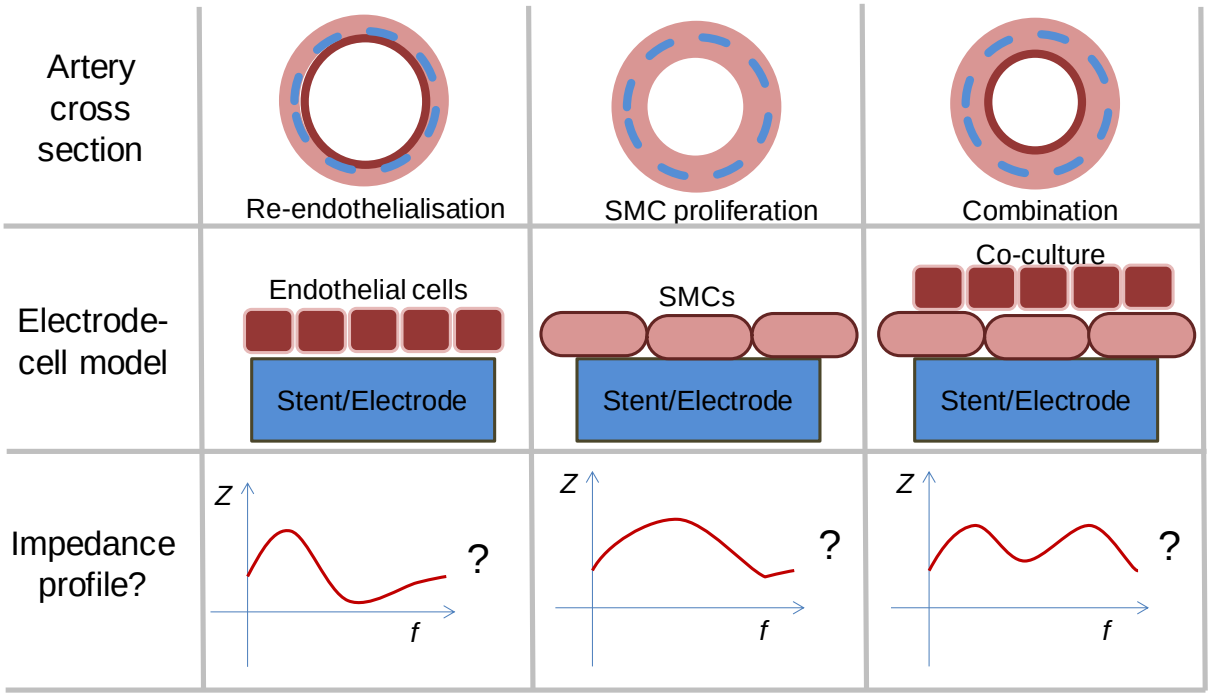

Figure 1.5 - Stent cellular regrowth scenarios and in vitro model schematic.

Part of translating the technology into a clinical application is to prove the concept is viable when using substrates that are suitable for use in vivo. Conducting polymers have been identified as a potential material whose conductivity allows impedance measurement to be taken on adhered cells yet could also encapsulate a therapeutic drug. Therefore included in the objectives is the measurement of cells using impedance spectroscopy with a conducting polymer substrate.

In reviewing the literature, an additional area of interest in cardiovascular disease was identified, impedance spectroscopy of gap junctions. This remains an unexplored area with only one paper publishing experimental data using fibroblast cells and two other purely theoretical papers. A study of gap junction inhibited cells is beneficial to the development of a self-reporting stent as a paucity of gap junctions has been linked to a dysfunctional endothelium which can lead to both restenosis and thrombosis. Should re-endothelialisation occur over the stent struts then an indication of the functionality of the endothelium would be useful to clinicians in assessing the arterial recovery. The analysis of inhibited gap junctions using agonists is restricted to end point invasive techniques and impedance spectroscopy would be able to provide some temporal resolution to this intervention. An investigation into the

impedance spectroscopy profiles of endothelial cells with and without blocked gap junctions would help provide information not only on the functionality of the junctions themselves but also give an indication as to the diagnostic sensitivity of a self-reporting stent.

1.31 Study objectives

The objectives of the study can be summarised as follows.

- Design and develop of an automated in vitro test system that can non-invasively carry out impedance sweeps of cell monolayers.
- Investigate the feasibility of using impedance spectroscopy to non-invasively characterise the following vascular cell types in clinically relevant populations.
    - Porcine smooth muscle cells
    - Porcine endothelial cells
    - Human Umbilical Vein Cells (HUVECs)
- Investigate the feasibility of using impedance spectroscopy to non-invasively characterise a direct co-culture of porcine endothelial and smooth muscle cells in clinically relevant populations.
- Investigate if a dysfunctional endothelial monolayer with inhibited gap junctions can be identified using impedance spectroscopy on a clinically relevant population.
- Investigate the feasibility of using conducting polymers as a substrate for a future self-reporting stent.

2. Theory

2.1. Theory of impedance spectroscopy

In the scenario whereby a direct current (I) is applied to a simple resistor with the potential (V) electrical resistance (R) obeys Ohms law in the following form.

$$R = \frac{V}{I}$$

Equation 2.1

The application of a sinusoidal voltage of frequency f to a simple resistor modifies the voltage and current elements of the above equation. In the case of alternating currents (AC) the term resistance is no longer used and the new term impedance denoted by Z is used. In this case the instantaneous voltage and current can be defined as below.

$$v_0 = V\,sin(\omega t)$$

Equation 2.2

$$i_0 = I\,sin(\omega t)$$

Equation 2.3

In the case of a simple resistor the impedance remains equivalent to the resistance however should an alternating voltage, be applied to a system that contains capacitive elements then Ohms law becomes an over simplification of the circuits response. The sinusoidal voltage induces an alternating current that is described as out of phase, or has a lag in relation to the applied potential. The resulting alternating current will (as with purely resistive elements) have a frequency-time component (ωt) but also a phase component (φ) or lag of the system as the capacative elements charge and discharge with a delay behind the applied potential.

Representing V_0 and I_0 graphically displays the phase element.

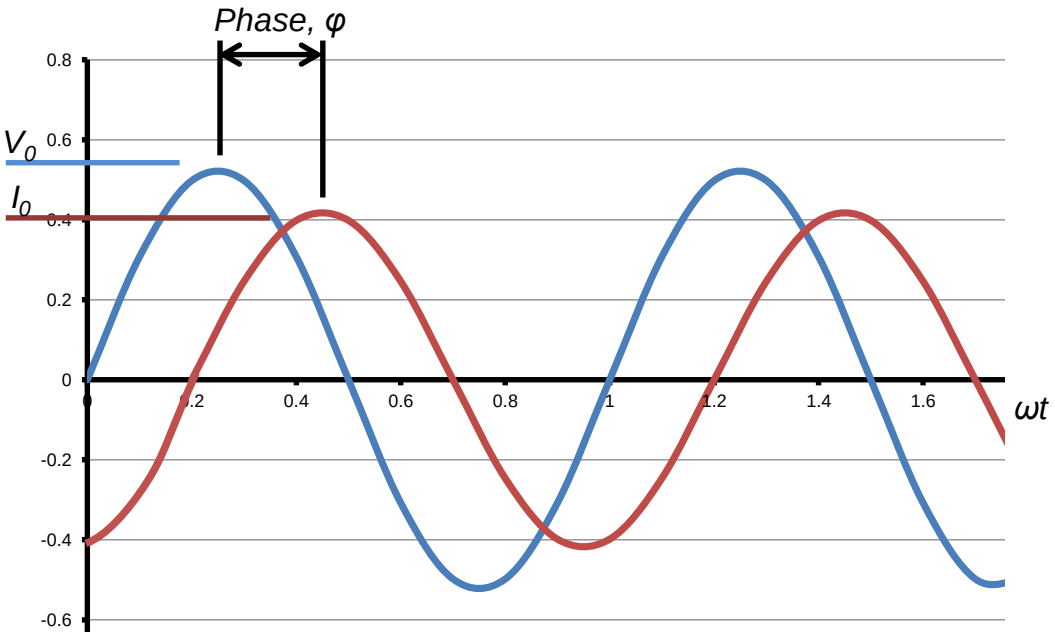

Figure 2.1 - Graphical representation of phase component of impedance, with sinusoidal applied potential (blue) and current (red).

Impedance can therefore be broken down into real and complex notation.

$$Z(\omega) = Z_{Re} + jZ_{Im}$$

Equation 2.4

Where

$$j = \sqrt{-1}$$

Equation 2.5

The phase angle φ, can be determined by ….

$$\varphi = tan^{-1}\left(\frac{Z_{Im}}{Z_{Re}}\right)$$

Equation 2.6

Applying an alternating current across a range of frequencies – known as a frequency sweep – values for the real and imaginary components of impedance can be determined. These are often denoted as Z' (real) and Z'' (imaginary) with absolute impedance represented as $|Z|$. The parameters Z real and Z imaginary are often referred to as the resistive and reactance components respectively. The real or resistance component can be considered the contribution to the impedance arising from current that is in phase with the voltage. The imaginary or reactance component is the impedance contribution arising from the current that is 90° out of phase with the applied voltage (Wegener, 2008). Complex plane plots of Z' (real) against Z'' (imaginary) and are known as Wessel or Nyquist plots. These are often used to represent the data gathered during impedance analysis, but are limited as they display no information on the frequency. For this reason bode plots of frequency against absolute impedance $|Z|$ or phase angle φ are employed to highlight frequency dependent phenomena. The Wessel plot is determined by the arrangement and magnitude of the electrical components that make up a circuit. Figure 2.2 displays the Wessel plots for some simple circuit arrangements, along with equations for real, imaginary and total impedance.

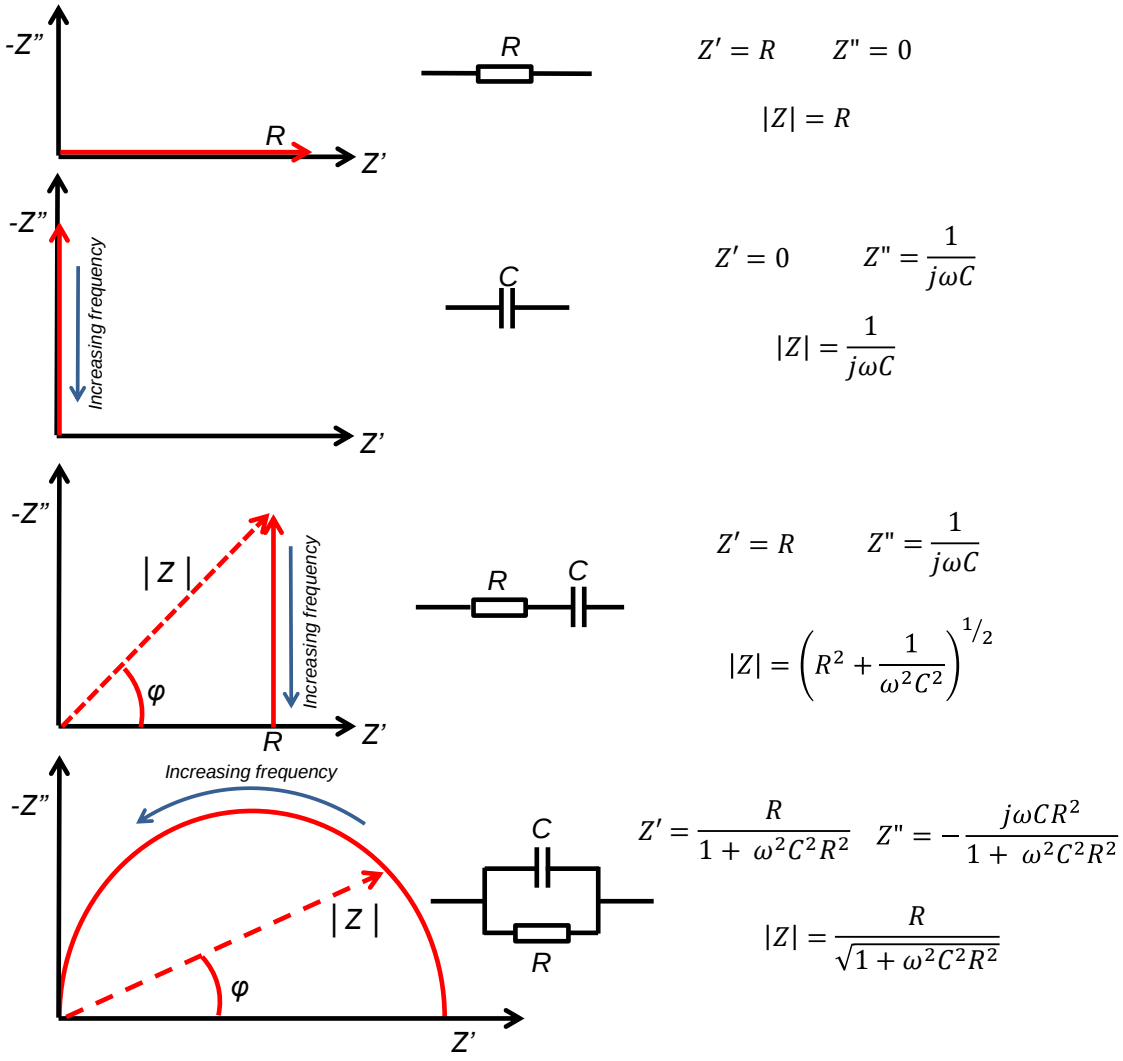

Figure 2.2 - Wessel plots of simple circuits with accompanying equations for real, imaginary and total impedance.

The circuit containing the resistor and capacitor in parallel (RC circuit) is of importance in the modelling of biological specimens, featuring extensively in the literature and is often simply referred to as an RC circuit. The derivation of the real and imaginary components of impedance and the impedance modulus for an RC circuit is detailed below.

Resistor and capacitor are in parallel therefore,

$$\frac{1}{Z} = \frac{1}{R} + \frac{1}{C}$$

Equation 2.7

$$C = \frac{1}{j\omega c}$$

Equation 2.8

$$\frac{1}{Z} = \frac{1}{R} + j\omega c$$

Equation 2.9

$$R = Z + j\omega cRZ$$

Equation 2.10

$$Z = \frac{R}{1 + j\omega Rc}$$

Equation 2.11

Split into real and imaginary parts, this becomes,

$$Z = \frac{R(1 - j\omega Rc)}{(1 + j\omega Rc)(1 - j\omega Rc)}$$

Equation 2.12

$$Z = \frac{R - j\omega R^2 c}{1 + \omega^2 R^2 c^2}$$

Equation 2.13

$$Z = \frac{R}{1 + \omega^2 R^2 c^2} + \frac{j\omega R^2 c}{1 + \omega^2 R^2 c^2}$$

Equation 2.14

$$Z = Z' + Z"$$

Equation 2.15

Where,

$$Z' = \frac{R}{1 + \omega^2 R^2 c^2}$$

Equation 2.16

And,

$$Z" = \frac{j\omega R^2 c}{1 + \omega^2 R^2 c^2}$$

Equation 2.17

When applying a frequency sweep to biological specimens the Wessel plots obtained are rarely as simple as the cases presented in Figure 2.2. A common plot is known as the Cole-Cole plot whereby the semi-circular profile seen in the RC circuit Wessel diagram becomes depressed with a centre that resides below the real axis. Resistors and capacitor circuit arrangements cannot produce such plots and consequently additional elements need to be considered.

2.2. Warburg impedance

One such additional element is the Warburg impedance. Electrochemical reactions can be limited by the rate of diffusion through a liquid. At the interface between a solution and an electrode, with an applied potential, ions are removed or added to the liquid in the immediate vicinity. A concentration gradient is therefore formed between the area immediately next to the electrode and the surrounding bulk solution. Diffusion will attempt to overcome the gradient with removal and addition of ions. The rate of diffusion of ions is limited by the properties of the bulk solution and this in turn can limit the reaction occurring at the electrode. In a scenario where an alternating voltage is applied, ions are unable to move in and out of the area surrounding the electrode at the required rate to maintain the flow of charge. This occurrence is accentuated further as the frequency of the alternating current increases. It has been shown that the voltage and the concentration are 45° out of

phase with one another for any given frequency. If this scenario occurs then the semi-circular Z', Z'' plot is no longer possible and forms a liner relationship known as the Warburg impedance, depicted in Figure 2.3.

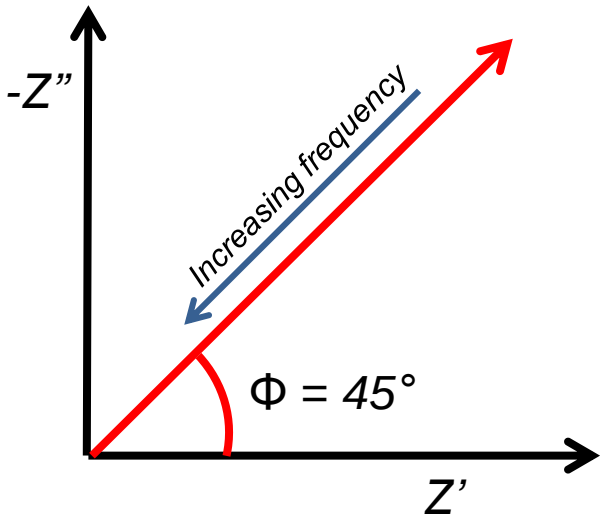

Figure 2.3 - Wessel plot of the Warburg impedance.

The Warburg impedance can be defined as..

$$Z_w = \frac{\sigma}{\sqrt{\omega}} - j\frac{\sigma}{\sqrt{\omega}}$$

Equation 2.18

Where,

$$\sigma = \frac{RT}{F^2 C_d \sqrt{2D}}$$

Equation 2.19

R is the universal gas constant, *T* is the temperature, *F* is the Faradays constant, C_d is the double layer capacitance and D is the diffusion coefficient.

Warburg impedance is often present when analysing biological cells, but is rarely identifiable as a straight line by itself as shown in Figure 2.3.

2.3. Electrical double layer

A conductor immersed in an electrolyte will become surrounded by the solution molecules, cations and anions as they adsorb onto the surface. How these species arrange themselves is known as the electrical double layer. Those that form the layer closest to the conductor surface are said to be within the inner Helmholtz layer, named after Hermann von Helmholtz who first proposed the model. This layer contains both solution molecules and specifically adsorbed anions, the centres of which denote the Inner Helmholtz Plane (IHP) at a distance x_1 from the conductor surface. Due to the formation of the adsorbed molecules creating the IHP, cations surrounded by solution molecules can only approach the surface of the conductor to a distance x_2. In the same fashion the centres of the solvated cations forms the Outer Helmholtz Plane (OHP). All distances in the solution greater than the OHP form the diffuse layer. The total charge densities, (σ) in each layer (OHP σ^d and IHP σ^i) can be summated to arrive at the charge density of the solution side σ^S. This must be balanced by the charge density of the conductor, $-\sigma^C$, as portrayed in the equation below (Bard and Faulkner, 2001).

$$\sigma^S = \sigma^d + \sigma^i = -\sigma^C$$

Equation 2.20

As a result of the adsorbed layer a conductor-electrolyte interface will act as a capacitor known as the electrical double layer and is also referred to as the interfacial capacitance. This behaviour is attributable to the two layers being oppositely charged with a dielectric area between them. Because the gap between the layers is small there is the potential for large capacitances to occur (Geddes, 1972). The electrical double layer is depicted schematically in Figure 2.4.

The ionic concentration dictates how large the diffuse layer becomes with studies exploiting this behaviour to control the distances labelled X_2 and X_1 (Venkatanarayanan, Keyes and Forster, 2013). In addition surface roughness can typically be positively correlated with electrical double layer capacitance (Malleo *et al.*, 2010).

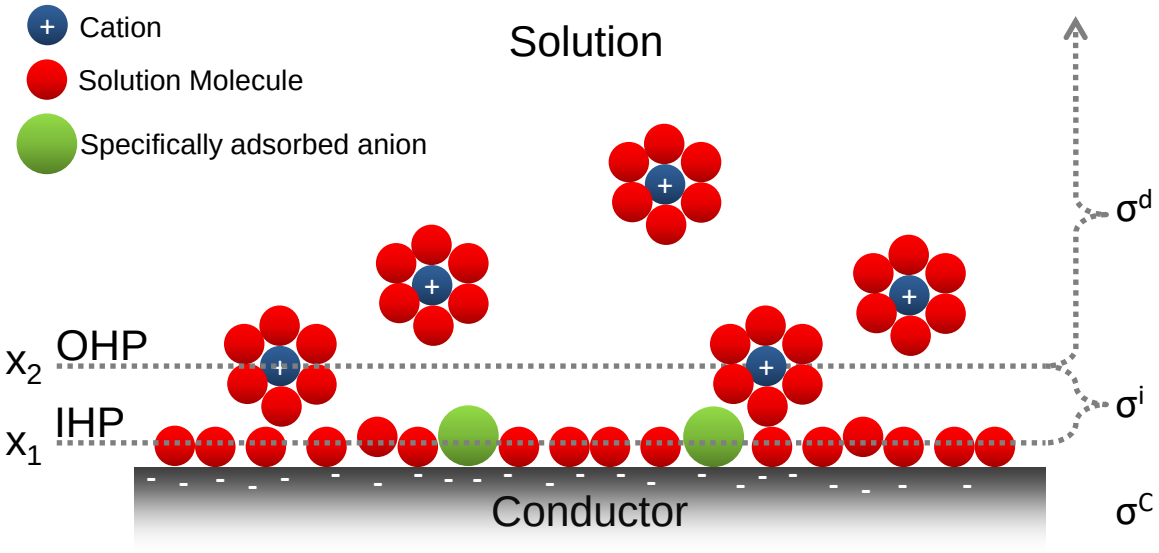

Figure 2.4- The electrical double layer (Bard and Faulkner, 2001).

The electrical double layer is often represented by an equivalent circuit as depicted in Figure 2.5.

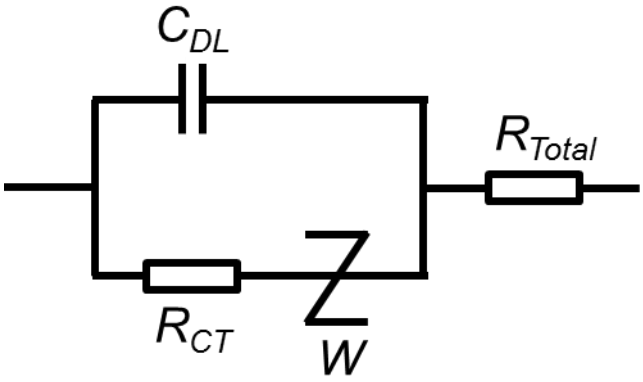

Figure 2.5 - Electrical double layer equivalent circuit (Mcadams *et al.*, 1995).

Where Z_w is the diffusion related Warburg impedance previously defined as…

$$Z_w = \frac{\sigma}{\sqrt{\omega}} - j\frac{\sigma}{\sqrt{\omega}} \quad or \quad Z_w = (1-j)\sigma\omega^{-0.5}$$

Equation 2.21

Comparison of the capacitive contribution arising from the electrical double layer can be made between materials as shown in Table 2.1.

Material	**Capacitance (Farads/m^2)**
Platinum	0.3
Platinum black	81.54
Iridium Oxide	28.72
Polypyrrole/PSS	312.18

Table 2.1- Capacitance values of materials used for thin film electrodes used in dielectric spectroscopy, derived from experimental data fitting into equivalent circuits (Malleo *et al.*, 2010).

2.4. Equivalent circuit modelling

With experimental data available and background knowledge of the system being tested it is possible to begin assembling a representative circuit. This process involves selecting electrical components that are deemed to have similar properties to the specimen being tested. The previously discussed interfacial capacitance of a thin film electrode is one such element that researchers often chose to include in their model.

Having determined a perceived circuit estimates can then be made for the values of the various components and iterative adjustments made until they match the experimental data. Should a sufficient fit be found then the experimental data can be quantified in terms of the modelled circuit elements. This is usually accomplished using dedicated software that provides a percentage error of the fitted values to the experimental data, enabling an assessment of the accuracy of the model. The process of using impedance spectroscopy measurements in conjunction with circuit modelling has been outlined by MacDonald, 1992, and is depicted in the flow diagram in Figure 2.6.

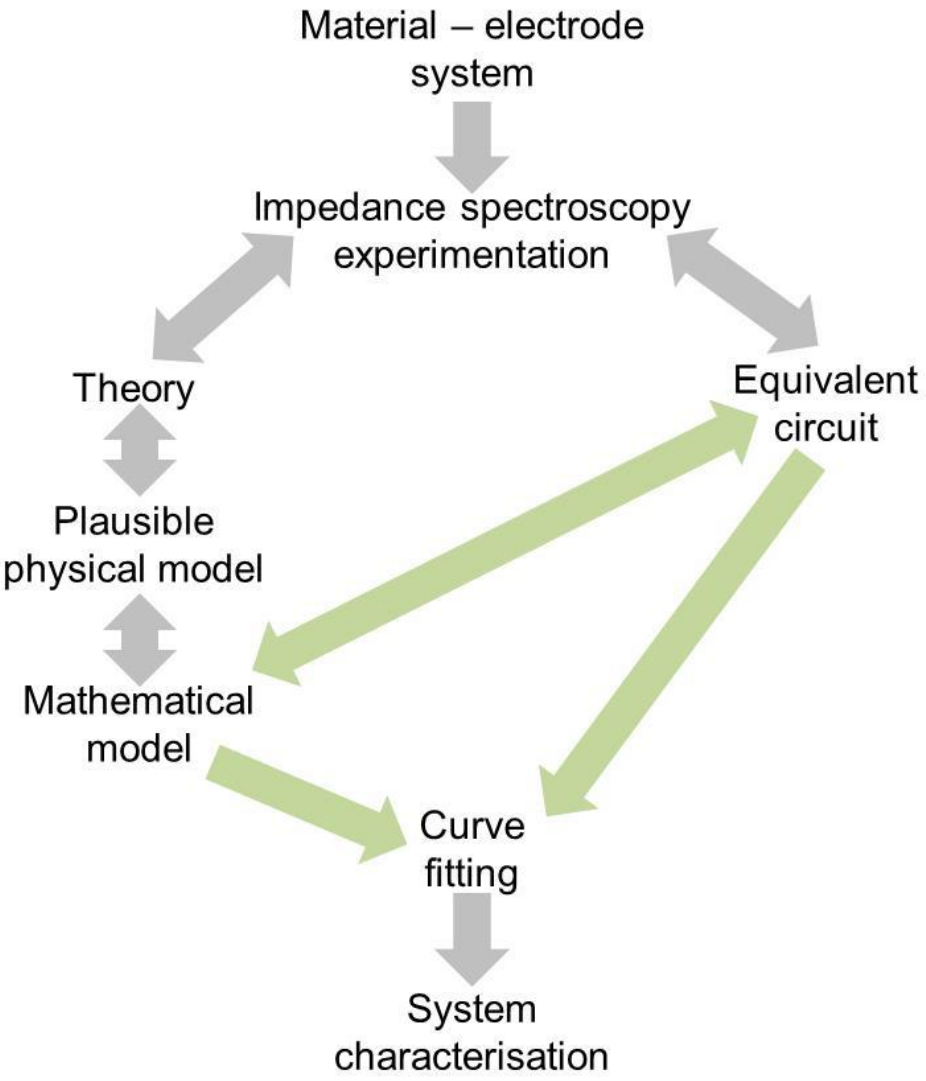

Figure 2.6 – Equivalent circuit modelling process. Arrows in green represent the stages of the process that are typically carried out in an iterative fashion using specialist software.

In the case of a cell the simplest equivalent circuit is a resistor and capacitor in parallel where the capacitor represents the cell membrane with its lipid bilayer and the cytoplasm is represented by the resistor. As an addition to the circuit Warburg impedance (W) can be added and also included in the circuit model below is the bulk solution resistance (R_{SOL}) of the surrounding media. This circuit shown in Figure 2.7 was first proposed by John Randles in 1947 and is often referred to in the literature as the Randles circuit.

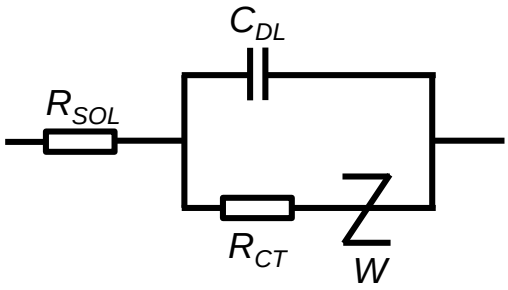

Figure 2.7 - The Randles circuit.

At high frequencies the capacitor will have the effect of short circuiting the charge transfer resistor causing the impedance to become analogous to the bulk solution resistance, shifting the semi-circular plot along the real axis. As previously alluded to the Warburg impedance element typically has its effect at low frequencies and this appends onto the semi-circular plot to create the complex plane profile depicted in Figure 2.8.

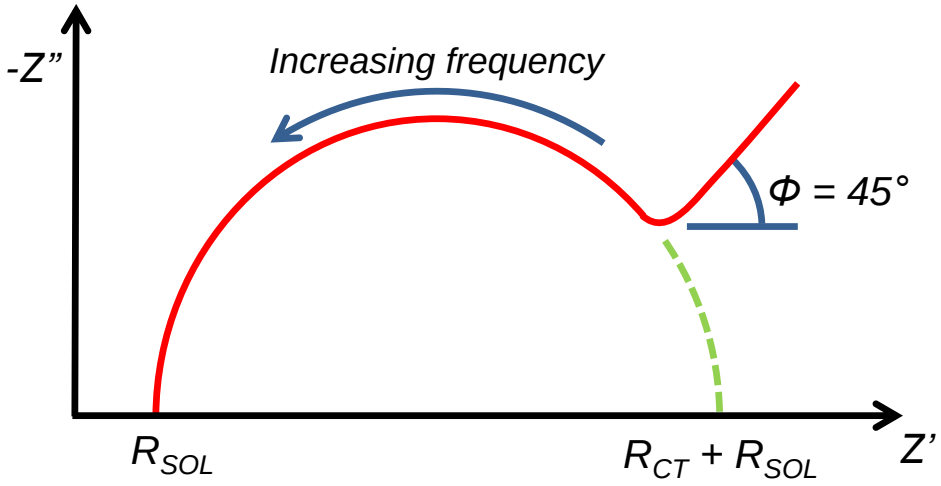

Figure 2.8 - Wessel plot of a Randles circuit showing the typical semi-circular plot of a RC circuit and an appended Warburg impedance at 45° constant phase angle.

Depending upon the analysis being undertaken additional components can be included to isolate the electrical properties of specific cell elements. The addition of extra circuit elements further modifies the derivation of Z’ and Z” becoming increasingly complex with software often used to perform the analysis. An example of a more complex equivalent circuit for a suspended cell is depicted in Figure 2.9.

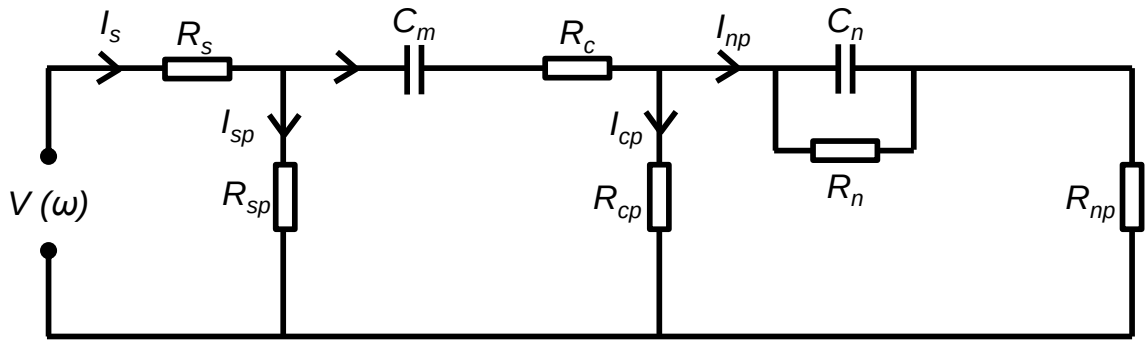

Figure 2.9 - Example of a complex equivalent circuit model to represent a suspended MBA-15 cell using resistive (R) and capacitive elements (C). The sub notations are defined as s external medium, sp the external medium adjacent to the membrane, m the phospholipid membrane, c the cytoplasm space, cp the cytoplasm adjacent to the nuclear envelope, n the nuclear envelope, and np the nucleoplasm space. (Ron *et al.*, 2010).

The addition of extra elements to the model allows for analysis of specific cellular properties, with the example in Figure 2.9 featuring dedicated components for the cell nucleus where R_{np} is the resistance of the nucleoplasm.

A simpler example of an equivalent circuit model for cells adhered to an electrode is shown in Figure 2.10 whereby separate sections represent the electrode and cell monolayer using an element known as the constant phase element (CPE) in parallel with resistance.

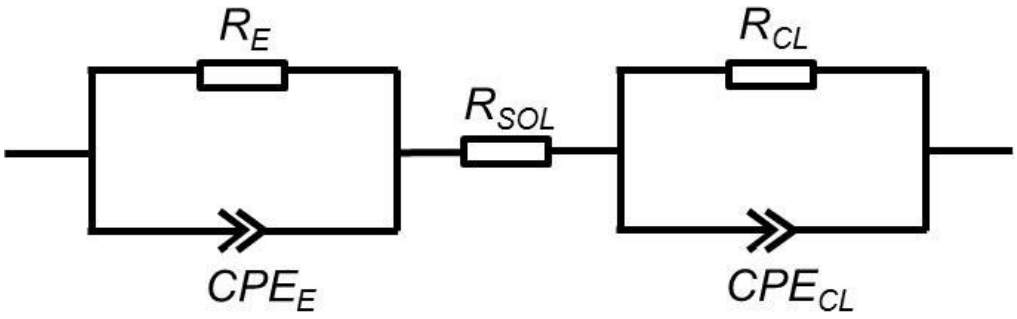

Figure 2.10 - Equivalent circuit model for cells adhered to a planar electrode where E denotes the combined parameter for both electrodes, SOL is the bulk solution and CL is the cell layer.

In the equivalent circuit shown in Figure 2.10 the CPE is included in both the electrode and cell model portions of the model. The CPE is, like the Warburg impedance, an example of an empirical circuit element that has no electrical analogue. It is included by researchers to model the non-ideal capacitance behaviour observed in their data and is sometimes referred to as pseudo capacitance. CPE behaviour has been attributed to time constant distributions in surfaces that arise from their dielectric properties, seen in biological samples such as skin (Jorcin et al. 2006, Orazem et al, 2013)

For the electrode component of the circuit shown in Figure 2.10 the CPE is included to model non-ideal capacitance behaviour that is thought to arise from the electrode surface roughness and non-uniform conductivity, (McAdams and Jossinet, 1996; Jorcin *et al.*, 2006), with the latter being an attribute more likely in larger electrodes. For the cell component this arrangement has been used in multiple published studies to model cells adhered to electrodes (Bouafsoun, Helali, Mebarek, *et al.*, 2007; Rahman, Price and Bhansali, 2007; Cho and Thielecke, 2008; Shedden, 2008).

The impedance of the constant phase element can be represented by the equation below (Bouafsoun, Helali, Mebarek, *et al.*, 2007; Rubinson and Kayinamura, 2009).

$$Z_{CPE} = \frac{1}{T(j\omega)^P}$$

Equation 2.22

Where $\omega = 2\pi f$, T and P are constants and are referred to in equivalent circuit modelling results as CPET and CPEP. P takes a value ranging between 1 and 0, such that when P = 1 Equation 2.22 is effectively modified into the equation for an ideal capacitor with T = C, as shown in the Wessel plot in Figure 2.2. The extensive use of CPEs in equivalent circuit modelling for biological specimens has been previously questioned by McAdams and Jossinet, 1996. They highlight that the CPE and the equivalent circuits into which it is included do not always accurately represent the biological system under investigation. Furthermore it is possible that 2 different circuits containing CPEs, or other circuit elements, can be found to fit to the same impedance data. A further consideration is in deriving a capacitance value from the

CPE with Orazem et al, 2013, warning that such derived values maybe inaccurate even if parameter P is above 0.9, or approaching ideal capacitor behaviour. These authors emphasis that those using CPEs in circuit modelling should be aware of these limitations.

Equivalent circuit modelling has the capability to enable a quantitative assessment of biological specimens being tested and can help to explain various phenomena observed during experimentation. However more complex models have the disadvantage of losing some of their accuracy and as previously mentioned there is the potential for different circuits to produce a fit for the same acquired data set (Kayinamura, Roberts and Rubinson, 2012). The pitfalls of circuit modelling have been highlighted in the literature and general recommendations are that the models should be simple, containing as few as elements as possible and fitted to data captured over a wide frequency range (Macdonald, 1992; McAdams and Jossinet, 1996; Malleo *et al.*, 2010).

2.5. Dispersions

In applying potentials at various frequencies to biological specimens the occurrence of dielectric dispersions must be considered. As previously detailed the lipid bilayer that comprises the membrane of a cell can be considered as capacitive with the opposing layers acting as two conductive plates separated by a distance of 3 to 5 nm. The application of a potential across the membrane in a scenario such as impedance spectroscopy results in charged ions accumulating on the opposing surfaces. The frequency that the potential is applied at is relevant as it determines the amount of time available for the charged ions to accumulate. Thus in analysing biological material the permittivity varies in a frequency dependent fashion with three frequency ranges showing distinct reductions in permittivity, referred to as dispersions. Figure 2.11 illustrates these dispersions along with the accompanying increases in conductivity.

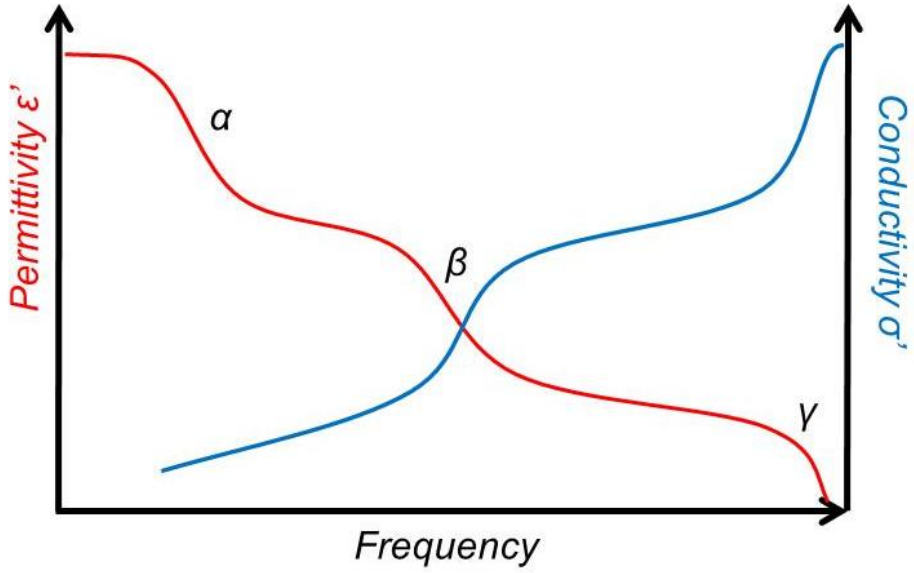

Figure 2.11 – Frequency dependency of permittivity (red) and conductivity (blue) of biological tissue with the dielectric dispersions α, β and γ.

At low frequencies there is time for the charged ions to build up and subsequently discharge causing more capacitive behaviour, resulting in a high permittivity such that the majority of the current flows around the cell. In the scenario of a potential being applied to cells adhered to an electrode - as is the case of experimentation detailed in this thesis - the current bypasses the cells and measures the extracellular space between them. The α dispersion in this frequency range is attributed to ionic diffusion processes at the membrane surface, although the precise causes remains disputed (Asami, 2007). As the frequency increases the time for the accumulation and discharge of ions is reduced and the membrane no longer becomes fully charged reducing its capacitive behaviour. The permittivity decreases as the current begins to flow through the intra cellular space and for cells on an electrode the variations in measurements can be considered to be representative of changes happening within the cells. The β dispersion arises from surface heterogeneities such as the presence of membrane pores or microvilli. Further increases in frequency result in there being insufficient time for the cell membrane to charge and it becomes purely resistive in behaviour. The γ dispersion observed at these frequencies is associated with the polarisation of water molecules (Gabriel *et al.*, 1996). For the measurement of cells on an electrode, measurements at these high frequencies do not reveal any significant information on the cells behaviour and are rarely used in the literature.

A schematic of current interactions with a cell and the effect of changes in the cell membrane are depicted in Figure 2.12.

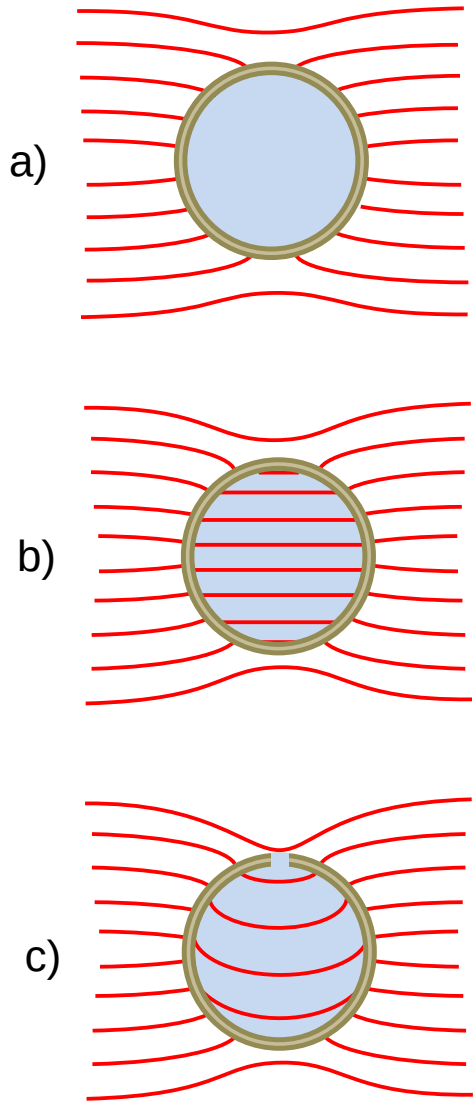

Figure 2.12 - Pictorial representation of current flow through a cell at various frequencies. a) At low frequencies the cell membrane shields the cytoplasm and organelles from the electric field, resulting in a high resistance to current flow. b) At higher frequencies the cell membrane resistance is progressively shorted out by the membrane capacitance and no longer performs its shielding function. Current flows through the cell and cellular resistance is reduced. c) The presence of a small conducting pore within the cell membrane creates a heterogeneous electric field inside the cell and cellular resistance is increased, often referred to as the Maxwell-Wagner effect. Adapted from Pethig & Kell 1987.

3 Materials and Methods

3.1 Chamber manufacture

3.1.1 Method

Cells were cultured in chambers that were based upon an existing design previously developed at the University of Strathclyde (Shedden, 2008). A number of alterations were applied to the original chamber to improve the design to make it more suitable for long term in-incubator measurements with the final embodiment used in tests described here. Chambers were manufactured by modifying a Lab-Tek cell culture 2 well chamber slide and a Falcon 35mm diameter petri dish. A thin gold patterned layer was applied to the surface of the petri dish using a vacuum deposition process. The pattern was created by placing a laser cut stainless steel mask onto the surface of the petri dish which was then put into a sputter coater containing a gold target. In total 5 coatings were applied creating a total coating thickness of 125nm. The thickness was calculated using formulae provided with the sputter coater and is detailed in the Appendix. Each coating step lasted 30 seconds each with a period of 2 minutes between coatings to allow cooling to take place, preventing the plastic dish from melting.

The pattern comprised one large, main electrode and 4 smaller opposing electrodes with dimensions as depicted in Figure 3.1. In impedance spectroscopy studies for a two electrode setup as described here the small electrode is sometimes referred as the working electrode and the larger electrode as the counter electrode (Wegener, 2008). The area of a small electrode is $7mm^2$ whilst the larger electrode is $100mm^2$ a ratio of 0.07. The area of each small electrode is of the same magnitude as the area over which cells regrow in a small stent as discussed in section 1.11 (Stent cell regrowth areas). Strain gauge wires were attached to the distal end of the electrodes with Silver Chloride Paint. The free ends of the wire were collated into a 5 way electrical connector that connected directly to the impedance analyser/multiplexer interface. The use of the connectors permitted easy removal of individual chambers from the incubator for media replenishment and microscopy imaging purposes.

The cell growth area was isolated by removing from a Lab-Tek slide the chamber housing and its accompanying silicone gasket. One of the cubes was then cut away to isolate a single cube. This was then adhered to the dish surface and thus over the gold electrode pattern by applying double sided tape, recreating the seal between the housing and the slide. The double sided tape was cut using a scalpel in such a way as to ensure that the tape was outboard of the silicone gasket seal. This method was used to eliminate any contact between the double sided tape and the cell media. During tests chambers were clamped between the upper lid and the underside of the dish using bulldog clips to further reduce the occurrence of leakages. Additional holes (<2mm diameter) were added to three of the upper sides of the cubes to permit appropriate atmospheric ingress and egress.

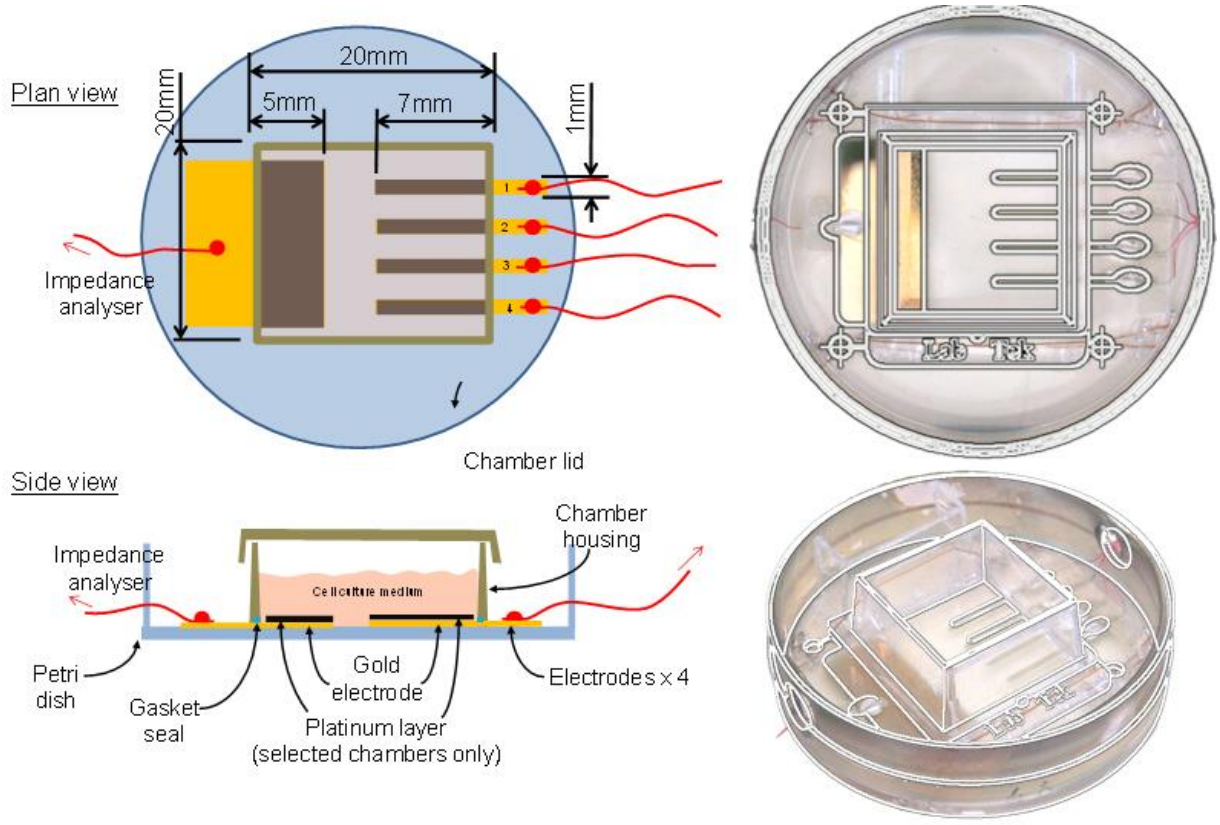

Figure 3.1 – Chamber design with cell culture surface and electrode dimensions (top left).

3.1.2 Electrode coating

Platinum black surface coatings were applied galvanostatically onto the patterned gold. The electrodes were first rinsed in distilled water and 1.5ml of Chloroplatinic acid platinising solution was then placed into the chamber. Platinising solution comprised 0.06M Chloroplatinic acid hexahydrate and 794µM of lead acetate in distilled water. A two electrode setup was used with the gold electrode to be coated set as the cathode and a 1mm diameter platinum wire as the anode. Coating of electrodes was applied with a current density of 0.43mA/mm^2 over 1.5 seconds. After coating the platinising solution was removed and the electrodes rinsed 3 times with distilled water. Platinum black electrodes were kept in 2ml of distilled water for 24 hours prior to usage in experiments.

Polypyrrole surface coatings were also applied in a similar fashion galvanostatically onto the patterned gold. The electrodes were first rinsed in distilled water. 1.5ml of aqueous Pyrrole 0.1M and Sodium Salicylate 0.1M was placed into the chamber. A two electrode setup was used with the gold electrode to be coated set as the cathode and a 1mm diameter platinum wire as the anode. Combined polypyrrole coating of electrodes was applied with a current density 0.011mA/mm^2 over 30 seconds. All material coating processes used a Solartron SI-1287 Electrochemical interface (Solartron Analytical, Farnborough, United Kingdom).

Release of salicylate was determined by storing the chambers containing the polypyrrole coated electrodes in 2ml of distilled water at room temperature, before sample removal and replacement with fresh distilled water every 24 hours up to 96 hours. Samples were analysed for salicylate concentration using a UV spectrometer (UV2401, Shimadzu corporation, Jiangsu, China). The absorbance at the wave length of salicylate (296nm) (Arbizzani *et al.*, 2007) was measured for each sample and then converted into a known mass by comparison with a calibration graph itself obtained from absorbance values of known solutions, this graph is included in the appendix.

3.1.3 Materials

Ethanol, Chloroplatinic acid hexahydrate, lead acetate, polypyrrole, sodium salicylate and Lab-Tek chambers were purchased from Sigma Aldrich, (Poole,

United Kingdom). Falcon petri dishes were purchased from Fisher Scientific (Loughborough, United Kingdom). Silver Chloride Paint and 5 way electrical connectors were purchased from RS (Corby, United Kingdom).

3.2 Atomic force microscopy (AFM)

Characterisation of platinum black and plastic culture ware surfaces was performed using an Asylum MFP-3D atomic force microscope (Asylum Research, Santa Barbara, USA). A Bruker SCANASYST-AIR cantilever with a spring constant of 0.4 N/m was fitted (Bruker Corporation, Camarillo, USA). Scans were taken at room temperature in contact mode. Scanned arrays comprised 256 x 256 pixel density of height data over a size of 5μm at a scan rate of 1*Hz*. Root mean square surface roughness was obtained from 3 sample points on a single platinum black electrode and 3 points on the plastic adjacent to the electrode.

3.3 Automated impedance spectroscopy system

The starting point for the system was the existing methodology used by Shedden, 2008. This involved carrying out experiments on cell monolayers through the removal of chambers from the incubator to an impedance analyser. The removal of chambers from the incubator into a non-clean environment in this manner increased the risk of infections developing and the cells under measurement were not able to be kept at 37˚C in an atmosphere of 5% CO2 conditions. The temporal resolution of the measurement using such a method was restricted to one measurement every 24 hours. Such a method also limited the number of chambers that could be experimented on at any one time. To address these issues it was decided that measurement of chambers should be carried out in an automated manner in the incubator, increasing the time resolution and reducing the risk of infection. This type of system resembles the commercial impedance spectroscopy systems described in section1.15 (Commercially available impedance spectroscopy systems).

A 32 channel multiplexer circuit was constructed that when integrated with bespoke software autonomously switches an impedance measurement procedure between 8 of the previously detailed chambers (4 electrodes per chamber). The system comprised an ADG732BUZ 32:1 multiplexer chip (Analog devices, Norwood, Massachusetts,

United States) an Arduino 2560 development board (Maplin, Glasgow) and an Autolab PGSTAT302N, (Metrohm, Herisau, Switzerland), a schematic is depicted in Figure 3.2. The multiplexer is of the same architecture (32:1) and manufacturer as used in 5 published studies on impedance measurement, (Smith, Thomas and Cornish, 2007; Sun *et al.*, 2010; Wissenwasser *et al.*, 2011; Reitinger *et al.*, 2012; Karimullah *et al.*, 2013) .

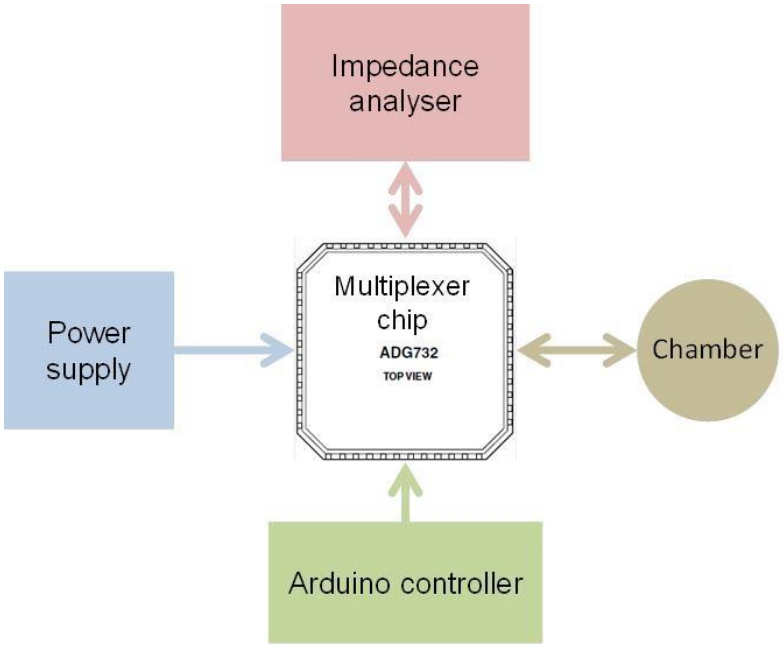

Figure 3.2 - Automated impedance spectroscopy system schematic.

Bespoke software for integrating the disparate componentry was developed using LabView software (National Instruments, Texas, United States). The performance of the system was characterised prior to use and these results are detailed in section 4.2 (System characterisation). A voltage amplitude of 50mV, peak amplitude with a frequency range of 1M*Hz* to 1.2*Hz* at 10 frequencies per decade was selected with no DC bias. The rationale for these parameters is detailed in section 4.2 (System characterisation). An image of the 8 chambers in the incubator is shown in Figure 3.3.

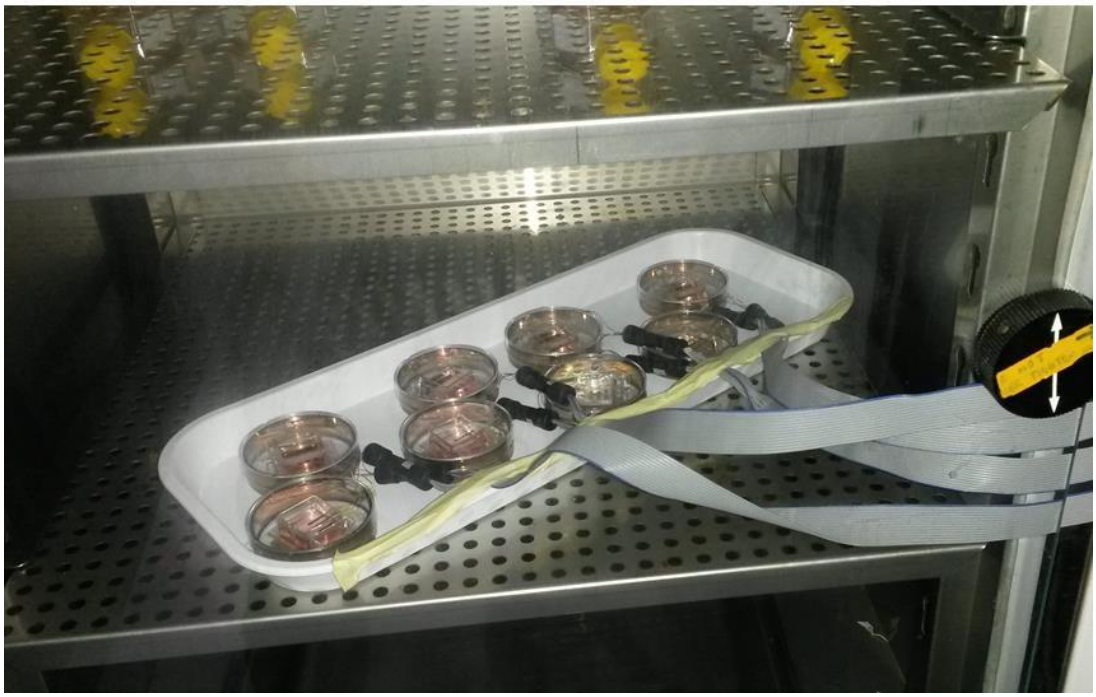

Figure 3.3- 8 chamber array located in the incubator.

3.4 Time lapse microscopy

3.4.1 Method

A bespoke system for capturing time lapse microscopy images of the cells as they settle and proliferate onto the electrodes was designed developed and tested. The system is similar in concept to the design published by Lynch et al, 2014. The lens and focussing wheel body was removed from a USB microscope and inverted on the supplied clamp and stand with a Moticam 10 positioned beneath. The whole inverted arrangement was compressed to prevent unwanted light penetrating through to the camera. The chamber to be imaged was placed on top of the inverted lens body and manoeuvred by hand until the desired electrode came into focus. Light intensity was tuned to ensure that the cells were visible through the electrode. As with the standard light microscopy used in this study, the intensity of light required to penetrate through the coated electrodes was often too high to permit observation of the surrounding cells attached to the clear culture ware plastic. A schematic and image of the time lapse arrangement in the incubator is shown in Figure 3.4.

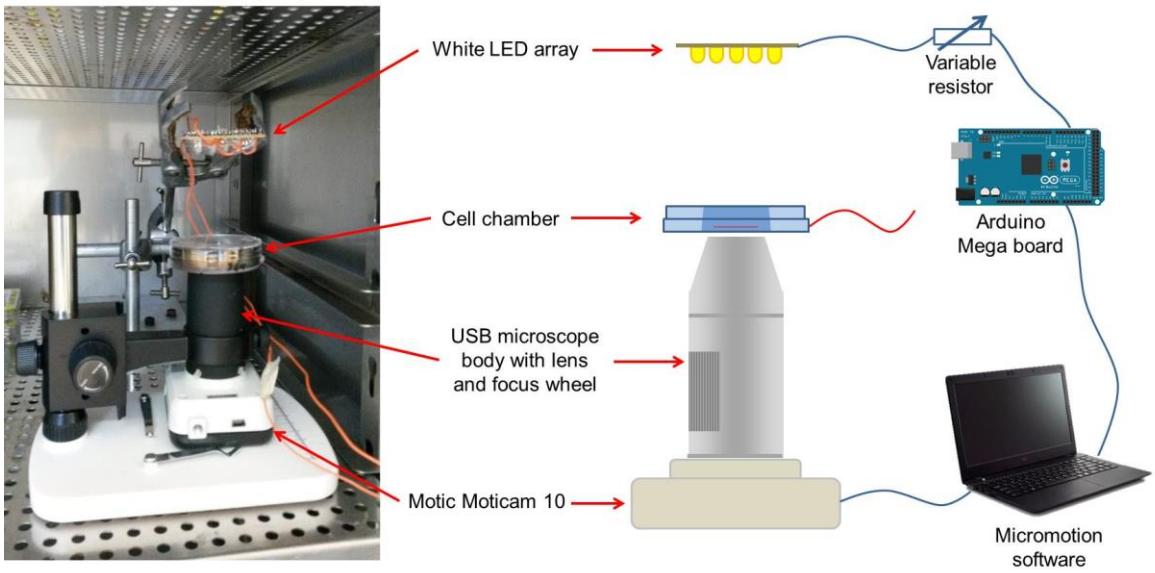

Figure 3.4 - Time lapse microscopy system image and schematic.

Lighting was provided by a 5 x 5 array of white LEDs arranged in series with a 220Ω fixed resistor all mounted onto a Vero board. The array was positioned 40mm above the surface being imaged. LED brightness control was achieved through the use of a 1kΩ potentiometer. The whole assembly was sterilised using ethanol and placed into the incubator with the required wires passing across the rubber seal thus maintaining the atmospheric integrity of the incubator. Image capture every 10 minutes was automated using μmanager software. An Arduino Mega development board was used in conjunction with the software to only turn on the lighting when capturing an image with the objective being to mitigate the effects of Phototoxicity on the cells (Lynch, Triajianto and Routledge, 2014). A bespoke LabView program developed for the project added a text overlay containing experimental information and a time stamp. Upon completion of the test Microsoft movie maker was used to assemble the saved images into a video format. Scale reference was provided by the width of the electrode as a known distance of 1mm. The software was briefly paused to allow the chamber being imaged to be removed from the incubator for media replenishment or in the case of co-culture experiments endothelial seeding. The electrode was aligned manually after being put back into the incubator and the imaging software restarted. Due to the short distance between electrodes and their high aspect ratio it was only

possible to perform time lapse microscopy on the end of one electrode for one chamber per test. Standard light microscopy was performed on the other non-time lapse imaged chambers with images captured every 24 hours.

3.4.2 Materials

USB microscope Crenova USB 2.0 5MP Digital microscope with accompanying clamp and stand was purchased from Amazon UK (Slough, United Kingdom). Nichia NSPW500GS-K1 white LEDs, vero board and 220Ω Vishay SFR16 Series 0204 Axial Metal Film Resistor were purchased from RS, United Kingdom (Corby, United Kingdom). 1kΩ dual gang potentiometer and Arduino mega board were obtained from Maplin (Glasgow, Scotland). μmanager is open source software available from www.micro-manager.org.

3.5 Cell culture

3.5.1 Porcine cells

Primary porcine smooth muscle cells were obtained by excising a left anterior descending coronary artery from a recently slaughtered porcine heart as highlighted in Figure 3.5a. The artery was sequentially rinsed in a 10% Penicillin/Streptomycin in phosphate buffer solution and smooth muscle cell culture medium to minimise the risk of infection and to prevent drying. External connective tissue was removed and the artery divided into approximately 2mm sections with the number of sections varying depending on the length of artery isolated. The isolated artery is shown in Figure 3.5b.

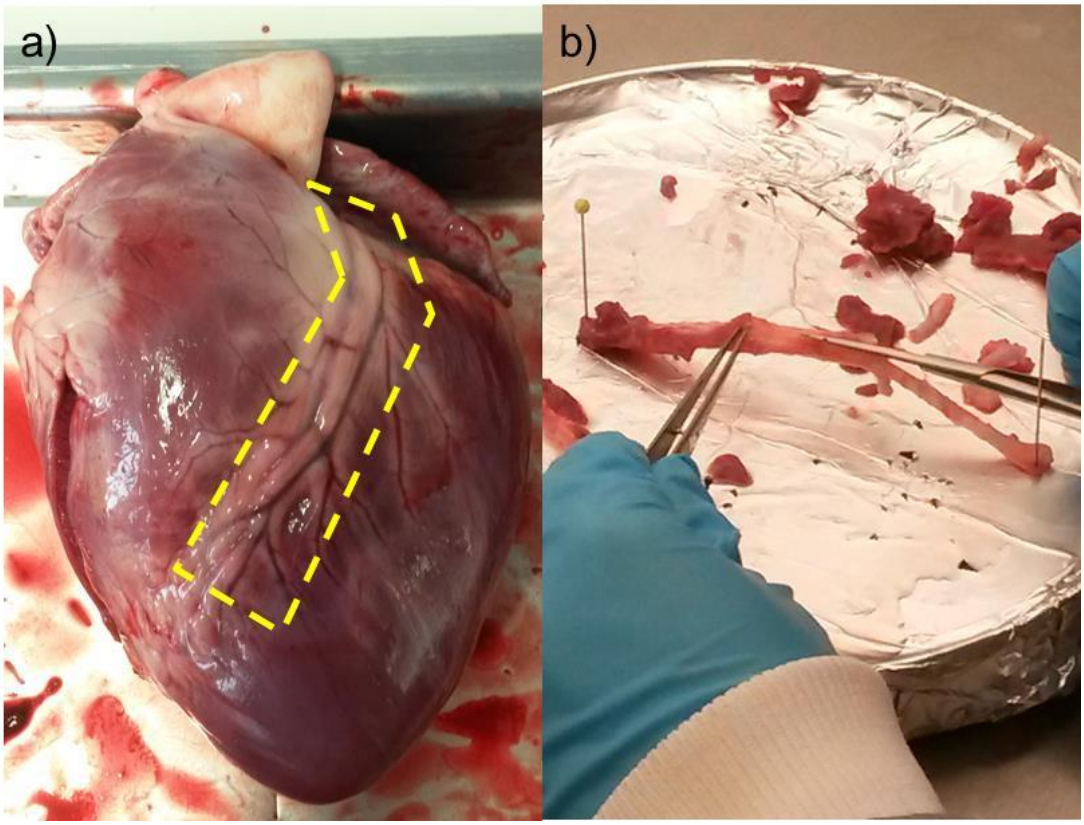

Figure 3.5 – a) Porcine heart with location of the left anterior descending coronary artery used for smooth muscle cell isolation outlined. b) Excised artery in the process of tissue removal prior to sectioning.

Sections were then placed in pairs into a T25 flask and immersed in smooth muscle cell culture medium which was changed every 48 hours. Following observation of smooth muscle cell outgrowth from the explants the sections were removed and cells cultured and passaged as normal. The time from dissection isolation to the explants removal was approximately 10 days.

Primary porcine endothelial cells were harvested by excising a pulmonary artery from the same porcine hearts as used for smooth muscle cell isolation and is depicted in Figure 3.6a and b. The artery was rinsed in endothelial cell growth media and a 10% Penicillin/Streptomycin in PBS solution to minimise the risk of infection and prevent drying. The luminal surface was exposed by slicing through the artery section and pinning flat. A scalpel blade was then lightly scraped over the luminal surface and rinsed in endothelial growth media to create a cell suspension. Care was taken not to scrape the same area more than once and remove non-endothelial cells

residing underneath the endothelium. Suspensions were transferred to T25 flasks with media replaced every 48 hours and passaged where monolayers approached confluency. All cells were maintained within a humidified chamber at 37°C (5% CO_2/95% air). Endothelial and smooth muscle cell lines derived from the same heart were given the same identification.

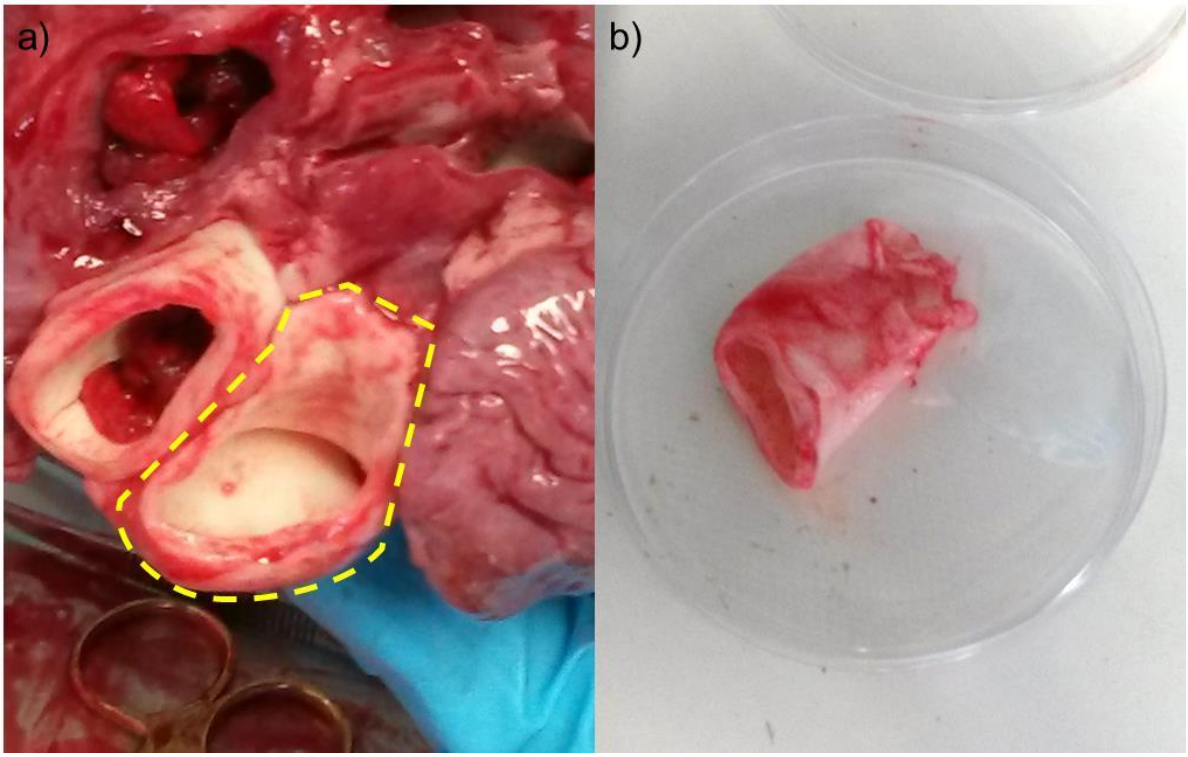

Figure 3.6 - a) Porcine heart with the Pulmonary artery used for endothelial cell isolation outlined. b) Removed pulmonary artery section.

3.5.2 HUVECs

To provide a comparison against a cell type more frequently used in the literature Human Umbilical Vein Endothelial Cells (HUVECs) were purchased from Lonza, passaged and maintained in a similar fashion to porcine cells using dedicated HUVEC media from the same supplier.

3.5.3 Materials

Smooth muscle cell media constituted a 50:50 mix of Waymouth's MB752/1 medium 200 and F-12 Nutrient Mixture (Ham) (Invitrogen, Paisley, Scotland), 9% foetal calf serum (European source) and 0.9% penicillin–streptomycin, (Sigma-Aldrich, Poole, United Kingdom). Primary porcine endothelial cell media comprised Medium 200 with 1.9% Low Serum Growth Supplement (Invitrogen, Paisley, Scotland) and 0.9% penicillin–streptomycin. HUVECs and HUVEC media (EGM2 BulletKit) were purchased from Lonza Group Ltd, (Basel, Switzerland). Porcine hearts were kindly donated by Robertson's Fine Foods, (Ardrossan, Scotland).

3.6 Cell experimentation

3.6.1 Method

Chambers were manufactured, as previously described, specifically for the test to be conducted and were not reused in later experimentation. Prior to commencement of each experiment chambers were prepared by sterilisation for 1 hour under UV light in a class II hood. All chambers lids were replaced and then then kept at 37°C until the moment of cell seeding or media addition. This was done to maintain cell suspension and media temperatures as it was thought that adding to a colder chamber would cause a drop in temperature, reducing the thermal stability in the initial minutes of the experimentation. This was deemed of particular importance as it is during this phase that the first impedance measurements are taken, against which all subsequent measurements are normalised. Normalisation of data is discussed further in section 4.8 (Electrode repeatability and data normalisation).

Chambers containing 2ml of media were seeded with endothelial cells, smooth muscle cells, or HUVECs at densities and at passage numbers stated in the specific results section. Seeding density was determined through cell counting with a haemocytometer. Control chambers contained 2ml of media only. Impedance sweeps of each electrode were taken at approximately 2.5 hour intervals. Media changes were typically carried out every 48 hours for both cell seeded and control chambers and where this regimen differed it is explicitly stated in the results. Endothelial cell tests from all species were typically run for a period of 96 hours, although were allowed to continue for a longer time where cells were observed to have proliferated more slowly over the electrodes. Variable growth rates in the same cell type can be expected in primary cell cultures from different sources. Experiments involving smooth muscle cells were run for a longer time period of up to 240 hours and co-culture tests also up to 240 hours. The discrepancy between the time period lengths of endothelial and smooth muscle cell tests is attributable to the different growth rates of the cell types.

The HUVEC test conducted was carried out in a similar fashion with a variation for one chamber. A single HUVEC seeded chamber was initially cultured in normal endothelial media as used for porcine cells and then after 48 hours changed to the HUVEC media as used in other chambers. This variation was carried out as an exploratory test to investigate the effect of different media formulations on the cells.

3.6.2 Light microscopy

Every 24 hours 10x and 4x magnification images were taken using a Moticam 10 microscope camera attached to an AE31 microscope (both Motic, China). Three 4x images were taken of each electrode providing a complete picture of cell coverage at that given time point. In addition 1, 4x image of the main electrode and 1, 10x image of each electrode tip were captured. Other areas of interest were also imaged where observed. Chambers were removed from the incubator such that upon their return they had at least 1 hour before the next impedance sweep was conducted. Chambers were out of the incubator for imaging for less than 5 minutes. This practice was adhered to in order to allow any thermal and atmospheric disturbance arising from their removal and replacement to stabilise. In some of the results presented

disturbances can be observed in impedance profiles after the removal of the chambers from the incubator for imaging. These disturbances return to their pre removal values or trends and were not deemed to be of consequence for any of the final results and conclusions presented in this study. The elevated level of light intensity required to image through the coated electrodes meant that the surrounding cells on the cultureware plastic were often not visible. Where cell coverage was observed to be different between the plastic and electrode areas this was noted and extra images taken. Control chambers were not subjected to microscopy imaging but were given a visual inspection for electrode damage and infections during media changes and at experiment end points. All light microscopy images were greyscaled prior to inclusion in the results sections of this thesis.

3.6.3 Co-culture experimentation

The growth of both cell types together, referred as a co-culture model provides a more accurate laboratory model of the vascular system than separate monocultures of endothelial and smooth muscle cells (Wallace and Truskey, 2010). For the purposes of fulfilling the aims and objectives of the work in this thesis the direct co-culture method was selected with the rationale for this decision outlined in section 1.28 (Co-culture experimentation). The method aimed to produce a layered structure of cells with an endothelial cell monolayer coating a sub confluent layer of smooth muscle cells.

A number of different co-culture options were tried with some unsuccessful procedures resulting in modification of the protocol for subsequent experiments. These modifications were changes in the composition of media used, level of SMC confluence attained before quiesecing and variation in the duration of SMC growth, and quiecesing phases. These changes are detailed in section 5.2.4 (Co-culture) to provide a guide as to the route taken to achieve a successful co-culture model. Figure 3.7 schematically depicts the distinct phases of a direct co-culture procedure. Smooth muscle cells were seeded onto the chamber surface and grown to varying levels of confluence before the addition of quiescent media. The smooth muscle cell growth was arrested in this manner to prevent the cells from attaining confluency after the endothelial cells had been seeded over them. A sub confluent smooth muscle layer

was considered to be more representative of in stent restenotic cell growth. Endothelial cells were then seeded directly on top of the smooth muscle cells and allowed to proliferate.

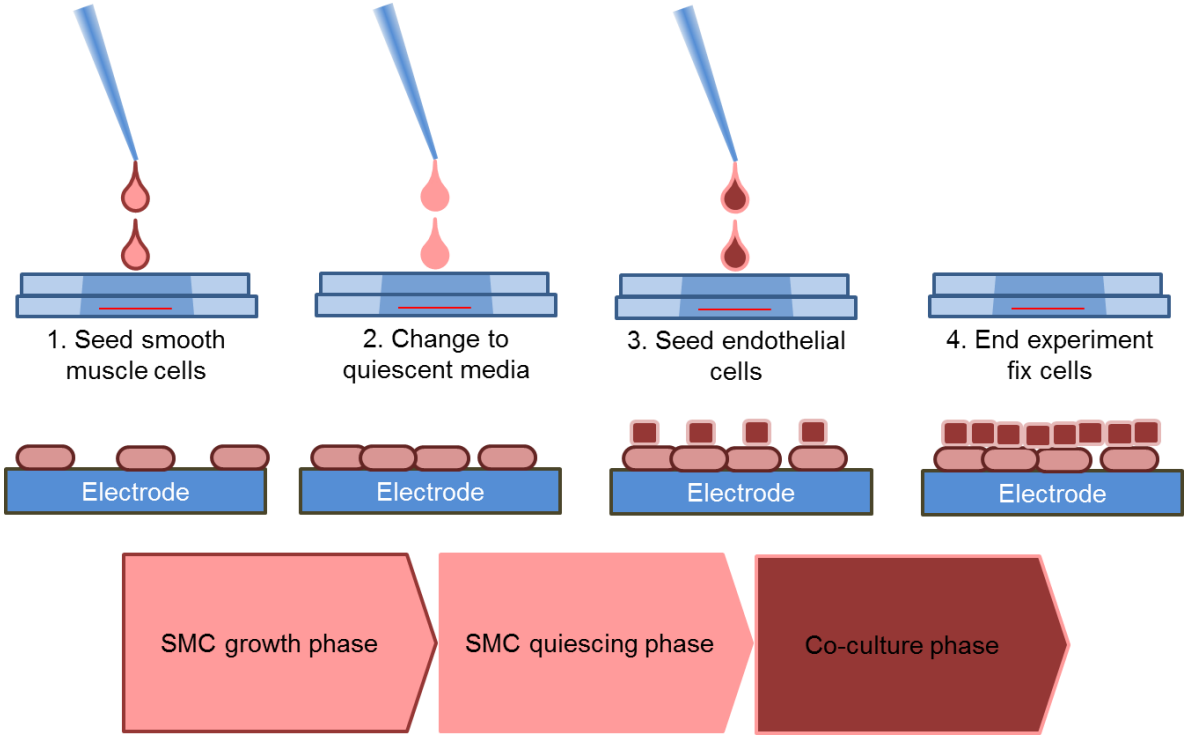

Figure 3.7 - Schematic procedure for cardiovascular cell co-culture.

Only porcine cells were used in co-culture experiments. Before co-culture was attempted in chambers the procedure was trialled in 2 separate experiments each with 4 petri dishes of the type used to manufacture the chambers. It was an experimental objective to seed endothelial cells onto smooth muscle cells that derived from the same heart, thus achieving a genetic match between the cells. However in practice timing the correct endothelial cell line to be available with the required amount of cells when the smooth cells finished their quiescent phase was not always possible and a different line was then used. Following completion of the trial test the cells were fixed in 10% formalin and stained for Von-Willebrand factor and DAPI as per the procedures detailed in section 3.7(Cell staining). The final co-culture experiment conducted in chambers was stained for α smooth muscle actin, DAPI and Von-Willebrand factor.

3.7 Cell staining

3.7.1 Method

Endothelial cell lines were assessed by staining cells for Von Willebrand factor expression, a commonly used endothelial cell marker (Patsch *et al.*, 2015). Blocking buffer consisting of 20% FCS in PBS was added to fixed cells for 1 hour. Rabbit polyclonal anti-von Willebrand factor antibody was then added at a concentration of 0.0025mg/ml in PBS and left overnight in a 4°C humid environment. Removal of primary antibody preceded rinsing in PBS and the addition of donkey anti-rabbit IgG Alexafluor 488 conjugated secondary antibody for 1 hour in the dark. Control steps were carried out through the addition of secondary and primary antibodies in isolation to endothelial cells derived using the same procedure, followed by imaging to check for non-specific binding. Smooth muscle cells were also stained for von-Willebrand expression.

Smooth muscle cells were characterised by staining cells for α smooth muscle actin expression (Patsch *et al.*, 2015). Blocking buffer was added to fixed cells for 1 hour and then removed. Conjugated CY3 mouse monoclonal anti-actin-alpha smooth muscle antibody was then added at a concentration of 0.0025mg/ml in PBS and left overnight in a 4°C humid environment. Controls were carried out by the addition of conjugated anti-alpha smooth muscle actin antibody to endothelial cells.

The final step in all staining procedures using cells cultured in chambers involved rinsing in PBS and removal of the cell culture cube to allow lens access. All fluorescent imaging was carried out using a Zeiss Axio Imager Z1 (Cambridge, United Kingdom). To improve the clarity of colour fluorescent microscopy images presented in the results section of this study the brightness was increased to 10% as defined by Microsoft word image adjustment parameters.

3.7.2 Materials

DAPI and anti-alpha smooth muscle actin antibody was purchased from Sigma-Aldrich, (Poole, United Kingdom). Rabbit polyclonal anti-Von Willebrand factor and donkey anti-rabbit IgG Alexafluor 488 conjugated secondary antibodies were purchased from Abcam (Cambridge, United Kingdom).

3.8 Endothelial functionality experimentation

Endothelial functionality experimentation was exclusively carried out on porcine endothelial cell monolayers. Cells were seeded and grown until confluency was observed in the same manner as previously described in section 3.6 (Cellular experimentation). Upon observation of confluency cell media was changed to a media containing a known gap junction mediator. Two gap junction inhibitors at two different concentrations were used, carbenoxolone (100μM and 50μM) and heptanol (0.5mM and 1mM). A gap junction enhancer, dipyridamole was also used (50μM). Cells were then cultured in the media containing the junction mediator for 4, 24 or 48 hours depending on the experimentation requirements. Control chambers contained seeded cells and received media changes as described above but with no gap junction mediators present.

A lucifer yellow scratch assay was used to assess the formation of gap junctions on the electrodes. Upon completion of the experiment the chamber to be subjected to the scratch assay was removed from the incubator and rinsed once in 37°C PBS. 2ml of 0.05% lucifer yellow in PBS was added to the chambers and then scratches made using a new scalpel blade. Scratches were performed by hand with one along the centre of the electrode and 4 equi-spaced on the main electrode, as shown in Figure 3.8. The chamber was then placed back in the incubator for 5 minutes to allow the dye to permeate from the scratch wound edge and through gap junctions, should they be present. After removal of the chamber from incubator the lucifer yellow solution was removed and the cells rinsed twice in PBS before fixing with 10% formalin for 10 minutes. Cells were then stored in PBS prior to fluorescence imaging. Gap junction fluorescence images were taken using a Zeiss Axio Imager Z1 at 10 x magnification with a wet emersion lens. Images were grey-scaled and had a scale bar added using the Zeiss software before saving. The coordinate reference system on the

microscope was utilised to capture images at specific points along the scratch to eliminate the possibility of operator bias. Figure 3.8 shows the points at which images were taken.

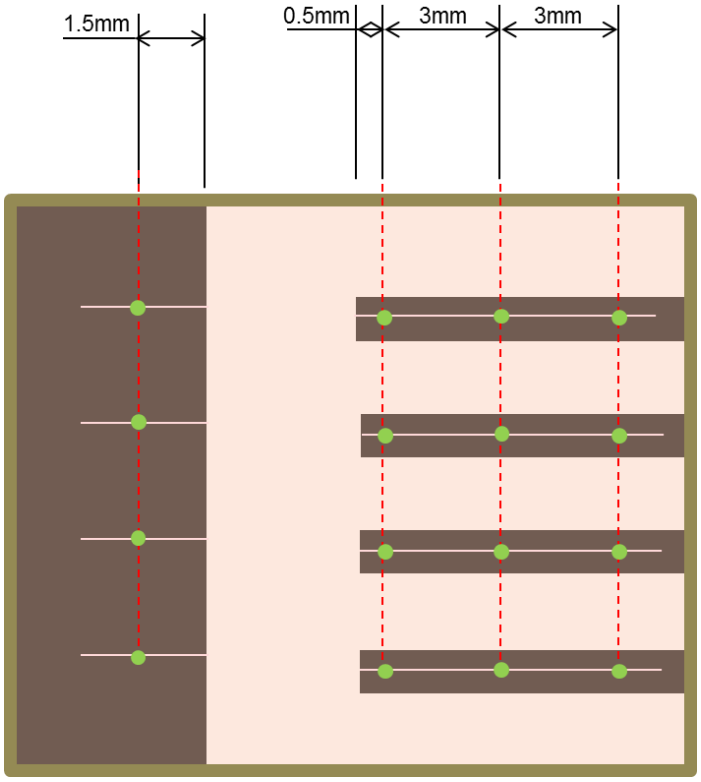

Figure 3.8 – Chamber- electrode plan drawing with positions of scratches and points at which images were captured for scratch assay analysis (green dots).

Post image analysis was carried out using ImageJ software. The procedure is similar to that used by Begandt et al, 2010, in analysing the amount of lucifer yellow scratch assay dye penetration through a monolayer. The 10x magnification images from the central portion of the scratch were analysed for each electrode. Firstly a 100 x 500 pixel rectangle was used to select an area of the image at a remote position from the scratch and any dye penetration as shown in Figure 3.9b. The plot profile function in the software was then used to provide a measurement of the mean pixel intensity for each pixel column in the selected area, providing a background level of intensity. Next a 400 x 500 pixel rectangle was positioned centrally on the right hand side of the scratch with its leftmost part aligning with the edge of the scratch. The same plot profile function was then used to obtain a quantitative measure of the dye

penetration. A screenshot of the box positioning and a typical plot obtained from it are shown in Figure 3.9a. As expected the pixel intensity caused by the presence of the dye in the cells rises in the zone adjacent to the scratch edge and then decays as the distance from the wounded cells increases. The data from the profile was tabulated and a mean pixel intensity value calculated. The background value was then subtracted from the intensity value of the area next to the scratch to obtain a measure of the amount of dye penetration and thus the level of gap junction permeability of the monolayer.

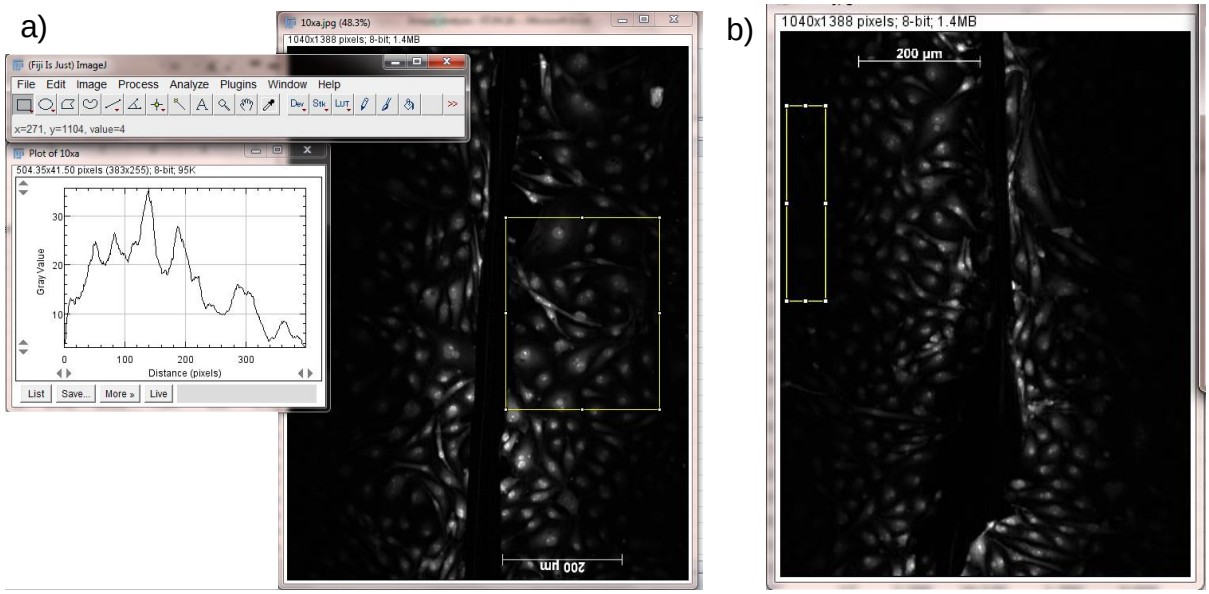

Figure 3.9 – Endothelial cell scratch assay analysis with ImageJ software. a) Dye perfused region of analysis adjacent to scratch and accompanying pixel intensity profile (insert).b) Typical background intensity region for subtraction from dye perfused region.

Tight junction formation was assessed in one endothelial dysfunction experiment through staining for Zonula Occludens, a protein that is associated with the regulation of tight junctions (Balda and Matter, 1998; Antonetti *et al.*, 1999; Shen *et al.*, 2011). Cells were fixed by adding 10% formalin for 15 minutes. Blocking buffer consisting of 20% FCS in PBS was added for 1 hour. Rabbit polyclonal anti-ZO1 primary antibody was then added at a concentration of 0.00166mg/ml in PBS and left

overnight in a 4°C humid environment. Removal of primary antibody preceded rinsing in PBS and addition of goat anti-Rabbit IgG (H+L) Secondary Antibody, Alexa Fluor® 594 conjugate for 1 hour in the dark. DAPI was applied at a concentration of 1μg/ml in PBS for 15 minutes. The final step involved rinsing in PBS and removal of the cell culture cube to allow lens access. Imaging was carried out using a Zeiss Axio Imager Z1 (Cambridge, United Kingdom). ZO-1 and DAPI fluorescent images of cells on electrodes were obtained at 40 times magnification using a wet emersion lens with the same coordinate reference system as described for gap junction imaging, however care was taken to capture images at points located away from the scratch. Control staining images using primary and secondary antibodies alone and then in combination are included in the appendix.

3.8.1 Statistical analysis

Statistical significance of total impedance variations and mean pixel intensity data was determined using MiniTab software with one way ANOVA analysis followed by Tukey's post-hoc multiple comparison tests. Values of $p < 0.05$ were considered statistically significant. Error bars displayed are ± standard error mean.

3.8.2 Materials

Lucifer yellow, carbenoxolone, 1-heptanol and dipyridamole were purchased from Sigma Aldrich, (Poole, United Kingdom). Rabbit polyclonal anti-ZO1primary antibody and goat anti-Rabbit IgG (H+L) Secondary Antibody, Alexa Fluor 594 conjugate was obtained from Thermo Fisher (Rockford, Illinois USA). ImageJ is open source software available from https://fiji.sc/#cite.

3.9 Equivalent circuit modelling

Data fitting to equivalent circuit models was performed using Z view software (Scribner associates, North Carolina, USA). Data was fitted in frequency range 1*Hz* to 100*kHz*. Fitting parameters used were a maximum number of iterations of 300, 0 optimisation iterations and complex fitting mode. Estimates were made for initial values and the circuit element parameters were limited to positive values only. Chi squared values are reported for fitted data and represent the square of the standard deviation between the captured original impedance data and the data fitted to the equivalent circuit.

4 System development

4.1 Automated measurement

Following construction of the system described in the materials and methods section 3.3 (Automated impedance spectroscopy system), a number of trials were carried out to test its functionality. To have the ability to perform impedance measurements at a rate and regularity beyond those that can be achieved manually the system needed to perform and record impedance spectroscopy measurements unaided. Two phases of testing were carried out to prove these capabilities.

Firstly the system was trialled out of the incubator on the lab bench. All multiplexer channels were connected to a test resistor capacitor circuit (RC) supplied with the autolab impedance analyser. This RC circuit is shown in the appendix section and for the purposes of the test provided the system with circuits similar to cell chambers to measure. From the initiation of the test with the bespoke LabVIEW software the system ran continuously for 18 hours before the RAM memory limit of the laptop was reached preventing further measurements. It was decided at this time that 18 hours was a sufficient length of time for the system to operate unaided enabling it to be left overnight before a reset could be done each morning and then again in the evening. Inspection of impedance sweep data revealed no effect of the reset. At this stage the functionality to begin the impedance sweep at any electrode in any of the chambers was added to the software system to allow the measurement sequence to continue in the correct sequence from the reset. A software modification added during the experimental phase of the project extended the maximum operating time and enabled the system to operate continually for the duration of the experiment, with up to 4 days demonstrated. This was achieved by running the LabVIEW program in continuous mode and using the number of previously saved files as a reference point for the next sweep.

The final stage of the automated trial period was to transfer from lab bench testing to the incubator environment. For the duration of this test the system was connected to 8 platinised electrode chambers containing smooth muscle cell growth media. The chambers were placed inside the incubator and the ribbon cables passed through the

incubator door rubber seal, maintaining the atmospheric integrity. Tests showed that the performance of the system on the lab bench was replicated with incubator measurements. Collectively these tests proved the capability of the developed system to carry out automated impedance spectroscopy sweeps of all 32 electrodes in the frequency range of 1*Hz* to 1M*Hz* at a time resolution of 2 hours.

4.2 System characterisation

The system was characterised by comparing the results of impedance sweeps through the constructed multiplexer system and software with those through the Autolab analyser alone using its supplied Nova sofware. A platinised chamber electrode containing smooth muscle cell growth media was measured directly with Autolab Nova software, this established a benchmark measurement for the total impedance through the multiplexer. Immediately afterwards the same chamber and electrode was attached to the automated system and measured with impedance sweeps performed with the developed software sequentially through all 32 channels of the multiplexer. By comparison with the benchmark measurement a percentage error for each frequency and channel measurement was then calculated using the equation below.

$$Total\ Z\ \%\ error = \frac{(Total\ Z\ no\ system) - (Total\ Z\ through\ system)}{(Total\ Z\ no\ system)} \times 100$$

The results are displayed in Figure 4.1.

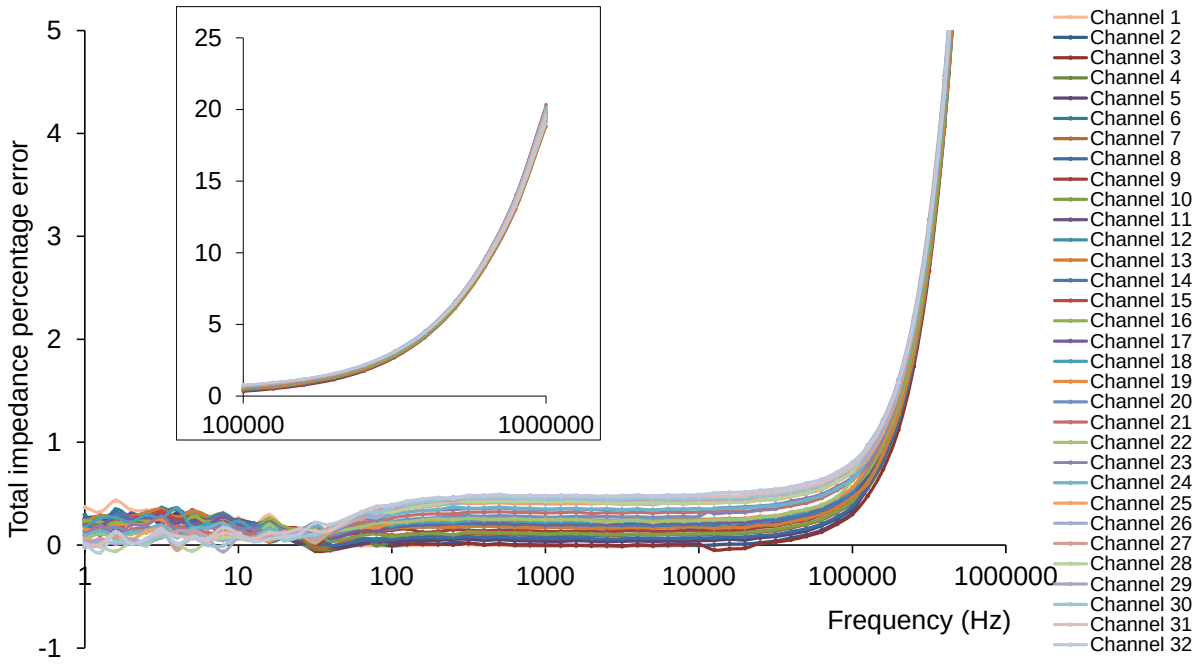

Figure 4.1- Automated impedance system characterisation in Smooth Muscle Cell media. Total impedance percentage error of measurements of a single platinised electrode through the developed system for each of the 32 multiplexer channels compared to measurements of the same electrode through the Autolab impedance analyser alone.

It can be seen from the graph that the system displays errors below 1% in the range 1*Hz* to 100*kHz*. Above 100*kHz* the errors rise rapidly with the system recording higher impedances than the benchmark measurement as shown in the insert graph in Figure 4.1. The time taken to complete all 32 sweeps was 2 hours and there is evidence of drift in the percentage errors occurring, with those channels measured closer in time to the benchmark measurement showing lower errors indicating that the true error between 1*Hz* and 100*kHz* is below 0.5%. These data show that the system is able to perform impedance sweeps with errors below 1% or better. Measurement of frequencies above 100*kHz* results in a high error that is repeatable but rises to as high as 20% at 1M*Hz*. Consequently all impedance measurements above 100*kHz* were disregarded from any of the experimental data presented in this thesis. Haas et al, 2010, also dismissed impedance data towards the 1M*Hz* range in their bespoke system after observing similar increases in magnitude that were attributed to multiplexer effects.

An additional reason for disregarding the use of impedance measurements above 100*kHz* is that reported results in the literature rarely use frequencies above this value. Table 4.1 displays frequencies from selected publications justifying the frequency band selection.

Frequency reported	**Cell type**	**Authors**
1*kHz*	Madin-Darby Canine Kidney Epithelial	(Karimullah *et al.*, 2013)
4*kHz*	Bovine aortic endothelial cells	(DePaola *et al.*, 2001)
4.6*kHz*	Adipose stem cell	(Jun *et al.*, 2013)
10*kHz*	Mesenchymal stem cells	(Reitinger *et al.*, 2012)
10*kHz*	CV1 – Kidney	(Ehret *et al.*, 1997)
10*kHz*	Restenotic lesion (in vivo, rabbit study)	(Süselbeck, Thielecke, Weinschenk, *et al.*, 2005)
10*kHz*	Rat aortic smooth muscle	(Haas et al. 2010)
31*kHz*	Porcine smooth muscle	(Shedden, 2008)
40*kHz*	Rat renal smooth muscle	(Balasubramanian *et al.*, 2008)
45*kHz*	Mesenchymal stem cells	(Angstmann *et al.*, 2011)
64*kHz*	Adipose stem cell	(Bagnaninchi and Drummond, 2011)

Table 4.1 - Example frequencies from the literature used for reporting impedance spectroscopy findings.

Selection of an excitation voltage was also guided by the available literature. Example voltage amplitudes used in studies and the cell types that there were applied are displayed in Table 4.2. A voltage of 50mV (peak amplitude) was selected for use in all of the experimentation presented here. This was deemed appropriate as being between the in vitro experiments carried out smooth muscle and endothelial cells

(200mV - Shedden to 100mV – Balasubramanian et al) and the clinically relevant data 10mV used by Süselbeck et al, where in vivo measurements were made of stenotic lesions using electrodes adhered to catheter delivered balloons. Furthermore voltages were applied against a set 0V (no DC bias) at the start of the impedance sweep, with no reference made to the open circuit potential.

Voltage amplitude	**Cell type**	**Authors**
80mV	Madin-Darby Canine Kidney Epithelial	(Karimullah *et al.*, 2013)
10mV	Mouse L929 fibroblast	(Rümenapp *et al.*, 2009)
100mV	Hela human cervix carcinoma	(Brischwein *et al.*, 2006)
35mV	Mesenchymal stem cells	(Reitinger *et al.*, 2012)
10mV	Restenotic lesion (in vivo, rabbit study)	(Süselbeck, Thielecke, Weinschenk, *et al.*, 2005)
200mV	Porcine smooth muscle, Endothelial cell and human epithelial	(Shedden, 2008)
100mV	Rat renal smooth muscle	(Balasubramanian *et al.*, 2008)

Table 4.2 –Example impedance voltage excitation amplitudes from the literature.

4.3 Electrode substrate

As discussed in introduction section 1.15 (Commercially available impedance spectroscopy systems), commercial impedance spectroscopy systems are sold with cell culture surfaces containing integrated gold electrodes. As a result cellular impedances studies published using measurements from gold electrodes predominate in the literature. As also discussed in the introduction an alternative and more

clinically relevant substrate for use in an implanted device is platinum black. Therefore all tests in the cell characterisation and endothelial functionality results sections were performed using platinised electrodes coated as described in section 3.1 Chamber manufacture. A comparison of the impedance characteristics obtained when using either a gold or platinised electrode can be seen in Figure 4.2.

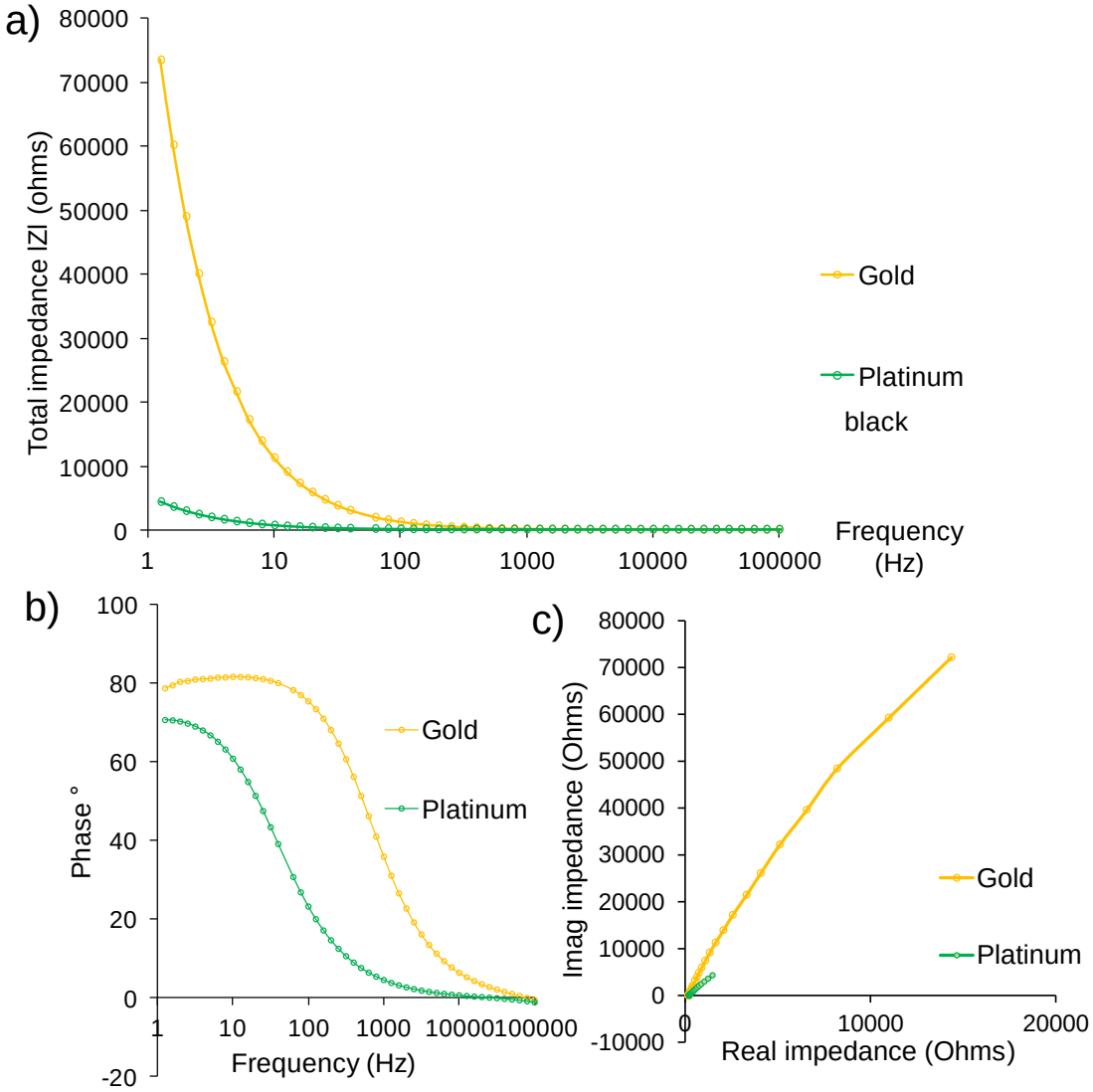

Figure 4.2 - Comparison of example gold and platinum electrodes in Endothelial cell media. a) Total impedance, b) Phase and c) Wessel plot.

The data demonstrates that the addition of a layer of platinum black over the gold reduces the impedance of the electrode, in particular at frequencies below 1000*Hz*.

4.4 Surface characterisation

Atomic force microscopy was used to characterise the surfaces of the platinised electrodes using the procedure described in section 3.2 (Atomic force microscopy). Also analysed for comparative purposes was the plastic culture ware surface. Table 4.3 shows the root mean square surface roughness for the two materials.

	Platinum black	Plastic culture ware
Mean RMS	12.77	3.20
SEM	3.47	0.33

Table 4.3 – Surface roughness defined by Root Mean Square (RMS) data from AFM scans. Data represents the mean value ± one standard error mean (SEM) (n=3).

Representative 3D images of the surfaces are shown in Figure 4.3 and provide a means of visually comparing the two surfaces.

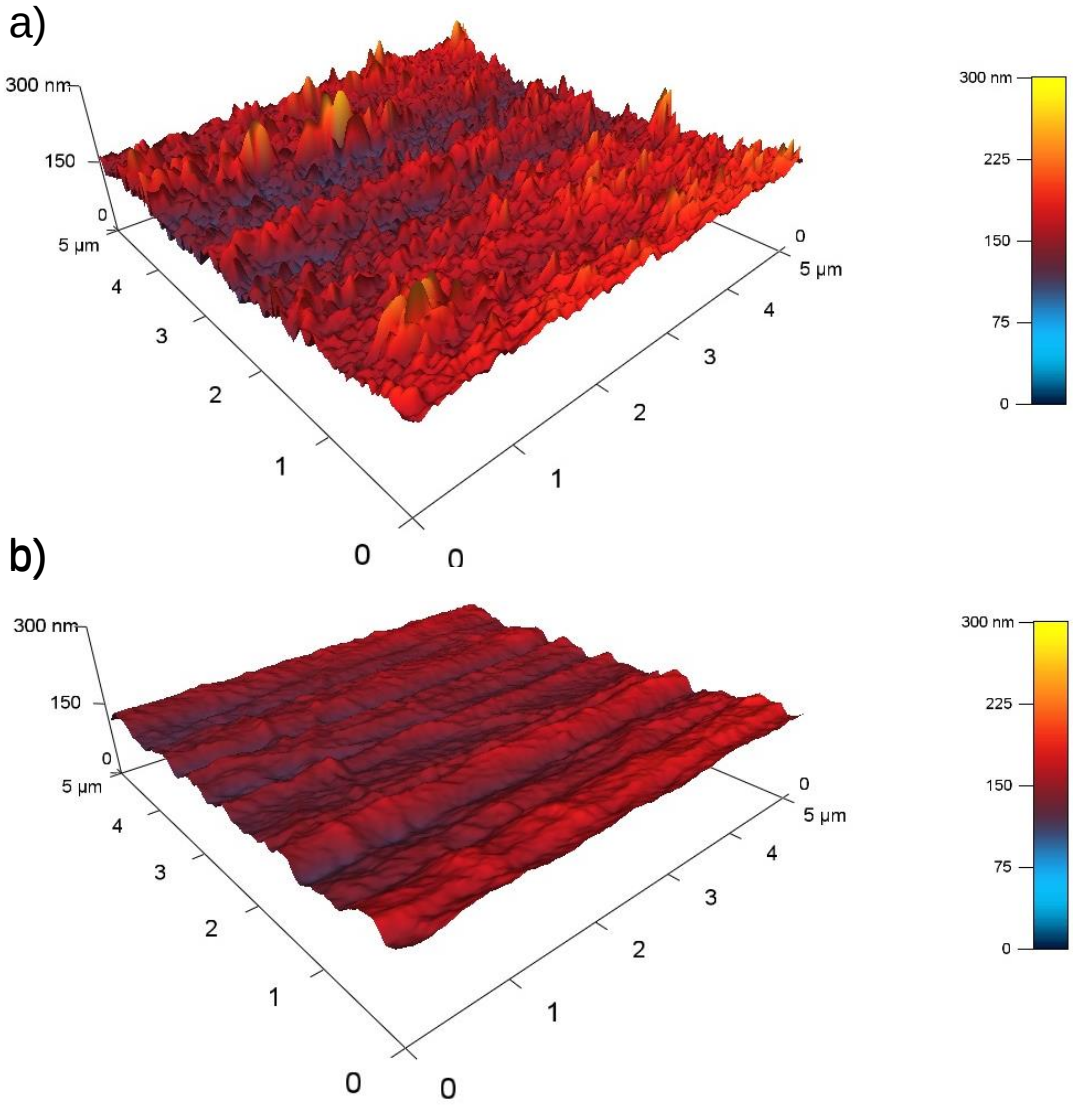

Figure 4.3 - Representative 3D AFM scan images of a) platinum black electrode and b) culture ware plastic.

The data demonstrates that the platinum black electrode surface is rougher than the surrounding plastic on which it is placed.

4.5 Time lapse microscopy

The integration of the time lapse microscope with the impedance system developed provided the opportunity to correlate observed changes at the cell-electrode interface with impedance changes. Importantly, these changes were observed without the need for expensive live-cell imaging systems with stage-top incubators and did not require the cells to be removed from the incubator. The time lapse system developed is described in materials and methods section 3.4 (Time lapse microscopy). It was tested by comparison of captured images taken in situ within the incubator with those obtained from the standard Motic light microscope. Figure 4.4 displays example images of electrode tips from the two microscopy methods. It can be seen from the images that the time lapse microscopy has a comparable resolution to light microscopy. Over the course of the experiments the time lapse imaging was able to reveal aspects of the cell motility, morphology and death which could then correlated with the available impedance data. An example time lapse microscopy video of HUVECs can be viewed in file HUVECs expt, supplied in the electronic appendix accompanying this thesis.

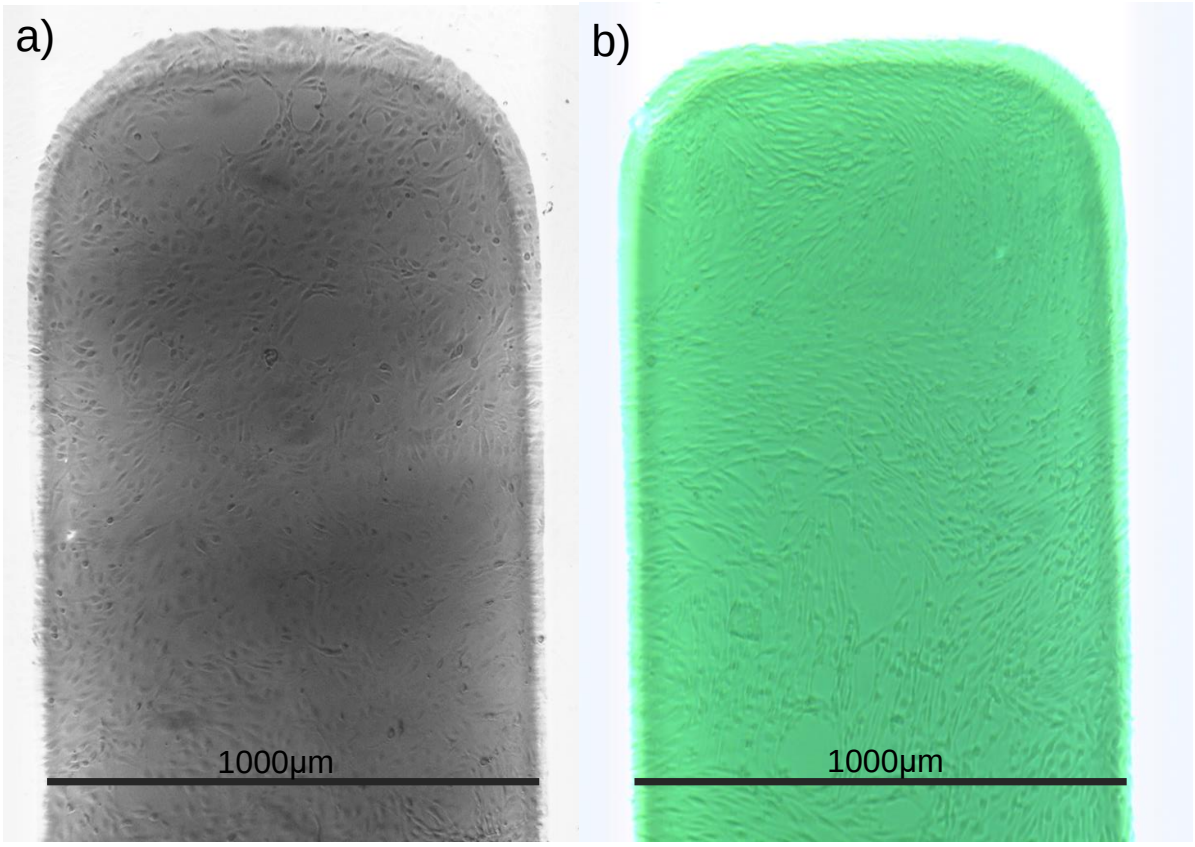

Figure 4.4 - Example light microscopy images of porcine endothelial cells on an electrode tip for standard light microscopy images taken every 24 hours (a) and for constructed time lapse microscope (b). Scale is provided by the known electrode width of 1000µm and by black scale bar of the same length.

4.6 Experimental data inclusion

Throughout the experimental phase it was necessary to remove some results from the final data analysis due to problems with the chambers. Over the course of all experiments data from 24% of all electrodes were removed. Data from chambers and individual electrodes were discarded for the following reasons.

Cell culture media leakage

Leakages were a particular issue in earlier experimental phases before a design change of clamping the culture cube onto the dish was employed. Media leakage onto electrodes created a number of uncontrollable current paths away from the electrodes and any cells that were adhered. The impedance data from any cell

chamber that was observed to have a leak was therefore considered unreliable and removed from any test set. In addition, microscopy images from leaking chambers were also discarded as the media provides a potential route for infection from the exterior of the chamber.

Electrode disconnection

On occasions the connection of the strain gauge wire to the gold base of the electrode became detached. The reasons for this detachment were observed to be poor application of the silver chloride paint during the manufacturing phase and excessive force applied to the wires on chamber removal for imaging and media replenishment. Impedance data from these chambers were discarded but in contrast to leaking chambers microscopy images were included in any analysis as these cells had undergone identical media changes and drug additions as chambers where electrodes remained connected. The absence of impedance sweeps applied to cells adhered to disconnected electrodes was not deemed to be of significance as the technique is considered non-invasive.

4.7 Impedance parameter selection

The real and imaginary components of impedance were measured, from which total impedance and the phase angle can be derived as described in theory section 2.1 (Theory of impedance spectroscopy). Amongst the stated objectives of this project was ascertaining if differences existed in the impedance profiles of cardiovascular cells for the purpose of characterising between them rather than analysing any particular aspect of their individual morphologies or behaviours. Inspection of the results throughout experimentation revealed that the greatest differences between the cell profiles were found in the imaginary component of impedance or the reactance, and it is these that are presented here. The reactance of a cell is determined by the capacitive effect of the cell membrane and various organelles within (Michaelis, Wegener and Robelek, 2013). It is a general rule for the impedance measurement of animal cells that the reactance measures the cells membranes and internal structures and organelles whilst the resistance measures the extracellular fluid (Wegener, 2008). Different cell types have varying structures, organelle and membrane arrangements that are tailored to their specific functionality. It is therefore reasonable

to assume that any measurements such as the impedance contributions from the reactance that measures these elements of the cell are more likely to reveal differences between cell types. For cell monolayers adhered to the surface of an electrode the measurement of their capacitive properties is particularly sensitive at high frequencies (Benson, Cramer and Galla, 2013). As an example reactance has been previously been used to characterise differentiating adipose derived stem cells at a frequency of 64*kHz* (Bagnaninchi and Drummond, 2011).

Some studies convert the reactance (Z") into an equivalent capacitance (C) value before presenting its variation in time and frequency (f) in 3 dimensional plots using the equation below (Stolwijk *et al.*, 2015).

$$C = \frac{1}{2\pi f Z"}$$

This manner of data interpretation relies on the assumption that the resistance and capacitance of the cells is in series (Wegener and Sieber, 1996). Converting the reactance in this fashion for the data gathered did not aid in characterisation of the cell types. The inclusion of the frequency in the equation to calculate capacitance results in any 3D plot being dominated by the frequencies at the lower end of the spectrum. Consequently the measured reactance was left unprocessed other than normalisation and forms the bulk of the cell characterisation data presented here. Where required, reference is made to the phase, real and total impedance parameters to explain cellular behaviour and to compare with existing results published in the literature.

A previously used method of cell characterisation utilises the total impedance normalised ratio calculated by dividing the total impedance of a cell covered electrode with the total impedance of the same cell free electrode as defined in Equation 24.

$$Total\ impedance\ normalised\ ratio\ = \frac{|Z|_{Cell\ covered\ electrode}}{|Z|_{Cell\ free\ electrode}}$$

Equation 24

When plotting this ratio for a confluent monolayer across a wide frequency range distinct ratio inflection points are revealed and are stated to be a characteristic impedance signature for that particular cell type. This impedance normalisation technique was introduced by Lind et al, 1990, was used by Shedden, 2008, to characterise cell monolayers adhered to gold electrodes and is the subject of a patent (Shedden *et al.*, 2009). Rümenapp et al, 2009, also used reductions in the same ratio to demonstrate the effect of toxic drugs on murine fibroblasts. As the experiments presented in this study use the same electrode dimensions and cell types as those used by Shedden this method of data presentation is included in the cell characterisation results.

A further stated objective was to investigate if a dysfunctional endothelial monolayer with inhibited gap junctions can be identified using impedance spectroscopy. A measure of an endothelial monolayer's functionality is its ability to form a selective barrier between the blood flow and the artery tissue. Impedance studies that analyse the barrier function of endothelial cell monolayers use the total impedance magnitude as a measure of the barrier properties, with higher values indicating increased barrier function and thus endothelium functionality (Benson, Cramer and Galla, 2013; Wegener and Seebach, 2014; Stolwijk *et al.*, 2015). Therefore results in the endothelial functionality section and the effects of gap junction modulation are presented as total impedance magnitude.

4.8 Electrode repeatability and data normalisation

The variation and distribution in total impedance between electrodes is presented in Figure 4.5.

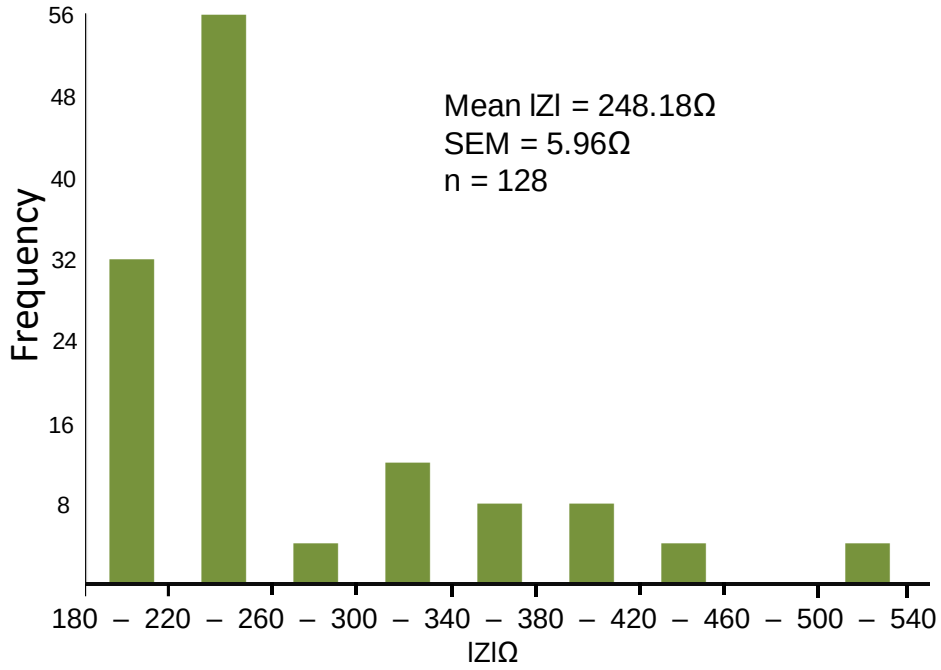

Figure 4.5 - Frequency distribution of |Z| for platinum black cell free electrodes in endothelial cell media. Data derived from first experimental total impedance measurements at 10kHz n =128.

The variation between electrodes in the same chamber and across all experiments shows that there existed an inherent variability in the manufacturing process. Consequently to enable comparison between impedance changes arising from cellular growth over all electrodes a normalisation was applied with all data subtracted from the first impedance measurements immediately after media addition to the chamber. Normalisation of impedance values in this fashion enabling comparison between electrodes and further statistical analysis has been previously reported in other impedance studies (Haas *et al.*, 2010; Benson, Cramer and Galla, 2013; Xu *et al.*, 2016) and is also applied to measurements made using commercially available systems. Normalisation using this first measurement also mimics the practice likely to be used in an in vivo self-reporting stent. A first measurement taken soon after stent expansion would be of bare stent struts in the same manner as with bare electrodes in this study immediately after seeding.

4.9 Control chambers

Control chambers in general exhibited minimal variation in impedance parameters in comparison to cell seeded chambers. Examples of electrode control reactance variation in chambers containing different media are shown in Figure 4.6 a, b and c. For each experimental data set – endothelial cells, HUVECs and smooth muscle cells - the control data was collated from all electrodes and a mean calculated for each frequency at a given time point in the experiment. This data processing method established a base control data set for each test that could be used to compare against the results from cell seeded chambers. The control averaged data is presented in Figure 4.6 d. In presentation alongside results from cell seeded electrodes the collated controls are labelled C and appear as orange lines in the data presented in section 5 (In vitro cell characterisation by impedance spectroscopy). The maximum standard error mean for the control value is stated in the figure caption if error bars are not visible at the scales used. The plots show that control electrodes were stable throughout the duration of the experiments and as will be demonstrated showed minimal reactance variation in comparison to cell seeded electrodes. The HUVEC controls shown in Figure 4.6 c and d experienced a minor fall in reactance 2 hours after media introduction. In the context of reactance variation arising from seeded HUVECs this fall was both in the opposite direction and of a low enough magnitude not to influence any interpretation of the results.

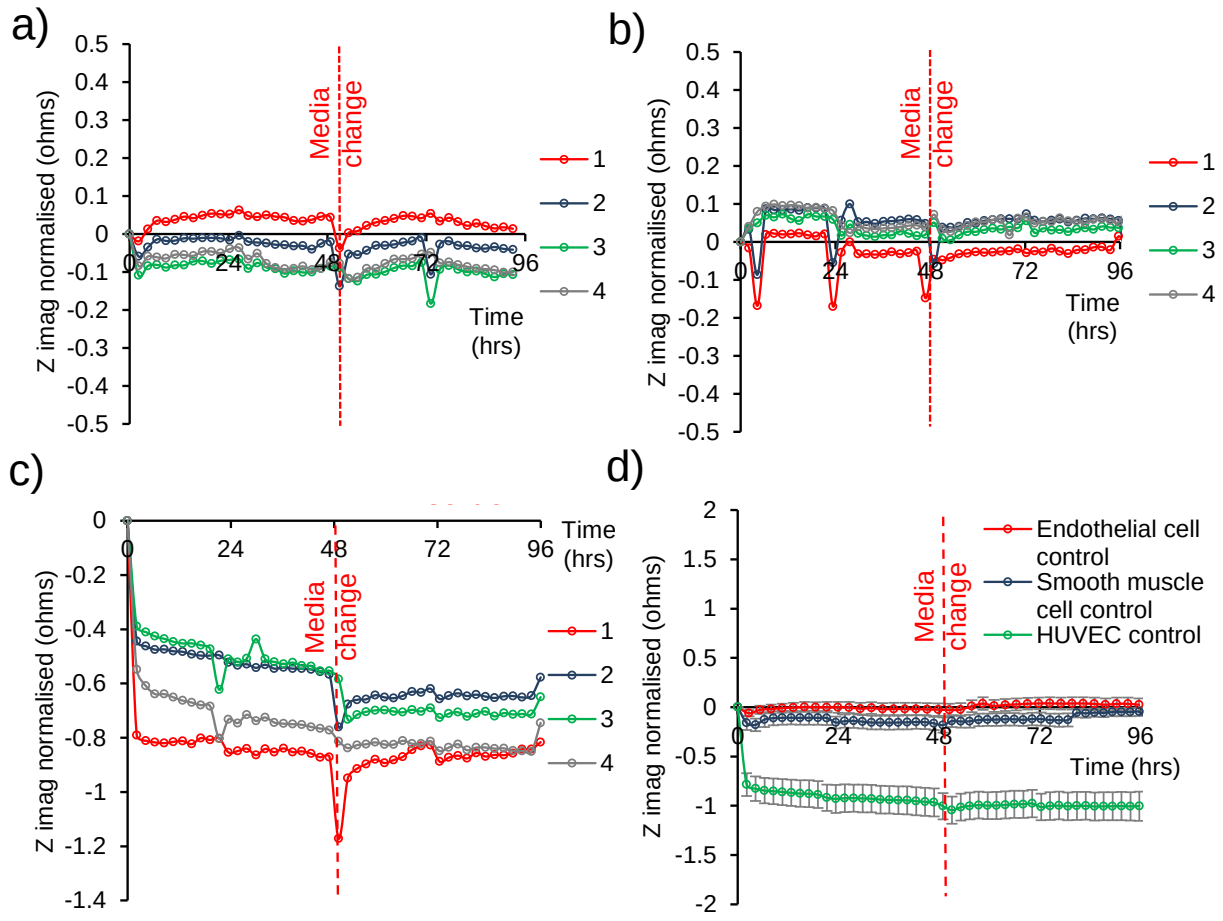

Figure 4.6 - a) b) c) Example control reactance profiles for electrodes 1 to 4 in the same chamber at 10kHz over 96 hours. a) Porcine endothelial media, b) smooth muscle cell media and c) HUVEC media. d) Collated control data for three media types. Error bars represent ± standard error mean, endothelial cell media n=33, smooth muscle cell media n=8, HUVEC media n= 10. Red dashed lines represent media changes.

Media changes often caused a localised fluctuation in reactance that was also observed in cell seeded chambers and can be seen in the region around the red dashed lines in Figure 4.6 a, b and c. These values stabilised back to pre-media change values within 2 impedance measurements at greatest, equating to 4 hours after media changes. Media change impedance fluctuations have been observed in other studies (Bagnaninchi and Drummond, 2011; Park *et al.*, 2011).

4.10 Discussion – System development

A stated study objective was to design and develop an automated in vitro test system that can non-invasively carry out impedance sweeps of cell monolayers. A period of design and development produced the system described in this section. The system had an automated temporal resolution of an impedance sweep of each electrode every 2 hours and represented an approximate tenfold step change increase in comparison to the previous system developed by Shedden, 2008. A time resolution of every 2 hours is typically less than those used in commercial impedance spectroscopy systems, however these are limited in the frequency range that can be applied. The ECIS system sold by Biophysics is limited to 11 frequencies across the range 0.0625*kHz* to 64*kHz* with such a sweep of a single electrode taking 10 seconds (Bagnaninchi and Drummond, 2011). The xCelligence system is capable of measuring a predetermined single frequency only, at a rate of 0.16 seconds per electrode (Grimnes *et al.*, 2015). 2 hours was deemed to be an appropriate balance between time resolution and frequency range and for the experiments conducted in the present study was a suitable match for the pace of proliferating cells. In future experiments the temporal resolution could be increased if required by reducing the number of electrodes being tested and reducing the frequency sweep range.

The application of platinum black coatings to the electrodes reduced their impedance. The measured impedances are comparable to published data for platinum black electrodes (Malleo *et al.*, 2010). Such impedance reductions from plain metal thin film electrodes can be attributed to an increased surface area for current flow owing to the coatings increased roughness (Cote and Gill, 1987; Franks *et al.*, 2005). A higher surface roughness has been considered a desirable attribute for stent surfaces seeking to encourage re-endothelialisation with the previously discussed Yukon Choice Stent being one such example (section 1.29 Conducting polymers).

During the experimental phase chambers were on occasion subject to electrode disconnection and leakages that in some experiments reduced the data set available for analysis. Whilst the issue of leakages was addressed with a design change the fragility of the wire connection to the electrode remained an issue throughout experimentation. Future chamber development work should focus on improving the

connection of strain gauge wire to the electrodes and reducing the time required to manufacture chambers, currently approximately 1.5 hours per chamber. Potential manufacturing efficiency improvements could be made by increasing the number of chambers placed in the sputter coater per coating session and the use of standardised jigs and fixtures for strain gauge wire application.

Throughout the system development stage and the later cell experimentation disconnected electrodes demonstrated clearly distinct impedance measurements with abnormally large magnitudes observed when compared to connected electrodes. When considering the final clinical objective of a self-reporting stent in an in vivo environment any abnormal impedance measurements immediately after deployment of a self-reporting stent could be an indication that a device malfunction such as strut fracture has occurred. Stent strut fracture occurrence rates of 1.5% have been identified and have been proposed as a cause of in stent restenosis (Lee *et al.*, 2009). Any atypical impedance measurements in the immediate post-stenting phase would inform clinicians that further assessment of stent deployment using non-invasive imaging techniques such as angiography is required.

An advantage of the developed system over the one used by Shedden is that it allows in-situ incubator measurements to be made, thereby reducing the probability of infections arising from regular removal of chambers for measurement. Maintaining chambers within the incubator also enables results to be gathered at appropriate atmospheric conditions without disturbance. This advance aligns the system both with commercial impedance spectroscopy equipment and bespoke impedance systems reported in the literature. The use of 8 chambers per test also increased the number of electrodes available for measurement to 32.

Table 4.4 compares specifications for the developed system (highlighted in red) with commercial systems (blue) and other bespoke systems reported in the literature (green). This demonstrates that the key parameters selected are comparable to other impedance spectroscopy systems. A notable exception is the area of the working electrode which is larger than those used in the majority of published systems. As previously stated in section 1.11 (Stent cell regrowth areas), the electrodes in this study have been shown to be comparable in area to the exposed surface of a stent

after implantation, thus measuring monolayers in clinically relevant numbers, a key advantage of the approach developed in this project.

By developing a bespoke system a substantial cost saving was achieved in comparison to commercially available impedance spectroscopy systems. Hardware costs were estimated at £12,000, of which £10,000 is the AutoLab analyser which has additional unused functionality beyond impedance spectroscopy measurements. The use of a more basic impedance analyser would reduce this price further providing a low cost system that could be replicated in other laboratories. It should also be considered that many of the components and equipment used in its construction are standard items commonly available in university laboratories, such as the sputter coater and LabView software. In comparison, an Applied BioPhysics Electric Cell system costs £32,000 with additional consumable costs (Giaever, 2016) and these initial hardware costs are a considerable barrier to researchers wishing to use impedance spectroscopy in their experiments. The developed system is also more flexible than commercial systems, for example allowing selection of the frequency range and excitation voltage. Customisation of the electrode size and shape is also achievable by changing the configuration of the mask used in the sputter coating process.

In summary it can be stated that the developed system fulfils the stated objective in section 1.31 (Study objectives). This enabled impedance spectroscopy measurements to be performed on the cellular regrowth scenarios presented in section 1.30 (Experimental rationale and aims). The results from these cell characterisation experiments are detailed and discussed in the following section 5 (In vitro cell characterisation by impedance spectroscopy).

System	Cell types tested	Excitation signal	Frequency	Electrode configuration	Working electrode area	Electrode substrate	Number of electrodes	Impedance analyser	Multiplexing method
Developed system	Porcine endothelial, smooth muscle, HUVEC	50mV	1*Hz* to 100*kHz*	2 - planar	7mm^2	Platinum black	32	Autolab pgstat302n	ADG732BUZ 32:1 multiplexer chip
Applied BioPhysics ECIS	Numerous in multiple published studies	10mV	0.0625*Hz* to 64*kHz*	2 - planar	0.05 to 3.985mm^2	Gold	8, 16 or 96	Bespoke to system	Bespoke to system
ACEA Xcelligence	Numerous in multiple published studies	Not reported	10*kHz*, 25*kHz* or 50*kHz*	2 - planar	Not reported	Gold	16, 48 or 96	Bespoke to system	Bespoke to system
(Venkatanarayanan, Keyes and Forster, 2013)	Ovarian cancer line SKOV3	25mV	0.1*Hz* to 100*KHz*	3 - planar	Not reported	Platinum	Not reported	CH Instruments 760D	None-Manual
(Karimullah *et al.*, 2013)	MDCK	80mV	20 *Hz* to 1M*Hz*	2 - planar	0.05mm^2	PEDOT	32	QuadTech 1420	ADG732BUZ 32:1 multiplexer chip
(Reitinger *et al.*, 2012)	Human mesenchymal stem	35mV	10*kHz*	2 - planar	3.6mm^2	Gold	12	Bespoke wireless system	ADG732BUZ 32:1 multiplexer chip
(Haas *et al.*, 2010)	Rat smooth muscle	10mV	500*Hz* to 5M*Hz*	2 - planar	Not reported	Gold	96	Agilent 4294A	Bespoke IMAT software
(Hildebrandt *et al.*, 2010)	Human mesenchymal stem	10mV	100*Hz* to 1M*Hz*	2 - planar	0.785mm^2	Platinum	16	Solartron 1260	Solartron multiplexing system
(Newbold *et al.*, 2010b)	MDCK, Mouse macrophage	0.5mA	Not reported	2 - planar	0.05mm^2	Gold	96	Tektronix, THS710	None-Manual
(Smith, Thomas and Cornish, 2007)	Bovine erythrocytes	Not reported	3*kHz* to 1M*Hz*	2 - planar	0.785mm^2	Not reported	25	Impedimed, SFB7	ADG732BUZ 32:1 multiplexer chip
(DePaola *et al.*, 2001)	Bovine aortic endothelial	1μA	4*kHz*	2 - planar	0.05mm^2	Gold	8	Not reported	PC

Table 4.4 – Specification comparison of the developed impedance spectroscopy system (red) with commercially available systems (blue) and published bespoke impedance spectroscopy systems (green).

5 In vitro cell characterisation by impedance spectroscopy

5.1 Introduction

The permanent implantation of a stent into a coronary artery is a common method for ameliorating vessel narrowing arising from atherosclerosis. Following the procedure the nature of cellular regrowth over a stent strut and the surrounding artery tissue is crucial to the long term success of the device. Optimal arterial wall healing is characterised by the rapid reformation of an endothelial cell monolayer over the exposed stent struts, thereby reducing the risk of thrombosis. The proliferation of smooth muscle cells, which in extensive layers can lead to narrowing of the vessel lumen, is an alternative cellular regrowth scenario. Current methods of re-endothelialisation diagnosis are limited by low resolutions or the requirement for invasive catheterisation (see sections 1.7 to 1.8 Re-endothelialisation and re-stenosis diagnosis). An implanted stent that is capable of using impedance spectroscopy to monitor re-endothelialisation and re-stenosis would therefore be of great potential benefit to clinicians and patients. The overall aim of the work detailed in this chapter was to investigate if vascular cell types could be non-invasively characterised in populations that are clinically relevant for a conceptual self-reporting stent. The specific study objectives targeted at achieving this aim are listed below.

- Investigate the feasibility of using impedance spectroscopy to non-invasively characterise the following vascular cell types in clinically relevant populations.
    - Porcine smooth muscle cells
    - Porcine endothelial cells
    - Human Umbilical Vein Cells (HUVECs)
- Investigate the feasibility of using impedance spectroscopy to non-invasively characterise a direct co-culture of porcine endothelial and smooth muscle cells in clinically relevant populations.

The general methods used in the pursuit of these objectives have been described in detail in section 3.6 (Cellular experimentation). Briefly cells were seeded into customised electrode chambers and grown to create a confluent, clinically relevant population. The automated impedance spectroscopy system previously detailed in section 4 (System development) was used to perform regular impedance measurements of these cell cultures. The results from each cell type and the co-culture experimentation are presented separately before results from equivalent circuit modelling are reported.

5.2 Results

5.2.1 Cell characterisation by immunofluorescence

The primary porcine cells obtained using the isolation methods described in section 3.5 (Cell culture) were characterised by immunofluorescence. Images from a representative sample of fluorescently stained cells are shown in Figure 5.1. Endothelial cell isolation procedure was verified through the positive staining for Von Willebrand factor (vWF) as shown in Figure 5.1a. Smooth muscle cell isolation was confirmed with the expression of smooth muscle alpha actin as shown in Figure 5.1b. Negative controls were used with the staining of smooth muscle cells for vWF and endothelial cells for smooth muscle alpha actin and images from a representative sample of negatively stained cells are shown in Figure 5.1c and Figure 5.1d.

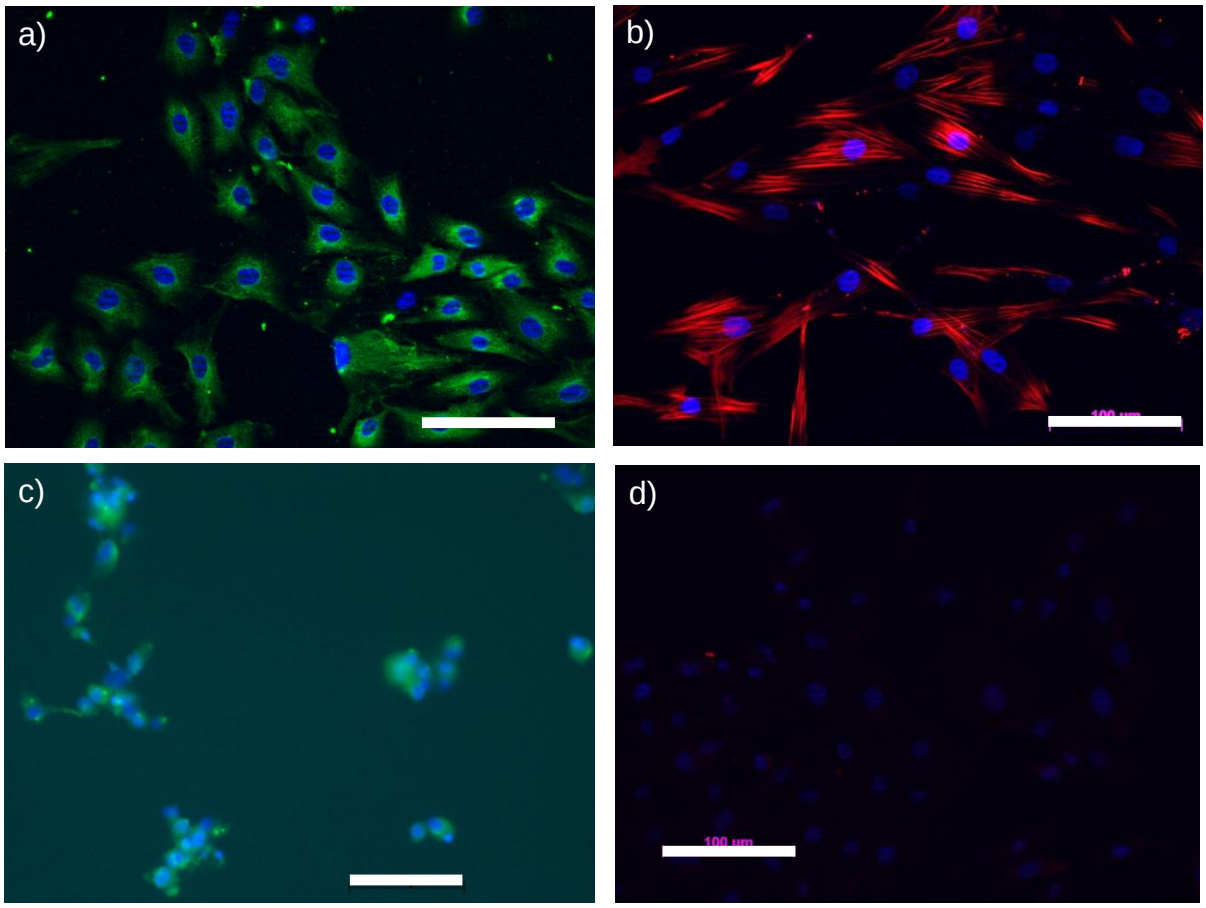

Figure 5.1 - Cell isolation characterisation. a) Endothelial cells positively staining for the marker Von Willebrand factor (green). b) Smooth muscle cells positively staining for smooth muscle alpha actin (red). Negative control, minimal Von Willebrand staining of c) smooth muscle cells (green). d) Minimal smooth muscle alpha actin (red) staining of endothelial cells. White scale bars are 100µm, all nuclei stained with DAPI (blue). Images were taken of cells at passage 2 and are representative of 15 observations. White scale bars are 100µm, all nuclei stained with DAPI (blue).

In addition to cell characterisation using fluorescent staining, the use of light microscopy revealed typical cobblestone morphologies for endothelial cells whilst smooth muscle cells demonstrated an elongated spindle appearance that when confluent aligned to appear as the hill and valley morphology reported in the literature (Figure 5.2) (Heydarkhan-Hagvall *et al.*, 2003).

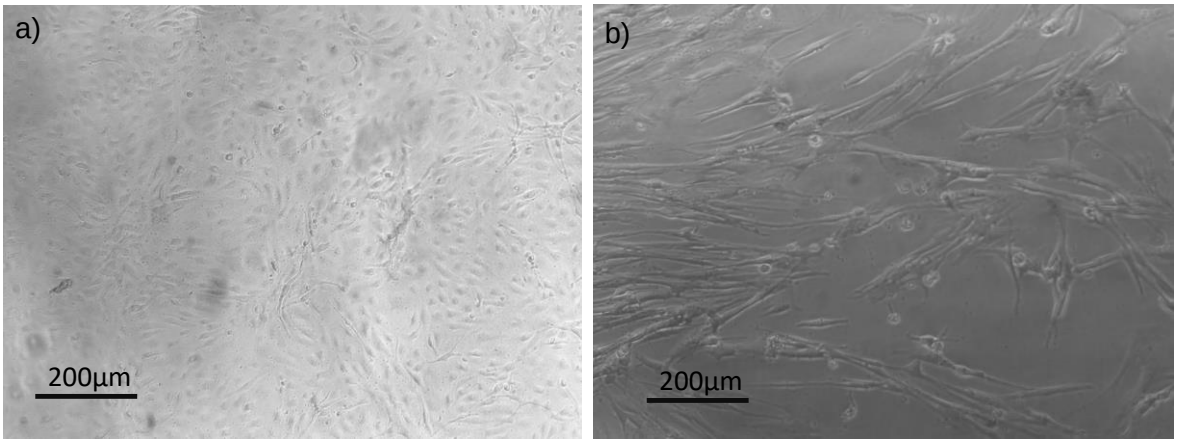

Figure 5.2 - Typical morphologies for cobblestone appearance endothelial cells (a) and elongated spindle shape smooth muscle cells (b).

5.2.2 Impedance based characterisation of endothelial cells

The introduction section of this thesis highlights that the nature of cellular growth over stent struts is critical to the long term success of the implant. Three cellular growth scenarios were discussed and in vitro models for each proposed as described in section 1.30 (Experimental rationale). The re-endothelialisation model adopted in the present study comprised the seeding of endothelial cells over thin film metal electrodes and monitoring their impedance profile as they proliferate towards confluency and beyond. In total 3 independent endothelial experiments were performed with a different porcine cell line used for each. Within each endothelial experiment the 8 available chambers were divided into those seeded with endothelial cells and media only cell-free controls. Within each chamber there are 4 electrode pairs providing 4 replicate impedance measurements. Experiment duration was 96 hours to prevent contact inhibition and cell detachment from occurring. Table 5.1 summarises the key parameters for each experiment.

Experiment	Duration	Passage no.	Seeding density (x 10^4 cells per cm^2)	Estimated time of 100% confluence	Chamber allocation
1	96 hours	P3	4.4 to 5.0	48 - 72 hours	4 cell seeded, 4 control
2	96 hours	P2	6.1 to 8.2	72 - 96 hours	4 cell seeded, 4 control
3	96 hours	P4	6.3 to 7.3	48 - 72 hours	7 cell seeded, 1 unused

Table 5.1 – Summary of porcine endothelial cell experiments. 100% Confluence estimation was assessed using light microscopy observations.

After removals for disconnections as detailed in system development section 4.6 (Experimental data inclusion), the data set for endothelial cells comprises 39 electrodes and control chambers with endothelial cell media totalling 33 electrodes. It is the electrodes that are referred to as n numbers in the presented data. This manner of data presentation mimics the convention in published impedance spectroscopy studies using commercial systems where the data from individual electrode pairs are averaged before further analysis.

Upon seeding, cells were observed to settle within the first 24 hours and then proliferate. No difference in cell morphology and growth rates was observed using light microscopy between those cells that settled on the platinum black electrodes and those on the plastic culture plate surface. Presentation of the entire reactance data in the 1*Hz* to 100*kHz* range can be attained with a 3D plot where time (hours) is the horizontal X axis, frequency (*Hz*) the horizontal Y axis and normalised reactance (Ω) the vertical Z axis. 3D Presentation of impedance parameter variation for cells adhered to a planar electrode has been previously reported although not for the reactance alone (Arndt *et al.*, 2004; Wegener and Seebach, 2014). A representative 3D reactance profile for endothelial cells seeded onto an electrode in the entire measured range of 1*Hz* to 100*kHz* range is shown in Figure 5.3a alongside data from the same electrode but presented in a reduced frequency range of 1*kHz* to 100*kHz*. As can be seen in Figure 5.3a, a 3D reactance plot that includes the full frequency range of 1*Hz* to 100*kHz* is dominated by high reactance values at frequencies below 1*kHz*, masking any variation at higher frequencies. More definition of the reactance can be attained by narrowing the 3D plot to the 1*kHz* to100*kHz* range as shown in Figure 5.3b. Furthermore as previously stated in section 4.2 (System characterisation), it is common for impedance studies to report findings in the *kHz* region and it this frequency range that the cell characterisation results will focus on.

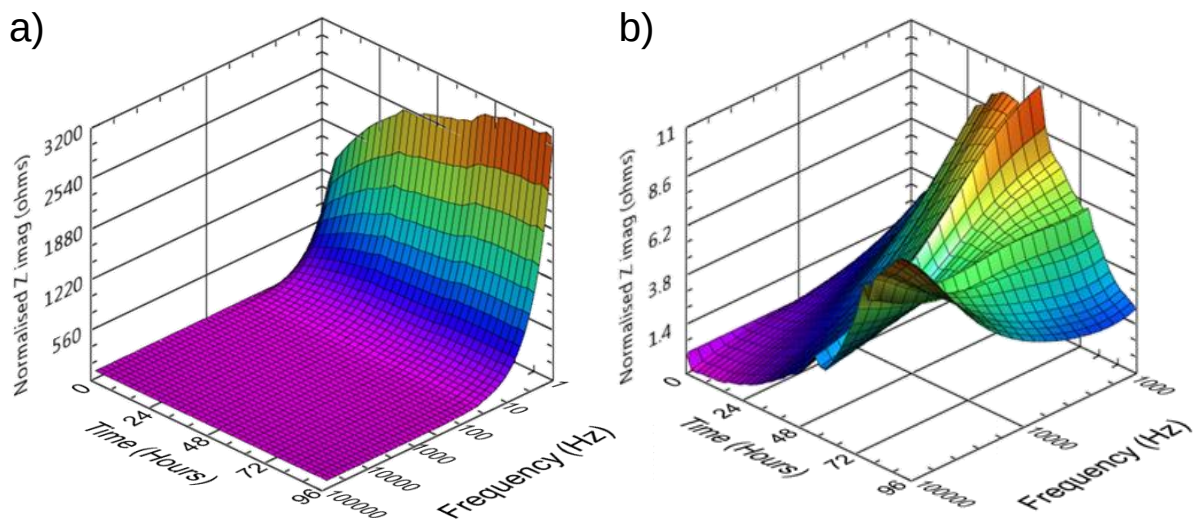

Figure 5.3 - Representative 3D reactance profiles for an electrode from experiment 1, seeded with porcine endothelial cells. a) Entire measured frequency range of 1Hz to 100kHz and b) reduced high frequency range of 1kHz to 100kHz .

The reactance was selected as the impedance parameter for cell characterisation purposes. As previously discussed in section 4.7 (Impedance parameter selection) published studies often convert the reactance into a capacitance value, however the inclusion of the frequency into the capacitance calculation equation can obscure data, particularly at high frequencies due to the large magnitudes. In the context of the experimental data presented here this can be observed by comparing the 3D profiles for reactance (Figure 5.4a) and capacitance (Figure 5.4b) from the same endothelial cell seeded electrode. It can be seen that the use of reactance preserves definition of profile features, especially in the 10*kHz* to 100*kHz* frequency range. This definition is important as multiple published impedance studies have selected specific frequencies within this range for data presentation, as shown previously in section 4.2 (System characterisation).

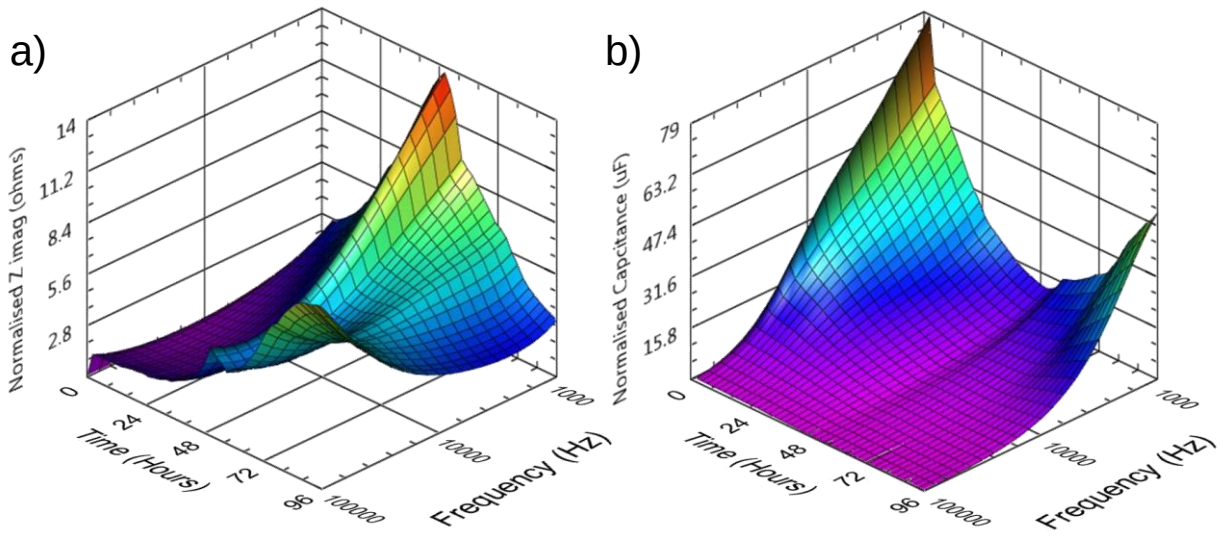

Figure 5.4 - Representative 3D profiles for an electrode from experiment 1, seeded with porcine endothelial cells range of 1kHz to 100kHz. a) Reactance and b) converted capacitance.

Representative reactance profiles from electrodes seeded with endothelial cells are presented in Figure 5.5 in the 1*kHz* to 100*kHz* frequency range along with light microscopy images of endothelial cell coverage of the electrode tips after 48 hours of culture.

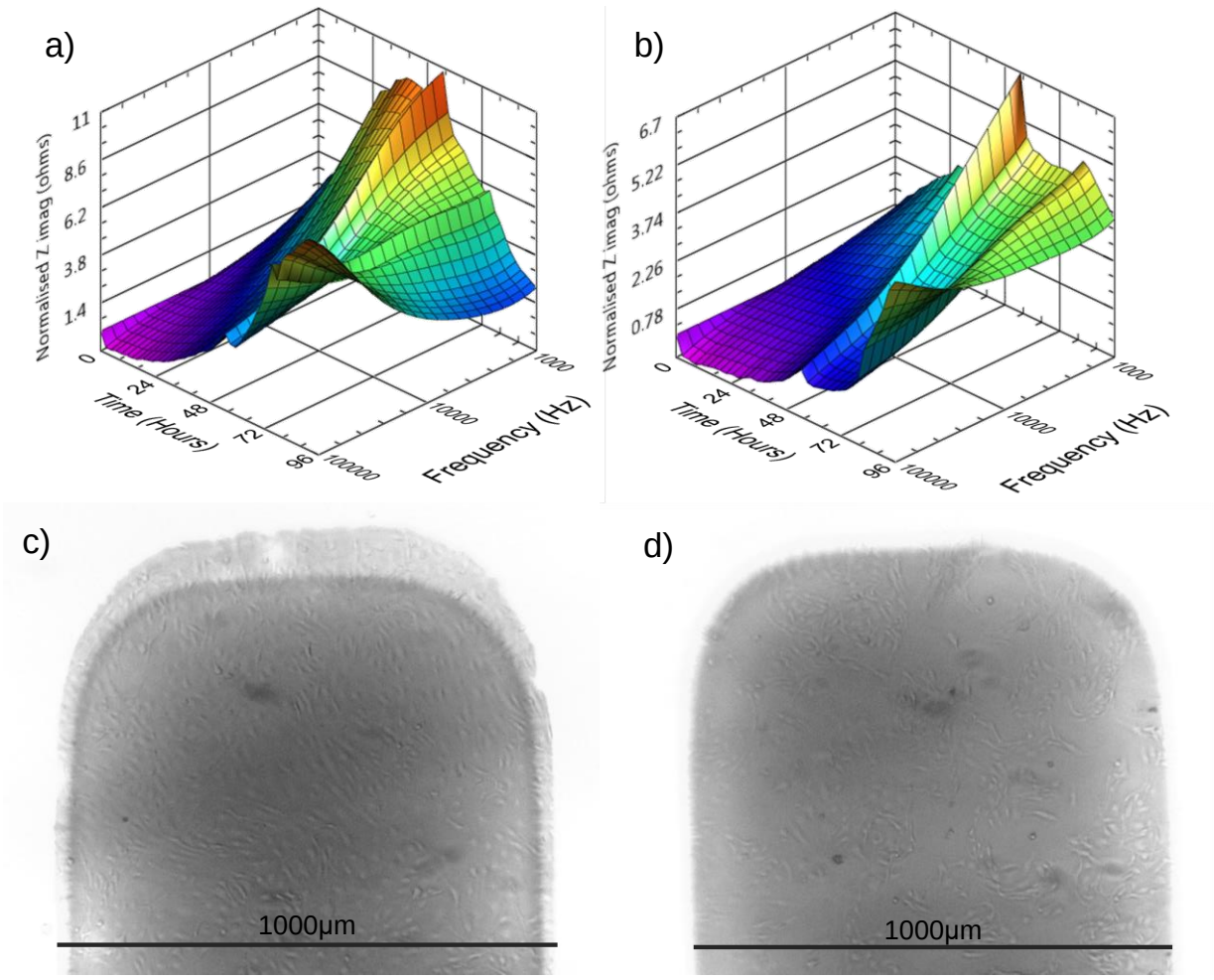

Figure 5.5 – a) and b) representative 3D reactance profiles of electrodes from endothelial cell seeded chambers in the frequency range 1kHz to 100kHz. Corresponding light microscopy images of cell coverage 48 hours from seeding for the same electrodes from experiment 1 (c) and experiment 2 (d). Scale provided by known electrode width of 1000µm and scale bar.

These Figure 5.5 plots indicate that the reactance has elevations and declines that are not uniform across all frequencies. Following cell seeding reactance is observed to climb but with differing rates, with lower frequencies showing greater rates in comparison to higher frequencies. Comparison between the two profiles shows that the reactance elevations and subsequent declines occurred at a faster rate for the electrode in Figure 5.5a and correlated with a higher observed cell growth rate. This can be seen in the 48 hour light microscopy tip images from the same electrodes shown below the plots where Figure 5.5c has attained a higher cell density in comparison to Figure 5.5d. Following confluence reactance declines first at low frequency (1*kHz*) and then progressively through to higher frequencies creating

distinctive endothelial cell double reactance peaks. The peaks are compressed or extended in the time domain for slow or rapidly proliferating cells respectively. Evidence for this can be seen in rapidly proliferating cells with a high level of electrode coverage shown after 48 hours in Figure 5.5c and the corresponding compressed 3D reactance profile in Figure 5.5a. In comparison slowly proliferating cells shown after 48 hours in Figure 5.5d had low electrode coverage causing the corresponding 3D reactance profile in Figure 5.5b to be extended, with electrode reactance at 1*kHz* only declining in the final 12 hours of the experiment.

The mean 3D reactance profile for all electrodes seeded with endothelial cells is shown in Figure 5.6a and also the reactance variation for all control chambers, (Figure 5.6b). The reactance Z axis scale is displayed as the same for both plots to allow comparison.

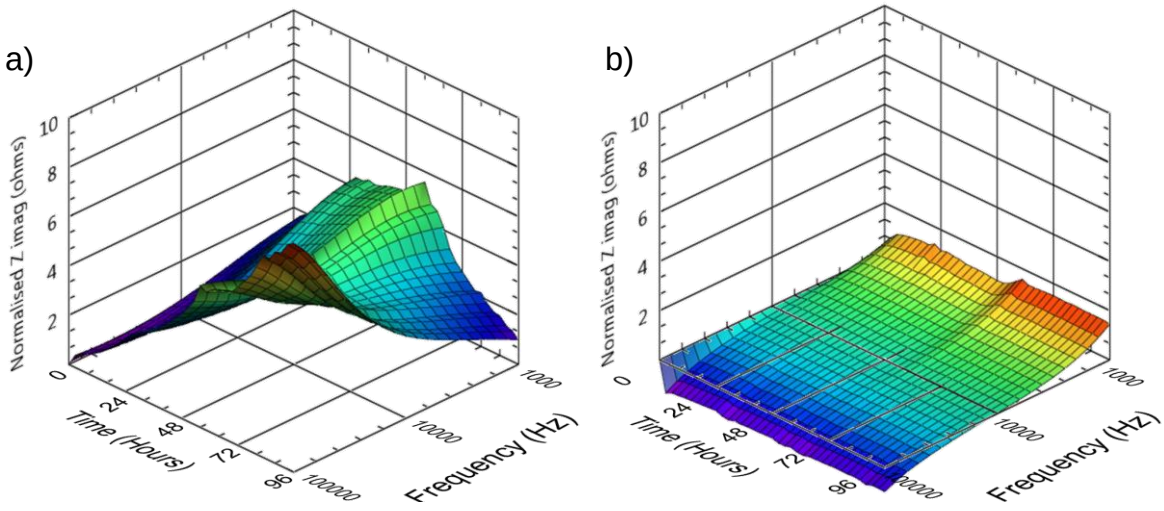

Figure 5.6 - Mean 3D reactance (z axis) variation over time (x axis) and across the frequency range1kHz to 100kHz (y axis). a) Porcine endothelial cell seeded electrodes (n=39, max standard error mean 0.91) and b) control electrodes (n=33, max standard error mean 0.40).

Further presentation of reactance variation can be attained by selecting a single frequency and displayed as an XY 2D plot with time as the X axis and the Y axis as normalised reactance. This manner of data presentation is the most commonly used method in the literature for depicting impedance parameter variation with time. The frequency of 10*kHz* has previously been used in multiple studies as detailed in section 4.2 (System characterisation), with the most relevant study being the in vivo 10*kHz* measurement of arterial lesions (Süselbeck, Thielecke, Köchlin, *et al.*, 2005), and represents the median of the 1*kHz* to 100*kHz* range presented in the 3D plots. Figure 5.7a shows the reactance profile of a representative chamber at 10*kHz* with accompanying light microscopy images demonstrating the proliferation of the cells over an electrode over time.

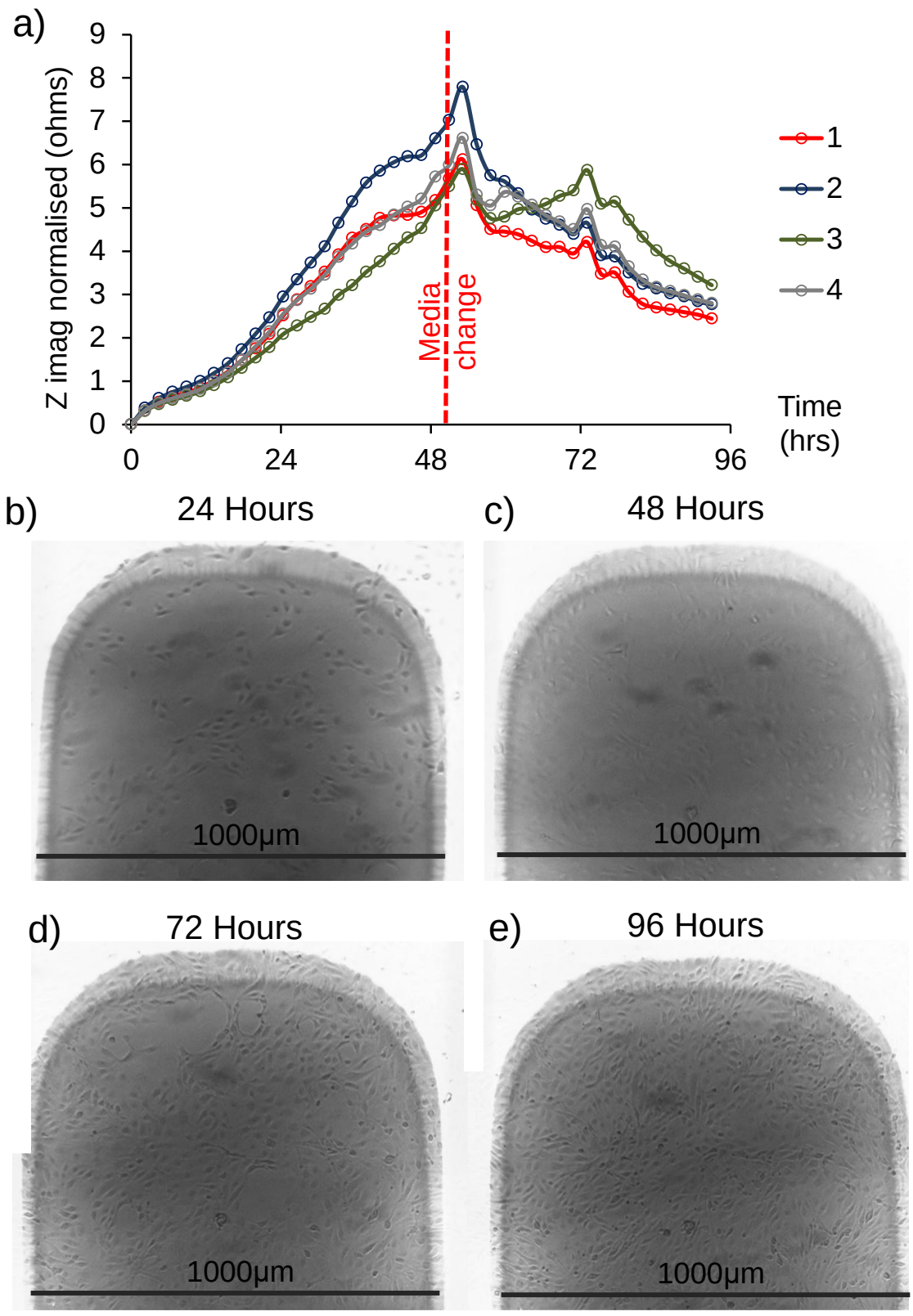

Figure 5.7 – a) 10kHz reactance profiles of electrodes 1 to 4 from a representative chamber seeded with porcine endothelial cells from experiment 1. Red line indicates media change. b), c), d), e) Periodic light microscopy images of electrode 3 showing cell proliferation progression. Scale bars are 1000µm.

The mean reactance profile for 10*kHz* for all electrodes measured is depicted in Figure 5.8 along with the mean for control values. The point of media change varied between experiments and is presented as time range band. It can be seen that the normalised reactance increases up to a peak value of approximately 5Ω after two days cell growth, before a gradual decay occurs to a final value of just over 3Ω in the remaining two days.

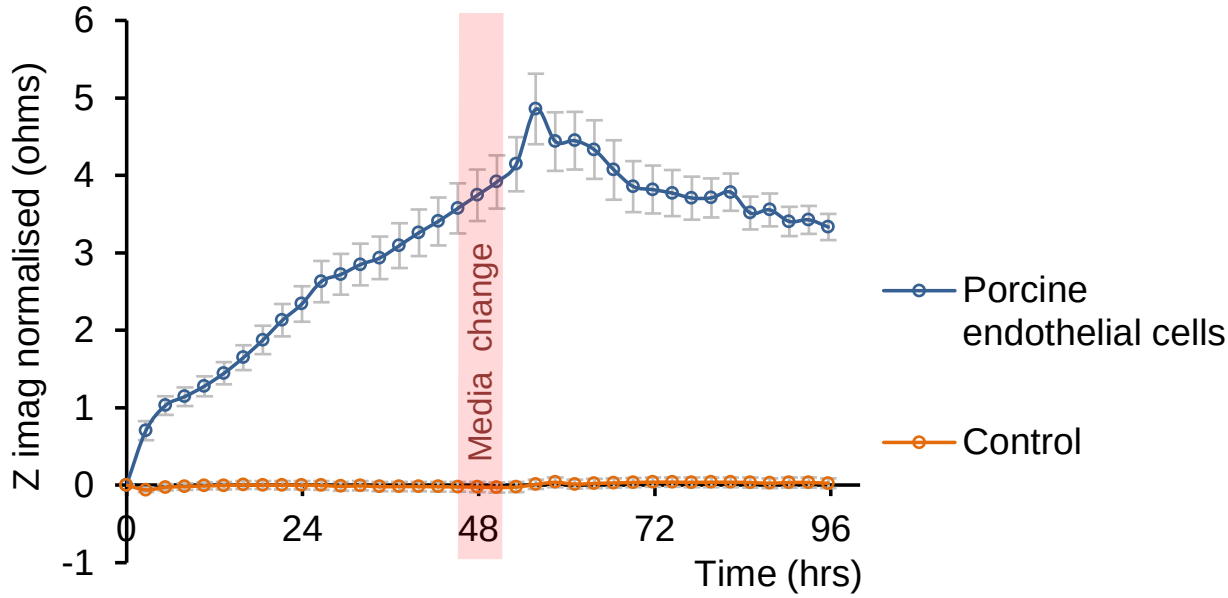

Figure 5.8 - Mean porcine endothelial cell reactance profile at 10kHz for all electrodes (n=39) and cell free control electrodes (n=33). Error bars are ± SEM with max control SEM = 0.04. Red band indicates region where media changes occurred.

An additional method of cell characterisation is the use of a total impedance ratio as previously detailed in section 4.7 (Impedance parameter selection). The mean ratio variation for porcine endothelial cells at 48 and 96 hours is depicted in Figure 5.9. The data shows a total impedance ratio inflection at 1260*Hz* at 96 hours where all electrodes in the data set had attained confluence.

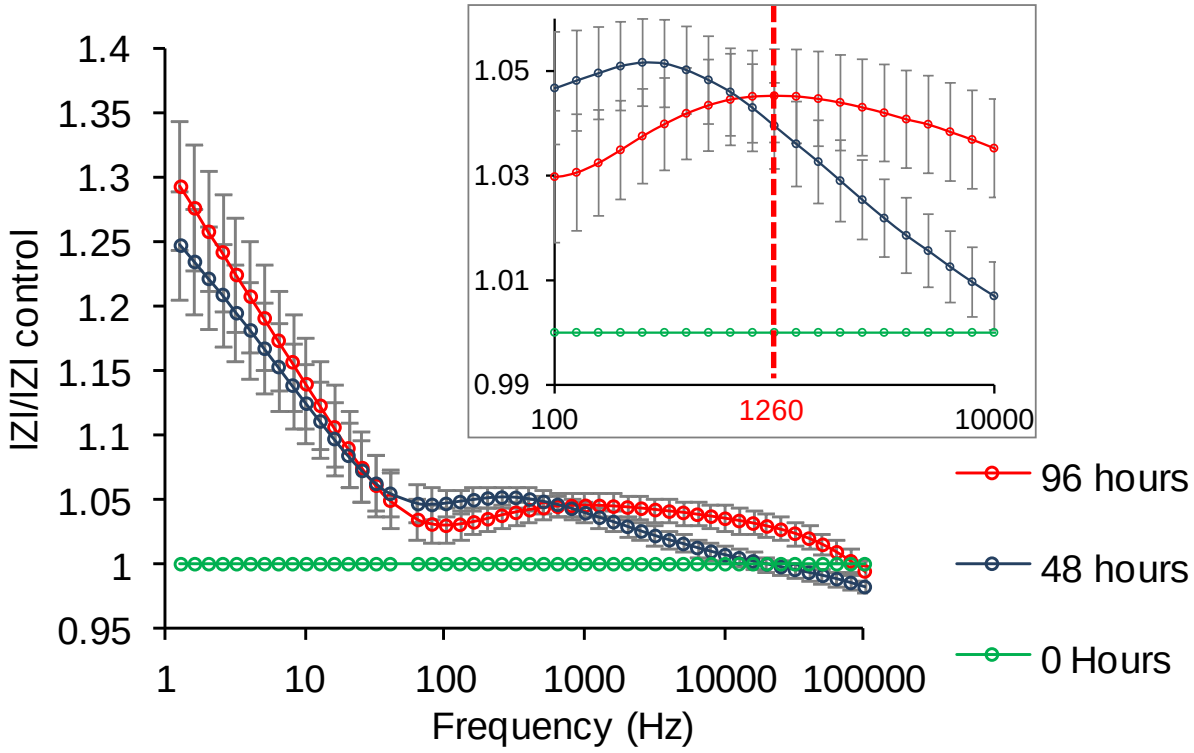

Figure 5.9 - Total impedance ratio for porcine endothelial cells seeded onto electrodes at 0, 48 and 96 hours. Insert shows reduced frequency range and an inflection frequency of 1260Hz. Error bars are ± SEM, n = 39.

5.2.3 Impedance based characterisation of smooth muscle cells

One source of smooth muscle cells was used to perform experimentation detailed in this section. 8 chambers were divided into 4 cell seeded and 4 media only cell-free controls with an experiment duration of 244 hours. After removals for disconnections as detailed in system development section 4.6 (Experimental data inclusion), the data set for seeded smooth muscle cells totalled 8 electrodes and 8 control electrodes with smooth muscle cell media only. Table 5.2 summarises the experimental parameters for the seeding of smooth muscle cells into chambers. Seeding densities were lower than endothelial cells as guided by the literature reflecting the size difference between the two cell types (Balasubramanian *et al.*, 2008).

SMC growth duration	244 hours
Seeding density (x 10^4 cells per cm^2)	2.6 to 3.1
Passage no.	P3
Estimated final confluency	100%
Chamber allocation	4 cell seeded, 4 control

Table 5.2 - Smooth muscle cell experiment parameter summary.

Presentation of the reactance variation over the entire frequency range for a representative smooth muscle cell seeded electrode is shown in the 3D plot in Figure 5.10a. It can be seen that the profile is dominated by the high reactance measurements in the 1*Hz* to 1*kHz* low frequency range. A comparison with the corresponding endothelial cell profile across the same frequency range shown in Figure 5.3a shows a similar profile. The 3D profile of the same smooth muscle cell seeded electrode but limited to the high frequency 1*kHz* to 100*kHz* range is depicted in Figure 5.10b and shows a greater level of reactance definition. As will be discussed further in later sections, this profile is distinct from endothelial cell seeded electrodes. These figures justify selection of a 1*kHz* to 100*kHz* range for presenting 3D reactance profiles.

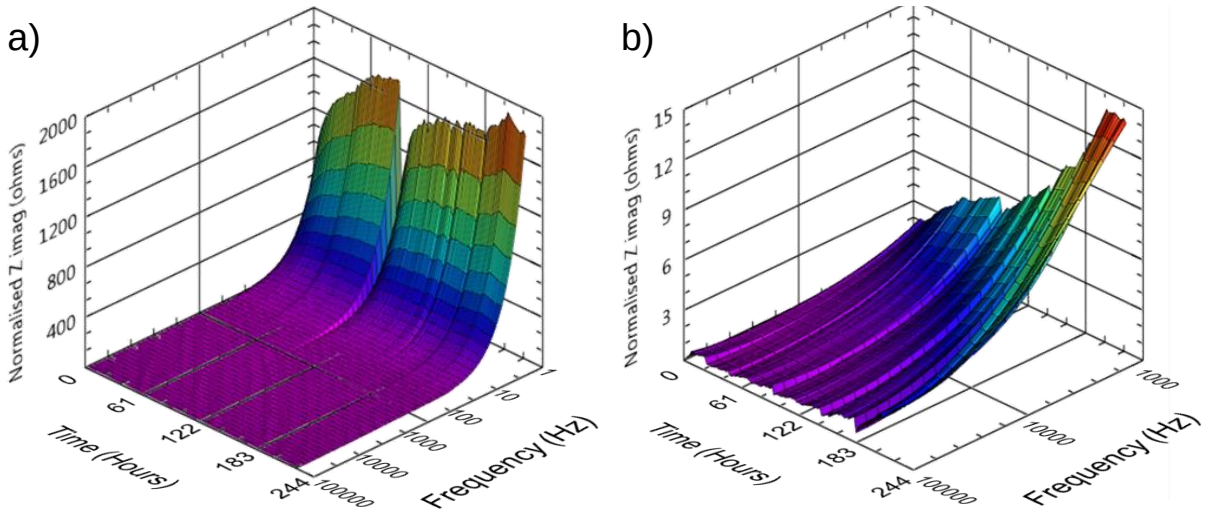

Figure 5.10 - Representative 3D reactance profiles for an electrode seeded with porcine smooth muscle cells. a) Entire measured frequency range of 1Hz to 100kHz and b) reduced high frequency range of 1kHz to 100kHz .

Mean 3D representation of the reactance in the frequency range 1*kHz* to 100*kHz* for electrodes seeded with smooth muscle cells and control electrodes with smooth muscle cell media only are depicted in Figure 5.11. The reactance Z axis scale is displayed as the same for both plots to allow comparison. The plots reveal that the magnitude of the reactance change for cell seeded electrodes (Figure 5.11a) is greatest at the lowest frequencies and minimal at the highest measured frequencies. The proliferation of smooth muscle cells did not produce dual reactance peaks in the same manner as endothelial cells. Control electrodes in smooth muscle cell media display minimal reactance variation in comparison to cell seeded electrodes.

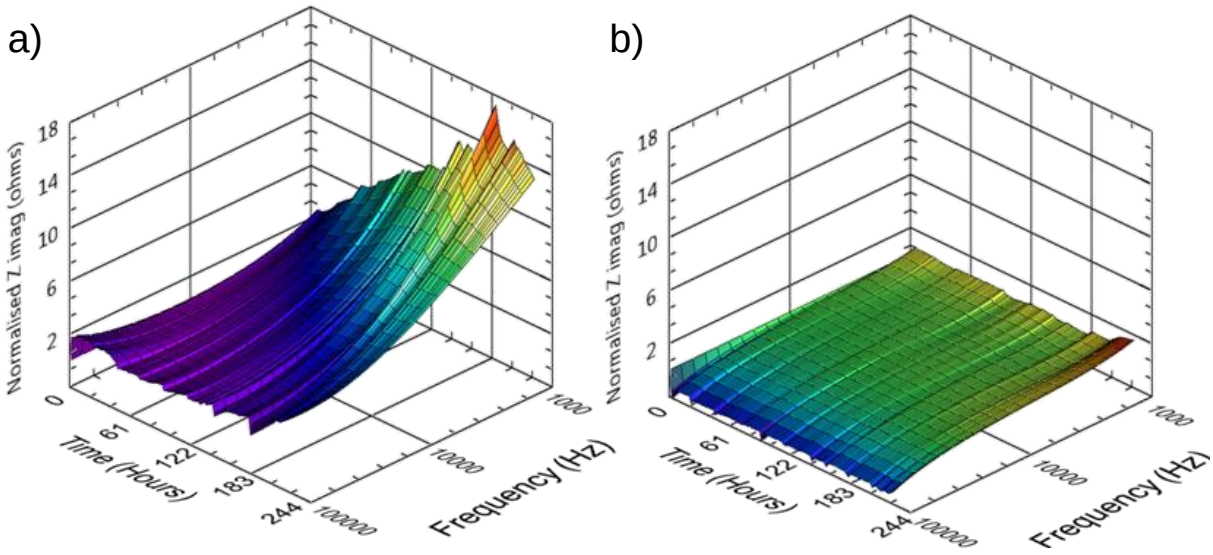

Figure 5.11 - Mean 3D reactance (z axis) variation over time (x axis) and across the frequency range1kHz to 100kHz (y axis). a) Smooth muscle cell seeded electrodes (n=8, max standard error mean 1.8606) and b) control electrodes (n=8, max standard error mean 0.778).

Selection of the frequency of 10*kHz* for 2D representation of smooth muscle cell data can be justified by reference to the literature, with previously published in vivo impedance measurement of smooth muscle cell laden stenotic lesions using this frequency (Süselbeck et al., 2005). Electrode time – reactance profiles at 10*kHz* from a representative chamber are shown in Figure 5.12. The data and images show the correlation between cell coverage of the electrode and the elevation in reactance as the cells proliferate to confluence, at which point the experiment was stopped to prevent contact inhibition from arising.

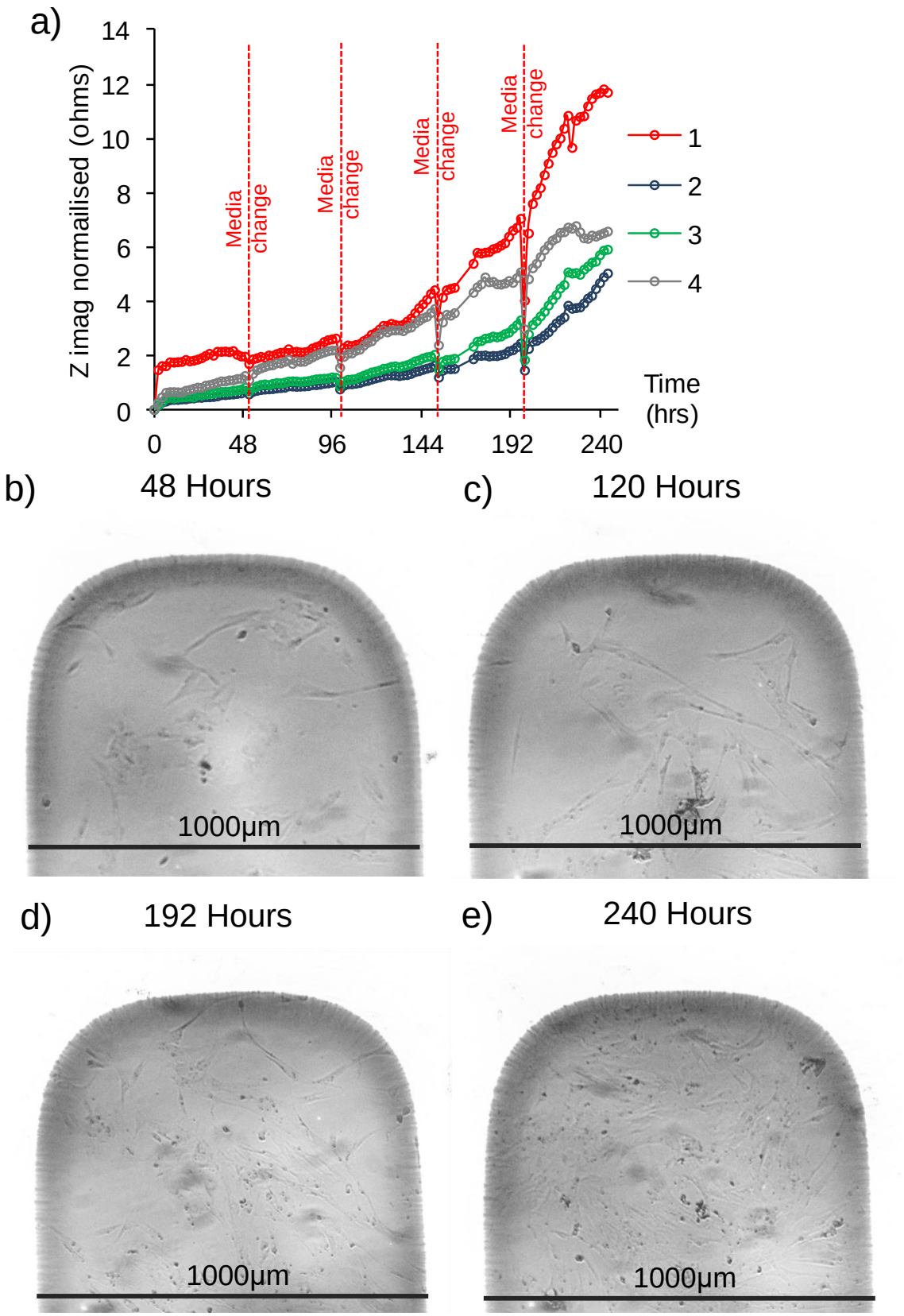

Figure 5.12 - a) 10kHz reactance profiles of electrodes 1 to 4 from a representative chamber seeded with porcine smooth muscle cells. Red lines indicate media changes. b), c), d), e) Periodic light microscopy images of electrode 3 showing cell proliferation progression. Scale bars are 1000µm.

Presentation of mean reactance variation at 10*kHz* can be seen in Figure 5.13. This demonstrates a rise in reactance as the cells settle and proliferate. Control electrodes did not experience the same elevations in reactance.

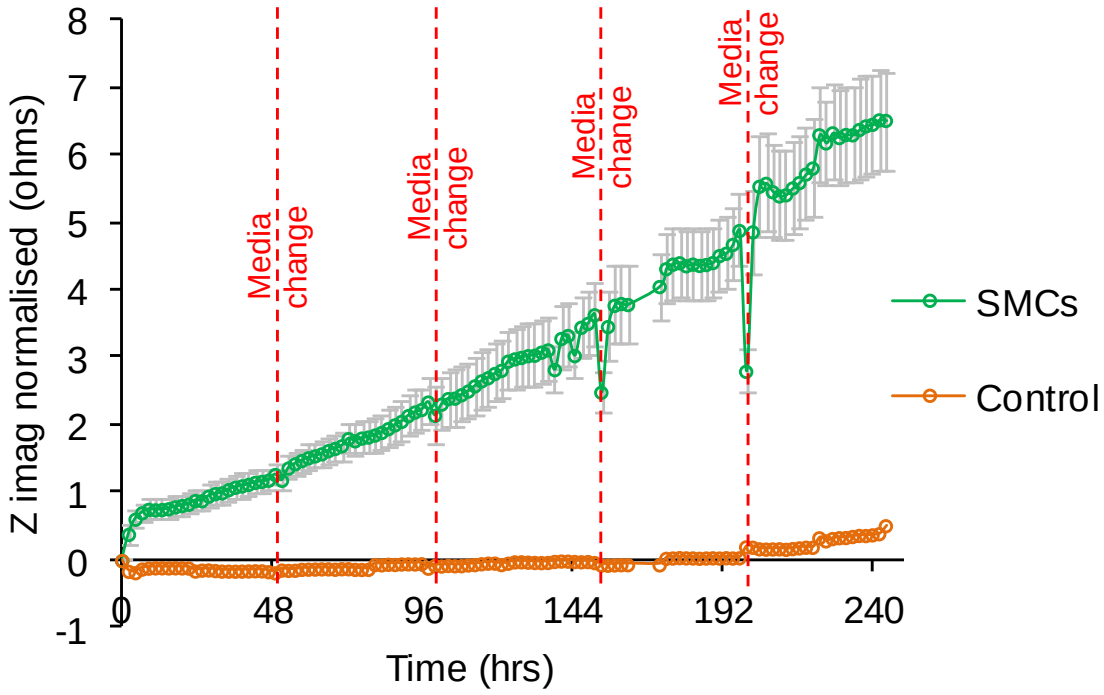

Figure 5.13 - Mean porcine smooth muscle cell reactance profile at 10kHz for all electrodes (n=8) and cell free control electrodes (n=8). Error bars are ± SEM with max control SEM = 0.74. Dashed red lines indicates region where media changes occurred.

The total impedance ratio previously shown for endothelial cells is depicted for smooth muscle cells in Figure 5.14. An inflection ratio at 40*HZ* can be seen.

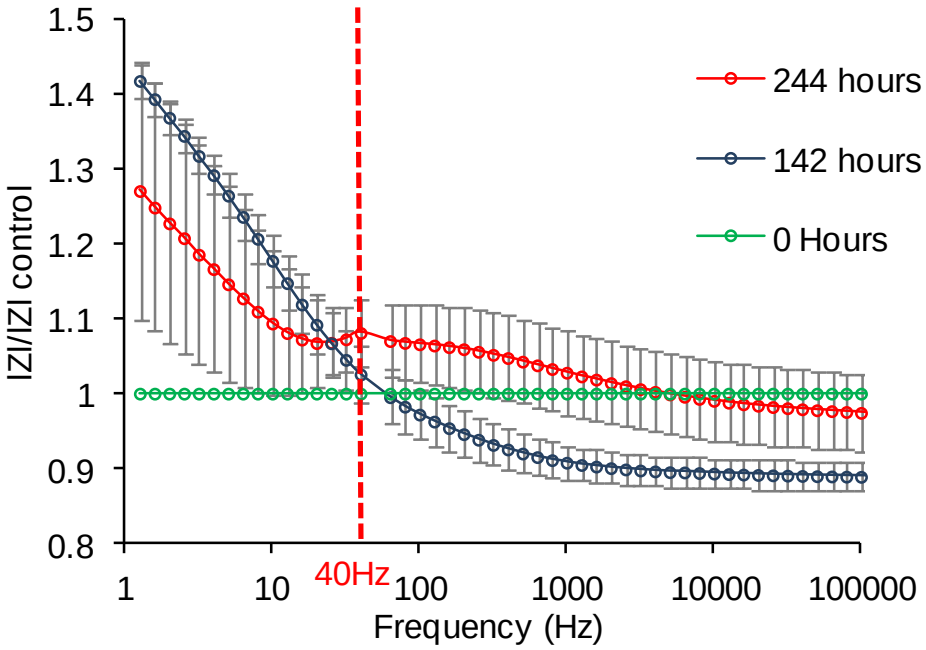

Figure 5.14 - Total impedance ratio for smooth muscle cells seeded onto electrodes at 0, 143 and 244 hours with a confluency inflection frequency of 40Hz. Error bars are ± SEM, n = 8.

5.2.4 Impedance-based characterisation of endothelial-smooth muscle cell co-cultures

As indicated in the materials and methods section a range of media and experimental durations were attempted for the co-culture of smooth muscle cells and endothelial cells until a final successful co-culture model was attained with confluency over the electrodes. Table 5.3 summarises the duration of the phases, media formulations used and observations from the light microscopy images. Supplementary observations have also been provided from the time lapse videos where available.

Experiment number	SMC seeding density ($x10^4$)	SMC passage no.	Growth phase duration	Growth phase observations	Quiescent media formulation	Quiescing phase duration	Quiescing phase observations	EC seeding density ($x10^4$)	EC and SMC cell line match?	CC media formulation	CC phase duration	Co-culture phase observations
Preliminary test A, 4 culture dishes only	NA	P4	120 hours	Low proliferation rate of cells, grown to 40% confluency before quiescing	F12, 0% FCS	72 hours	Cells appeared healthy with retention of SMC morphology	3.9 to 5.9	No	5 parts F12, 1 part EC media	192 hours	EC confluency observed 144 hours after seeding. Cell sheet detachment in 2 dishes at 168 hours and 192 hours post EC seeding.
Preliminary test B, 4 culture dishes only	1.2	P4	144 hours	Settled cells attaining 40-50% confluency before quiecsing.	F12, 0% FCS	96 hours	Cells appeared healthy with retention of SMC morphology.	5.8	No	5 parts F12, 1 part EC media	168 hours	ECs settle but proliferate slowly over SMCs. Test stopped prior to EC confluence to prevent cell sheet detachment.
Chamber experiment 1	1.6 to 2.1	P2	24 hours	Grown to 30% confluency before quiescing	SMC media, 0% FCS	72 hours	Cell death obsevered through quiescing phase, test aborted. Software crash between 48 and 67 hours - no data available.	NA	NA	NA	NA	NA
Chamber experiment 2	3.8	P3	48 hours	Few cells settled, short spindle morphology. Test aborted.	NA	NA	NA	NA	NA	NA	NA	NA
Chamber experient 3	3.8	P4	72 hours	Settled cells attaining 50-60% confluency before quiecsing.	F12, 0% FCS	48 hours	Cell death obsevered immediately after addition of quiescent media	4.5	No	5 parts F12, 1 part EC media	48 hours	ECs failed to settle and also died.
Chamber experiment 4	4.0	P2	24 hours	Settled cells attaining 25-35% confluency before quiecsing.	SMC media, 0.5% FCS	48 hours	Time lapse observations shows initial balling up of cells which then recover spindle SMC morphology after 8 hours.	6.0	Yes	5 parts F12, 1 part EC media	48 hours	Introduction of ECs causes death of the majority of SMCs. ECs themselves fail to settle and die.
Chamber experiment 5	3.8	P4	115 hours	Settled cells attaining 60-70% confluency before quiecsing.	SMC media, 0.5% FCS	28 hours	Cell death observed in C5 only. Time lapse observations shows initial balling up of cells which then recover spindle SMC morphology after 8 hours.	9.0	No	SMC media, 0.5% FCS	96 hours	ECs grown in SMC media, 0.5% FCS for 24 hours prior to seeding. Confluency of EC layers observed 48 hours after seeding.

Table 5.3 - Co-culture experimentation parameter summary and observations.

Two preliminary tests were conducted in 4 cell culture dishes which aimed to establish an outline procedure and assess if co-culture was feasible using the primary porcine cell lines available. In both tests the smooth muscle cells appeared healthy exhibiting spindle shape morphology. The quiescing phase with serum free F12 media did not result in any noticeable cell death or change in the cells morphology (Figure 5.15a). Following seeding of endothelial cells they proliferated and covered the smooth muscles (Figure 5.15d). Different endothelial growth rates were observed with test A attaining confluence 144 hours after seeding. However in 2 out of the 4 plates the cell sheet became detached from the plastic. This provided an indication that co-culture should not be continued once endothelial cell confluency is believed to have occurred. Cell sheet detachment was not observed in any of the subsequent experiments. Light microscopy revealed that within the early stages of co-culture identification of individual cell types from their morphology was possible in areas where both cell types were not layered on top of one another (Figure 5.15b). However later stage co-culture results in a cross hatch appearance as shown in Figure 5.15d, where identification of individual cells and their shape is difficult due to layering. This is distinct from the smooth muscle hill and valley and endothelial cobblestone morphologies seen when cultured in isolation.

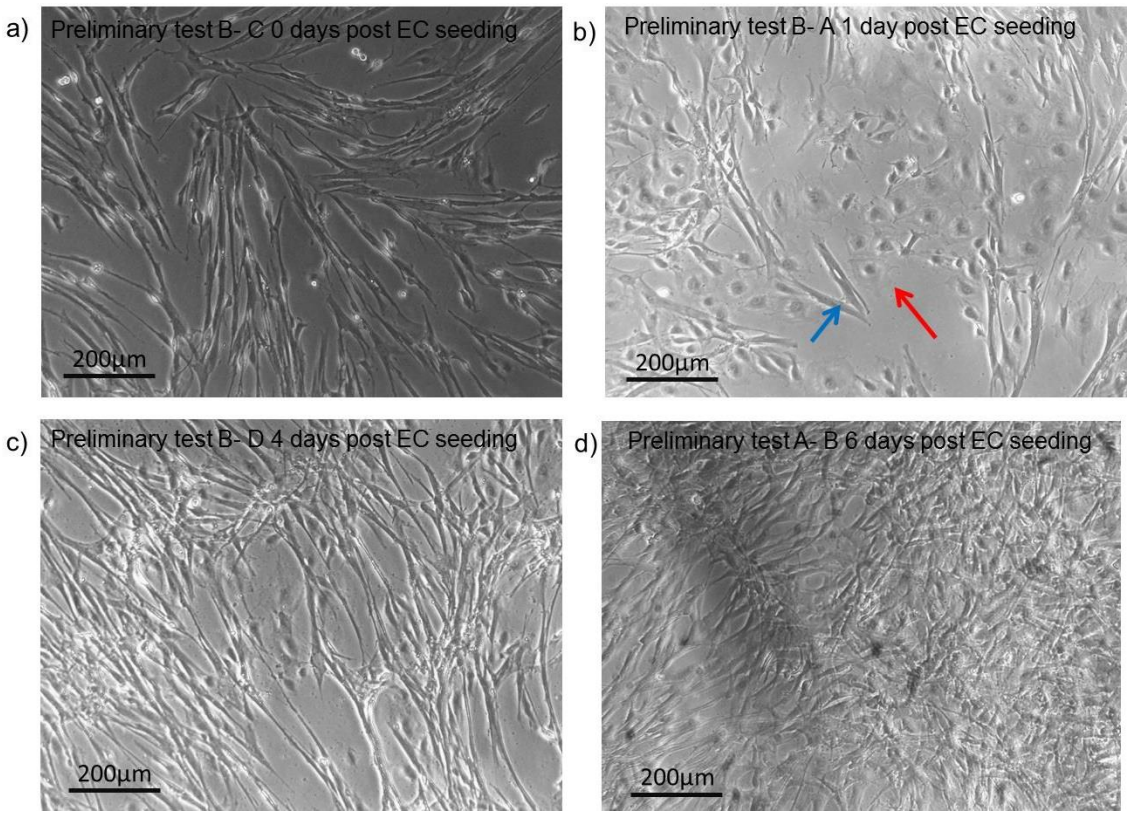

Figure 5.15 – Light microscopy images from preliminary co-culture tests at various time stages. a) Post quiescent phase smooth muscle cells immediately prior to endothelial cell seeding. b) Co-culture 1 day after endothelial cell seeding with smooth muscle cell (blue arrow) and endothelial cell (red arrow) morphologies visible. c) Co-culture 4 days after endothelial seeding, identification of cell morphologies becomes more difficult as cells layer over one another. d) Co-culture 6 days after endothelial cell seeding displaying a cross-hatch pattern.

Plates from test B were stained for von-Wildebrand Factor (vWF) and with DAPI. vWF staining technique is often used in the published literature as a specific marker for endothelial cells. The objective in staining a co-culture model with for vWF was to identify those cells that were endothelial cells in the cell layer cells and it was assumed that unstained cells would be smooth muscle cells. Images from the staining are depicted in Figure 5.16.

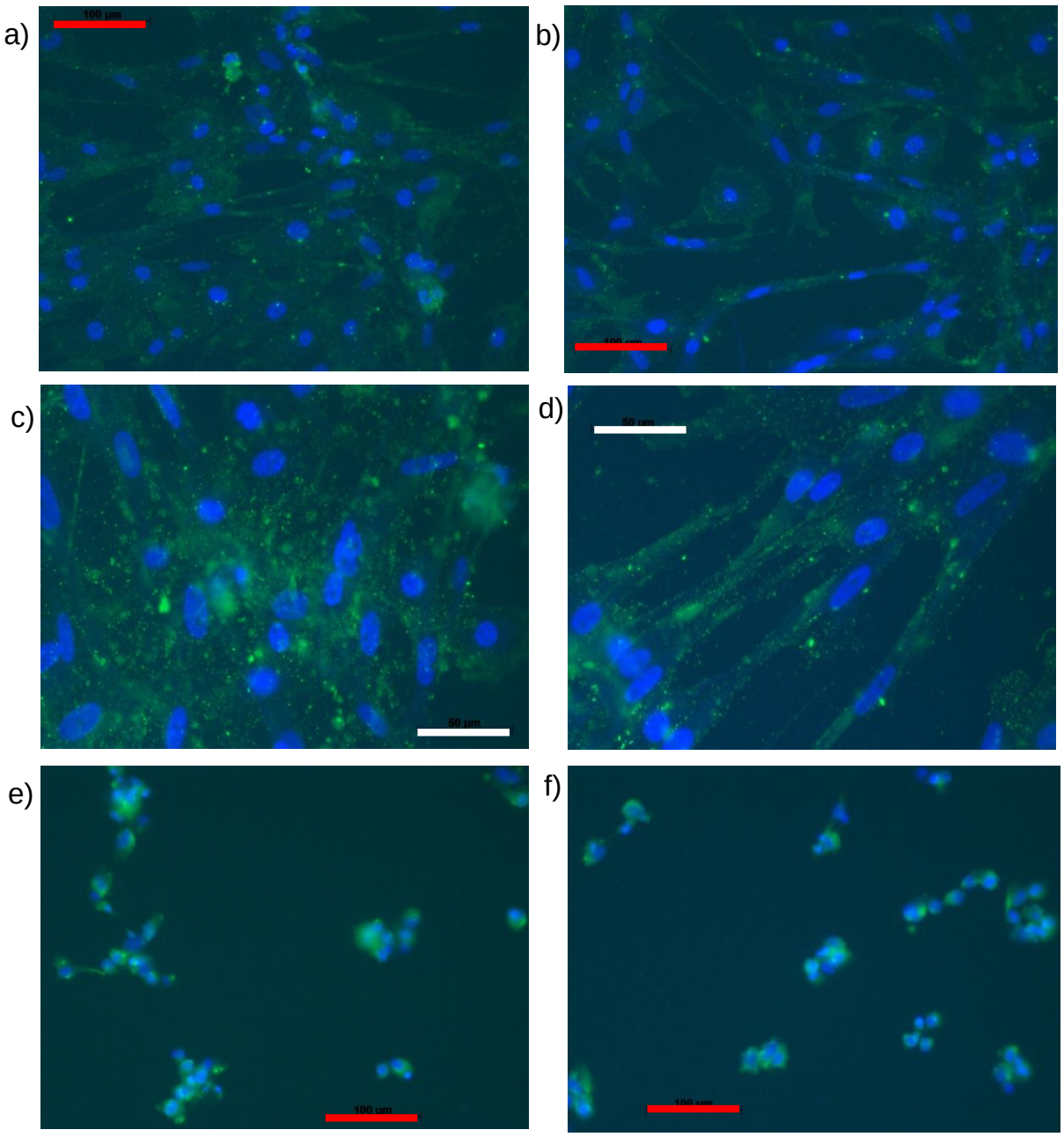

Figure 5.16 – a) to d) Von-Willebrand and DAPI stained co-culture from preliminary test 2,. e) and f) control images of cells from smooth muscle cell isolation procedure cultured alone Von-Willebrand and DAPI stained. White scale bars 50µm red scale bars 100µm.

The stained images show that all visible cells have stained positively for vWF with each DAPI nucleus surrounded by green. The image shown in Figure 5.16d shows cells with an aligned spindle shape morphology typical of smooth muscle cells but positively stained with vWF. These results provided a guide that the use of vWF staining alone is not suitable for smooth muscle and endothelial cell co-culture when attempting to identify between the two cell types. α smooth muscle actin used to

stain co-cultures in experiments presented later on in this section was not available for these preliminary tests.

Due to co-culture tests involving both endothelial and smooth muscle cells it was necessary to change to media of different compositions at specific points in the experiments. Examples of cell free control chambers where such changes were performed are shown in the presented impedance profiles as coloured dashed lines with descriptions in the accompanying caption. Across all of the co-culture experiments these changes caused low variations in the control profiles, indicating that the reactance of the electrodes was not heavily influenced by the media composition.

Following preliminary testing, cells were seeded into chambers containing platinum black electrodes for impedance testing. The first 2 experiments in chambers with impedance measurements failed to achieve the later stages of co-culture, with the smooth muscle cells failing to settle or dying throughout the quiescing phase. Consequently these tests were not seeded with endothelial cells and were aborted.

Experiment 3 also showed a high level of smooth muscle cell death following the addition of quiescent media. This is evident in the microscopy images in Figure 5.17, which depict an electrode with healthy smooth muscle cells (Figure 5.17a) at 48 hours that subsequently die in the early stages of the quiescing phase (Figure 5.17b) . However an attempt was still made to seed endothelial cells into these chambers. These failed to settle and can be seen in the cell death debris shown in Figure 5.17c. These observations were also confirmed with the time lapse microscopy video and can be found in the electronic appendix referenced file name Co-culture expt 3.

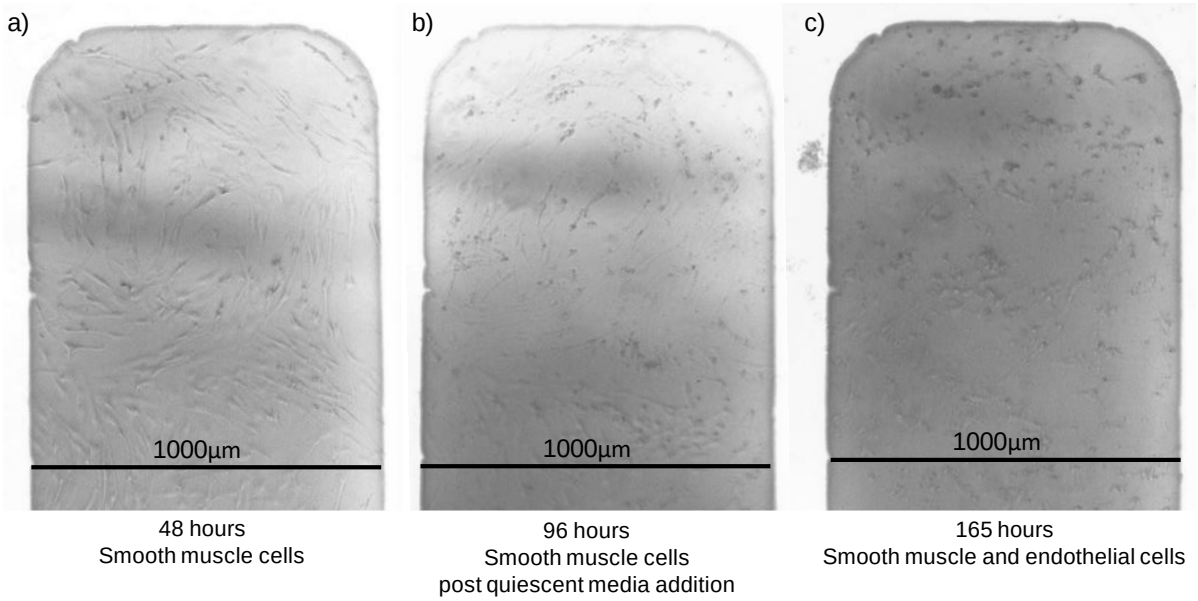

Figure 5.17 – Light microscopy electrode tip images from co-culture experiment 3. Scale provided by known electrode width of 1000µm.

The observed behaviour in experiment 3 was correlated with the reactance profile shown in Figure 5.18. The effect of the addition of the quiescent media in comparison to control profiles can be seen with a sharp drop in reactance following quiescent media addition (dashed green line) indicating that cell death occurred rapidly. Endothelial cell introduction (dashed blue line) caused an initial elevation in reactance followed by a decline, agreeing with light microscopy and time lapse observations.

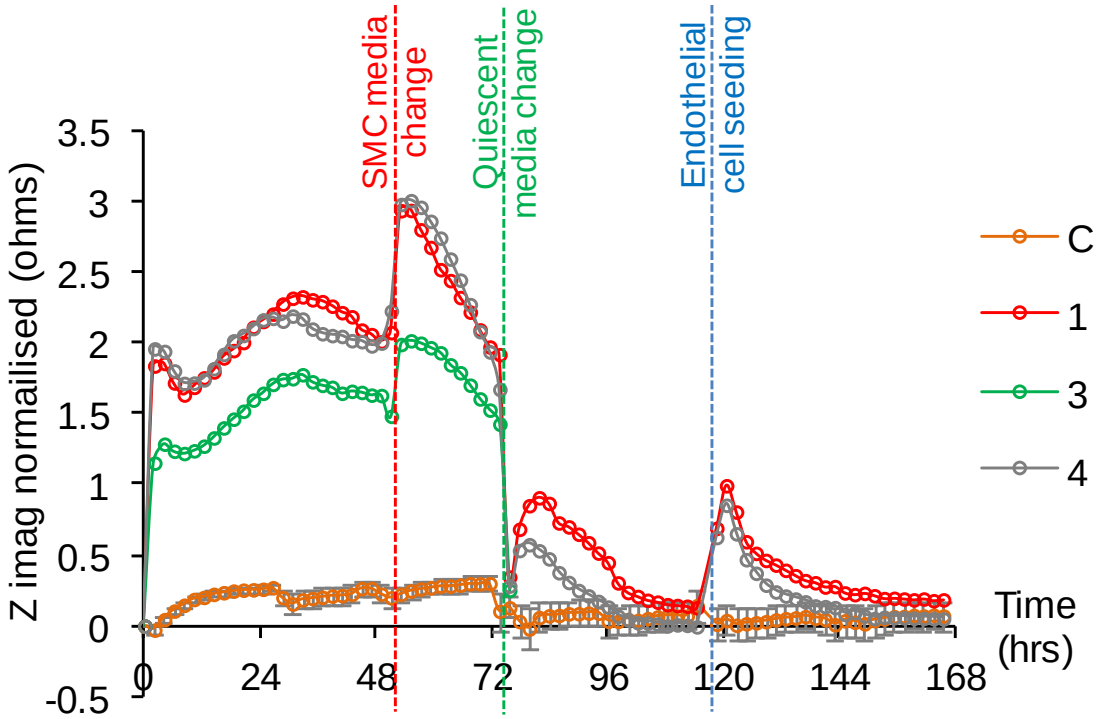

Figure 5.18 – 10kHz electrode reactance profiles from a representative chamber in co-culture experiment 3. Red line indicates smooth muscle cell media change, green line quiescing media introduction (F12, 0% FCS) and blue line endothelial cell seeding with co-culture media (5 parts F12, 1 part porcine endothelial cell media). Combined experiment 3 control data shown in orange (C), error bars are ± SEM, n=12.

A change was made to the quiescing phase in experiment 4 with the use of smooth muscle cell media supplemented with 0.5% level of FCS rather than the 0% used in previous experiments. This modification was made to prevent the death of smooth muscle cells seen on the addition of serum free media formulations. Furthermore, low serum levels are also reported in the literature as a quiescent step (Stone *et al.*, 2013). Smooth muscle cells survived the quiescing phase in experiment 4 although the inspection of the time lapse video showed the cells changing into a more spheroid shape in the first 4 hours, losing their normal elongated spindle morphology. 8 hours into the quiescing phase the cells had recovered and returned to their normal shape. The time-lapse video can be found in the electronic appendix, file reference Co-culture expt 4. Comparison with the impedance data in Figure 5.20 shows a drop in reactance and a subsequent recovery followed by a steady decline. The seeding of

endothelial cells into the chambers over the layer of smooth cells caused the death and detachment of the majority of the smooth muscle cells and can be best seen in the time-lapse video in the electronic appendix, file reference Co-culture expt 4. Pre and post endothelial cell seeding light microscopy images are also shown in Figure 5.19. Those cells that survived this early co-culture phase grouped together in star shape clusters that shrunk in size as more cell death occurred, leaving larger and larger patches of the electrode uncovered. From the time lapse microscopy there was also a reduction in the motility of these remaining cells. In addition to seeding of the endothelial cells at this point a change to culture media was also used which comprised 5 parts F12 and 1 part endothelial cell growth media. Therefore this media contained no FCS but a low amount (0.38%) of low serum growth supplement that forms a constituent of the endothelial cell media. Although this media formulation was successfully used in the co-culture phase during the preliminary testing stage it did not translate to a successful endothelial seeding phases in tests carried out on electrodes.

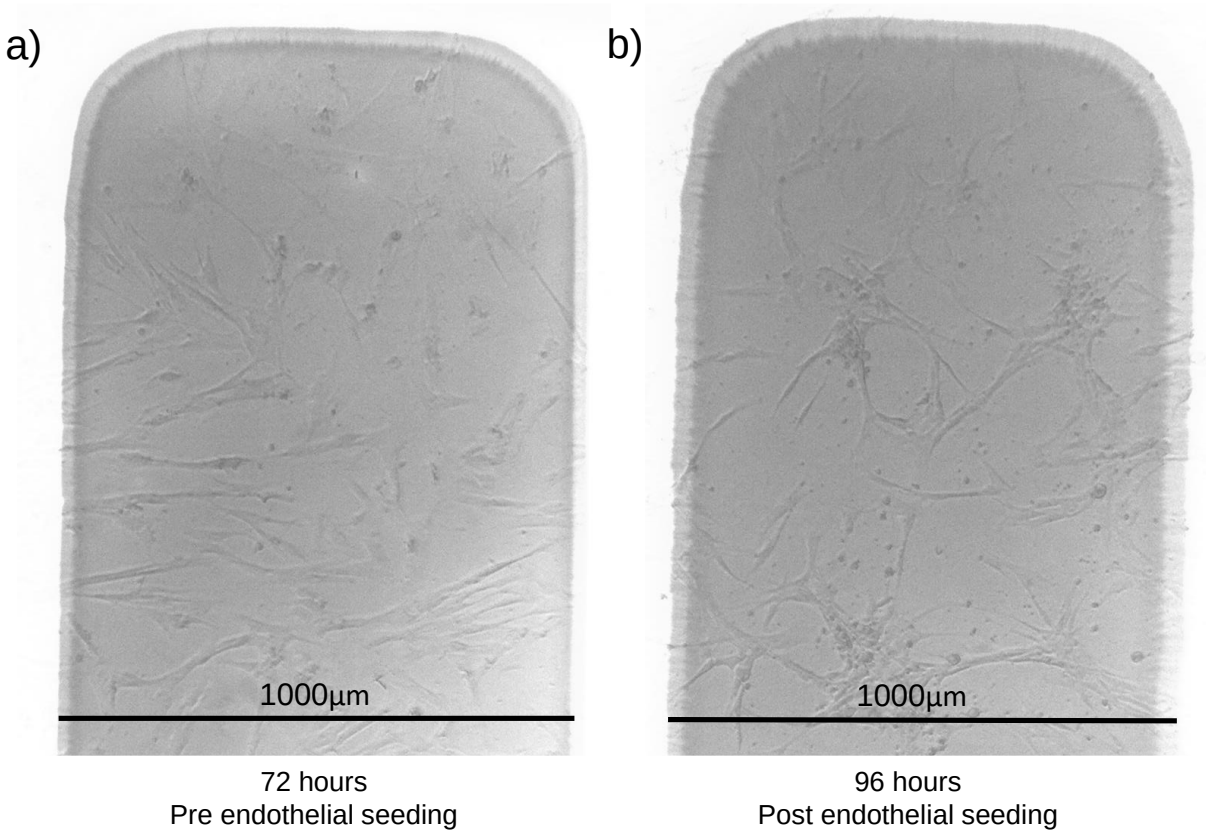

Figure 5.19 – Light microscopy of electrode tip images from co-culture test 4 showing pre and post endothelial seeding cell coverage. Scale provided by known electrode width of 1000µm.

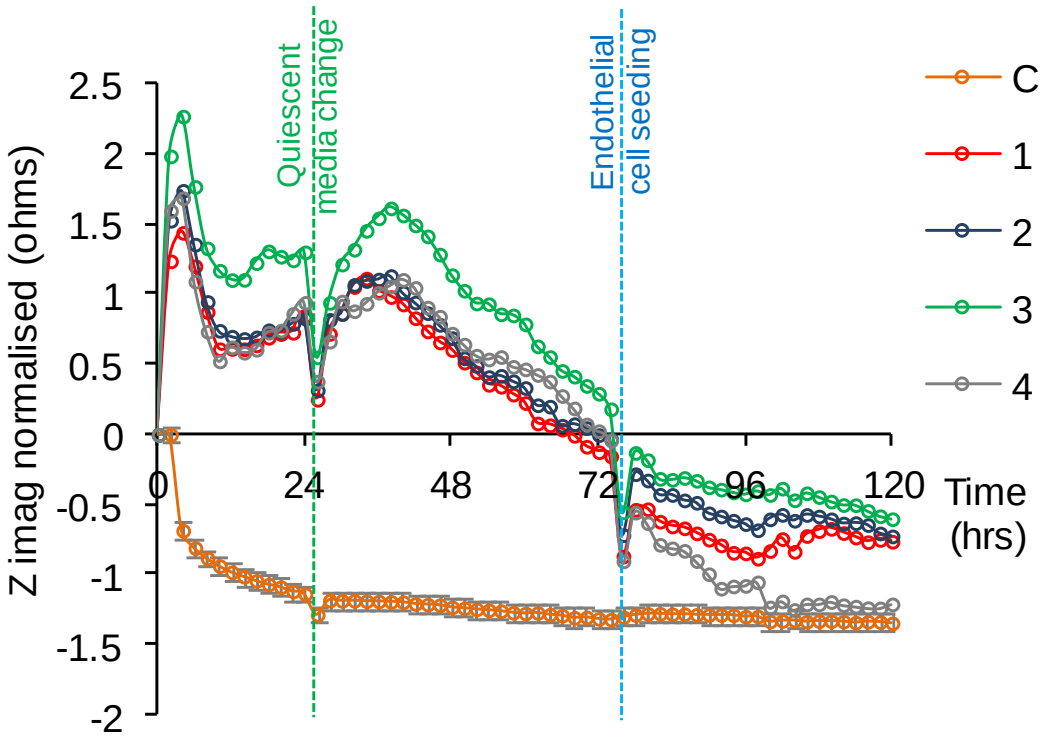

Figure 5.20 – 10kHz electrode reactance profiles from a representative chamber in co-culture experiment 4. Green line indicates quiescing media introduction (smooth muscle cell media, 0.5% FCS) and blue line endothelial cell seeding with co-culture media (5 parts F12, 1 part porcine endothelial cell media). Combined control (C) data shown in orange, error bars ± SEM n=12.

Experiment 5 repeated the procedure of experiment 4 with the only modification being that endothelial cells were cultured in 0.5% FCS smooth muscle cell media for 24 hours prior to their seeding onto the quiesced smooth muscle cells. The intention behind this variation was to allow the endothelial cells to experience changes to their culture conditions in advance of their seeding rather than experiencing a change in media and introduction to co-culture all at once as in previous experiments where endothelial cells failed to settle. Smooth muscle cells were seeded and grown to a higher level of confluence (70%) than in previous co-culture experiments (25% to 60%). Time-lapse observation revealed that the quiescing phase caused a repeat of the spheroid morphology formation in the initial 8 hours, followed by a recovery. Time-lapse video can be found in the electronic appendix, file reference Co-culture expt 5. The mean percentage reduction in total impedance following addition of quiescent media is shown in Figure 5.23 for smooth muscle cell seeded electrodes and bare control electrodes. This figure is included to enable comparison of the

quiescing stage with data from a previously published impedance study investigating smooth muscle cell phenotypic switching and is discussed further in section 5.3.5 (Impedance monitoring of endothelial and smooth muscle cell co-culture). The results demonstrate that the addition of quiescent media caused a reduction in total impedance measured two hours hence.

Evidence that experiment 5 attained a co-culture of smooth muscle and endothelial cells can be observed in the immunofluorescence imaging carried out on completion of the experiment. Chambers were fixed and stained using DAPI, anti α smooth muscle actin antibody – a smooth muscle cell marker – and finally anti vWF antibody – an endothelial cell marker. The use of α smooth muscle actin – shown in red – enabled the positive identification of smooth muscle cells in the co-culture layer, with an elongated spindle shape and actin strands clearly visible in the images shown in Figure 5.22. Figure 5.22 also shows the distribution of smooth muscle cells on the electrodes a and b demonstrating that they are sub confluent as desired in the proposed restenosis model. The coverage of smooth muscle cells is reduced in comparison to endothelial cells and lower numbers were to be found towards the tips of the electrodes, concurring with the light microscopy observations of their confluency level before endothelial cells were seeded.

The vWF staining showed the same evidence of positive staining of all cells including those that stained positively for α smooth muscle actin. Examples of these cells are shown in Figure 5.21. These images reinforce the findings from the staining of the preliminary co-cultures where cells with smooth muscle morphologies were observed to have positively stained for vWF. Those cells that stained positively for vWF factor but not α smooth muscle actin and these cells are most likely to be the endothelial cells introduced at 140 hours. Collectively these images suggest that a co-culture in vitro model of smooth muscle and endothelial cells was established over the electrodes.

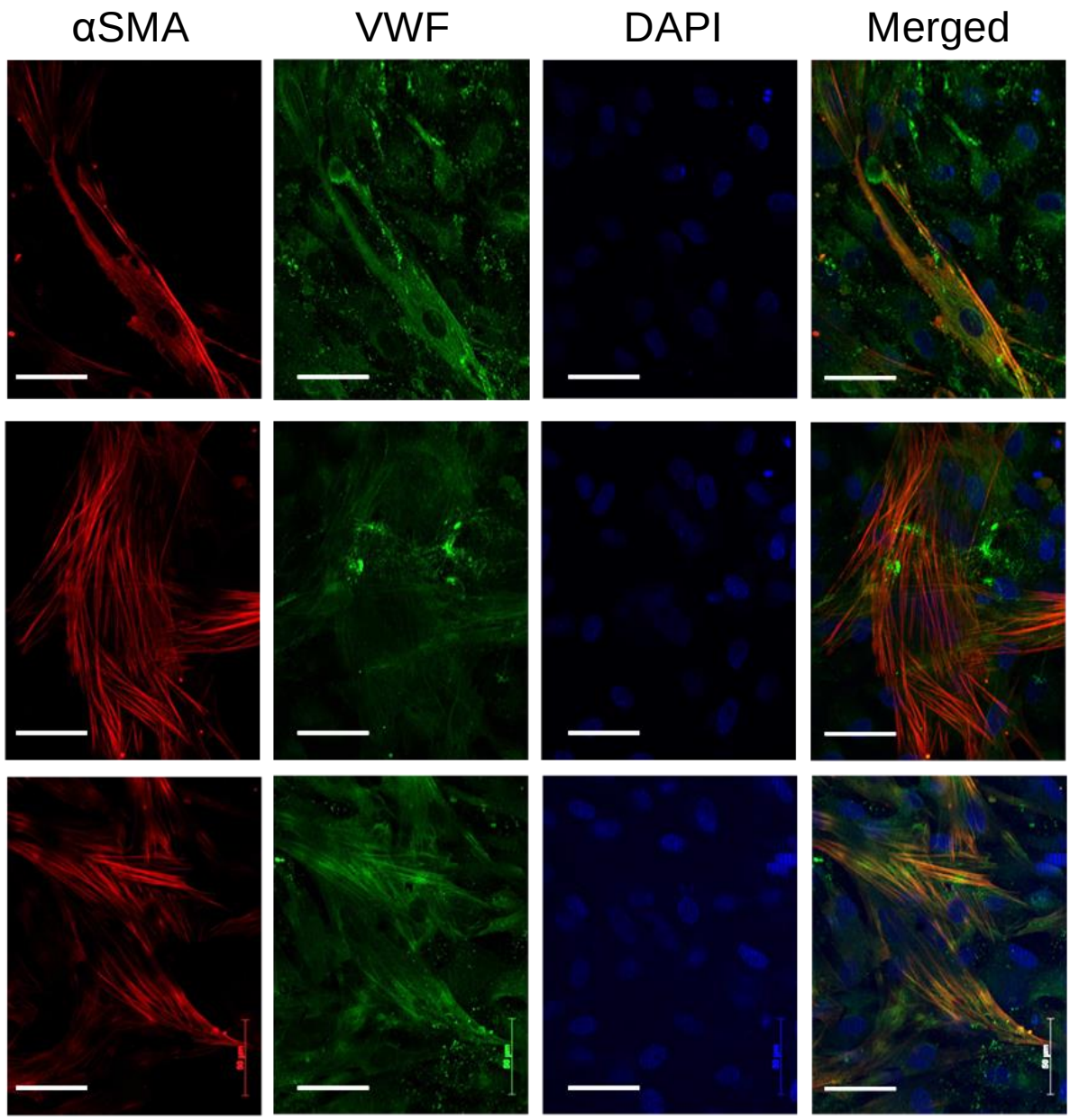

Figure 5.21 – Stained cells, co-culture test 5, α smooth muscle actin (red), Von-Willebrand factor (green) and DAPI (blue). Images are taken from electrode surfaces, white scale bars are 50µm, and are representative of 5 replicate electrodes.

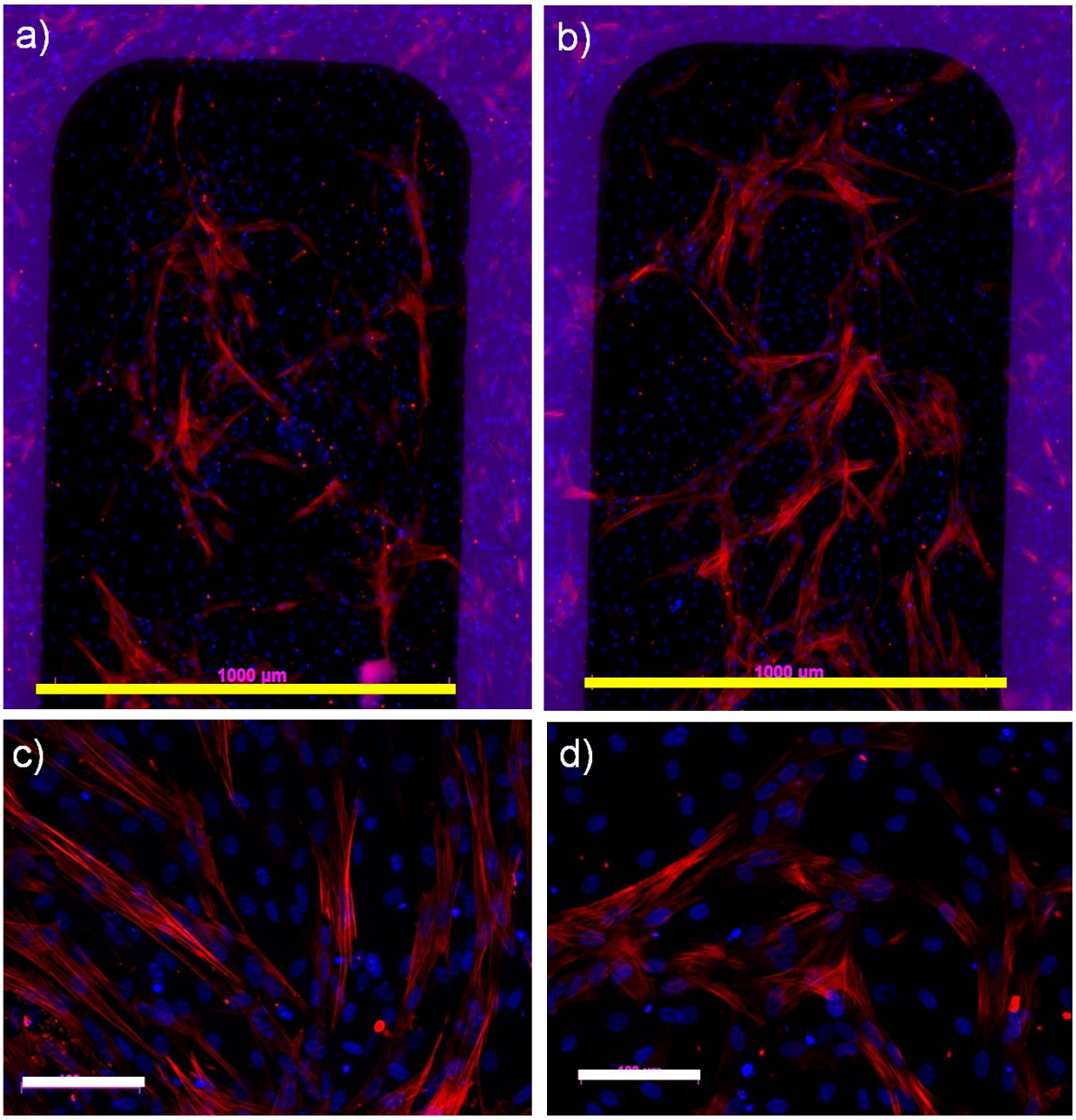

Figure 5.22 – α smooth muscle actin (red) and DAPI (blue)stained cells, co-culture test 5. Electrode tips at 5x magnification a), b) and electrode surface detail at 20x magnification c) and d) Yellow scale bars are 1000µm and white scale bars are 100µm.

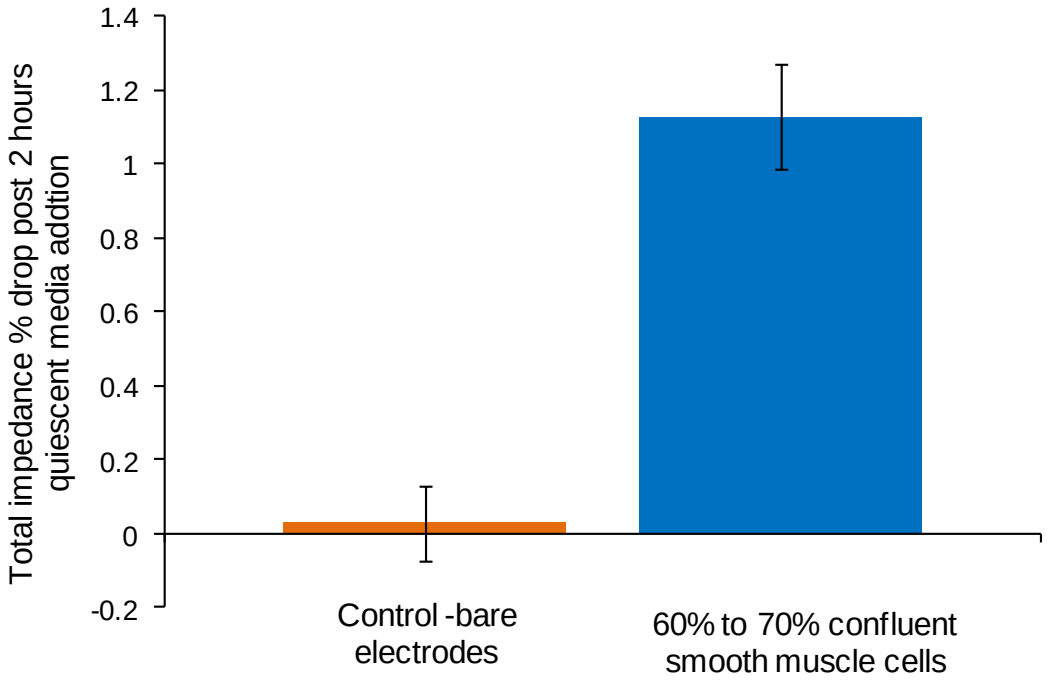

Figure 5.23 – Percentage total impedance reduction at 100kHz after introduction of quiescent 0.5% FBS media to electrodes covered with 60% to 70% confluent smooth muscle cells (n =15) and control bare electrodes (n=7). Error bars are ± SEM.

Endothelial cells were observed to have settled onto smooth muscle cells with the exception of a single chamber where they and the smooth muscle cells were seen to die in a similar fashion to test 4. Proliferation of endothelial cells appeared to be slow for the first 24 hours after seeding. Thereafter endothelial cells began to grow over the smooth muscle cells and covered the electrode with confluence observed between 192 and 216 hours resulting in the cross hatched appearance previously observed in the preliminary co-culture tests (Figure 5.24). The co-culture phase duration was 96 hours which was a typical duration of an endothelial test for the given seeding density. In addition it was believed to be sufficiently short to prevent the possibility of the cell sheet detachment in the same manner as observed in preliminary test A.

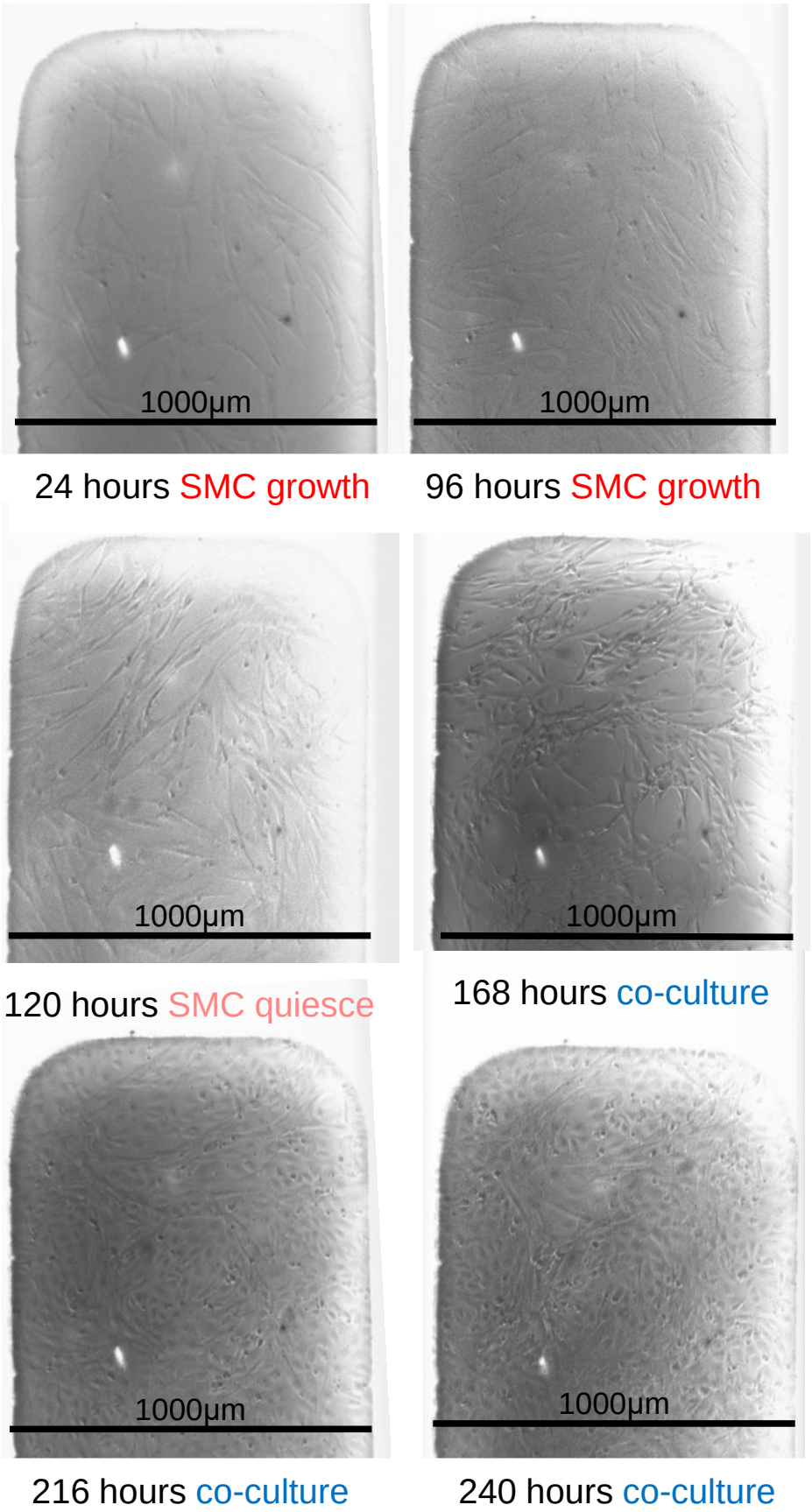

Figure 5.24 – Light microscopy of electrode tips, co-culture experiment 5. Scale bars are 1000µm.

Figure 5.26 shows the experiment 5 mean reactance profiles for cell seeded electrodes and control electrodes at a frequency of 10*kHz*. A notable aspect is that the control profile fell significantly within the first 48 hours of the experiment. This behaviour was also evident in the control profiles in co-culture test 4 but with reduced magnitudes. The cell profile in Figure 5.25 also showed early phase reactance declines in contrast to previously presented cell seeded electrodes at this 10*kHz* frequency. The instability of the control electrodes is thought to be contributing to the cell electrode decline and at this frequency obscuring expected elevations in reactance. No specific cause for this change in the electrode behaviour was discovered although an enforced variation in the chamber manufacturing procedure may be a cause. A different sputter coater had to be used that required more coatings to achieve a gold layer of sufficient thickness that could be platinum black coated. Periodic 24 hour reductions seen can be attributed to manual disturbances when chambers were removed from the incubator for light microscopy.

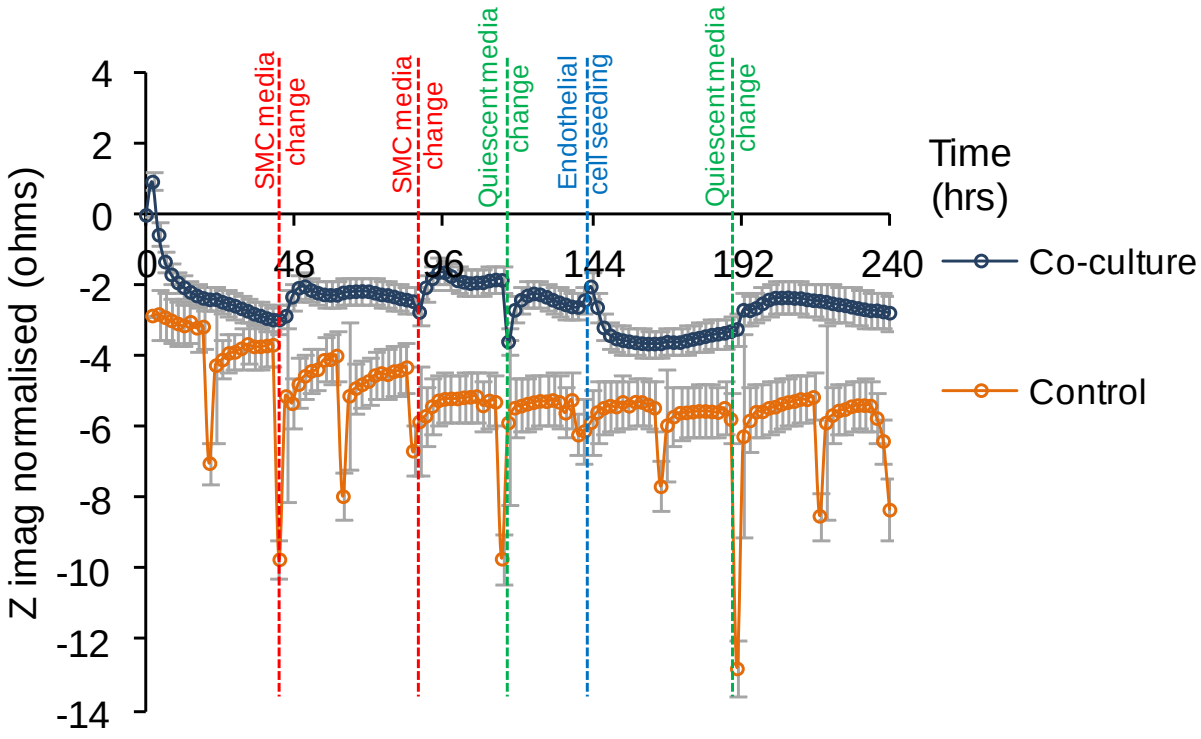

5.25 – Mean reactance profile at 10kHz for cell adhered co-culture electrodes from experiment 5. Red line lines indicate smooth muscle cell media changes. Green line indicates quiescing media introduction (smooth muscle cell media, 0.5% FCS) and blue line endothelial cell seeding with smooth muscle cell media, 0.5% FCS. Mean control (C) data shown in orange. Error bars ± SEM, co-culture electrodes n= 15, control electrodes n=7.

The greatest differences between the control and cell seeded chambers were seen at higher frequencies, consequently the mean reactance data from cell seeded for co-culture test 5 at 100*kHz* are shown in Figure 5.26. Inspection of the control reactance profiles shows large fluctuations following media changes that subsequently stabilised to pre media change values. Additional periodic 24 hour control fluctuations coincided with occasions where cell seeded chambers were removed from the incubator for light microscopy imaging and it is thought that accidental disturbance of the control chambers occurred at this point. No significant control variation was seen following the change from proliferative smooth muscle cell media to quiescent media at 115 hours.

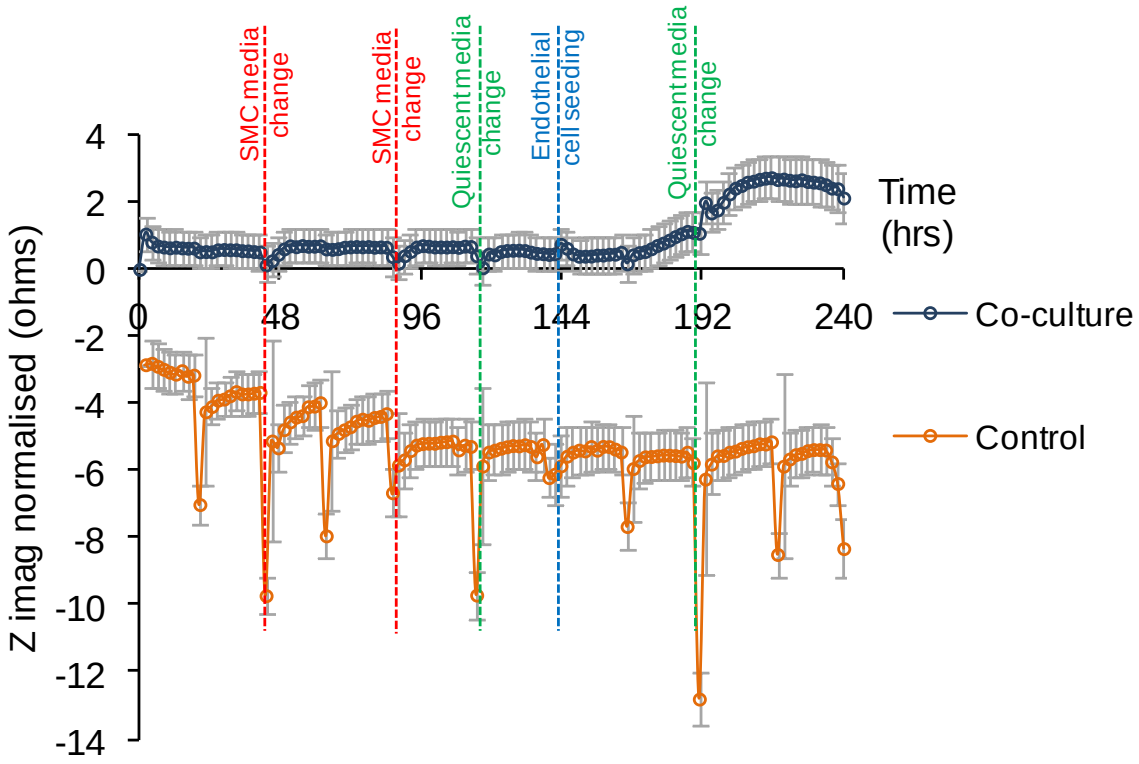

Figure 5.26 – Mean reactance profile at 100kHz for cell adhered co-culture electrodes from experiment 5. Red line lines indicate smooth muscle cell media changes. Green line indicates quiescing media introduction (smooth muscle cell media, 0.5% FCS) and blue line endothelial cell seeding with smooth muscle cell media, 0.5% FCS. Mean control (C) data shown in orange. Error bars ± SEM, co-culture electrodes n= 15, control electrodes n=7.

Data from cell seeded chambers at 100*kHz* is shown in Figure 5.27 without control data to highlight changes in impedance arising from the adhesion and proliferation of cells over the electrodes. The smooth muscle cell proliferation observed with light microscopy and time-lapse images in the initial 115 hours did not cause corresponding reactance elevations. This result is in contrast to previous experiments where smooth muscle cells were seeded onto electrodes using comparable seeding densities and is potentially a cell induced impedance effect that has been obscured by the previously detailed control instability. The introduction of endothelial cells at 140 hours caused either a fall or no significant change in the reactance values for an initial 24 to 48 hours indicating slow growth (Figure 5.27 a,b,d and e). This behaviour was confirmed with light microscopy images showing patches of the electrode still visible at 168 hours (Figure 5.24). Proliferation of endothelial cells observed between 168 and 240 hours correlates with rises in reactance which then levelled out and then began to fall in the final 24 hours of the experiment creating an endothelial cell post confluence peak in the same manner as measured in experiments seeding endothelial cells only. The post confluence peak was attained first in chamber 8 and microscopy observation revealed that endothelial cells proliferated to confluence at a faster rate in this chamber and can be seen in the time-lapse microscopy video of this chamber. No increases were measured in the single chamber where endothelial cells were observed failing to settle (Figure 5.27c) and these reactance values were excluded from the mean data set. Mean data from electrodes is shown in Figure 5.27f.

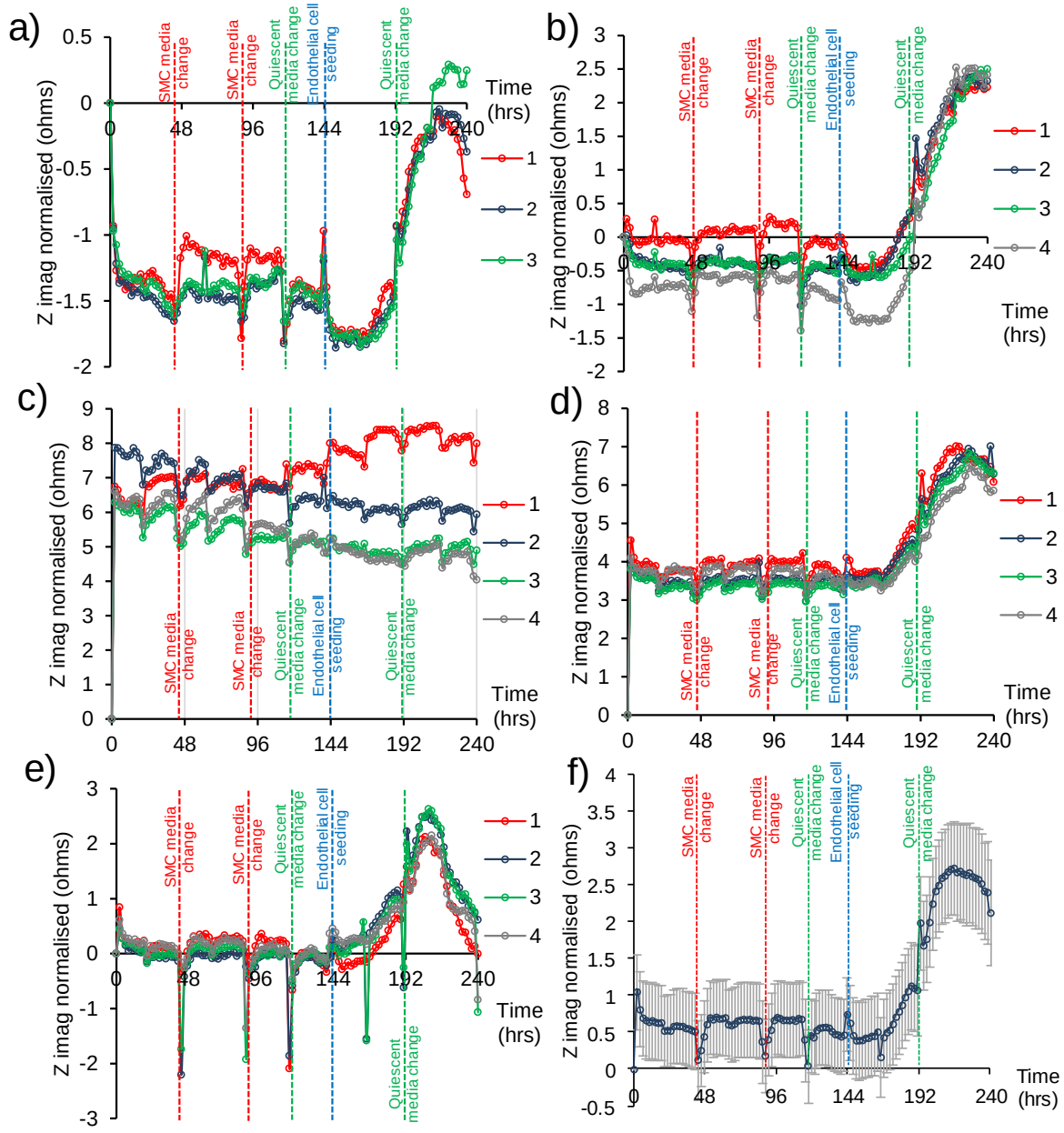

Figure 5.27 – a) to e). Co-culture test 5 chamber reactance profiles at 100kHz. Red line lines indicate smooth muscle cell media changes. Green line indicates quiescing media introduction (smooth muscle cell media, 0.5% FCS) and blue line endothelial cell seeding with smooth muscle cell media, 0.5% FCS. f) Mean reactance for cell adhered co-culture electrodes from experiment 5, error bars ± SEM, co-culture electrodes n=15.

The changes in impedance arising from endothelial cell seeding and subsequent proliferation were not measurable across the whole frequency range. Figure 5.28a and b shows representative 3D reactance electrode profiles. Inspection reveals that the reactance increases following endothelial cell introduction are most prominent at

frequencies above 10*kHz* although as previously suggested the variation in control chambers may account for the loss of sensitivity to cellular behaviour at low frequencies. Figure 5.28c and d show a reduced high frequency range of 10*kHz* to 100*kHz* with the endothelial cell introduction at 140 hours clearly visible as an elevation in the reactance.

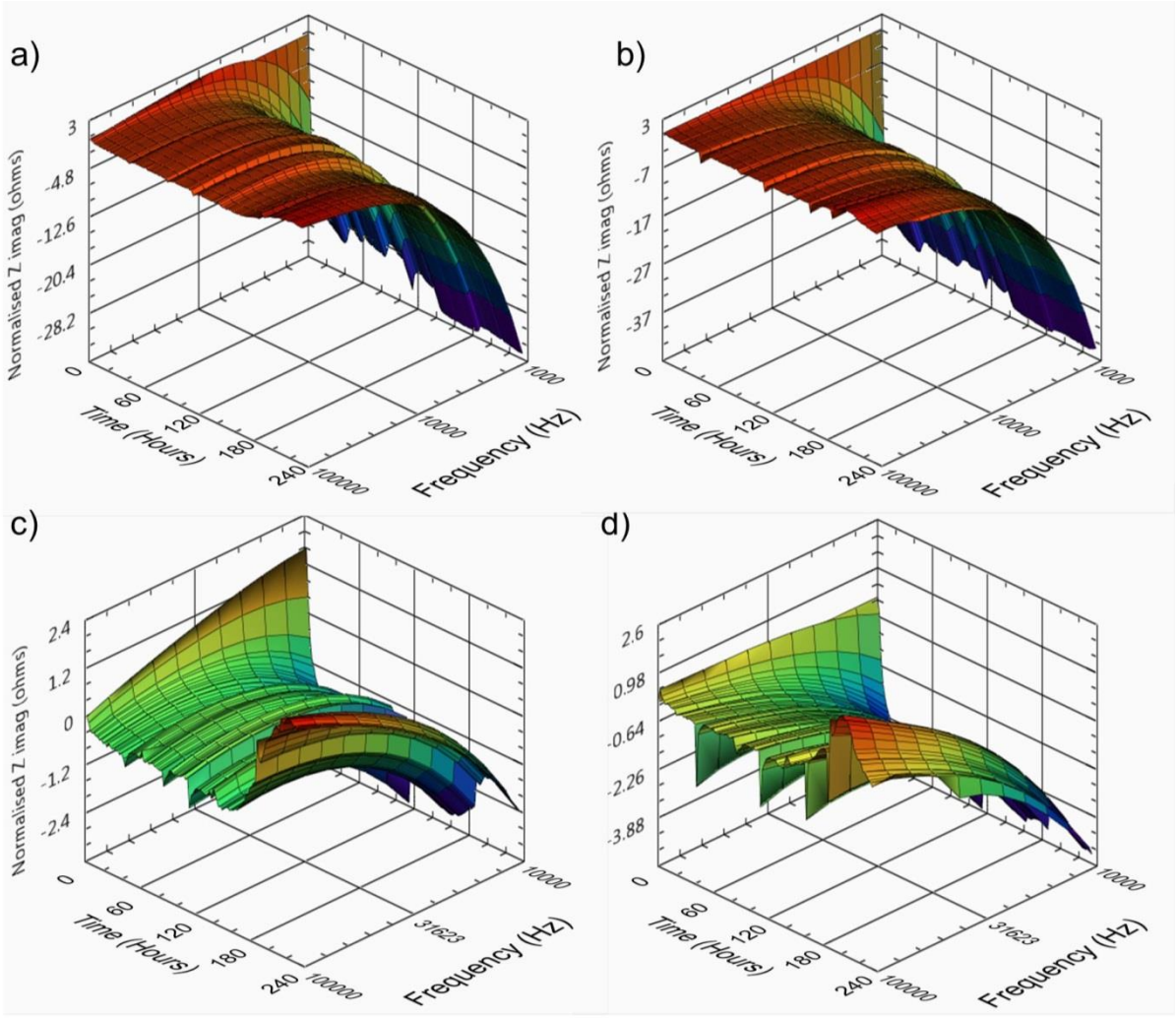

Figure 5.28 – 3D reactance profiles of representative co-culture test 5 electrodes in the frequency range 1kHz to 100kHz (a and b) and 10kHz to 100kHz (c and d).

The total impedance ratio previously shown for endothelial cells is depicted for smooth muscle cells in Figure 5.29. Data are presented for the different stages of co-culture establishment, proliferating smooth muscle cells, quiescent smooth muscle cells and finally co-culture. Initial inspection reveals minimal differences between the co-culture phases, however shallow inflection peaks can be observed in 1*kHz* to 100*kHz* range as shown in the Figure 5.29 insert. A shallow inflection ratio shift at

from 2*kHz* for quiesced smooth muscle cells to 5*kHz* when a co-culture of endothelial and smooth muscle cells had been established.

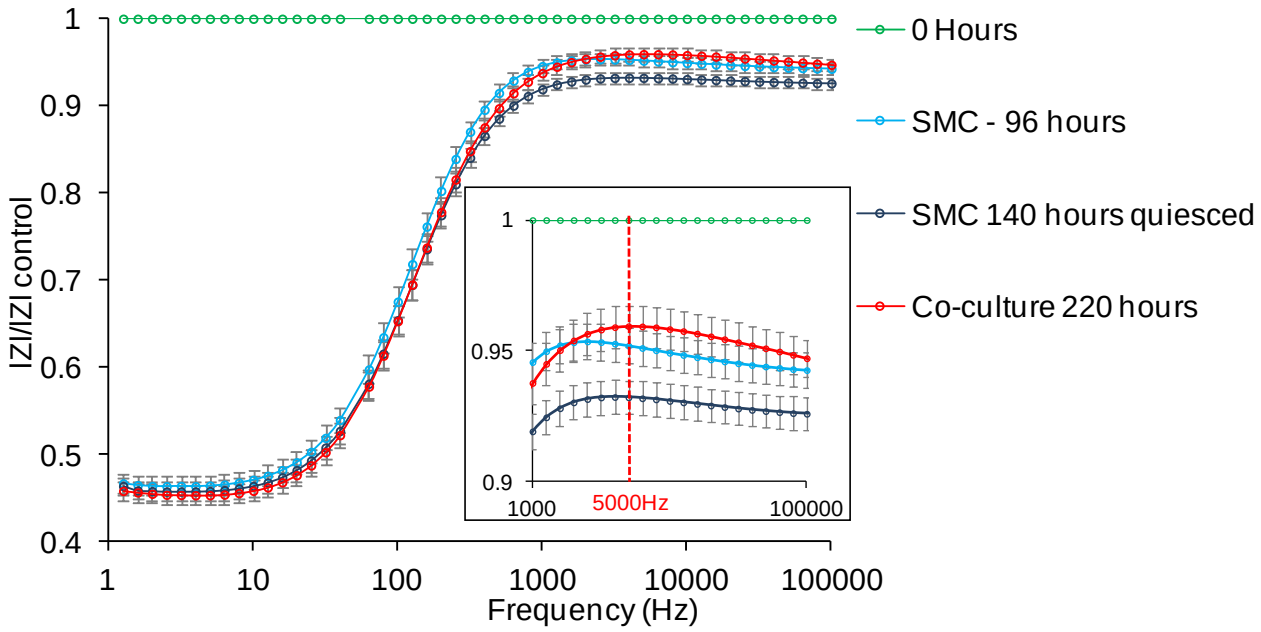

Figure 5.29 - Total impedance ratio for stages of co-culture establishment on electrodes at 0 hours, proliferating smooth muscle cells at 96 hours, quiescent smooth muscle cells at 140 hours and co-culture at 244 hours. Insert shows a reduced frequency range and a co-culture inflection frequency of 5000Hz. Error bars are ± SEM, n=15.

5.2.5 Impedance based characterisation of human umbilical vein endothelial cells (HUVECs)

The results presented thus far are all from primary porcine cell lines, however it is known that there are species dependent differences in cells, which may give rise to differences in impedance characteristics. Therefore it was decided to investigate if the results observed would be replicated in human endothelial cells, thereby enhancing the clinical relevance of the study. A commonly used human cell type in the literature are Human Umbilical Vein Endothelial Cells (HUVECs) and these were selected for use in the present study. HUVECs were seeded into 5 chambers for one experiment. Cells (P4) were seeded onto electrodes into the chambers at densities in the range 4.1 to 5.1 x 10^4 cells per cm^2, 3 cell-free chambers were used as controls with media only. For one of the cell chambers standard endothelial cell media used in porcine cell experiments was used, and replaced at 48 hours with HUVEC media. This procedure was followed as a trial to determine the effect of different media on HUVECs. The remaining 4 chambers received HUVEC media for the duration of the experiment. Settling and proliferation of the cells was observed with confluence attained in all chambers between 24 and 48 hours. Time lapse microscopy observations revealed that HUVECs cells had a far greater level of motility when compared to porcine endothelial cells and can be seen in the video referenced HUVECs expt in the electronic appendix. Reactance data from a representative chamber is shown in Figure 5.30 alongside light microscopy images revealing a post confluence peak in a similar trend to those observed in the previous porcine endothelial cell studies (see Figure 5.8).

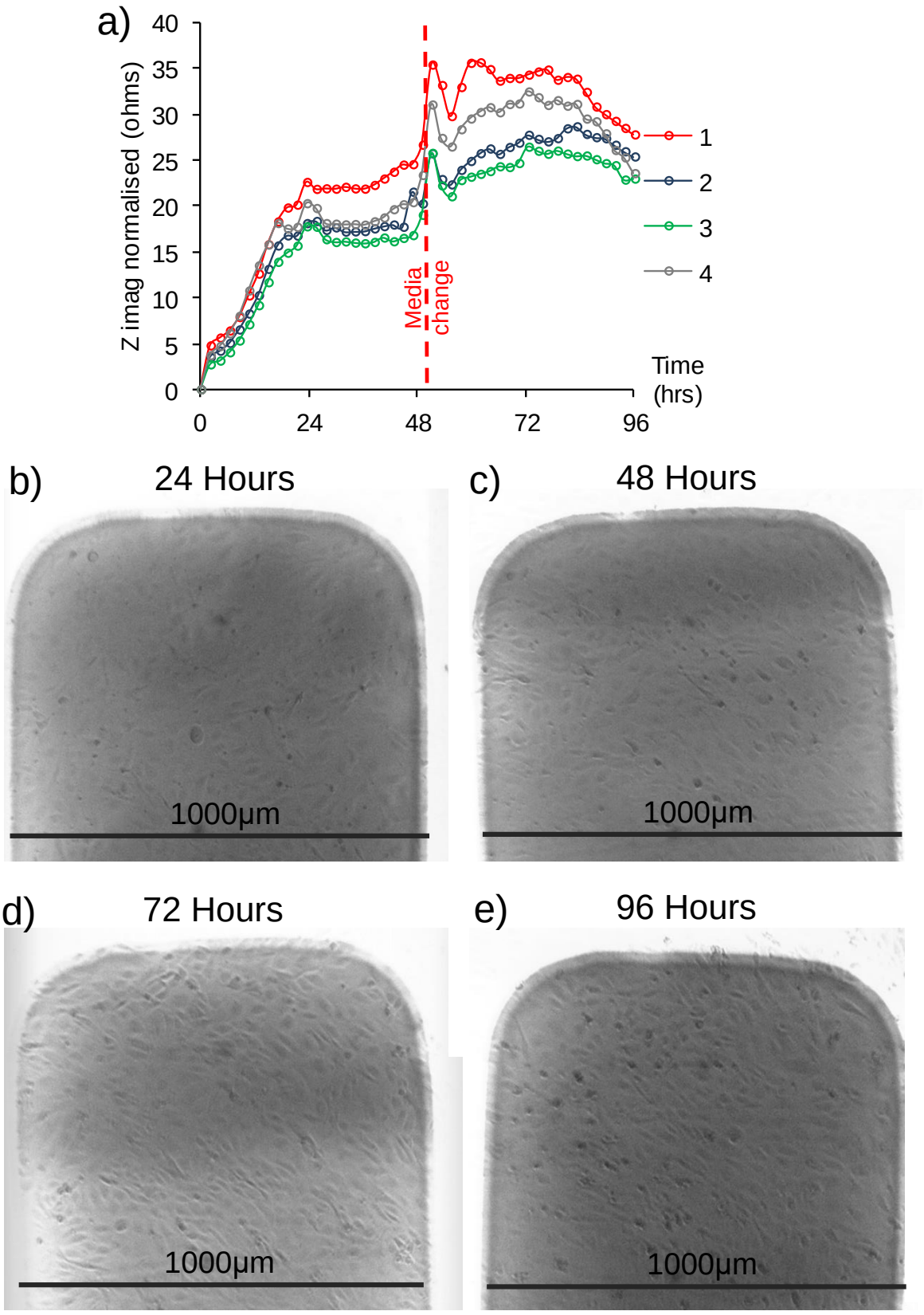

Figure 5.30 – a) 10kHz reactance profiles of electrodes1 to 4 from a representative chamber seeded with HUVECs. Red line indicates media change. b), c), d), e) Periodic light microscopy images of electrode 1 showing cell proliferation progression. Scale bars are 1000µm.

Mean reactance variation for all electrodes is shown in Figure 5.31 along with controls. The single chamber that experienced a change in media composition is not included in the data set. A post confluence decline in reactance is clearly visible from approximately 74 hours onwards.

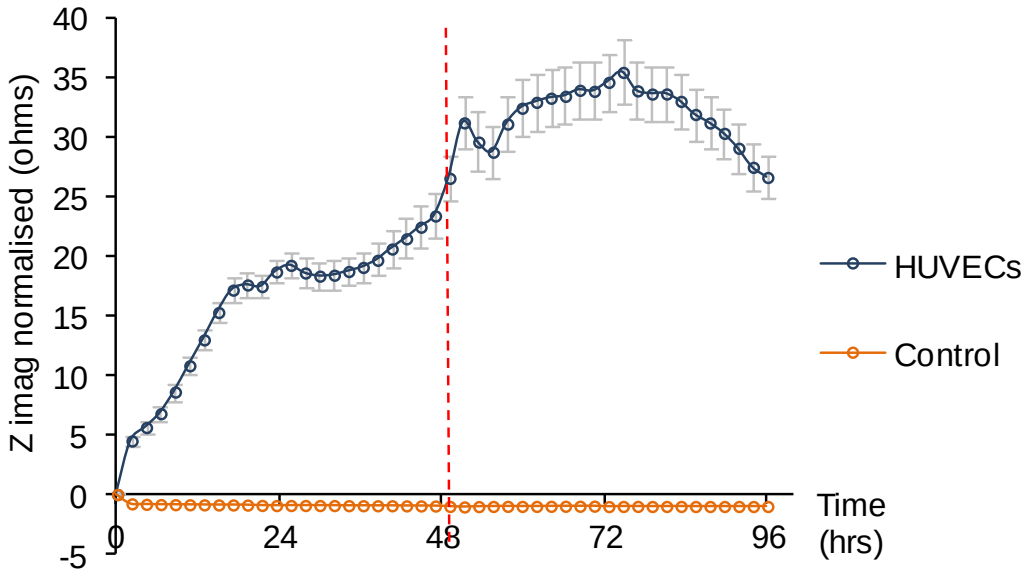

Figure 5.31 - Mean HUVEC reactance profile at 10kHz for all electrodes (n=14) and cell free control electrodes (n=10). Error bars are ± SEM with max control SEM = 0.148. Red line indicates media change.

Mean 3D plots of HUVEC reactance are shown in Figure 5.32 alongside mean control reactance. These plots reveal differences between HUVEC reactance and the previously presented porcine cells. The HUVECs displayed a post confluence peak being maximal in the frequency range 25*kHz* to 40*kHz*, whilst porcine cells displayed a higher frequency peak and a distinctive double peak signature.

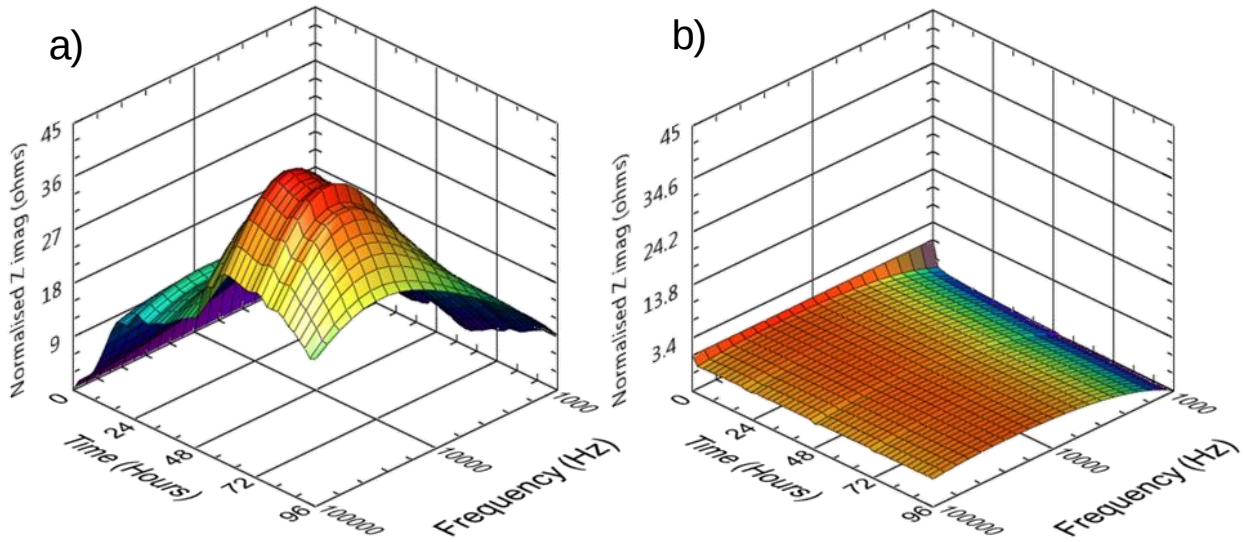

Figure 5.32 - Mean 3D reactance (z axis) variation over time (x axis) and across the frequency range1kHz to 100kHz (y axis). a) HUVEC seeded electrodes (n=14, max standard error mean 3.351) and b) control electrodes (n=10, max standard error mean 1.0544).

The single chamber in which porcine endothelial cell media was used followed by a change to HUVEC media induced a significant variation in reactance. This can be seen in the representative 3D reactance electrode reactance profile shown in Figure 5.33 along with light microscopy images of cells before and after media change. The chamber showed a post confluence peak at a lower frequency range and a drop in reactance following the media change at 48 hours followed by a recovery phase, with no differences in cell coverage. An additive present in the HUVEC media and not in the porcine media was Vascular Endothelial Growth Factor which may be responsible for the difference.

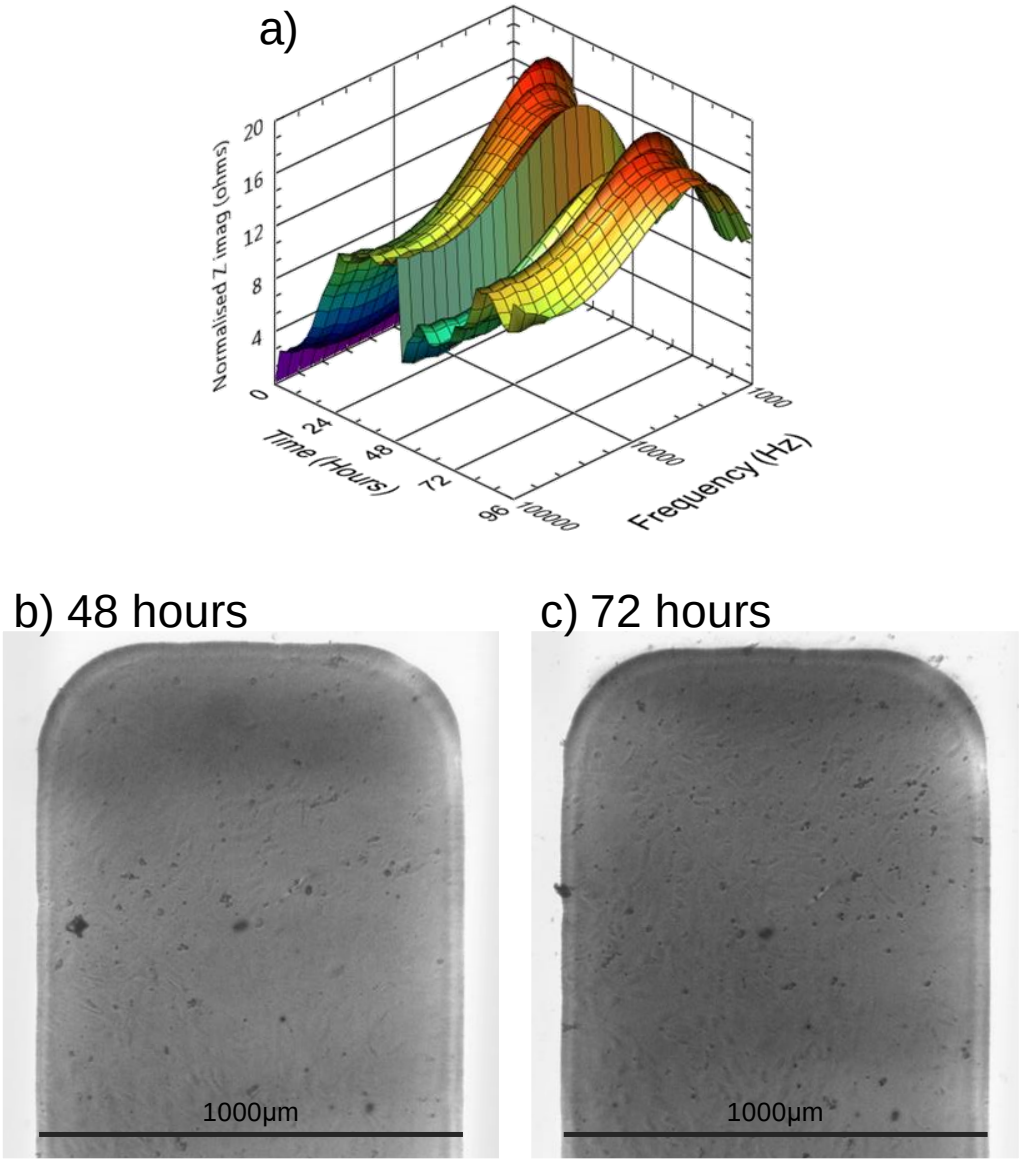

Figure 5.33 – a) 3D electrode reactance profile seeded with HUVECs and cultured in porcine endothelial cell media up to 48 hours where media change to HUVEC media occurred. Corresponding light microscopy images of cells before media change b) and after c). Scale bars are 1000µm.

The total impedance ratio is depicted for HUVECs in Figure 5.34. An inflection ratio at 794*Hz* can clearly be seen, with an increasing magnitude over time.

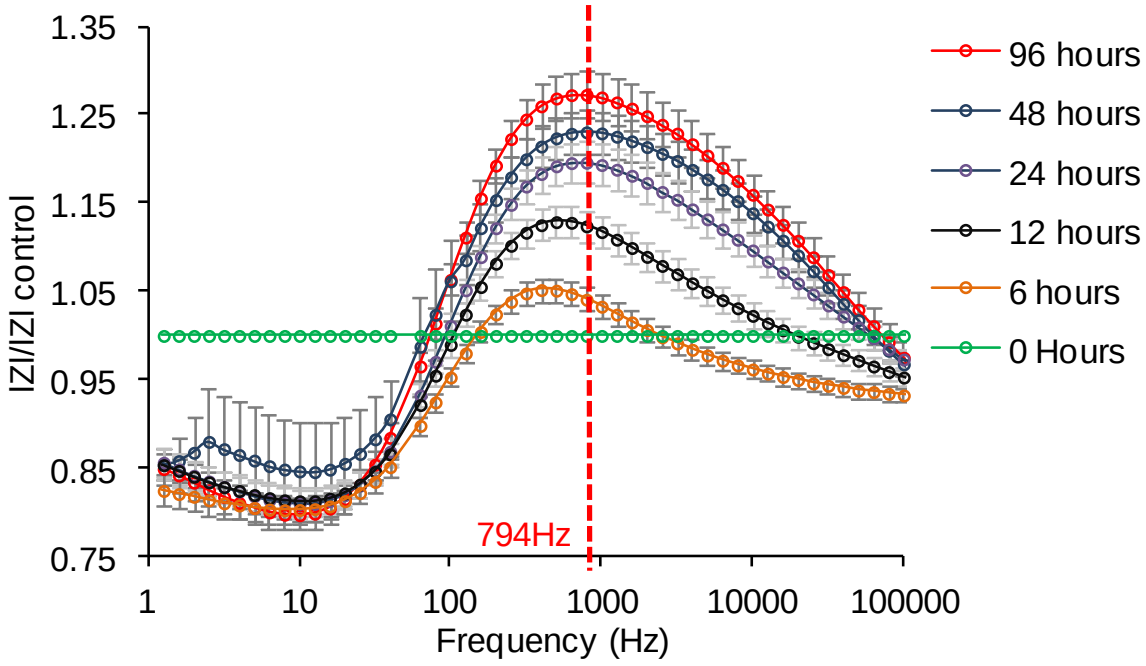

Figure 5.34 - Total impedance ratio for HUVECs seeded onto electrodes at 0, 48 and 96 hours. Red dashed line indicates an inflection frequency at 96 hours of 794Hz. Error bars are ± SEM, n = 14.

5.2.6 Summary of key cell characterisation data

To permit comparison between the different cell types examined in this study, Figure 5.35 displays the mean 2D reactance profiles and their respective 3D reactance plots for the previously detailed experimentation of endothelial cells, smooth muscle cells, HUVECs and co-culture. Comparison of reactance values between the 3 cell type experimented on as monolayers are shown in Table 5.4. The 2D plots highlight a similar elevation in reactance observed in all the cell types as they proliferate over the electrodes. The magnitude of this rise is cell dependent, with HUVECs producing a maximum of around 35Ω compared to values of around 5Ω and 7Ω for the porcine endothelial and smooth muscle cell cultures respectively. Both HUVECs and porcine endothelial cells show a post confluence decline in reactance (Figure 5.35 a and b) that was not visible in the smooth muscle cell data (Figure 5.35c). Inspection of the 3D reactance plots displaying a wider frequency range reveals that variations in reactance are not uniform across the frequency spectrum. Porcine endothelial cells showed a characteristic double peak (Figure 5.35e) whilst HUVECs exhibit a single peak (Figure 5.35d). Smooth muscle cells exhibited no such reactance peaks in the measured frequency range (Figure 5.35f).

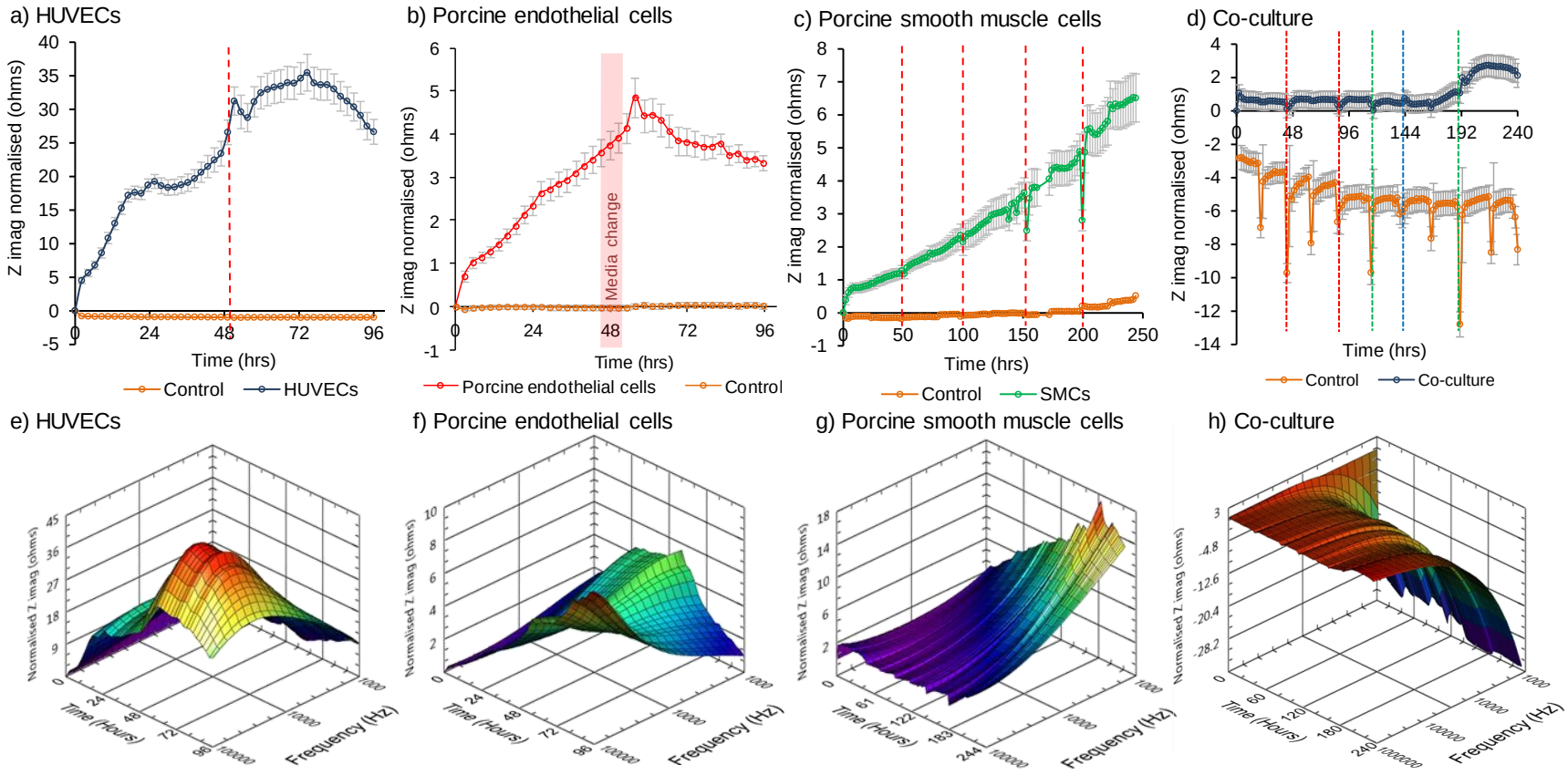

Figure 5.35 – Mean reactance profiles at 10kHz for a) HUVECs, b) porcine endothelial cells, c) porcine smooth muscle cells and d) co-culture at 100kHz. Error bars are ± SEM. HUVEC n = 14, control max SEM = 0.148, n = 10. EC n = 39, control max SEM 0.04, n = 33. SMC n = 8, control max SEM 0.11, n = 8, co-culture n= 15, control max SEM = 0.717 n=7. Mean 3D reactance electrode profiles e) HUVECs max SEM = 3.35, f) ECs max SEM = 0.91, h) SMCs max SEM = 1.86 and i) co-culture max SEM = 2.88.

		Reactance on experiment completion (Ω)					
	n	1*kHz*	SD	10*kHz*	SD	100*kHz*	SD
Endothelial cell control	33	1.45	0.46	0.02	0.07	-0.98	0.17
Endothelial cells	39	1.00	0.90	3.33	0.17	9.30	0.77
Smooth muscle cell control	8	1.60	0.13	0.52	0.11	-1.12	0.46
Smooth muscle cells	8	13.06	0.82	6.51	0.72	3.78	0.94
HUVEC control	10	-6.87	1.06	-1.00	0.15	-1.52	0.38
HUVECs	14	9.28	1.03	26.64	1.85	24.84	1.23

Table 5.4 - Reactance values on experiment completion for the 3 cell monotypes tested.

Total impedance ratios for confluent cells at the end of their respective experiments from the 4 data sets are shown in Figure 5.36.

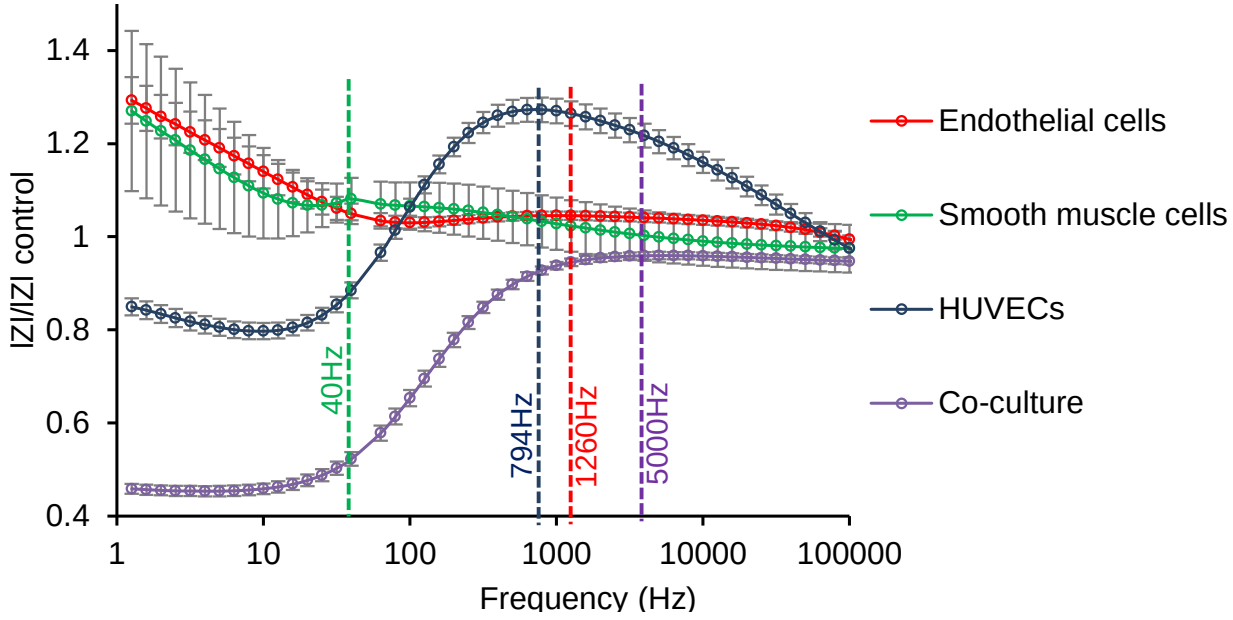

Figure 5.36 – Mean total impedance ratio for confluent monolayers of porcine endothelial cells (n=39), smooth muscle cells (n=8), co-culture (n=15) and HUVECs (n=14) seeded onto electrodes. Red dashed line indicates an endothelial cell inflection frequency of 1260Hz. Green dashed line indicates a smooth muscle cell inflection frequency of 40Hz. Purple dashed line indicates a co-culture inflection frequency of 5000Hz Blue dashed line indicates a HUVEC inflection frequency of 794Hz. Error bars are ± SEM.

5.2.7 Equivalent circuit modelling

The use of equivalent circuits enables the assignment of electrical components to cellular features and when fitted to experimental data allows these elements to be quantified. As discussed in section 2.4 (Equivalent circuit modelling), a range of circuit models are available. The selected circuits for the purposes of analysing the results presented in this study are those previously used by Shedden, 2008. Results from bare electrodes were fitted against the circuit shown in Figure 5.37. This circuit uses a minimal number of elements an approach that helps to maintain accuracy when attempting to fit data (Macdonald, 1992; Malleo *et al.*, 2010). Previously the circuit was used to model gold electrodes, which differ from the platinum black electrodes used in this study. However a resistor and constant phase element has been used in the literature to model platinum black coated electrodes, demonstrating the relevance of using the circuit for the results gathered here (Franks *et al.*, 2005). In the case of the cell seeded chambers this circuit was used to fit the first impedance sweep taken in the first 5 minutes after seeding before the cells settled onto the electrodes. Data was fitted using Z view software which calculated a value for each element and an associated error. The size of the error is an indication of the confidence that can be assigned to each value.

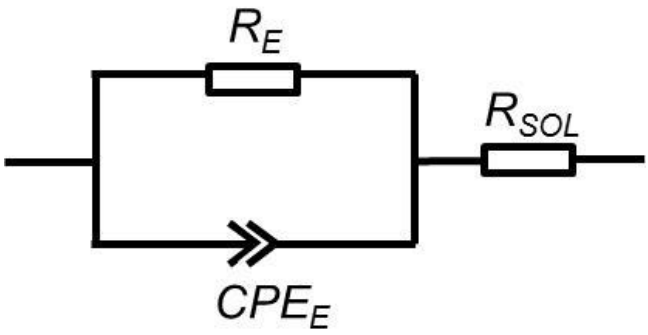

Figure 5.37 - Equivalent circuit model for bare platinum black electrodes in cell media. R_E and CPE_E represent the resistance and constant phase elements of the combined electrodes respectively. R_{SOL} represents the resistive component of the cell media.

Results from cell covered electrodes were fitted against the circuit shown in Figure 5.38 using Z-View software as detailed in section 3.9 (Equivalent circuit modelling). The cell layer is also modelled using a resistor and constant phase element. This arrangement has been used in multiple published studies to model cells adhered to

electrodes (Bouafsoun, Helali, Mebarek, *et al.*, 2007; Rahman, Price and Bhansali, 2007; Cho and Thielecke, 2008; Shedden, 2008). Whilst the CPE model must be treated with caution it is be used in this study to compare the development and growth stages of different cells in culture on an electrode surface.

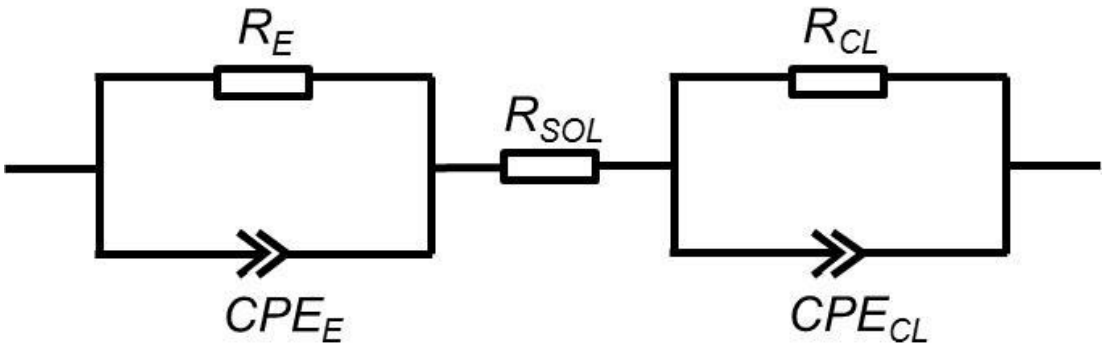

Figure 5.38 - Equivalent circuit model for platinum black electrodes with an adhered cell monolayer in cell media. R_E and CPE_E represent the resistance and constant phase elements of the combined electrodes respectively. R_{CL} and CPE_{CL} represent the resistance and constant phase elements of the cell monolayer respectively. R_{SOL} represents the resistive component of the cell media.

Results from different media compositions are shown in Table 5.4. CPET and CPEP values are defined in section 2.4 (Equivalent circuit modelling, Equation 23). Wessel and bode diagrams are shown with the fitted data curve and original data for Endothelial cell media in Figure 5.39 and demonstrates the closeness of the fit. The data shows that the electrode resistance is constant between the controls. This result is unsurprising as cell media would not be expected to alter the resistance of the electrodes. CPET values for electrodes in HUVEC media were found to be approximately halved when compared to the other 2 media types. This could be attributed to differences in the interfacial capacitance caused by variations in electrolyte concentrations between the media or that the electrodes used in the HUVEC test had a lower surface roughness than those measured on the samples characterised in section 4.4 (Surface characterisation). Such a difference is unlikely to be attributable to serum content as of the 3 media SMC contained a higher concentration of serum (10%) in comparison to Endothelial (2%) and HUVEC (2%).

	Control media					
	Endothelial	**Error %**	**SMC**	**Error %**	**HUVEC**	**Error %**
R_E	133150Ω	10.116	131750Ω	9.3829	135690Ω	5.1593
$CPET_E$	30.482μF	0.41838	35.314μF	0.35754	15.516μF	0.37271
$CPEP_E$	0.84705	0.1173	0.8357	0.8357	0.87218	0.0935
R_{SOL}	217.2Ω	0.104	247.1Ω	0.0822	273.7Ω	0.1022
Chi^2	0.0003701		0.00025535		0.000326	

Table 5.4 - Equivalent circuit modelling parameters for control platinum black electrodes in different cell media.

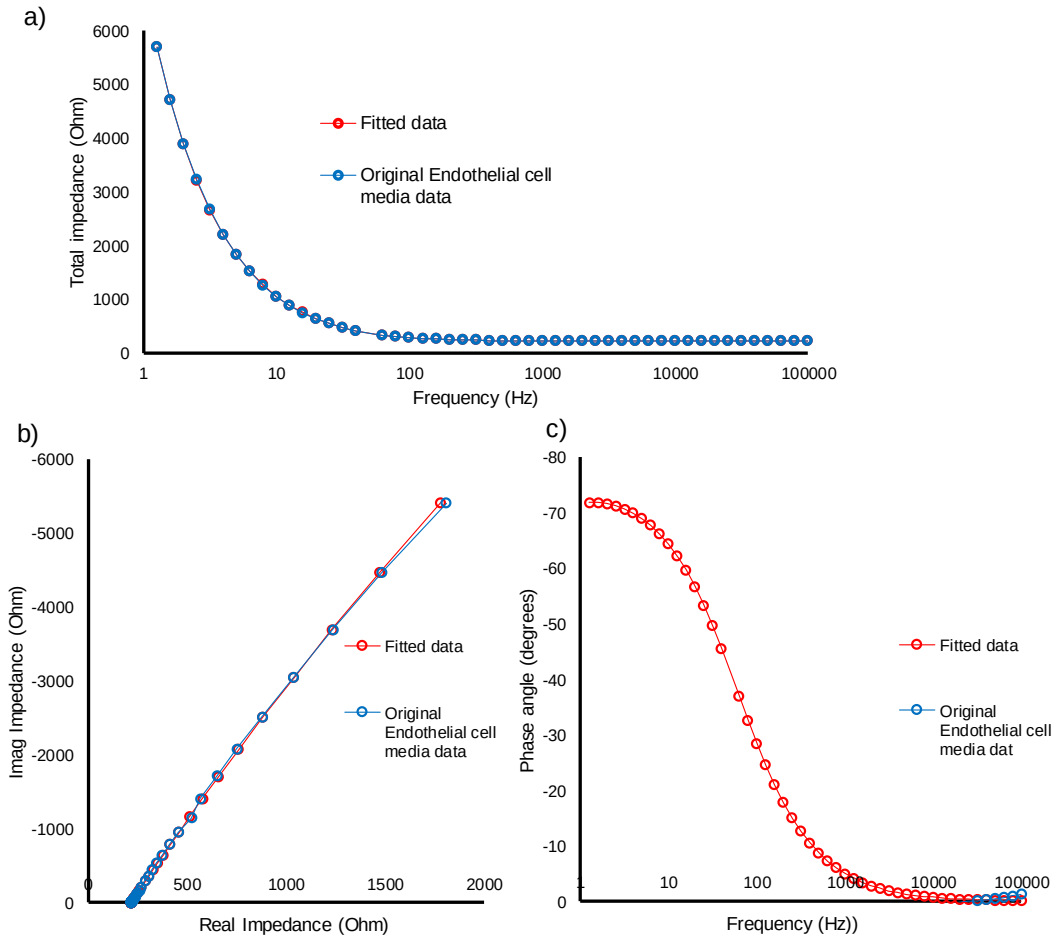

Figure 5.39 – Graphical comparison of equivalent circuit impedance fitted data and original data for electrode in endothelial cell media. a) Total impedance, b) Wessel plot and c) Phase.

Equivalent circuit fitted values for a porcine endothelial cell test at various time points are shown in Table 5.5. For the test fitted, the cells were observed to have attained confluence by 48 hours. As would be expected the solution resistance remains constant throughout the course of the experiment. The values for the electrode elements varied once the cells had adhered to the electrode with over a

threefold increase in electrode resistance, a halving of CPET and an elevation in CPEP indication a move to more capacitive behaviour. These data would appear to suggest that the electrodes were not stable throughout the duration of the experiment however this is contradicted by plots of measured impedance parameters for control chambers which demonstrate a high degree of stability. As the data for 0 hours is comparable to the endothelial media control data in Table 5.4 it is possible that components of the impedance contribution arising from the cells have been included in the models electrode elements. Values for the cell layer show a decline in resistance and a large increase elevation in $CPET_{CL}$. Also evident is a drop in the $CPEP_{CL}$ value showing that the confluent cell layer has behaved less like an ideal capacitor as the confluent layer has matured. However an increase in the errors of the cell layer values at 96 hours suggest that the circuit used has become less representative of an endothelial layer adhered to a platinum black electrode.

	Porcine endothelial cells					
	0 hours	**Error %**	**48 hours**	**Error %**	**96 hours**	**Error %**
R_E	160220Ω	18.326	335400Ω	16.669	400060Ω	9.1297
$CPET_E$	30.157μF	0.63123	17.172μF	0.4996	16.18μF	0.25118
$CPEP_E$	0.84559	0.16648	0.90486	0.14523	0.91203	0.078164
R_{SOL}	197.1Ω	0.16267	189.9Ω	0.19636	193.7Ω	1.3078
R_{CL}	-	-	42.06Ω	3.9705	29.11Ω	16.867
$CPET_{CL}$	-	-	44.622μF	19.4	121.97μF	41.586
$CPEP_{CL}$	-	-	0.73949	3.0232	0.31578	17.075
Chi^2	0.0008334		0.0002136		0.000050555	

Table 5.5 - Equivalent circuit modelling parameters for proliferating porcine endothelial cells.

The fitted values for a smooth muscle cells experiment are shown in Table 5.6. The cells at 144 hours in this experiment had attained 50% to 60% confluency and were 100% confluent at 244 hours. The solution resistance remains stable throughout the experiment and is comparable to the value from the control experiment. The electrode elements show the same instability as the endothelial results from Table 5.5 with an increase in resistance and a fall in $CPET_E$ once cells had adhered and proliferated across the electrode. These variations are again contradicted by the stability of the measured control impedance data again indicating that cellular impedance contributions have been included into the electrode component values.

Values from the fitted cell layer elements demonstrated a stability not seen in the porcine endothelial cells and HUVECs.

	Smooth muscle cells					
	0 hours	**Error %**	**144 hours**	**Error %**	**244 hours**	**Error %**
R_E	177750Ω	8.516	822970Ω	48.883	434240Ω	20.667
$CPET_E$	27.312μF	0.52109	15.978μF	0.68807	15.66μF	0.54335
$CPEP_E$	0.85256	0.07543	0.91521	0.21558	0.91899	0.16712
R_{SOL}	246.2Ω	0.12816	226.7Ω	0.19622	269.7Ω	0.20792
R_{CL}	-	-	49.62Ω	7.4678	52.8Ω	5.6371
$CPET_{CL}$	-	-	86.601μF	23.935	91.474μF	23.013
$CPEP_{CL}$	-	-	0.72781	4.0934	0.65923	4.1072
Chi^2	0.00059565		0.00035033		0.00023144	

Table 5.6 - Equivalent circuit modelling parameters for proliferating porcine smooth muscle cells.

The fitted data parameters for HUVECs are shown in Table 5.7. Cells were observed to have reached confluency before 48 hours. The electrode data displays similar trends to those seen for porcine endothelial and smooth muscle cell tests with a rise in resistance once cells settled onto the electrode. Cell layer resistances were higher than other cell types. Elevated cell layer resistance is often correlated with a high barrier function.

	HUVECs					
	0 hours	**Error %**	**48 hours**	**Error %**	**96 hours**	**Error %**
R_E	152040Ω	6.0621	417340Ω	17.476	467220Ω	19.981
$CPET_E$	11.185μF	0.49677	12.588μF	0.52333	12.8μF	0.56873
$CPEP_E$	0.88366	0.11509	0.91373	0.1432	0.91713	0.16981
R_{SOL}	200.3Ω	0.15938	161.2Ω	2.3199	150.5Ω	2.9009
R_{CL}	-	-	145.4Ω	3.5461	190.8Ω	4.4145
$CPET_{CL}$	-	-	23.403μF	14.401	98.758μF	14.18
$CPEP_{CL}$	-	-	0.48506	3.4822	0.3726	4.5467
Chi^2	0.0005842		0.00018969		0.00015901	

Table 5.7 - Equivalent circuit modelling parameters for proliferating human umbilical vein endothelial cells.

5.3 Discussion

The results from the immunofluorescence imaging and each of the cell regrowth scenarios will be discussed individually before a more general discussion on the relevance of the results to the wider project aims.

5.3.1 Cell characterisation by immunofluorescence

The overall objective of the work presented in this section was to determine the feasibility of using impedance spectroscopy in a self-reporting stent to monitor re-endothelialisation or re-stenosis. This was assessed through in vitro experimentation of cell cultures that modelled these post-stenting regrowth scenarios. It was therefore necessary to firstly use standard, invasive cell staining techniques to characterise the cell types that would be subsequently analysed by the impedance methods developed in this study. The immunofluorescence results provided evidence of successful endothelial cell isolation with positive staining for the endothelial marker von Willebrand factor (Figure 5.16a). The expression of von Willebrand factor is a commonly utilised marker for endothelial cells. Light microscopy observation of a cobblestone appearance (Figure 5.2a) typical for endothelial cells gave further confidence in the isolation procedure (Becker *et al.*, 2001; Bouafsoun, Helali, Mebarek, *et al.*, 2007). Successful smooth muscle cell isolation was evidenced through observation of expression of the marker α smooth muscle actin (Figure 5.16b), an extensively used marker of smooth muscle cells throughout the literature (Chung *et al.*, 2002; Rowlands and Cooper-White, 2008; Sakamoto, Kiuchi and Sato, 2011). A further indicator of smooth muscle cells is the observed hill and valley morphology (Figure 5.2b) associated with their in vitro, monolayer culture (Kinard *et al.*, 1997; Heydarkhan-Hagvall *et al.*, 2003). Negative controls showed minimal von Willebrand factor expression in cells from the smooth muscle cell isolation procedure (Figure 5.1c) and minimal α smooth muscle actin expression in those cells isolated using the endothelial cell procedure providing additional corroborative evidence. Collectively the results presented here provide confidence that the cell isolation procedures used throughout the course of this study were able to isolate the stated primary porcine vascular cell types.

5.3.2 Impedance monitoring of endothelial cells

The first of the key objectives within this study was to investigate if impedance spectroscopy could be used to characterise endothelial cells grown in clinically relevant populations. The experimental proliferation of endothelial cells over the electrodes correlated with variations in impedance measurements. Specifically there was a gradual rise in electrode reactance as the cells settled and then proliferated over the surface of the electrode (Figure 5.8) and this endothelial cell impedance spectroscopy trend concurs with previously published findings. This trend is often presented as a decline in the capacitance of the electrode following cell seeding and has been observed in data from endothelial cells (Michaelis *et al.*, 2012; Benson, Cramer and Galla, 2013; Zobel, Hansen and Galla, 2016) and other cell types (Campbell *et al.*, 2007). As previously detailed in section 4.7 (Impedance parameter selection) capacitance is derived in these studies from the reactance and approximates to the inverse of the reactance. This is demonstrated by comparing the plots shown in Figure 5.4. The capacitance (Figure 5.4b) declines as the cells proliferate and replace the higher capacitance of the electrode (Michaelis, Wegener and Robelek, 2013). Inversely the reactance for the same electrode (Figure 5.4a) shows an elevation from the time point of cell seeding, as the cells proliferate and cover the electrode. This can also clearly be seen in Figure 5.8 as the reactance increases in the first 48 hours after cell seeding.

It was observed that a confluent monolayer of endothelial cells was established after approximately 48 hours of culture. After this point a decline in reactance that was frequency and time dependent was then observed, with decreases occurring first at 1*kHz* and later towards 100*kHz*. These effects are best visualised in the 3D plots shown in Figure 5.5 and b as well in the mean reactance 3D plot in Figure 5.6a. The effect of this frequency dependant behaviour was to create a distinct double reactance peak. Examination of the literature has not revealed the presentation of frequency dependant reactance variation in this manner. Wegener and Seebach, 2014, present 3D frequency dependant variation of total impedance for an unspecified endothelial cell type in the range 10*Hz* to 100*kHz* with no time dependent peaks. As an aside the authors emphasise the wealth of information that 3D presentation of impedance data acquisition across a wide frequency range can provide (Wegener and Seebach, 2014). In experiments on porcine endothelial cell monolayers on gold electrodes of the same dimensions as those presented in this

study, Shedden, 2008, observed a fall in the total impedance 2 days after confluence in the 1*kHz* to 1M*Hz* frequency range. It may be that the declining reactance contributed to this fall, however the reactance data alone and its frequency dependency is not presented to permit confirmation.

The measured reactance declines that created the double peaks visible in the 3D presentation of the data always occurred following observation of confluence. This suggests that the reactance peaks arise from changes in the cells as they transition into a mature endothelial layer. With the available impedance data, microscopy images and literature it is not possible to assign a definitive reason for the observed reactance decline and the following suggestions must remain conjectural. Michaelis et al, 2013, disrupted the cytoskeleton and cell to cell junctions of epithelial cells causing a steep rise in the measured capacitance. A decline in reactance may therefore represent changes in the cytoskeletal and junctional arrangements in the endothelial cells particularly as the latter may only form in confluent monolayers. An alternative proposed explanation involves the excretion of an extracellular matrix by the cells. The filling of the space between the basolateral membrane and the electrode would cause the cells to elevate. A number of studies have investigated the effect of cellular adhesion to proteins already existing on the electrode (Wegener, Keese and Giaever, 2000; Hartmann *et al.*, 2007; Newbold *et al.*, 2010b). None have investigated the effect of extracellular matrix excretion by the cells themselves and the effect this would have on the impedance properties of cell monolayers. An argument against this hypothesis is that smooth muscle cells too will secrete an extra cellular matrix and as will be discussed in the next section 5.3.3 (Impedance monitoring of smooth muscle cells) the reactance profiles from these cells display no reactance peaks. It is also plausible that the reactance declines may well be the result of cumulative cellular maturation effects that arise on formation of an endothelial cell monolayer.

As previously stated no definitive explanation is readily forthcoming from the literature regarding the reasons why endothelial cells should display the measured reactance profile. In seeking to attribute a cause for the absence of post confluence reactance declines in the literature it should be considered that the focus of the majority of impedance spectroscopy studies carried out on endothelial cell monolayers focus on the measurement of the effect of agonist introduction rather

than as a method for comparing against other cells types. Furthermore as shown in section 4.10 (Discussion – System development) the system developed and used in the experiments presented here measures impedance over a frequency range and at a temporal resolution that is only available when using bespoke impedance spectroscopy systems. The majority of the impedance studies published use one of the available commercial systems that restrict high resolution, wide frequency range measurement. Consequently researchers using these systems to measure impedance variation in endothelial cells would not have the data available to observe the frequency dependant reactance variation. In gathering data over a wide frequency range the results presented here were able to provide high resolution reaction profiles for the re-endothelialisation in vitro model that could be compared against the other cellular regrowth scenarios.

5.3.3 Impedance monitoring of smooth muscle cells

The previously stated objective was to investigate the feasibility of using impedance spectroscopy to non-invasively characterise smooth muscle cells in clinically relevant populations. The proposed smooth muscle cell scenario was achieved as demonstrated with the light microscopy images of electrodes depicting confluent monolayers in clinically relevant populations. Smooth muscle cell proliferation caused a rise in the reactance that was correlated with the coverage of the electrodes in a similar fashion to endothelial cells. The 3D visualisation of reactance variation with both time and frequency revealed that its rate of elevation was frequency dependent. This smooth muscle cell reactance behaviour is best visualised in the 3D plot depicted in Figure 5.11a which shows a distinct upward inflecting sweep reactance profile. Lower frequencies showed a higher rate of reactance increases in comparison to high frequency measurements. Reactance declines after confluence did not occur, which is in stark contrast to the endothelial cell data measurements shown in section 5.2.2 (Impedance based characterisation of endothelial cells). The data in Table 5.4 also demonstrates the difference in reactance values between the smooth muscle cells and endothelial cells. On completion of experimentation smooth muscle cell covered electrodes had a 1*kHz* mean reactance of 13.06Ω compared to 1Ω for endothelial cells. At the higher 10*kHz* smooth muscle cell reactance was reduced to 6.51Ω whilst endothelial cells climbed to 3.33Ω and at the highest frequency of 100*kHz* the endothelial reactance (9.30Ω) was greater than smooth

muscle cells (3.78Ω). At this time point, from low to high frequencies smooth muscle cells showed reactance declines in contrast to increases for endothelial cells.

As previously described in section 1.19 (Impedance spectroscopy and smooth muscle cells) the seeding of smooth muscle cells onto electrodes and the performance of impedance spectroscopy measurement has received less research attention than endothelial cells and as such there is a reduced number of published impedance to compare the data gathered and presented here against. Balasubramanian et al, 2008, previously observed that renal rat smooth muscle cell proliferation over gold electrodes precipitated a decline in capacitance and thus can be equated to an elevation in the reactance. This impedance behaviour is similar to the endothelial cell studies described in section 5.3.2 (Impedance monitoring of endothelial cells) where the increasing coverage of the cells replaces the capacitance of the electrode lowering the capacitance. Balasubramanian et al carried out their measurements using the Biophysics ECIS system, on gold 0.05mm^2 electrodes, using a single frequency of 4*kHz* over the course of 5 hours with no microscopy images. Therefore meaningful comparison with the reactance rate variation presented here, in the 1*kHz* to 100*kHz* frequency range over 240 hours is limited. In another key study, Haas et al, 2010, were able to characterise a change in aortic rat smooth muscle phenotype as measured through changes in the frequency dependent variations in total impedance magnitude. They did not present time dependent reactance or derived capacitance variation in their findings, again limiting comparison with the results presented as part of this study. A further difference between the results presented here and the two cited smooth muscle cell impedance studies is that they all performed their experiments on gold working electrodes that were considerably smaller than the 7mm^2 electrodes used in the developed system. The set of smooth muscle cell results collected for this study can therefore be stated to make a contribution to the existing knowledge in the field of impedance spectroscopy analysis of the cell type through the use of large clinically relevant populations.

5.3.4 Impedance monitoring of HUVECs

HUVEC experimentation was included in the study to provide comparative impedance spectroscopy measurements against a cell type that has been commonly used in published impedance studies (Rahman, Lo and Bhansali, 2006; Rahman, Price and Bhansali, 2007; Seebach *et al.*, 2007; Szulcek, Bogaard and van Nieuw

Amerongen, 2014) and also cardiovascular stent research, (Prasad *et al.*, 2005; Yeh *et al.*, 2006).

The data gathered from the HUVEC experimentation display different reactance profiles to both the smooth muscle cells and the porcine endothelial cells. No variable peak is noticeable with the HUVECs, with only a single peak visible in the 3D profiles (Figure 5.32). In common with the porcine endothelial cells the peak was visible only once the cells had achieved confluency and it is possible that additional peaks may exist at frequencies beyond the 100*kHz* limit of the developed system. Measurement of HUVECs beyond 100*kHz* is hindered by the difficulties in obtaining reliable high frequency data through multiplexers as previously shown in section 4.2 (System characterisation). However Rahman et al, 2007, reported that total impedance measurements on HUVECs in the 1M*Hz* to 100M*Hz* range displayed no distinct peaks, indicating that the lower frequency range used in the present study was appropriate. The experimental end point reactance data presented in Tale 5.4 also demonstrates the differences between HUVEC and porcine endothelial cells. At 1*kHz* HUVECs had a final value of 9.28Ω, compared to 1.00Ω for endothelial cells. At 10*kHz* HUVEC reactance rises to 26.64Ω and porcine endothelial cells was 3.33Ω. At the highest frequency measured HUVEC reactance had fallen slightly to 24.84Ω, whilst porcine endothelial cells had approximately trebled to 9.30Ω.

As shown in Table 5.4 HUVEC monolayers demonstrated considerable higher reactance magnitudes when compared to porcine arterial source endothelial cells. Maximum mean reactance in the 1*kHz* to 100*kHz* range for HUVECs was 35Ω, compared to 7Ω for porcine arterial cells. The difference in reactance magnitude provides another potential method of non-invasively characterising between the cell types.

Although the use of HUVECs represents a change in both cell species and vascular tree source location from the porcine endothelial cells it can be said that the impedance results provide an indication of the sensitivity of the system in terms of cell characterisation. Endothelial cells isolated from different locations in the vasculature have been found to display heterogeneity in terms of marker expression, barrier function, structural features and junction formation (Aird, 2007a). It would therefore be expected that the cumulative effect of such differences would give rise to variations in the impedance profiles measured in cells isolated from different

species and locations within the artery tree. No studies have directly compared the impedance profiles of endothelial cells from different vasculature locations and the present study is the first to indicate that impedance spectroscopy is capable of discerning endothelial cell type. Comparison of endothelial heterogeneity using impedance spectroscopic techniques is therefore a potential avenue for future study. In the context of the objectives of the study the HUVEC findings provide confidence that the use of reactance measurement across a wide frequency range is able to characterise different cell types.

The single HUVEC seeded chamber that was cultured initially in porcine endothelial media and then changed to HUVEC media revealed an immediate fall in reactance that then recovered after 24 hours, and is best visualised in Figure 5.33a. That a change in media can induce such a prominent change in impedance profiles without inducing cell death indicates that the introduction of an agonist in the HUVEC media has caused a change in the cell monolayer that cannot be seen through light microscopy. The most obvious difference between the two media is the presence of Vascular Endothelial Growth Factor (VEGF) in the introduced HUVEC media. This is included by the manufacturer to increase proliferation of the cells allowing researchers to rapidly expand populations for their experiments. VEGF however, has been shown to have a detrimental effect on endothelial cell monolayer barrier function, inhibiting tight junctions (Wang, Dentler and Borchardt, 2001) and gap junctions too (Thuringer, 2004). That a change in a media from one with no VEGF to one with VEGF causes a drop in impedance is therefore to be expected and is in agreement with published impedance studies where VEGF is introduced to endothelial cell monolayers on electrodes. In such studies impedance falls are associated with a loss of barrier function. Hyun et al, 2015, correlated VEGF introduction with capacitance elevations and a disruption of the tight junction proteins ZO-1 and claudin-5. Becker et al, 2001, showed a VEGF dose dependent fall in transendothelial resistance and an associated actin cytoskeletal remodelling. The results for this single chamber show that the composition of the media and in particular the inclusion of growth factors can have a substantial effect on the impedance profiles of cell monolayer cultures. The data also indicates that the system developed in the present study would be able to measure any disruption of endothelium barrier function induced through the addition of agonists, as will be further explored in section 6 (Endothelial functionality).

Inspection of the time-lapse microscopy revealed that HUVECs had a high level of motility throughout the duration of the experiment. Impedance fluctuations arising from the micromotion of endothelial cells on the electrode surface observed in published studies are not evident in the measurements presented here (Giaever and Keese, 1991; Opp *et al.*, 2009; Benson, Cramer and Galla, 2013; Szulcek, Bogaard and van Nieuw Amerongen, 2014). An explanation can be found in the fact that the area of the working electrodes used in the experiments presented here is significantly greater than those used in the cited studies, at least by a factor of 140. On such large clinically relevant monolayers impedance fluctuation arising from individual cell micromotion becomes averaged out over a large population.

5.3.5 Impedance monitoring of endothelial and smooth muscle cell co-culture

Impedance spectroscopy investigation of a smooth muscle and endothelial cell co-culture was stated as a key objective in section 1.31 (Study objectives) and was one of the three in vitro cell regrowth models proposed in section 1.30 (Experimental rationale and aims). Establishing co-cultures of the type developed in the present study, where the two cell types are in direct contact within a common media and are not grown on separate surfaces, is a particularly complex challenge. A significant period of experimental development therefore preceded the establishment of the model on the electrodes. To the authors knowledge this represents the first study that has successfully achieved a smooth muscle – endothelial cell co-culture for the purposes of impedance spectroscopy measurements.

The development stage enabled key parameters to be established for the smooth muscle cell growth, quiescing and endothelial seeding stages that comprise the establishment of an in vitro co-culture model as previously detailed in section 3.6 (Cellular experimentation). The final experimental procedure represents an amalgamation of procedural steps with the method adopted most closely based on the model originally reported by Wallace et al, 2007, with the key modification of pre-culturing endothelial cells in co-culture media for 24 hours media prior to direct seeding onto the smooth muscle cell layer as performed by Lavender et al, 2005.

Von Willebrand factor and α smooth muscle actin markers were used on completion of the co-culture experimentation with the intention being to confirm the establishment of a smooth muscle cell and endothelial cell culture. Positive staining

of smooth muscle cells for von Willebrand factor was observed for those cells grown in co-culture (Figure 5.16 and Figure 5.21). This can be explained as it is a known signalling molecule between the two cell types with published effects on smooth muscle cells (Qin *et al.*, 2003; Zhang *et al.*, 2012). Any von Willebrand factor expressed by the endothelial cells in the duration of the experiment will bind to smooth muscle cell receptors and be visible in the fluorescent microscopy. The method of von Willebrand factor signalling between the cell types is likely to be extracellular owing the large 500 to 20000kDa size of the von Willebrand factor protein (Furlan, 1996). This is far in excess of the 1kDa limit for gap junctions that link endothelial and smooth muscle cells as part of intercellular myoendothelial junctions, discussed in section 1.24 (Myoendothelial junctions). It would not be expected to find microscopy evidence of myoendothelial gap junctions from the imaging methods used. Smooth muscle cells cultured in isolation that were not exposed to von Willebrand factor expressed by endothelial cells did not stain positively. This result provides further verification that an in vitro co-culture model is a more accurate representation of the in vivo scenario as smooth muscles cells cultured in isolation would not be subject to the presence of von Willebrand factor which is only one example of a signalling molecule between the two cells. When double stained cells that were positive for von Willebrand factor but not α smooth muscle actin can be considered as endothelial cells. These results provided evidence that a direct co-culture was established attaining the in vitro model proposed in 1.31 (Experimental rationale and aims). There is no published information in the literature on the use of either marker in co-cultures with researchers using experimental end point analysis techniques such as magnetic bead attachment to separate cell types (Heydarkhan-Hagvall *et al.*, 2003; Wallace and Truskey, 2010) . It can therefore be stated that the von Willebrand factor and α smooth muscle actin immunofluorescence results can contribute guidance for in vitro studies where the confirmation of an endothelial – smooth muscle cell co-culture is required.

The time-lapse microscopy images captured during the quiescing stage, during which the media serum content was reduced from 10% to 0.5%, showed smooth muscle cells changed morphology in the initial 4 hours, taking on a spheroid or rounded shape. There exists evidence in the literature from time-lapse observations of smooth muscle cells morphology changes when undergoing a phenotypic switch. Sandison et al, 2016, recorded smooth muscle cell rounding as they transitioned from a

contractile to a proliferative, migratory phenotype induced through the addition of media containing 10% FBS. The cells presented here have undergone the opposite change in their culture conditions with serum removal from the culture media. The rounding observed is likely to be a morphological change as cells transition phenotype, however additional experimentation aimed at ascertaining phenotypes before and after serum removal would be required. In the context of co-culture experimentation the observation of this behaviour provides a guideline for future tests that the smooth muscle quiescing stage should be longer than 8 hours to allow sufficient time for phenotypic transitioning to take place.

Further evidence for phenotypic switching can be seen in the total impedance changes following the reduction of serum content in the media from 10% to 0.5%. A small percentage fall in total impedance was observed for smooth muscle cell seeded electrodes during this stage, in contrast to minimal changes in control values, as shown in Figure 5.23. This result is in agreement with published data where Haas et al, 2010, observed a reduction in total impedance during the same smooth muscle cell phenotypic switching event. However the magnitude of the impedance fall measured by Haas et al was far in excess of that in the data presented here, with a 40% reduction comparing against 1.12%. A potential cause for this difference is that the procedure for co-culture requires the smooth muscle layer to be sub-confluent during the quiescence stage, in contrast to the fully covered electrodes used by Haas et al. Consequently a portion of the current flow will have been through the uncovered areas of the electrode rather than the quiescing smooth muscle cells, thereby reducing the contribution of the cells to the electrodes impedance and truncating any variations arising from phenotypic switching. The study by Haas also differed in their use of primary rat smooth muscle cells on gold electrodes. This result provides further evidence, alongside the time-lapse microscopy, that a change from a synthetic, proliferative phenotype to a contractile quiescent phenotype was induced in the co-culture model as intended. This switch from a contractile to proliferative phenotype is thought to be the key driver in atherosclerosis plaque development and in the restenosis response that characterises the arterial response to stent induced injury, as previously described in 1.2 (Atherosclerosis) and 1.3 (In stent restenosis). The findings presented both here and elsewhere suggest that this switch can be characterised non-invasively, in coronary artery smooth muscle cells,

suggesting the potential capability of impedance spectroscopy for the screening of new drugs that seek to modulate this switch for therapeutic benefit.

The time-lapse microscopy captured for the endothelial cell seeding stage shows the cells settling over the smooth muscle cells and proliferating to confluence, providing further corroborative evidence alongside the immunofluorescence microscopy that a co-culture had been established on the electrodes. The video capture of endothelial cells and smooth muscle establishing an in vitro co-culture is to our knowledge a further unique research finding with no examples available for comparison in the literature.

Following endothelial cell seeding onto smooth muscle cells reactance elevations achieved a maximal value approximately 48 hours after cell introduction followed by a decline creating distinct peaks, best visualised in Figure 5.27. The presence of reactance peaks following the seeding of endothelial cells can be attributed to the formation of an endothelial monolayer and evidence for this can be found in a number of features in the data set collected. Firstly, the peaks are of the same profile and occur over the same time period as previously observed in the endothelial cells data where cells were seeded alone onto electrodes within the same seeding density range as shown in previously in section 5.3.2 (Impedance monitoring of endothelial cells). In addition, the time variation in reactance peaks between chambers correlated with the light and time-lapse microscopy observed progress of endothelial cell proliferation. Electrodes where cells proliferated more quickly reached a reactance peak sooner than was observed on slowly proliferating electrodes. The clear existence of the reactance peak in the data reveals that the co-culture impedance profile is dominated by the endothelial cells in the double layer. These results provide some confidence that in the in vivo scenario of a self-reporting stent, should smooth muscle cells proliferate over the struts and subsequently become re-endothelialised then it will be evident in the impedance data. As previously stated impedance spectroscopy measurements on a double layer of smooth muscle and endothelial cells in co-culture is unique and as such there are no published studies available for comparative input.

5.3.6 Equivalent circuit modelling

The results from the equivalent circuit modelling show that a constant phase element in parallel with a resistor provides a good model for platinum black electrodes in cell media with comparable results to published values in the literature (Franks *et al.*, 2005). However once cells have adhered to the electrodes the selected model loses its accuracy. The electrode components of the model showed an instability that was not evident in the unprocessed impedance data presented elsewhere in this study. This is best evidenced by the increases in the electrode resistive component (R_E) which should remain stable throughout. At the completion of each experiment R_E increased by 2.5 times for Endothelial cell experiments, 2.4 times for smooth muscle cells and 3.07 for HUVECs. This shows that cellular impedance contributions have been incorporated into the models electrode components. Such instability was not observed by Shedden, 2008, in her experiments using the same cell types on gold electrodes of the same dimensions with a maximal 1.3 times increase. The model used in this study may not be suitable for cells adhered to platinum black electrodes. Of further concern for the circuit modelling results was the high errors assigned to constant phase element values with Endothelial cell layer CPE_T errors rising to 41%. Consequently the circuit modelling data is of limited use for characterising between the cell types. Future work should aim to develop a more accurate circuit model to fit with the available data. It maybe that a different circuit is required for cellular elements once confluency has been attained, adding a further level of dynamic complexity to equivalent circuit modelling.

5.3.7 Cell characterisation with the total impedance ratio

As discussed in section 4.7 (Impedance parameter selection) a method developed by Shedden, 2008, used the total impedance ratio to determine characteristic peaks at frequencies that were proposed as being specific to each cell type. Tested by Shedden were porcine endothelial cells and smooth muscle cell monolayers on electrodes of the same dimensions as those used in this study. A comparison can be made between the total impedance ratio peaks found by Shedden and those determined from the data presented here, as shown previously in Figure 5.36. Table 5.8 compares the peak frequencies from the two studies with all experimented cell types.

Cell type	Present study	Shedden study
Porcine endothelial	1260*Hz*	22387*Hz*
Porcine smooth muscle	40*Hz*	2512*Hz*
MDCK	Not tested	794*Hz*
HUVEC	794*Hz*	Not tested
Co-culture	5000*Hz*	Not tested

Table 5.8 - Peak total impedance ratio comparison between present study and Shedden, 2008, for various cell types once confluency was attained.

It can be seen from the data in Table 5.8 that the peak total impedance frequencies differ between the two studies. In seeking an explanation it is important to state the experimental differences between the two studies. The excitation voltage applied in current study was 50mV which compares with 200mV used by Shedden. No other published study has used an excitation voltage above 200mV on cells directly adhered to electrodes. Examples of excitation voltages from other studies have been previously detailed in the system specification comparison table in section 4.10 (Discussion – System development). Although 200mV can be considered high in the context of published impedance studies there is no defined limit at which an excitation voltage can no longer be considered non-invasive. Furthermore there is no evidence that the use of different excitation voltages can alter the total impedance ratio frequency peaks. An additional key difference between the studies is the electrode substrate material, with the results in the present study carried out on platinum black electrodes as opposed to gold electrodes by Shedden. Other published studies have measured impedance variations on confluent monolayers of the same cell types through modification of the electrode substrate through protein adherence although none specifically analysed the total impedance ratio (Wegener, Keese and Giaever, 2000; Bouafsoun, Helali, Othmane, *et al.*, 2007; Newbold *et al.*, 2010b). Therefore analysis of the data presented here alongside those published by Shedden and elsewhere indicates that comparison of impedance parameters for the purposes of cell characterisation is material specific and is only valid when performed on electrodes from the same substrates. As will be seen and discussed in the later section 7 (Conducting polymer substrate testing), results from conducting polymer electrodes lend credence to this proposal.

5.3.8 Relevance of results to a self-reporting stent

5.3.8.1 Re-endothelialisation

The data from the in vitro re-endothelialisation model presented in section 5.2.2 (Impedance based characterisation of endothelial cells) indicates that a self-reporting stent has the potential to be able to detect any re-endothelialisation of the stent struts. The progression of the reactance as the monolayer approached, attained and went beyond confluency suggests that a self-reporting stent would be able to characterise between a partially and fully re-endothelialised stent. Identification of complete endothelial cell coverage would be an indicator that the patient is at a lower risk chance of in stent thrombosis development.

The differences between the smooth muscle and endothelial cell reactance profiles indicate that impedance spectroscopy measurements from a self-reporting stent may be able to characterise the cell type coverage. Smooth muscle cells do not form an anti-thrombotic barrier between the stent struts and the circulating blood in the same fashion as endothelial cells and the non-invasive measurement of their proliferation and absence of endothelial cells would show that the patient has a higher risk of in stent thrombosis. The observation of a distinct endothelial cell profile in the co-culture results also demonstrates that endothelialisation may be possible even with a smooth muscle cell substrate.

It is not known if the frequency dependent reactance peaks observed to be characteristic of endothelial cells will be repeated in an in vivo scenario and this is therefore a key research question in any future development of a monitoring device. The frequency ranges over which the in vitro reactance peaks where determined provide guidance that a self-reporting stent will be required to perform impedance measurements over the same or similar ranges in order to provide sufficient data resolution for re-endothelialisation characterisation. This is of relevance in considering the technical development of a self-reporting stent were the circuitry should be designed to target frequencies that are only required to characterise the cell regrowth scenarios and the in vitro results suggest that for re-endothelialisation the range of $1kHz$ to $100kHz$ is suitable. The measurement of frequencies that are not required for cellular regrowth characterisation would lead to extraneous circuitry and consequently additional unnecessary device volume. Future in vivo testing of a prototype device would enable further determination of key frequencies.

Should a self-reporting stent be able to provide data to clinicians that re-endothelialisation has taken place over the struts then this would have implications for the patient's future treatment. As discussed in section 1.5 (Drug-eluting stents), following stenting patients undergo an extended course of anti-platelet and anti-coagulant drug therapy aimed at reducing the possibility of thrombus development on the exposed stent surface. The formation of an endothelial layer over the struts provides an antithrombotic surface reducing the likelihood of thrombus development. With the knowledge that such a cellular regrowth scenario has occurred clinicians can reduce or cease the patient's drug therapy. This is of particular importance for those patients with additional conditions that are exacerbated by the use of anti-platelet drugs. No current monitoring technique, invasive or non-invasive, has the capability to determine that re-endothelialisation has taken place.

5.3.8.2 In stent restenosis

The in vitro smooth muscle cell proliferation model is proposed in section 1.30 (Experimental rationale) and comprises the establishment of a monolayer of smooth muscle cells over the electrodes. As discussed in 1.2 (In stent restenosis) the disease is characterised by the excessive proliferation of smooth muscle cells resulting in neo-intimal growth that ultimately occludes blood flow. The smooth muscle cell proliferation model used here may be considered to be representative of the very early stages of the disease. The growth of single layers of smooth muscle cells is asymptomatic and as such the identification of this a scenario in-vivo would be of little clinical relevance. Further discussion on the importance of smooth muscle cell growth in monolayers in-vivo is limited by the lack information on the cellular growth of in stent-restenosis in its very early stages. This is in part due to the currently available diagnostic techniques being only able to discern the later stages of the disease where smooth muscle proliferation and extra cellular matrix excretion has created a large lesion. In the context of the proposed cellular regrowth scenarios over a conceptual self-reporting stent the results presented are indicative that the proliferation of smooth muscle cells would give rise to impedance variations that could provide an early diagnosis of in stent restenosis.

The co-culture results show that even with smooth cells as a substrate re-endothelialisation is detectable using impedance spectroscopic techniques. However should this scenario be detected in vivo by a self-reporting stent it is not currently

known if this is an indicator of a successful cell regrowth outcome whereby the endothelial layer prevents thrombus formation, restenosis and neoatherosclerosis. An alternative cell growth scenario is the continued proliferation of smooth muscle cells and the accompanying extracellular matrix excretion, underneath the endothelium ultimately leading to a restenotic lesion that can be considered late in stent restenosis. In this case detection of smooth muscle cells might also be a very early indicator of the disease. A self-reporting stent would ideally be able to determine the level of neo-intimal growth allowing clinicians to predict when a patient will develop in stent restenosis symptoms. Post-mortem studies inspecting restenotic lesions have shown the presence of an intact endothelium in cases involving both bare metal and drug-eluting stents (Nakano *et al.*, 2013). Whilst providing a crucial insight into the disease pathology, such end point analysis techniques cannot ascertain at what point the endothelium formed nor if its presence attenuates or accelerates the growth of the lesion. The continual layering of proliferating smooth muscle cells may also be evident in the impedance measurements from a self-reporting stent. As discussed in section 1.30 (Experimental rationale) the creation of this thicker intimal layer scenario on electrodes is not possible using in-vitro cell culture techniques, although evidence from in-vivo impedance measures published elsewhere provide a guide as to the use of impedance spectroscopy in measuring stenotic lesions. As previously detailed in section 1.8 (Restenosis diagnosis - invasive techniques) impedance measurements taken using electrodes attached to a catheterisation balloon were able to differentiate between diseased lesions and healthy disease-free surrounding tissue. The data was captured from the inside of the artery and as such measured lesions from the opposite side of the neointimal growth to the proposed self-reporting stent, however they demonstrate that impedance spectroscopy can measure larger thicknesses of tissue (Süselbeck, Thielecke, Köchlin, *et al.*, 2005). These in vivo results represent the opposite time point in the disease progression to the mono and double layers presented in this study. Collectively the data from this study and published elsewhere can be used to make a case that a self-reporting stent would potentially be able to characterise the initiation and progression of in stent restenosis.

5.3.8.3 In vivo discernment of cell regrowth scenario

The impedance signature of the stent immediately after it has been implanted would be used as the reference data against which later data points would be normalised. Whilst the control measurements representing bare electrodes in the data presented here remained stable the in-vivo impedance measurements from a self-reporting stent will also to remain stable, over a clinically relevant period, potentially in excess of 12 months. It is assumed that if the in-vivo data fails to deviate significantly away from the reference value as shown in the cell free control values then it will be an indication that the stent remains bare and exposed to the blood flow. As discussed in section 1.6 (Stent thrombosis) a bare stent increases the patients risk of thrombosis. It is the occurrence of the re-endothelialisation signature within the early stages after stenting that would be a key marker of the desired cellular regrowth. This would allow clinicians to make an informed decision on the removal of any antiplatelet therapy courses. Any delay in this re-endothelialisation signature would be indicative of a lack of re-endothelialisation and represent a stent implant that is at a higher risk of restenosis or thrombosis.

Inevitably there will remain a temporal aspect to any diagnosis of the aforementioned scenarios. In seeking to understand how cellular regrowth rates would influence the reactance profiles additional in vitro testing where endothelial and smooth muscle cells are seeded across a wider range of densities than those used in the experiments presented here would show how the reactance profiles are influence by proliferation rates. However in vitro testing would only to be able to provide a guide to the rates of re-endothelialisation and restenosis as there is a paucity of information regarding the in vivo time progression and sequences of restenosis and re-endothelialisation in humans. As discussed in section 1.4 (Re-endothelialisation) animal studies have provided some information on the time progression of re-endothelialisation but there remains a gap between these and the observed rates in humans. Comparison between the time course of re-endothelialisation in in vivo animal studies and data available from humans indicate that the cell proliferation impedance signatures measured in this study would be considerably extended in an in vivo scenario.

5.4 Limitations

A number of limitations for the experimental work presented in this section should be acknowledged and are discussed here. Wider limitations applicable to all of the work presented in this thesis are discussed in section 8.7 (General study limitations).

5.4.1 Re-endothelialisation mechanism

The modelling of post-stenting cellular regrowth in the experiments was initiated by the seeding of cells onto the electrodes. In the case of an implanted stent in a coronary artery the regrowth is thought to be initiated by migration of cells from the edges of the strut (Pérez de Prado *et al.*, 2011). This represents a difference in the regrowth pattern between the study and the in vivo scenario although the attachment of circulating endothelial cells can be considered similar to cell seeding.

5.4.2 Restenosis model thickness

In stent restenosis is characterised by neo-intimal growth of smooth muscle cells to the extent whereby a lesion becomes large enough to occlude blood flow. The in stent restenosis models presented here are made from a confluent monolayer of smooth muscle cells or a co-culture with a sub confluent monolayer of smooth muscle cells and a monolayer of endothelial cells. Consequently a more accurate model would constitute multiple layers of smooth muscle cells that accumulate over time. Achieving this depth of growth is difficult in vitro as the lower layers detach from the substrate having been unable to receive sufficient nutrients from the media as the upper cell layers form a barrier. Larger in vitro 3 dimensional culture is possible by using engineered scaffolds and hydrogels into which cells can be seeded. Inevitably the gels and scaffold will have their own impedance properties that would themselves require characterisation.

5.4.3 Co-culture smooth muscle cell phenotypes

A further limitation for the co-culture model is that the smooth muscle cells were in a quiescent state during the stage where endothelial cells were seeded and grown. It is however the proliferative synthetic phenotype that predominates during the progression of in stent restenosis. The smooth muscle cells were quiesed as part of the co-culture procedure and this stage is part of all of the published procedures for the co-culture of endothelial and smooth muscle together. However none of the

studies were aiming to create a representation of diseased tissue and a more accurate in vitro model for in stent restenosis would have been proliferative smooth muscle cells underneath the endothelium.

5.4.4 Growth rate clinical relevancy

Although variable growth rates were observed and measured between cell types there was no active control over how quickly or slowly the cells were allowed to proliferate. The time taken to confluence was also influenced by the seeding densities used for each cell type which were deliberately kept within a relatively narrow range to maintain experiment to experiment repeatability. The in vivo rate of re-endothelialisation and in stent restenosis in vivo may be highly variable, a situation that a self-reporting stent will need to contend with. A greater range of cell growth rates would therefore have added a level of clinical relevance to the results.

5.5 Future work

As discussed previously the re-endothelialisation mechanism used in this study is not wholly accurate of cell proliferation over the stent struts in vivo. An experiment that could investigate a different proliferation mechanism of endothelial cells would initially involve the seeding of cells over the electrodes as presented here. A high voltage current could then be applied to kill and detach the cells on the electrode. The confluent viable cells on the culture plastic adjacent to the electrode would then be able to migrate and proliferate onto the new bare platinum black surface in the same fashion as over stent struts in vivo. The same experimental procedure could also be repeated for smooth muscle cells.

Although extensively thick layers of cells are difficult to achieve in vitro it still may be possible to create multiple smooth muscle cells layers that would model in stent restenosis at a later stage than the single layer or co-culture models present here. The periodic re-seeding of smooth muscle cells onto electrodes whilst recording impedance measurements could provide a guide as to how the impedance profile will change in vivo as the disease progresses. This experimentation could be continued until the lowest level of cells detach from the electrode due to contact inhibition or starving of nutrients.

Matching the in vitro growth rate of seeded cells with the rate with the re-endothelialisation and in stent restenosis development observed clinically in humans

would more accurately align the in vitro models with the in vivo, clinical pathology. The rate of progression of both scenarios in humans is likely to be slower with an average development time for late stage in stent restenosis of 5.5 months (Dangas et al., 2010). Experimentation aimed at achieving this objective could aim to influence in vitro rates through lower seeding densities or modulation of nutrients and growth factors in the media. In this regard smooth muscle cell experimentation will be required to overcome the paradoxical challenge of maintaining a slow growth rate for the proliferative synthetic cell phenotype that is responsible for in stent restenotic lesion growth.

5.6 Summary

Overall it can be stated that impedance spectroscopy is able to characterise between endothelial cell growth and smooth muscle cell growth in vitro. Characteristic reactance peaks for endothelial cells at high frequency (100*kHz*) showed 10.5 fold increases in comparison to control electrodes whilst smooth muscle cells only showed a 4.4 fold increase at the same frequency. At lower 1*kHz* frequencies this comparative trend was inverted with smooth muscle cells showing a 7.2 fold increase of control values whilst endothelial cells showed a 0.45 times reduction (values derived from data shown in table Table 5.4). Reactance comparison at other time points also showed differences across the 1*kHz* to 100*kHz* frequency range, best visualised in 3D presentation of the data.

This result makes impedance spectroscopy a good candidate technology for the in vivo measurement of cell growth scenarios over stent struts. The results in this section have shown that impedance spectroscopy can be used, in vitro, to characterise endothelial monolayers and that the technique has the potential - when translated to an in vivo environment - to be able to inform clinicians which cellular regrowth scenario has taken place over an implanted stent. As discussed in section 1.4 (Re-endothelialisation) the functionality of an endothelium is of importance in preventing disease states such as in stent restenosis and thrombosis, therefore additional knowledge on endothelial monolayer functionality would be of great benefit to clinicians. Impedance spectroscopy assessment of endothelial dysfunction as induced through the inhibition of gap junctions is detailed and discussed in the following section 6 (Endothelial layer functionality).

6 An investigation into the use of impedance spectroscopy for monitoring endothelial cell layer function

6.1 Introduction

The ability of an implanted stent to assess the function of the endothelial cell layer that forms over stent struts would be an additional capability aiding in the clinical monitoring of vessel healing. As previously discussed, the establishment of a healthy functional endothelium over the implanted stent struts following implantation is the gold standard of cellular regrowth scenarios. However endothelial layers are known to exhibit different levels of functionality and the knowledge that re-endothelialisation is complete is not necessarily a guarantee that thrombus development, restenosis or neoatherosclerosis will be prevented. In vitro experiments have revealed that drug-eluting stents can be associated with endothelial dysfunction (Finn, Nakazawa, *et al.*, 2007). Although endothelial dysfunction can be characterised by a number of features a key aspect that has been used as an indicator of such dysfunction is a loss of barrier function, whereby the endothelium no longer acts as a selective barrier between the blood and the artery tissue (Tesfamariam, 2016).

The introduction chapter has described the critical role, that, gap junctions play in the establishment of healthy endothelial layer (see section 1.23 Gap junctions). Furthermore, a paucity of gap junctions has been linked to a dysfunctional endothelium and is associated with regions where atherosclerotic plaques form (Ebong and Depaola, 2013). Gap junctions are inter-cellular channels that allow for the exchange of ions, metabolites and other signalling molecules across the monolayer. As these junctions are only able to form between cells whose monolayers are in contact with one another, any variation in their electrical properties would only be measurable once the monolayer had achieved confluency.

The work described in this chapter aimed to recreate one aspect of a dysfunctional, endothelial monolayer by blocking gap junctions. The intention was to transition the

confluent endothelial cell monolayer on the electrodes from a healthy functional state to a dysfunctional state through the addition of drugs known to inhibit gap junctions. There are currently no published studies that have used impedance spectroscopy to analyse the inhibition of gap junctions in endothelial cells. We hypothesised that the use of impedance spectroscopy measurements throughout the process would enable the characterisation of the transitional phase and ultimately dysfunction. An important aspect in achieving this experimentally is the selection of a gap junction inhibitor that has previously demonstrated efficacy in endothelial cells.

6.2 Gap junction mediators

One of the primary areas of research for blocking gap junctions is Neuroscience, where inhibitors are used to reduce intercellular communication between neurons (Juszczak and Swiergiel, 2009). A wide variety of compounds have been found to have an inhibitory effect on gap junctions and consequently there is no dedicated class of drugs (Salameh and Dhein, 2005). A further consideration is that the mechanism of action is not certain for the majority of gap junction inhibitors (Dhein, 2004; Brisset, Isakson and Kwak, 2009). Some of these agents have been found to be specific for a given connexin whilst others are non-specific and have an inhibitory effect on multiple connexins. Connexins are transmembrane proteins that assemble into larger hemi channels, one half of a gap junction (see section 1.23 Gap junctions). It should also be considered that many gap junction blocking compounds have inhibitory effects on hemi channels comprised of the other class of transmembrane proteins, the pannexins. Furthermore, some drugs have secondary actions resulting in them often being referred to as “dirty”. These effects must be considered in any analysis involving gap junction inhibition. Examples of gap junction inhibitors with secondary effects are Thrombin, previously detailed as being an inhibitor of tight junctions and Vascular Endothelial Growth Factor (VEGF) which encourages cell proliferation. In the context of experimentation on endothelial cells the selected agent should also be known to act on the three connexins expressed by this cell type, Cx37, Cx40 and Cx43. The two selected gap junction inhibitors that meet this criterion, and which were therefore used in this study, were carbenoxlone and heptanol. Brief information on these two compounds is detailed below.

- The 18-α-glycyrrhetinic acid derivative carbenoxolone is described as a non-specific gap junction blocker (Pelegrin and Surprenant, 2006). It has been

demonstrated to be an effective blocker of connexin gap junctions, connexin hemi-channels and Panx-1 hemi channels (Lohman and Isakson, 2014). In bovine endothelial cells following gap junction blocking with carbenoxolone up regulation of Cx43 was discovered in a negative feedback response mechanism (Sagar and Larson, 2006). It is one of the most commonly used inhibitor of gap junctions in research, therefore allowing results from this study to be compared against a wider range of other studies.

- Heptanol is a long chain alcohol and is another widely used inhibitor of gap junctions. The drug is thought to be incorporated into the lipid bilayer and consequently reduces the open probability of gap junctions (Takens-Kwak *et al.*, 1992; Salameh and Dhein, 2005). Its efficacy has been demonstrated on the connexins Cx 37, Cx40 and Cx43 that make up endothelial cell gap junctions (D'hondt *et al.*, 2009). As is often found with other gap junction inhibitors there is an accompanying blocking effect on connexin hemi-channels, however in contrast to the aforementioned carbenoxolone, heptanol has been found to have no effect on Panx-1 hemi channels (Pelegrin and Surprenant, 2006). Heptanol is part of a different class of drugs to carbenoxolone, therefore being a good alternative inhibitor for experimentation.

Beyond gap junction inhibition more recent research by Begandt et al, 2010, has identified an agonist that can increase the formation of gap junctions between cells. The drug Dipyridamole has been highlighted as having an enhancing effect on the formation of gap junctions and a dual mechanism of action has been proposed, whereby each of these actions results in the increase of cyclic Adenosine Monophosphate (cAMP) within the cell. This in turn activates protein kinase A, an important mediator of gap junction formation. In the present study it was decided that dipyridamole could provide a positive control for gap junction inhibition and was included in the plan for the endothelial functionality experiments.

6.3 Section aims and objectives

Previously section 1.31 (Study objectives) defined the study's objective with regards to endothelial functionality as follows.

- Investigate if a dysfunctional endothelial monolayer with inhibited gap junctions can be identified using impedance spectroscopy on a clinically relevant population.

Specific aims for the experimentation detailed in this section that aimed to address this objective are listed below.

- Investigate if the carbenoxolone induced inhibition of gap junctions in endothelial monolayers can be characterised using impedance spectroscopy.
- Investigate if the dipyridamole induced enhancement of gap junctions in endothelial monolayers can be characterised using impedance spectroscopy.
- Investigate the dose dependency of carbenoxolone induced gap junction inhibition in endothelial monolayers using impedance spectroscopy.
- Investigate if the heptanol induced inhibition of gap junctions in endothelial monolayers can be characterised using impedance spectroscopy.
- Investigate the dose dependency of heptanol induced gap junction inhibition in endothelial monolayers using impedance spectroscopy.
- Investigate the link between gap junction inhibition and tight junction formation in endothelial monolayers using impedance spectroscopy.

6.4 Experimental structure

Gap junction experiments were carried out as described in section 3.8 (Junction experimentation). In total 4 experiments were performed and details of these are summarised in Table 6.1. Endothelial cells were seeded into chambers and grown until confluency was observed by light microscopy. The gap junction mediator was then added as part of a standard media change and the experiment then continued for either 4, 24 or 48 hours. The principal end point analysis technique was a lucifer yellow scratch assay, previously discussed in section 1.25 (Gap junction assessment) and the methodology used described in section 3.8 (Junction experimentation). This assay permitted fluorescence microscopy imaging to assess the level of intercellular communication through gap junctions. The final experiment (4) also used anti ZO-1

antibody staining to investigate the formation of tight junctions, using the procedure described in section 3.8 (Junction experimentation).

Experiment	Object of experiment investigation	Seeding density (x 10^4 cells/cm^2)	Passage no.	Gap junction mediator chamber allocation	End point analysis
1	Gap junction inhibition / enhancement	6.25	3	3x Carbenoxolone 100 µM	Lucifer yellow scratch assay
				3x Dipyridamole 50 µM	
				2x Control cells	
2	Carbenoxolone dose dependancy	4.125 to 4.5	3	3x Carbenoxolone 100 µM	Lucifer yellow scratch assay
				3x Carbenoxolone 50 µM	
				2x Control cells	
3	Heptonol gap junction inhibition	4.5 to 6.25	5	3x Heptanol 100 mM	Lucifer yellow scratch assay
				3x Heptanol 50 mM	
				2x Control cells	
4	Tight junction formation	6	4	3x Carbenoxolone 100 µM (end point analysis 4 hours post dosage)	Lucifer yellow scratch assay
				3x Carbenoxolone 100 µM (end point analysis 24 hours post dosage)	Anti ZO-1 antibody.
				2x Control cells	

Table 6.1 - Summary details of four experiments performed to assess endothelial gap junctions (1-4) and tight junctions (4).

6.5 Data presentation

As previously discussed in the system development section 4.7 (Impedance parameter selection), total impedance was selected as the parameter to provide a measure of an endothelial layers functionality. The frequency of 10*kHz* has previously been justified and used to present impedance spectroscopy measurements of cell monolayers and used in the present study to characterise cell types (section 5 - In vitro cell characterisation by impedance spectroscopy). In the context of endothelial cell dysfunction the *kHz* range has been previously used to measure the barrier function of cell monolayers (Benson, Cramer and Galla, 2013; Wegener and Seebach, 2014; Stolwijk *et al.*, 2015). Consequently all 2D plots in this section use total impedance data measured at 10*kHz*. Inspection of the 3D dimensional profiles for dosed cells also demonstrates the frequency range over which mediator addition effects occurred. Figure 6.1 shows representative 3D total impedance profiles for an undosed control electrode (Figure 6.1a) and a carbenoxolone dosed electrode (Figure 6.1b), demonstrating that the effect of dose addition occurs across the depicted 1*kHz* to 100*kHz* range. It can be seen in Figure 6.1b that the introduction of 100µM

carbenoxolone at 48 hours causes a decrease in the total impedance in comparison to dose free cells (Figure 6.1a).

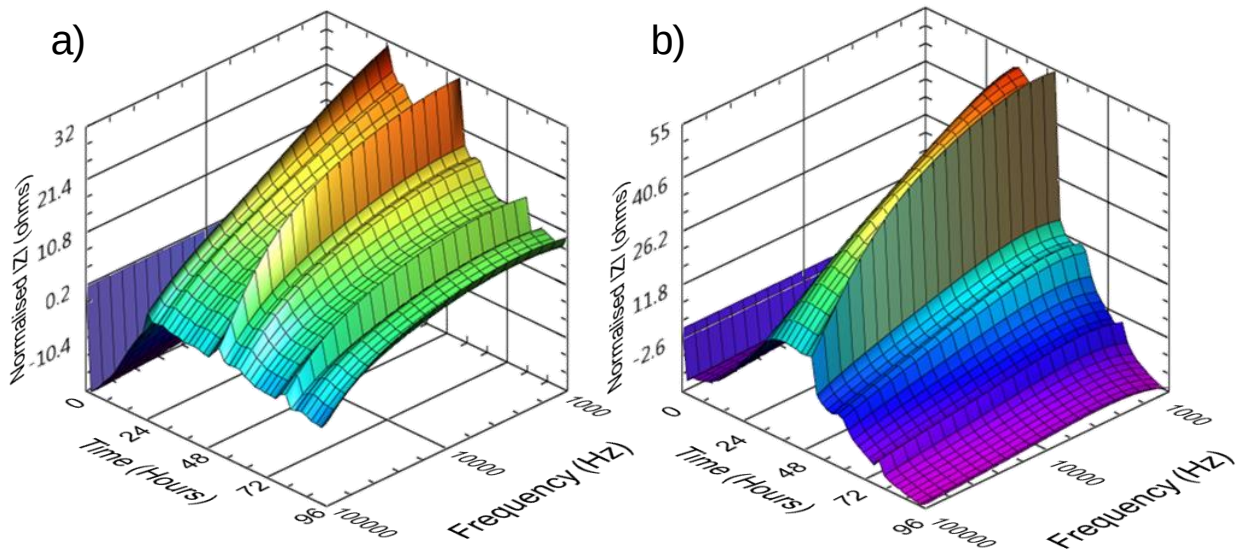

Figure 6.1 - Representative electrode 3D normalised total impedance (z axis) variation over time (x axis) for endothelial cells across the frequency range 1kHz to 100kHz (y axis). a) Control with media change at 48 hours and b) 100µM carbenoxolone dosed cells at 48 hours. Data representative of 12 electrode pairs.

Total impedance data presented for gap junction experiments was normalised against the data point immediately before mediator addition, all subsequent points therefore represent the total impedance response of cells under the influence of the drugs. Data presentation in this manner has been previously used by Arndt et al, 2004, to demonstrate the cytotoxic effect of agonists on endothelial cells. An example of total impedance profiles for electrodes from a representative chamber and the corresponding profiles after the described normalisation are shown in Figure 6.2. The two plots show that presentation of the data in this manner allows the effect of the addition of mediators to be more clearly elucidated.

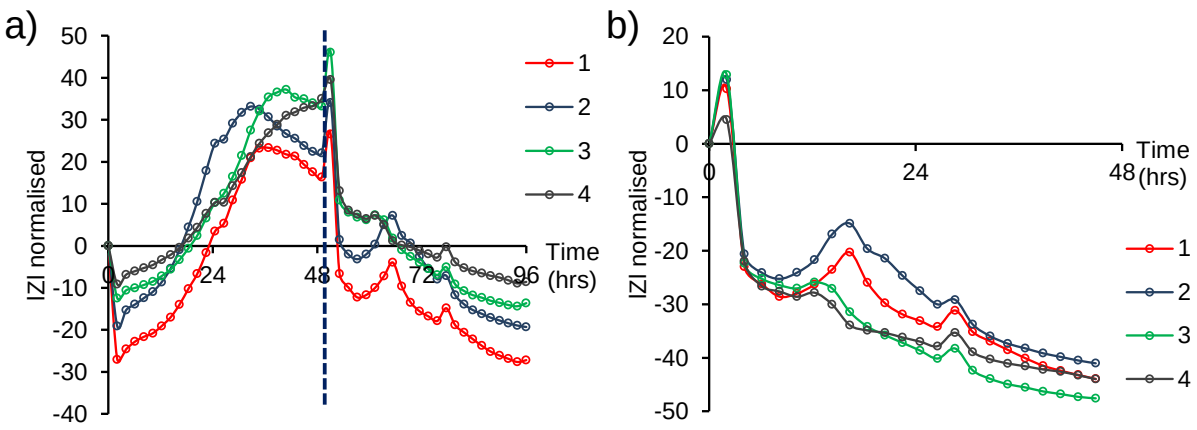

Figure 6.2 – Total impedance electrode profiles at 10kHz from a representative chamber in experiment 1. a) Data normalised against first measurement, blue dashed line represents carbenoxolone 100µM dosing. b) Data normalised against impedance value immediately prior to carbenoxolone 100µM dosing.

All electrodes displayed a rise in total impedance as the cells first settled and began to proliferate, covering the electrode, in a similar manner to data from the endothelial characterisation experiments. The measured values also corresponded to the observed cell coverage from the periodic light microscopy images and the time lapse videos. Once confluence was observed gap junction mediators were added to the cells. The response of the cells to these gap junction mediators will now be presented.

6.6 Results

6.6.1 Experiment 1 - Carbenoxolone and dipyridamole

Experiment 1 aimed to compare the impedance characteristics of endothelial cells dosed with a gap junction enhancer (dipyridamole - 50μM) and a gap junction inhibitor (carbenoxolone - 100μM). The cells were observed to have attained confluency after 50 hours of culture, at which point the media was changed to media containing the aforementioned gap junction mediators. Concentrations for the various agonists were derived from published experimental data (Sagar and Larson, 2006; Begandt *et al.*, 2013). Following addition of either drug there were no observable variations in cell behaviour from the light microscopy images. Example light microscopy images of cell monolayers pre and post mediator introduction are shown in Figure 6.3. Time lapse microscopy captured carbenoxolone 100μM dosed cells also showed no significant change in comparison to pre-dosed behaviour. Experiment 1 time lapse video is referenced as Junction expt 1 - CBX 100uM in the electronic appendix.

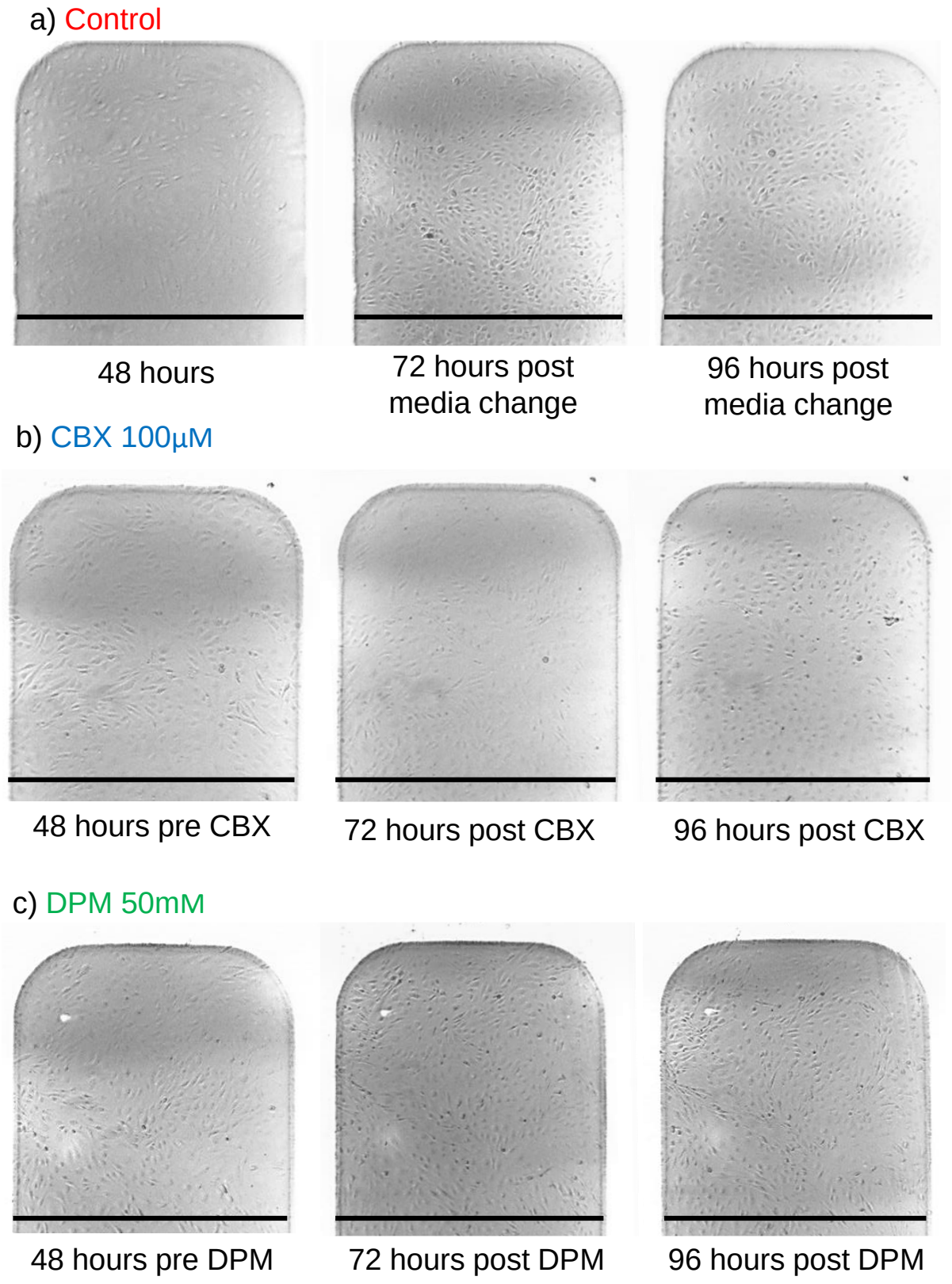

Figure 6.3 - Light microscopy of electrode tips, from experiment 1. a) Control, b) 100µM Carbenoxolone (CBX) dosed cells, c) 50µM dipyridamole (DPM) dosed cells. Scale bars are 1000µm. Images are representative of 12 dipyridamole and carbenoxolone dose electrodes and 8 control electrodes.

Total impedance variations at 10*kHz* after drug additions for experiment 1 are depicted in Figure 6.4. The introduction of carbenoxolone, dipyridamole and media alone precipitated an initial rise in total impedance in the first two hours, a disturbance that is typical for the introduction of media to cell monolayers. Thereon in the total impedance dropped with divergence between the data sets apparent in the magnitude of these falls. Cells exposed to gap junction enhancer dipyridamole demonstrated only small reductions in total impedance following its introduction and when compared to control cells show an enhanced level of total impedance. Small impedance fluctuations at 28 hours can be attributed to disturbance of the chambers where they were removed from the incubator for light microscopy imaging.

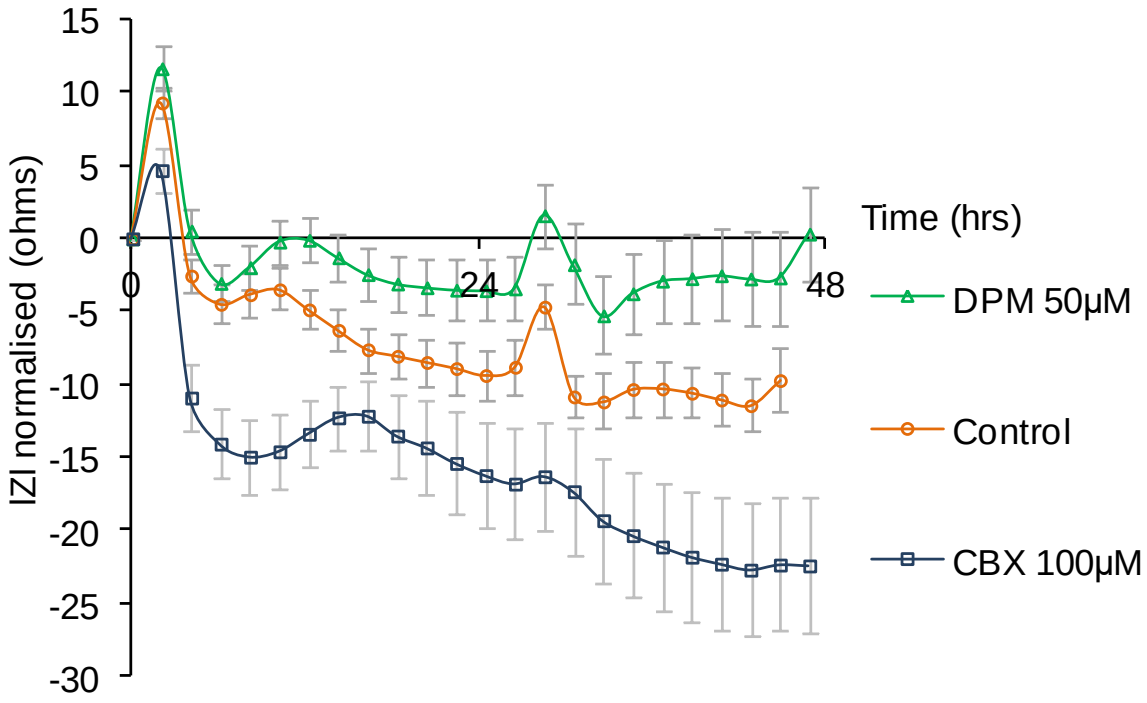

Figure 6.4 – Mean total impedance profiles at 10kHz following gap junction mediator addition to confluent endothelial cells on platinum black electrodes in experiment 1. Error bars are ± standard error mean, carbenoxolone (CBX) 100µM n=12, dipyridamole (DPM) 50µM n=11, and control n=7.

The mean total impedance drop 4 hours after dosing for each mediator and controls are shown in Figure 6.5, with statistical significance assessed using one way ANOVA followed by Tukey's post-hoc multiple comparison test as described in section 3.8.1 (Statistical analysis). 4 hours was selected as a time point as this would

allow sufficient time for normal fluctuations from media addition to stabilize. Such a time point of assessment also aligned with examples in the literature (Sagar and Larson, 2006; Begandt *et al.*, 2015). Carbenoxolone exhibited a statistically significant reduction in monolayer total impedance on the electrodes. The dipyridamole induced enhancement was not assessed to be statistically significant.

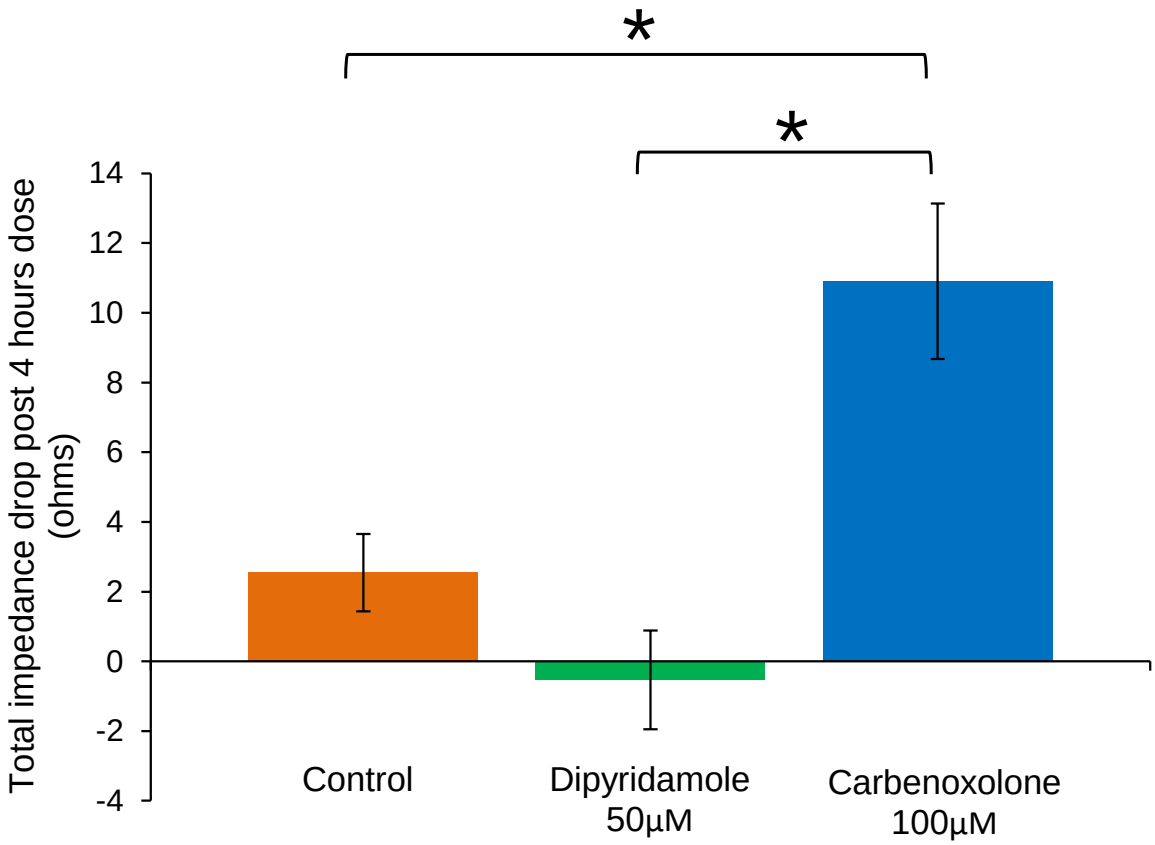

*Figure 6.5 – Mean total impedance reduction at 10kHz 4 hours after gap junction mediator addition, error bars are ± standard error mean, control n = 8, dipyridamole n = 11, carbenoxolone n = 12 . * denotes statistical significance, p < 0.05.*

After the last impedance measurement had been performed, 48 hours after agonist addition, the cells within the chambers were scratch assayed in the presence of 0.05% Lucifer yellow and fixed in 10% formalin. Assessment of gap junction formation was achieved using a lucifer yellow scratch assay as described in section 3.8 (Junction experimentation). Representative lucifer yellow scratch assay images from experiment 1 of dosed and control cells are shown in Figure 6.6. Control and dipyridamole 50µM chambers show a clear dispersion of lucifer yellow through gap junctions away from the scratch (Figure 6.6 a and b) demonstrating the presence of

gap junctions in the monolayers. Dye penetration from carbenoxolone 100µM dosed cells, shown in Figure 6.6c, was clearly reduced in comparison to controls and principally limited to those cells immediately adjacent to the scratch edges, indicating that a reduction in gap junctions had been achieved.

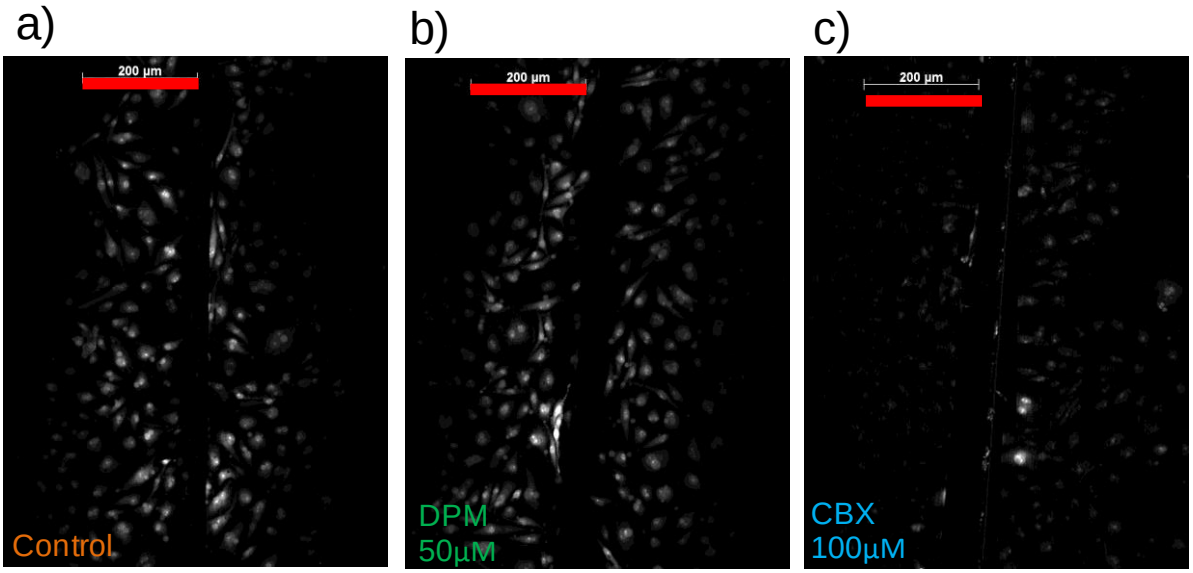

Figure 6.6 – Lucifer yellow (0.05%) scratch assay fluorescence microscopy images of endothelial cell monolayers on electrodes from experiment 1 48 hours after dosing. a) control – no dosage, b) dipyridamole 50µM and c) carbenoxolone 100µM. Red scale bars are 200µm. Images are representative of 12 dipyridamole and carbenoxolone dose electrodes and 8 control electrodes.

The images obtained from the scratch assays were processed using ImageJ software as described in section 3.8 (Junction experimentation). The results of this analysis, which have expressed the level of fluorescence as a mean pixel intensity for each treatment are shown in Figure 6.7. Carbenoxolone was found to significantly reduce the dye penetration compared to untreated controls further confirming the fall in intercellular communication via gap junctions observed in Figure 6.6c. Dipyridamole significantly enhanced dye penetration compared to controls, in agreement with the image shown in Figure 6.6b. These results confirm that carbenoxolone (100µM) prevents intercellular communication through the inhibition of gap junctions and that dipyridamole (50µM) increases intercellular communication within confluent endothelial cell layers.

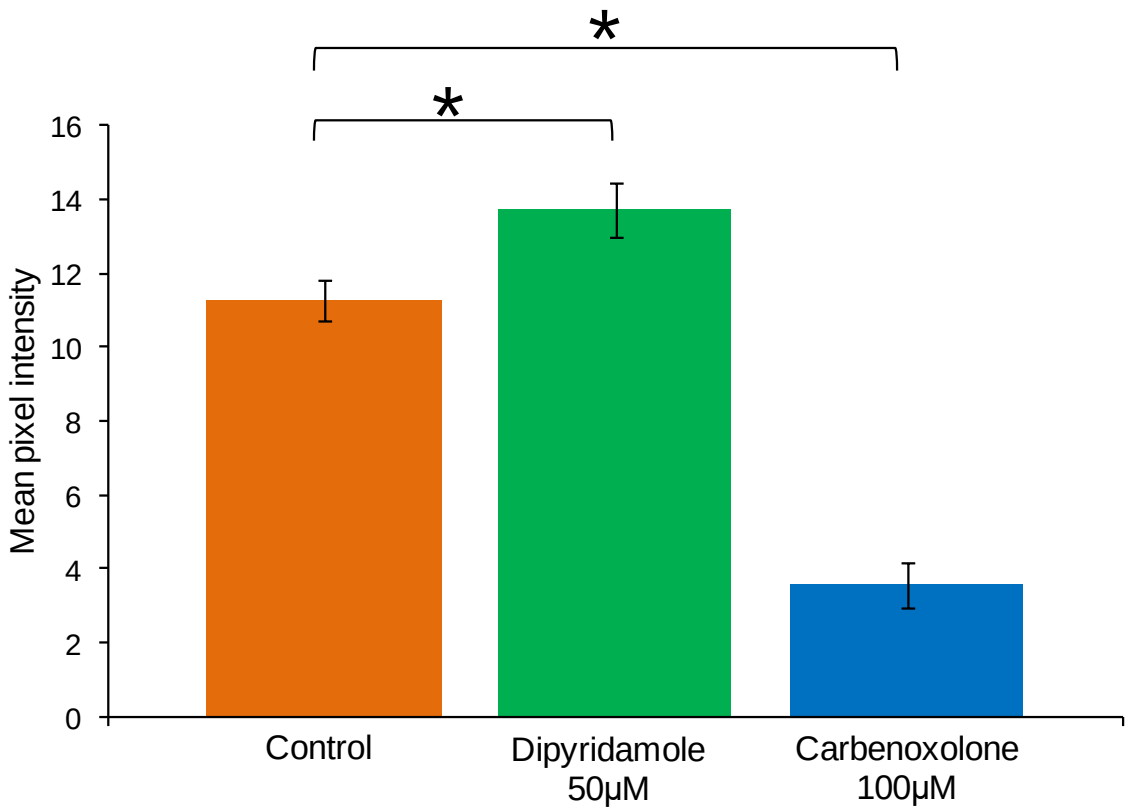

*Figure 6.7 - Mean pixel intensity from lucifer yellow scratch assay regions on electrodes. Error bars are ± standard error mean, control n = 8, dipyridamole n = 12, carbenoxolone n = 12. * denotes statistical significance, p < 0.05.*

6.6.2 Experiment 2 - Carbenoxolone dose dependency

Experiment 2 aimed to determine if the carbenoloxolone induced total impedance drops seen in test 1 were dose dependant. Two concentrations of carbenoxlone were examined, as guided by the literature (100µM and 50µM) (Pelegrin and Surprenant, 2006; Sagar and Larson, 2006). Figure 6.8 shows the total impedance response following dosing of the cells at these concentrations. The addition of carbenoxolone at 100µM concentration resulted in a decline in total impedance after inhibitor addition followed by a recovery after 24 hours and then a decline until the experiment was concluded 48 hours later. Carbenoxolone at 50µM induced the same trends but with reduced magnitudes in the initial 24 hours after dosing before falling to the same values as 100µM dosed cells after 48 hours. By comparison, cells on control electrodes with no gap junction inhibitor added showed an elevation in total impedance that then stabilised. Both 50µM and 100µM dosed cells showed a recovery in impedance values between 12 and 24 hours before a final decline in the remaining experimental time.

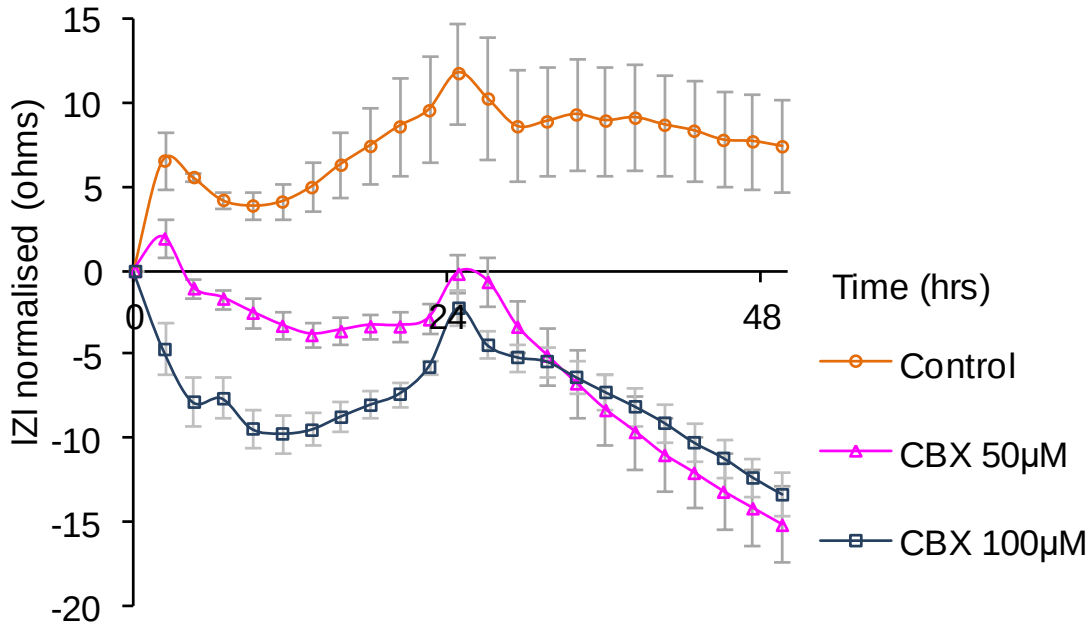

Figure 6.8 - Mean total impedance profiles at 10kHz following gap junction mediator addition to confluent endothelial cells on platinum black electrodes in experiment 2. Error bars are ± standard error mean, control n=7, carbenoxolone (CBX) 50µM n=9 and carbenoxolone 100µM n=10.

Differences between the dosed cells are evident in comparing the total impedance drop between the concentrations 4 hours after introduction, as shown in Figure 6.9. Total impedance differences between control, 50µM and 100µM dosed cells were found to be statistically significant. These data indicate that the reduction in endothelial cell monolayer total impedance caused by carbenoxolone is dose dependent for the two concentrations examined in this study.

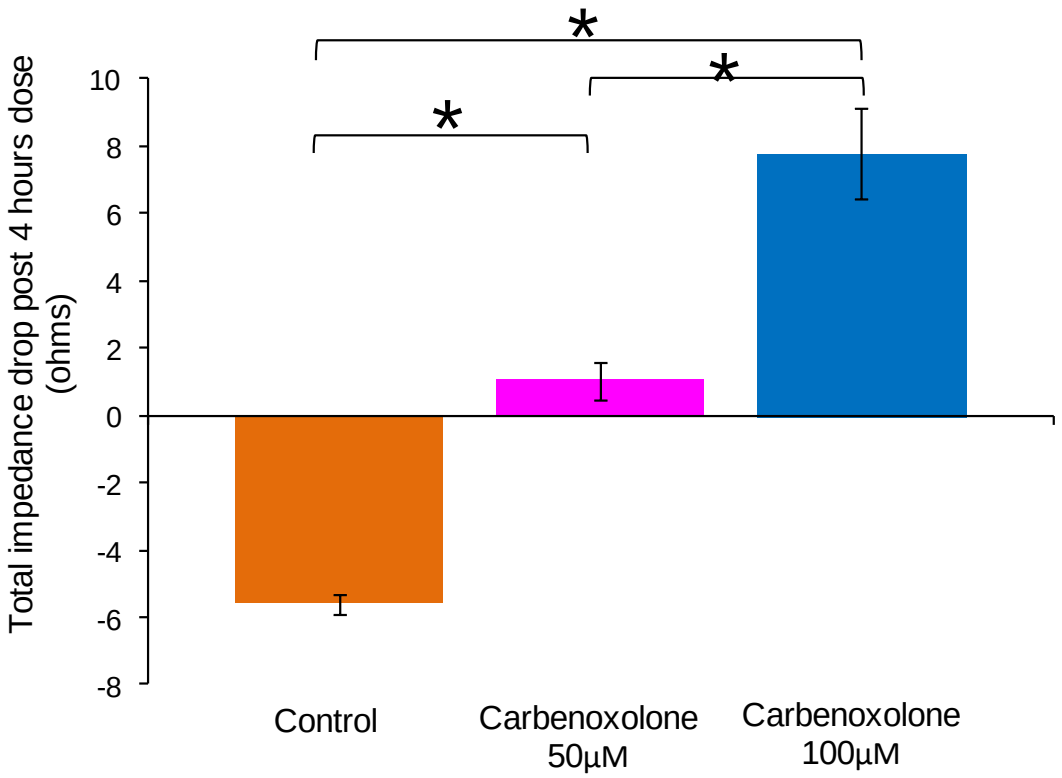

*Figure 6.9 – Mean total impedance reduction at 10kHz 4 hours post carbenoxolone addition, error bars are ± standard error mean, control n = 7, carbenoxolone 50µM n = 11, carbenoxolone 100µM n = 11 . * Denotes statistical significance, p < 0.05.*

Light microscopy images and-time lapse video showed no differences in cell coverage or morphology between the pre and post mediator addition stages as evidenced by the time-lapse video referenced file name Junction expt 2 - CBX 50uM in the electronic appendix.

Control electrode images of the lucifer yellow scratch assay (Figure 6.10a) show dye penetration from the wound edge, via gap junctions and across the monolayer. Whilst minimal dye transfer from the wound edge was seen in the 50µM and 100µM carbenoxolone dosed cells (Figure 6.10 b and c). Subsequent image analysis, shown in Figure 6.11, revealed that the mean pixel intensity observed at both concentrations was found to be significantly different from control values. Carbenoxolone 50µM and 100µM dosed cells were not found to be statistically significantly different from one another. These results show that whilst the total impedance drops following carbenoxolone addition appear to be dose dependant the scratch assay analysis did not reveal such a dose dependant response.

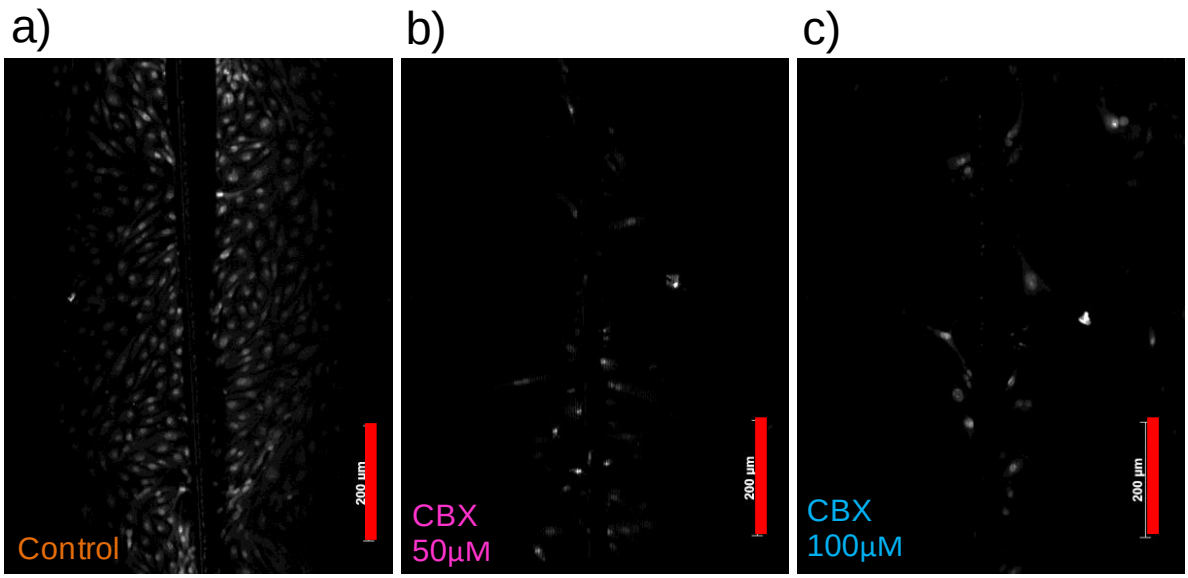

Figure 6.10 – Representative lucifer yellow (0.05%) scratch assay fluorescence microscopy images of endothelial cell monolayers from experiment 2 48 hours after dosing. Electrodes dosed with a) control – no dosage, b) carbenoxolone 50µM and c) carbenoxolone 100µM. Red scale bars are 200µm. Images are representative of 11 carbenoxolone 50µM electrodes, 10 carbenoxolone 100µM electrodes and 8 control electrodes.

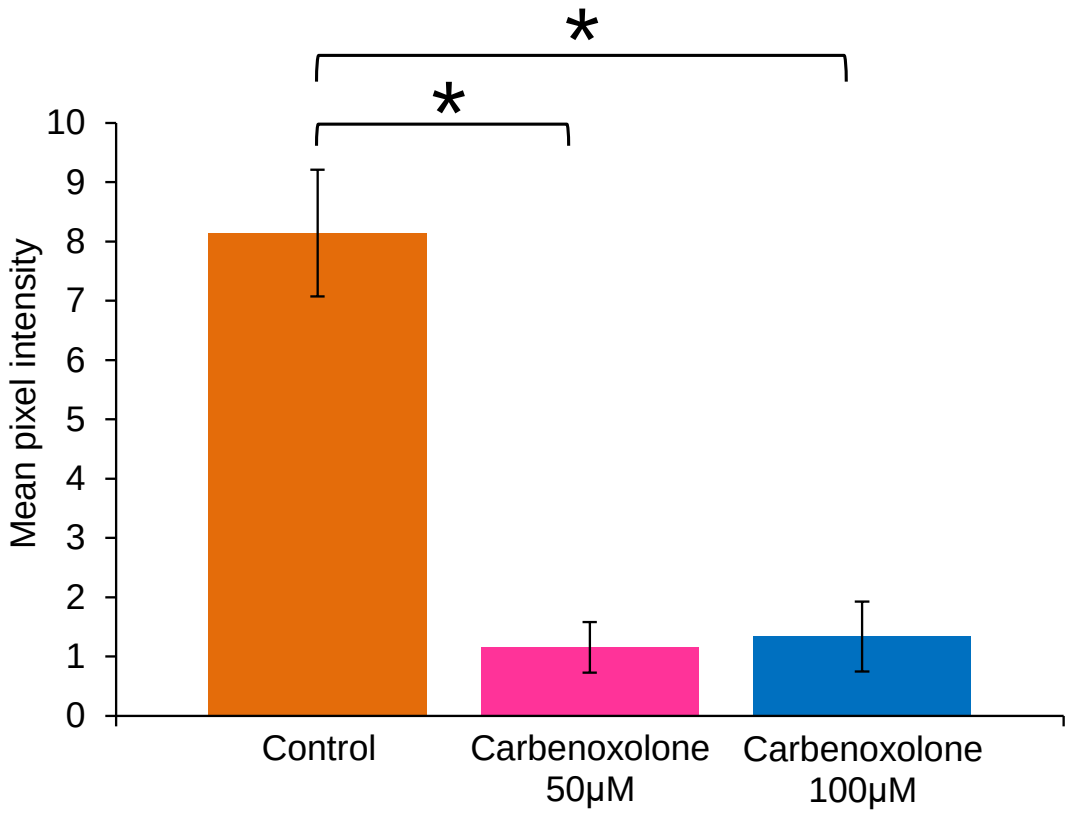

*Figure 6.11 - Mean pixel intensity from lucifer yellow scratch assay regions. Error bars are ± standard error mean, control n = 8, carbenoxolone 50µM n = 11, carbenoxolone100µM n = 10 . * Denotes statistical significance, p < 0.05.*

6.6.3 Experiment 3 - Heptanol dose dependency

Experiment 3 aimed to discern if the measured impedance behaviour seen in carbenoxolone dosed cells was repeated using a different gap junction inhibitor; heptanol. Confluent endothelial cell monolayers were dosed with heptanol at concentrations of 0.5mM and 1mM. These concentrations were based on those used in previous studies (Spray, Ye and Ransom, 2006; Asfour *et al.*, 2010). Light microscopy images and time lapse video showed no differences in cell coverage or morphology between the pre and post mediator addition stages as evidenced by the time-lapse video referenced file name Junction expt 3 - HPT 1mM in the electronic appendix. Total impedance profiles for junction test 3 are shown in Figure 6.12. All cells showed drops in total impedance within the first 8 hours. However the magnitude of the falls was greatest for 1mM dosed cells, then 0.5mM and finally control exhibiting a minimal reduction. All categories then showed some recovery in total impedance, an effect which also appeared to be dose dependent.

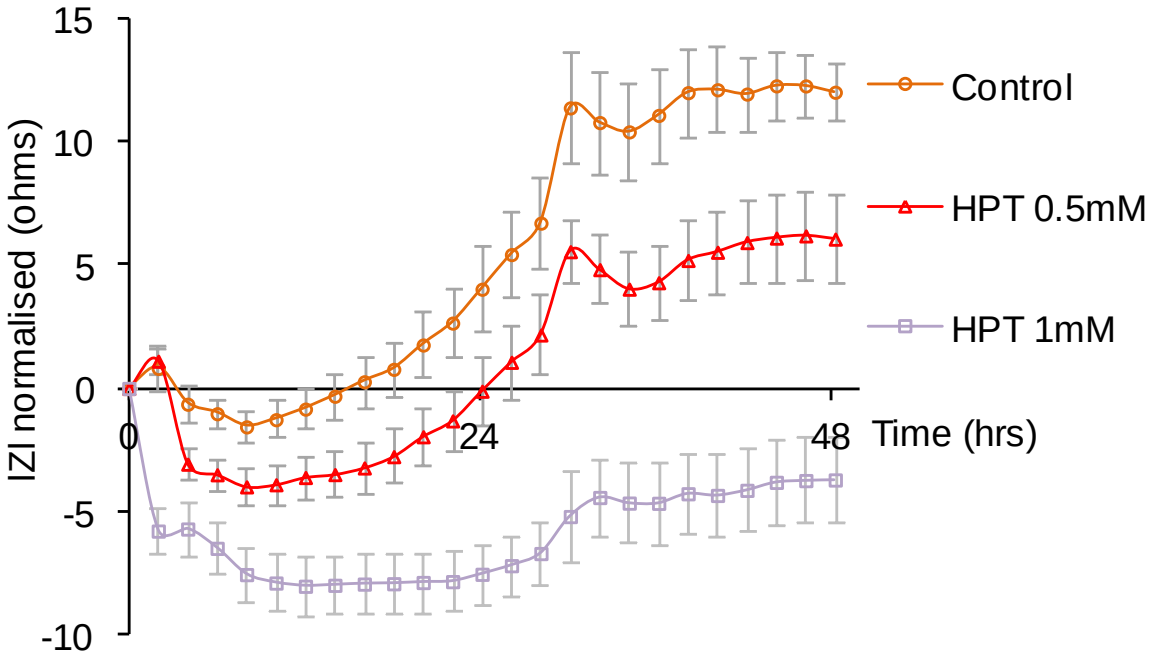

Figure 6.12 - Mean total impedance profiles at 10kHz following gap junction mediator addition to confluent endothelial cells on platinum black electrodes in experiment 3. Error bars are ± standard error mean, control n=4, heptanol (HPT) 0.5mM n=8 and heptanol 1mM n=11.

The post 4 hour total impedance drop data are shown in Figure 6.13. Heptanol (1mM) was assessed as statistically significant when compared to control values. However the fall measured for 0.5mM heptanol was assessed as being not statistically significant when compared to control values. The magnitudes of the total impedance drops were reduced for heptanol when compared to carbenoxolone, however it should be noted that this compares different cells taken from different isolations.

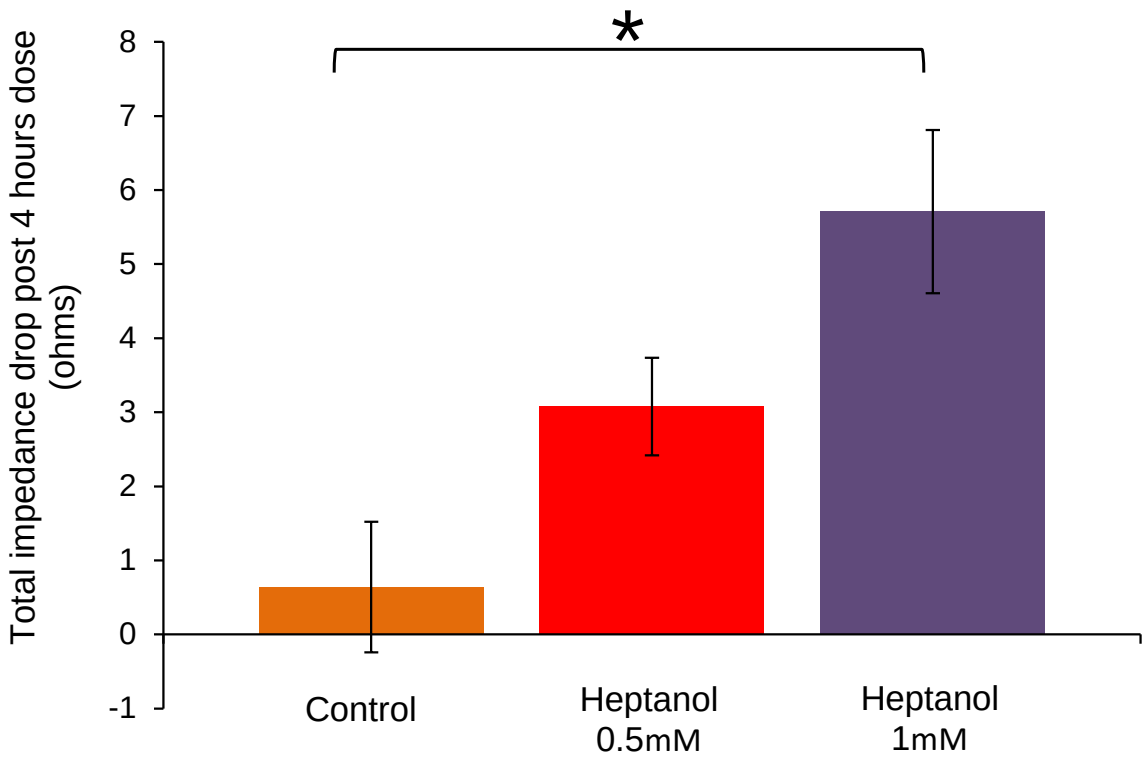

*Figure 6.13 – Mean total impedance reduction at 10kHz following heptanol addition, error bars are ± standard error mean, control n = 3, heptanol 0.5mM n = 8, heptanol 1mM n = 11. * Denotes statistical significance, $p < 0.05$.*

Gap junction inhibition was confirmed by the scratch assay images shown in Figure 6.14 and the results of the analysis of the dye penetration using ImageJ software are shown in Figure 6.15. Dye transfer was assessed as being reduced in both 0.5mM and 1mM heptanol dosed cells and was statistically significant in the case of 1mM. Dye transfer in 1mM dosed cells was reduced when compared to 0.5mM and was also statistically significant showing a dose dependent response. All heptanol dosed cells showed a larger amount of dye transfer compared to those dosed with carbenoxolone, although as previously stated the experiments were conducted on cells deriving from different isolations.

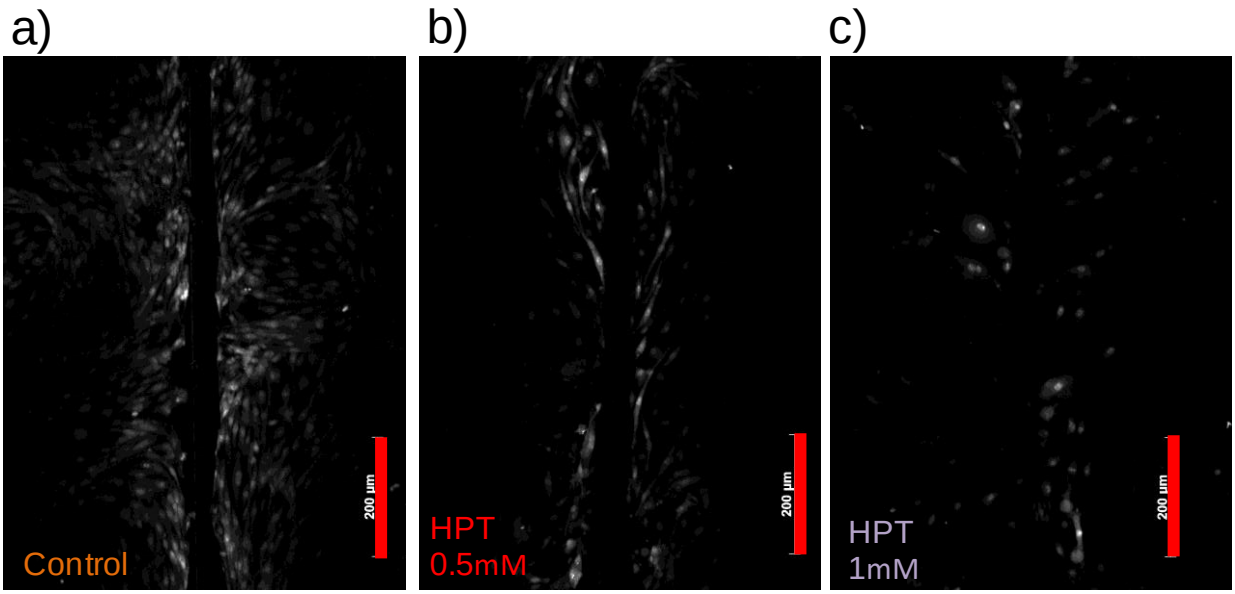

Figure 6.14 - Representative lucifer yellow (0.05%) scratch assay fluorescence microscopy images of endothelial cell monolayers from experiment 3 48 hours after dosing. a) control – no dosage, b) heptanol 0.5mM and c) heptanol 1mM. Red scale bars are 200µm. Images are representative of 12 heptanol 0.5mM electrodes, 10 heptanol 1mM 100µM electrodes and 8 control electrodes.

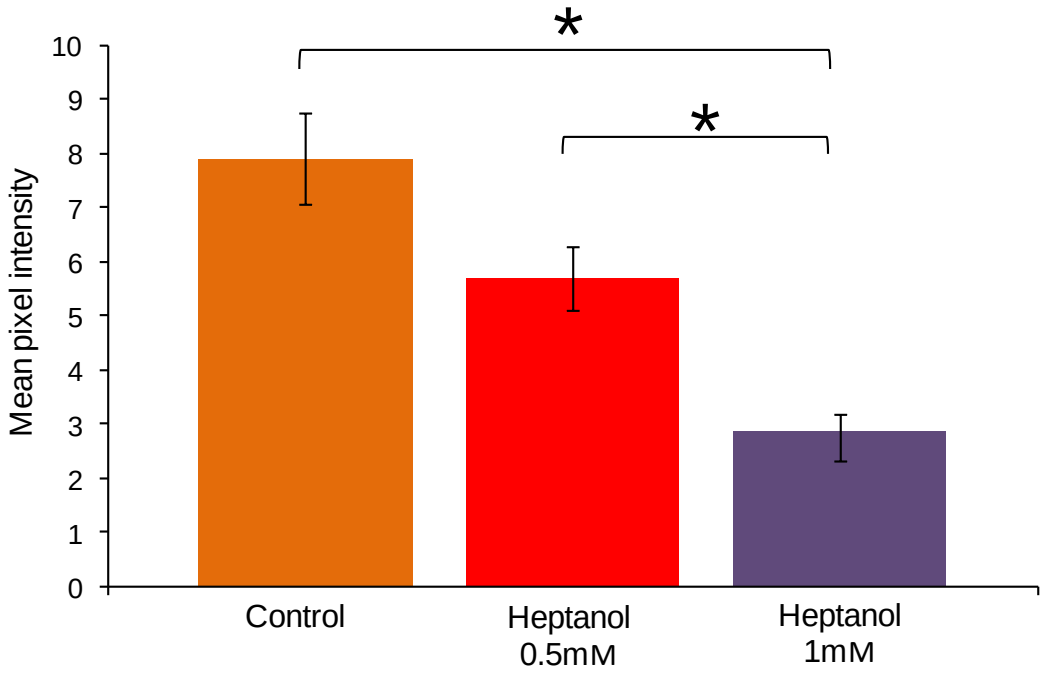

*Figure 6.15 - Mean pixel intensity from lucifer yellow scratch assay regions. Error bars are ± standard error mean, control n = 8, heptanol 0.5M n = 12, heptanol 1mM n = 10 . * Denotes statistical significance, p < 0.05.*

6.6.4 Experiment 4 - Tight and gap junction inter dependency

The final junction test aimed to determine if there was a link between gap junction inhibition and the expression of tight junctions. The drops in impedance parameters observed in experiments 1 to 3 may be loss of barrier function in the endothelial layer (Benson, Cramer and Galla, 2013; Stolwijk *et al.*, 2015). The barrier function of endothelial cells is primarily provided and regulated by the formation of tight junctions between adjacent cells (Clark, 2009). It was therefore hypothesised that the recovery of total impedance values after gap junction inhibition seen in the previous tests may be due to the reformation of tight junctions. In order to investigate this hypothesis in experiment 4, impedance measurements in chambers were stopped at either 4 or 24 hours after the addition of the gap junction inhibitor. At this point ZO-1 and lucifer yellow staining methods were then used to analyse for the formation of both tight and gap junctions respectively. The positive expression of ZO-1 is associated with the formation of tight junctions (Nagasawa *et al.*, 2006). Control chambers were continued without media changes only for 24 hours.

The experiment was performed in the same manner as experiments 1 to 3, with seeded cells grown up to 100% confluence before the addition of media containing 100μM carbenoxolone. Carbenoxolone was selected as the gap junction inhibitor, as the results from previous junction experiments demonstrated it to be a more effective inhibitor, evidenced in the magnitude of total impedance falls when compared to heptanol dosed cells, best visualised by comparing Figure 6.9 and Figure 6.13.

Light microscopy images and time lapse video showed no differences in cell coverage or morphology between the pre and post mediator addition stages as shown in the time-lapse video from the carbenoxolone 24 hour data set referenced file name Junction expt 4 - CBX 100uM in the electronic appendix. Time—total impedance profiles following dosing for the 3 data set categories of 4 hours, 24 hours and controls can be seen in Figure 6.16. Control cells displayed a relatively small decline in impedance over the first 10 hours, before stabilising for the remainder of the 24 hour period. In the 24 hour carbenoxolone group, an initial decline over the same period as seen with the control cells was observed, although the magnitude of this fall was much greater than the control. A steady increase in impedance towards the control values then occurred between 10 and 24 hours. In the 4 hour carbenoxolone data set, the fall in total impedance was similar in magnitude to the 24 hour

carbenoxolone group reported in the same graph and observed previously in experiments 1 and 3.

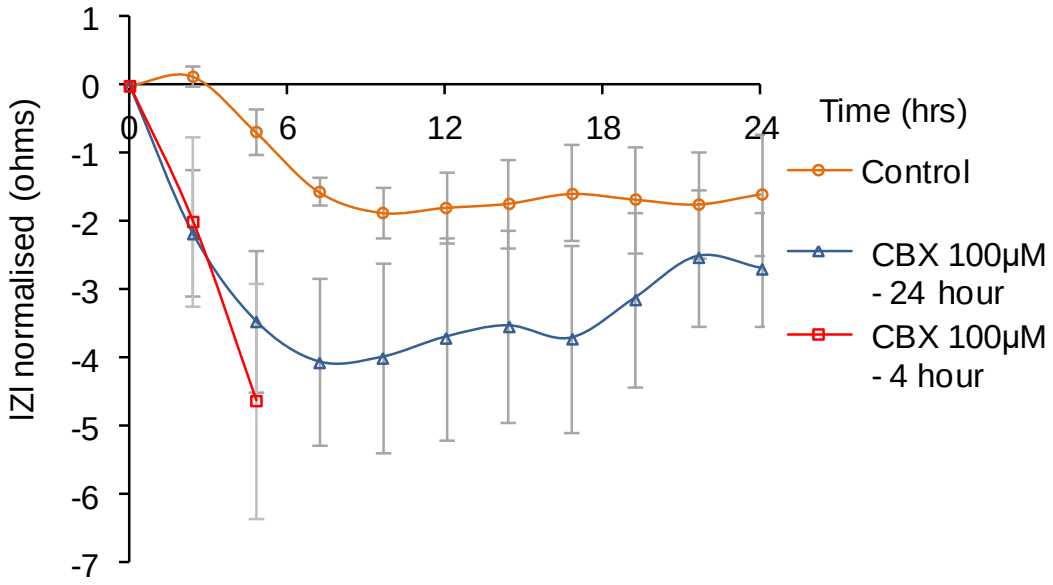

Figure 6.16 - Mean total impedance profiles at 10kHz following gap junction mediator addition to confluent endothelial cells on platinum black electrodes in experiment 4. Error bars are ± standard error mean, control n=5, carbenoxolone (CBX) 24 hours 100µM n=9 and carbenoxolone 4 hours 100µM n=7.

Representative lucifer yellow scratch assay images of the experiments described above are shown in Figure 6.17 with the accompanying ImageJ analysis results provided in Figure 6.18. As seen previously in experiments 1 and 2, carbenoxolone significantly inhibited gap junction communication compared to control cells. A difference in dye penetration was discerned between the 2 dosed data sets, with the 24 hour group showing less intercellular communication than those cells measured 4 hours after dosing. This indicates that the time taken for carbenoxolone to inhibit junctions extends beyond 4 hours after dosing. These observations are supported by the quantitative data shown in Figure 6.18.

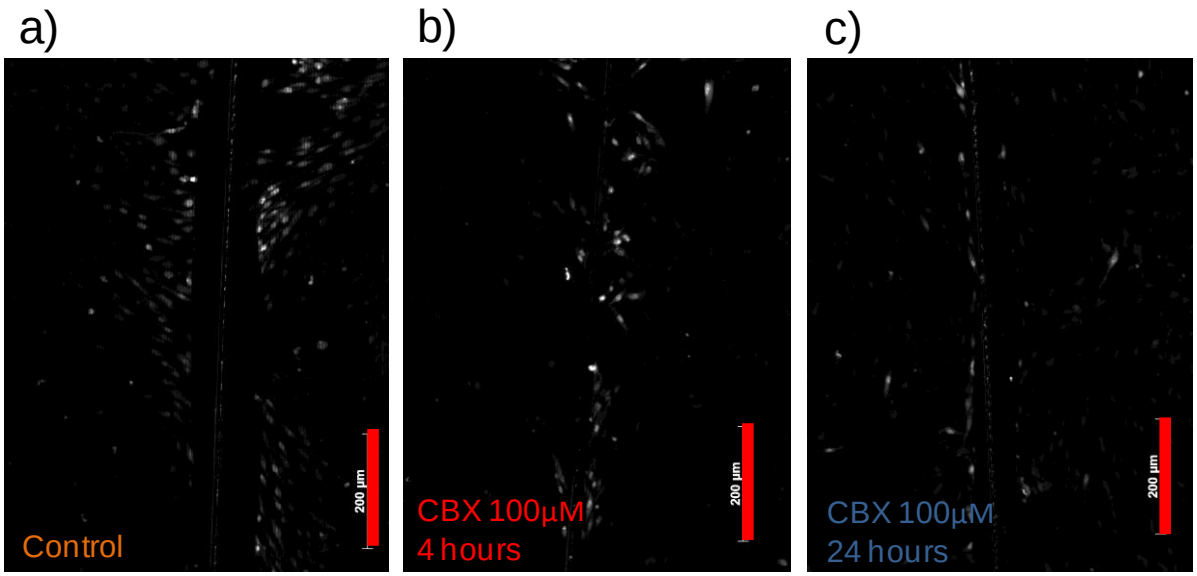

Figure 6.17 – Representative lucifer yellow (0.05%) scratch assay fluorescent microscopy images from junction experiment 4. a) Control 24 hours after media addition only. b) 4 hours after carbenoxolone 100µM dose addition. c) 24 hours after carbenoxolone 100µM dose addition. Red scale bars are 200µm. Images are representative of 12 for 4 hour data set, 11 for 4 hour data set and 8 control electrodes.

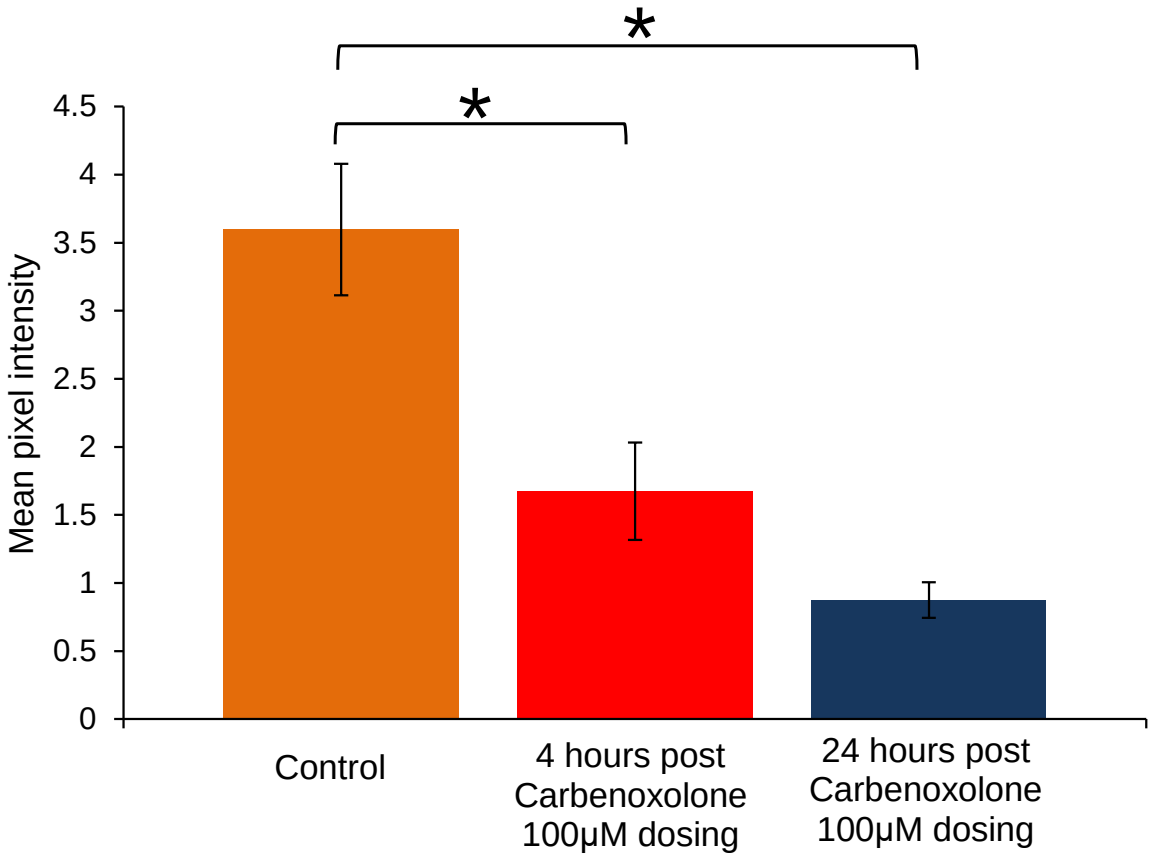

*Figure 6.18 - Mean pixel intensity from lucifer yellow scratch assay regions. Error bars are ± standard error mean, control n = 8, 4 hours after carbenoxolone 100µM dose n = 12, 24 hours after carbenoxolone 100µM dose n = 11, n = 10. * denotes statistical significance, p < 0.05.*

Fluorescent microscopy images of ZO-1 expression are shown in Figure 6.19. It can be seen from the images that no discernible differences in ZO-1 expression can be determined between the control, 4 hour and 24 hour data sets, showing that carbenoxolone does not influence the expression of ZO-1. The location of ZO-1 expression was observed to be primarily in the cytoplasm and not localised to the cell membrane.

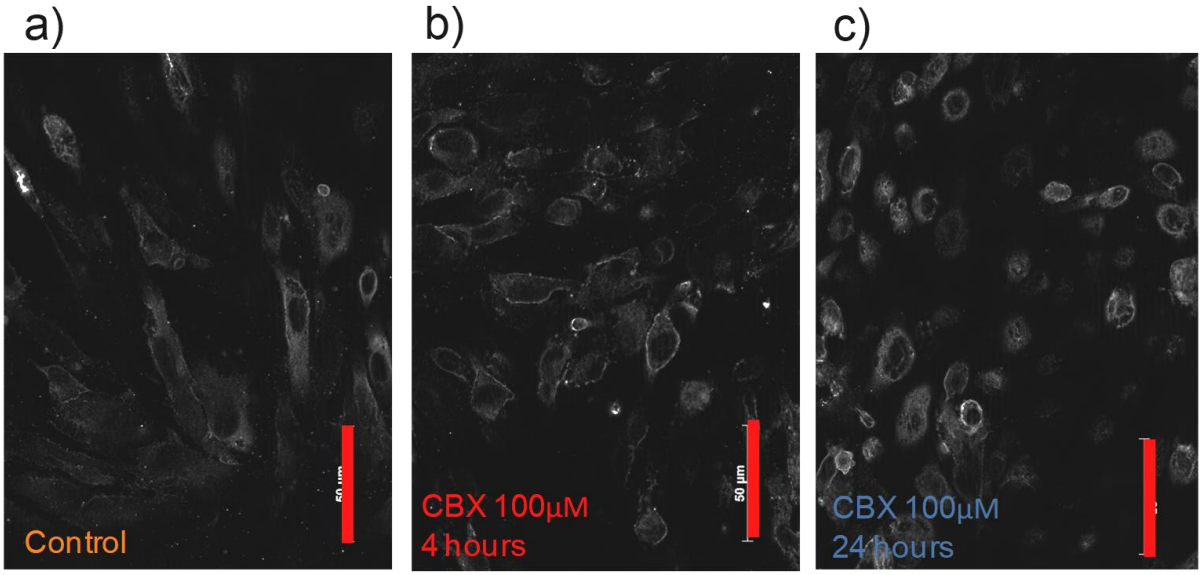

Figure 6.19 – Representative greyscaled fluorescent microscopy images showing ZO-1 expression from experiment 4. a) Control 24 hours after media addition only. b) 4 hours after carbenoxolone 100µM dose addition. c) 24 hours after carbenoxolone 100µM dose addition. Red scale bars are 50µm. Images are representative of 12 for 4 hour data set, 11 for 4 hour data set and 8 control electrodes.

6.7 Discussion

The overall objective of this study was to investigate if a dysfunctional endothelial monolayer induced through the inhibition of gap junctions can be identified using impedance spectroscopy in clinically relevant cell populations. Endothelium dysfunction has been linked to the development of in stent restenosis and thrombosis (Kubo *et al.*, 2015; Tesfamariam, 2016). It is therefore anticipated that the capability to measure dysfunctional endothelium in a self-reporting stent would be a useful tool for clinicians and researchers seeking information on the re-endothelialisation process. The results presented here show that total impedance falls following the creation of a dysfunctional endothelium through the inhibition of gap junctions. This provides evidence that an impedance-based self-reporting stent has the potential to monitor endothelial cell monolayer functionality. To our knowledge, the use of impedance spectroscopy to non-invasively monitor gap junction modulation in endothelial cell cultures, as described in this study, has not been previously reported in the literature. This represents a novel approach, with the potential to provide very useful insights within a number of areas of cardiovascular research. Whilst our initial

focus has been on analysis of the relevance of our findings to the development of a self-reporting stent, it is clear that they can help contribute to knowledge and understanding of endothelial cell to cell junctions and their relationship to various aspects of cardiovascular disease. The following discussion will therefore consider these aspects first, before returning to a more general discussion on the relevance of the results to a self-reporting stent concept.

Time-lapse microscopy of gap junction inhibited cells affirms observations from the light microscopy images that the variation in total impedance observed throughout this study was not likely to be due to morphological changes in the cells or cell death events. Furthermore the drop in impedance parameters was evident in experiments using 2 separate, widely used gap junction inhibitors. The correlation of results from different drugs in this way increases confidence that the inhibition of gap junctions is the primary initiator in the mechanism that precipitates a fall in total impedance and is not a subsidiary action of the drugs.

The impedance response of confluent endothelial cell monolayers to carbenoxolone was determined to be dose dependent 4 hours after drug addition (Figure 6.9). As previously stated the measurement of impedance for gap junction inhibited endothelial cells is unique and no studies are available for comparison. The dose dependent nature of carbenoxolone induced gap junction inhibition has previously been shown in endothelial cells by Sagar and Larson, 2006. The group demonstrated a carbenoxolone dose dependent response in bovine endothelial cells with a 30% reduction in lucifer yellow dye transfer at 50μM and 80% at 100μM. However dye transfer results from the present study did not show dose dependency, with 50μM causing a 76% fall and 100μM a 74% reduction (Figure 6.11). A key difference between the two studies that may account for the discrepancy in the 50μM results is that the dye transfer data presented here was collected after 48 hours of exposure to carbenoxolone as opposed to only 30 minutes by Sagar and Larson. It is possible that the gap junction inhibition as induced by carbenoxolone has its own time dependent profile. Given that the data shown in this study for 50μM and 100μM dosed cells showed near identical reductions in dye transfer after 48 hours such an inhibition profile may be asymptotic towards an 80% reduction. Evidence of this can be seen in Figure 6.18 where 100μM dosed carbenoxolone dosed cells were assessed by dye

transfer at 4 and 24 hours, and show a time dependent reduction of 54% and 76% respectively.

A dose dependent total impedance response was not found to be statistically significant 4 hours after heptonal dosing (Figure 6.13). However inspection of the longer term post-dosing total impedance measurements (Figure 6.12) reveals clear dose dependency trends between undosed, 0.5mM and 1mM dosed cells. The lack of dose dependency after four hours may suggest that the mechanism of gap junction inhibition for heptanol is slower than that for carbenoxolone. A further potential explanation is that heptanol is a less potent inhibitor of gap junctions than carbenoxolone at the concentrations used in this study. Additional evidence for this hypothesis can be found in the reduced magnitude of impedance falls for heptanol dosed cells (maximum of 5.7Ω for 1mM, Figure 6.13) in comparison to those induced by carbenoxolone (maximum of 10.9Ω for 100μm, Figure 6.5). Dye transfer measurements demonstrated dose dependency when measured 48 hours after dosing. Heptanol dose dependency has previously been shown for communication between cardiomyocytes (Takens-Kwak *et al.*, 1992) and in dye transfer in rat epithelial cell monolayers (El-Sabban, Martin and Homaidan, 1998) and rat cardiomyocytes (Li *et al.*, 2012). The present study however is the first to report heptanol dose dependency with regards to impedance falls and dye transfer in endothelial cells.

The reduction in total impedance caused by the inhibition of gap junctions from carbenoxolone and heptanol was not anticipated from the pre-experimental analysis of the literature discussed in section 1.26 (Electrical assessment of gap junctions). Although no studies have extensively used impedance spectroscopy to investigate gap junction formation, two studies have developed theoretical models that predict that the formation of gap junctions would cause a decrease in the overall impedance values (Gheorghiu, Balut and Gheorghiu, 2002; Asami, 2007). Thus, their inhibition experimentally should initiate a rise in impedance and conversely dipyridamole induced enhancement should cause a fall. These predictions are in clear contrast to the results observed in the present study, where the use of gap junction blockers led to impedance falls whilst gap junction enhancement produced elevations in impedance. It should be considered that the assumptions required to develop the models proposed by Gheorghiu et al and Asami do not accurately reflect the in vitro experimental scenario used in this study. The cells are considered as a non-specific

generic type structured as dielectric, spheroid shells suspended within an electric field rather than a monolayer adhered to an electrode surface. None of these assumptions however, are likely to be sufficiently significant enough to cause such contrary differences in the results from the theoretical models and the experimental data presented here. Both studies model gap junction inhibition in isolation and do not consider subsidiary effects that their closure may have on other cellular mechanisms. It is therefore possible that the observed reduction in total impedance, seen consistently throughout the results presented in this study, is caused by one or more subsidiary mechanisms not included in the theoretical models.

Measurement of total impedance falls indicates an increase in the permeability of the endothelial cell layer and thus a reduction in the monolayers barrier function. Reductions in total impedance measurements have been shown previously by other researchers to correlate with a corresponding reduction in the monolayers barrier function (Sun *et al*., 2010; Szulcek, *et al*, 2014; Bischoff *et al*., 2016). Evidence linking the gap junction mediation induced in this study with endothelium barrier function can also be found in the literature. Nagasawa et al, 2006, showed a drop in transendothelial resistance and paracellular flux measurements of porcine blood brain barrier and rat lung endothelial cells following the dosing of gap junction blockers 18 β-glycyrrhetinic and oleamide. 18 β-glycyrrhetinic acid is an analogue of carbenoxolone. The study continued transendothelial resistance measurement for 12 hours after gap junction inhibitor dosing. Significantly, after an initial fall it was observed that there was a recovery in transendothelial resistance values, in a similar fashion to the total impedance recovery seen in the data in present study. Nagasawa et al did not however continue the inhibition of gap junctions beyond 12 hours and thus will not have observed longer term post dosage behaviour. Furthermore the microporous membrane used in transendothelial resistance experimentation prevents the use of light microscopy observations. The images and time-lapse microscopy shown here provide novel insights into the behaviour of endothelial cells with inhibited and enhanced gap junction formation. Nagasawa et al also demonstrated that this reduction in barrier properties was not associated with a change in the expression of a range of proteins associated with tight junction formation including ZO-1, in agreement with the fluorescent microscopy images shown in Figure 6.19 in section 6.6.4 (Experiment 4 - Tight and gap junction inter dependency). This study by Nagasawa et al represents the closest published experimental approximation to the

results presented here and provides corroborative evidence linking gap junction inhibition and endothelium barrier function.

Only one published study has been found that used the combination of gap junction inhibition and impedance spectroscopy to investigate cells adhered to electrodes. Asfour et al, 2010, observed a reduction in mouse fibroblast monolayer total impedance at 5*kHz* after Heptanol dosing at a single 1mM concentration. This study correlates with the data presented here however in different cell types, with fibroblasts not forming selective monolayer barriers in vivo. Evidence from fibroblasts is therefore of limited relevance in comparison to the endothelial functionality results presented here.

Expression of the tight junction marker ZO-1 was examined in carbenoxolone dosed endothelial cells at either 4 or 24 hours after inhibitor addition. The rationale behind such experimentation was to determine if gap junction inhibition and the associated time dependent total impedance variations were due to a corresponding modulation in tight junction formation. The lack of change in ZO-1 expression between cells as measured 4 and 24 hours after gap junction inhibition seen in experiment 4 indicates that both the 4 hour decrease and 24 hour recovery in cell layer barrier function is independent of tight junction formation. As previously stated, this finding correlates with observations made by Nagasawa et al. Therefore the post dosage recovery in barrier function after 24 hours seen in carbenoxolone and heptanol dosed cells may be the detection of an unknown compensatory mechanism, whereby an alternative mechanism has been used by the cells to restore their barrier function. The ZO-1 imaging shows that the compensatory mechanism can be reasonably assumed to not involve tight junctions. In addition the observed paucity of gap junctions in the scratch assays images at both 4 and 24 hours demonstrate that barrier function recovery does not involve an elevation in intercellular communication. Compensatory mechanisms are a known phenomenon in studies using knockout mouse models (Lohman and Isakson, 2014). Work directed at studying this mechanism would enable new insights into how endothelial monolayers actively control their permeability. It was further observed from the ZO-1 expression images (Figure 6.19) that the marker was primarily expressed in the cytoplasm and not localised to the cell membrane. This can be taken as evidence that the endothelium had attained maturity, as ZO-1 is known to be membrane localised during the initial

stages of tight junction formation but then is found to be distributed within the cytoplasm during the later stages of junction maturation (Dejana, Corada and Lampugnani, 1995).

An alternative cause of the 24 hour recovery may be the result of inhibitor drug metabolisation. The depletion of the drug in the media would enable the previously inhibited normal mechanism mediating the high barrier function to recommence. However there is evidence from the scratch assay images taken after 48 hours and also 24 hours that gap junctions are inhibited throughout the post dose period. It would be expected to see an increase in gap junction formation if the drug concentration in the media had become reduced. Further discussion of this idea is hindered by current lack of understanding as to the precise nature of the mechanism of action for carbenoxolone and heptanol in inhibiting gap junctions (Dhein, 2004; Brisset, Isakson and Kwak, 2009).

The results from the dosing of endothelial cells with dipyridamole demonstrated an enhancement of gap junction formation as assessed through dye penetration scratch assay image analysis. This result is in agreement with the research published by Begandts et al, 2010, 2013, 2015, all be it at decreased magnitudes. They observed a 50% increase in dye transfer for dipyridamole 50μM dosed aortic bovine endothelial cells, compared to 22% for the data presented here on pulmonary porcine endothelial cells. The differences may be attributed to the different cells used or be indicative of the variability in the manual application of applying a scratch to monolayers as highlighted by Abbaci et al, 2008. The enhanced gap junction communication seen in the scratch assay analysis data presented here correlates with an increase in total impedance parameters when compared to dose free control values. This result allows a link between an increase in dipyridamole induced gap junction expression and barrier function enhancement to be established and is a novel finding. Discerning a mechanism explaining these findings is not possible with the available information from the experiments and will require further work. Begandt et al did not examine barrier function or expression of any of the associated proteins associated with tight junction formation, nor did their experiments include a gap junction inhibitor to act as a negative control.

The data from the junction experiment using the gap junction enhancer dipyridamole indicates the potential of this drug as a candidate for encapsulation in drug-eluting

stents. Current drugs encapsulated in stent surfaces such as rapamycin and paclitaxel have had success in reducing the likelihood of in stent restenosis but have been shown to attenuate the proliferation of endothelial cells as highlighted in section 1.5 (Drug-eluting stents). The dipyridamole results show that the drug has a positive effect on the barrier function of endothelial cells and increases intercellular communication, both desirable effects that can reduce the risk of thrombosis and restenosis (Tesfamariam, 2007). Although this was not specifically examined in this present study, evidence from the light microscopy images (Figure 6.3c) suggest that it achieves these beneficial effects without compromising the adhesion and viability of the cells. Inspection of the literature into the actions of dipyridamole on vascular cells reveals it to have an anti-proliferative effect on smooth muscle cells with recommendations for its therapeutic use in restenosis (Singh *et al.*, 1994; Dixon *et al.*, 2009). Dipyridamole has also been clinically used in combination with aspirin to provide anti-platelet therapy (Sacco *et al.*, 2008) and as a coronary artery vasodilator (Rossen *et al.*, 1991). All of these effects are considered beneficial in a post-stenting environment.

The results presented here used the inhibition of gap junctions to artificially create a dysfunctional endothelium, however gap junction inhibition is one of many ways that endothelial cells can become dysfunctional. Examples from the literature include the addition of thrombin (Rabiet *et al.*, 1996) and the blocking of ion channels (Callies *et al.*, 2011). The inhibition of gap junctions caused a reduction in the barrier properties of the endothelial cell layer recreating a dysfunctional endothelial monolayer as proposed in 1.32 (Study objectives). Impedance spectroscopy measurements were able to clearly distinguish between endothelium transitioning from the functional to the dysfunctional. When considering the implications of these findings in the development of a self-reporting stent they provide confidence that impedance spectroscopy has the potential to provide a measurement of the health of a newly reformed endothelial layer over the stent struts. Such real-time data would be of use to clinicians wishing to make informed decisions on therapeutic interventions.

6.8 Limitations

The resolution of gap junction inhibitor concentrations applied in this study was restricted to two each for Heptanol and Carbenoxolone. Consequently, clarification of dose dependent impedance response is not possible. Of interest would have been the determination of minimal and maximal limits for the total impedance variation, as induced by gap junction inhibition. A further study limitation is that the gap junction enhancer dipyridamole was used at a single concentration only. As a result it is not known if the measured increase in total impedance and dye penetration is dose dependent. Of particular interest would have been the determination of an upper limit on the enhancing effect of dipyridamole, providing enhanced guidance and information on the proposed therapeutic potential of the drug.

A limitation in the work presented in this section is that a link between gap junction inhibition in endothelial cells and a decline in its anti-thrombotic studies has not been yet been investigated in the published literature. Although as discussed in the introduction section 1.23 (Gap junctions) a link between the inhibition of gap junction connexins in coronary endothelial cells with disease states of hypertension, hypotension and atherosclerosis has been established (Begandt *et al.*, 2013; Ebong and Depaola, 2013). However, the dysfunctional endothelium induced here cannot be definitively associated with an endothelium with reduced anti-thrombotic properties and as such at an increased risk of in-stent thrombosis.

The dye penetration scratch assay method has known variability that can be associated with the requirement to manually apply a scratch to the cell layer, although the use of image analysis software, such as ImageJ has been shown to reduce this (Abbaci *et al.*, 2008). Consequently the dye transfer data presented here may have higher variation than if an alternative method of assessment was used. The gold standard in this regard has been cited as being freeze fracture electron microscopy (Hanani, 2012). This however requires specialist equipment that was not available during the endothelial dysfunction experimentation stage.

6.9 Future work

The previously cited limitations in drug dose concentrations could be addressed with a range of simple repeat experiments. Multiple concentrations of dipyridamole should be applied with the ranges used by Begandt et al, 2013, used a guide. Greater dose resolution for the gap junction inhibitors would increase confidence in the dose dependent results presented here. Heptanol in particular should be dosed onto confluent endothelial cells at higher concentrations than those presented here, as it was shown to cause less marked reductions in total impedance when compared to carbenoxolone.

Work focusing on using the developed system to investigate cardiovascular disease could include a number of studies analysing the effect of blocking gap junctions on endothelial cells. The barrier property recovery phase observed after gap junction inhibition requires further investigation, with future experimentation aiming to confirm the existence of the recovery phase through the use of gap junction blocker washout and blocker reapplication protocols as used in other studies (Salameh and Dhein, 2005). If confirmed then the investigation should then focus on identifying a mechanism. Such work should examine differential expression in proteins at the beginning and end of the recovery phase, in a similar fashion to the already tested ZO-1 which showed no variation in expression. Studies using cells derived from junction related gene knockout mice could also be performed. If the recovery phase is proven to be a compensatory mechanism this would provide an intriguing insight into the temporal reaction of cells to drugs. A further investigation into whether gap junction inhibition effects seen in endothelial cells are repeated in cells grown in co-culture would add a level of clinical relevance to this experimentation.

6.10 Summary

In summary it can be said that the present study adds several novel contributions to the current understanding of gap junction and barrier function interdependency in endothelial cell monolayers. The link between gap junction inhibition and a loss of barrier function has been established with different agonists, carbenoxolone and heptanol, to those previously published by Nagasawa et al. This adds further evidence that gap junctions are essential to a healthy endothelium through the maintenance of its barrier function. The use of impedance spectroscopy to investigate the role of gap junctions in endothelial cell monolayers is unique and provides a new method of non-invasive assessment. The measurement of a dose dependent response for these agonists, as measured by impedance spectroscopy, has not been reported and represents an additional novel finding. Further novel understanding can be found in the measurement of endothelium barrier enhancement through an increase in dipyridamole induced, gap junction formation. Although a previous research group has established a link between dipyridamole and gap junction expression the group did not analyse the effect that the resulting increase in intercellular communication would have on barrier function (Begandt *et al.*, 2010).

In linking gap junction inhibition and barrier function, this study has highlighted the difficulties in translating theoretical cell models into empirical measurements, as an intervention in one cellular mechanism can initiate unforeseen changes in other mechanisms. If it were possible to inhibit gap junctions in isolation without causing additional cellular reorganisation then the theoretical results may hold true. The interdependent relationship between gap junctions and the endothelium barrier function seen in the results presented here and elsewhere in the literature hinders correlation of the theoretical and experimental approaches.

The experimentation detailed in this section has demonstrated the capability of impedance spectroscopy in assessing endothelial functionality, indicating its potential suitability for usage in a self-reporting stent. In seeking to translate this medical device concept into a clinical environment, impedance measurements of endothelial monolayers adhered to substrates that could potentially act as both a drug-eluting and measurement surface would be beneficial. This work is detailed in the following section 7 (Conducting polymer substrate testing).

7 Conducting polymer substrate testing

7.1 Introduction

In seeking to translate the concept of a self-reporting stent into a clinical setting experimental data on materials likely to be used in vivo will be required. As previously described in section 1.29 (Conducting polymers) conducting polymers are a unique class of materials that have two particular features that make them an excellent candidate material for use as a coating for a self-reporting stent. Firstly their conductivity makes them a suitable substrate for monitoring the progression of post stenting cellular regrowth through impedance spectroscopy. Secondly, conducting polymers are able to encapsulate drugs in a similar fashion to the current polymer coatings used on drug-eluting stents. Consequently these materials are a potential enabling technology that would allow the creation of a self-reporting, drug-eluting stent. Therefore the objective of the work detailed in this section was to investigate the feasibility of using conducting polymers as a substrate for a future self-reporting stent. Polypyrrole is one such conducting polymer that has been widely used in a variety of biomedical applications (Guimard, Gomez and Schmidt, 2007). It can be readily coated onto metal substrates, through the process of electropolymerisation in the presence of a suitable dopant ion. A limited number of studies have investigated polypyrrole as a coating for coronary stents (Weiss *et al.*, 2003; Arbizzani *et al.*, 2007; Okner *et al.*, 2009). It was therefore selected for use in the work presented here with the anti-inflammatory drug, salicylate being used as the dopant ion. Salicylate has been previously used as a dopant in polypyrrole thin film coatings (Kontturi, Pentti and Sundholm, 1998; Cascalheira *et al.*, 2003; Arbizzani *et al.*, 2007).

An aqueous solution of pyrrole with salicylate was used to produce a series of polypyrrole coated electrodes via a process of galvanostatic electropolymerisation, as described in section 3.1.2 (Electrode coating). The impedance characteristics of these coated electrodes were then characterised by impedance spectroscopy. Endothelial cell adhesion and growth on the polypyrrole coated electrodes was then monitored over time using the methods previously described in section 3.6 (Cell experimentation).

7.2 Results

7.2.1 Polypyrrole coated electrode characterisation

A comparison of the impedance properties of the polypyrrole coated gold electrodes with the platinum black coated and uncoated gold used in this study is depicted in Figure 7.1. The results demonstrate that the addition of the polypyrrole coating to gold electrodes lowers the total impedance of the electrode in a similar manner to platinum black at frequencies below 10*kHz*. At lower frequencies, the total impedance of polypyrrole is closer to the uncoated gold than platinum black.

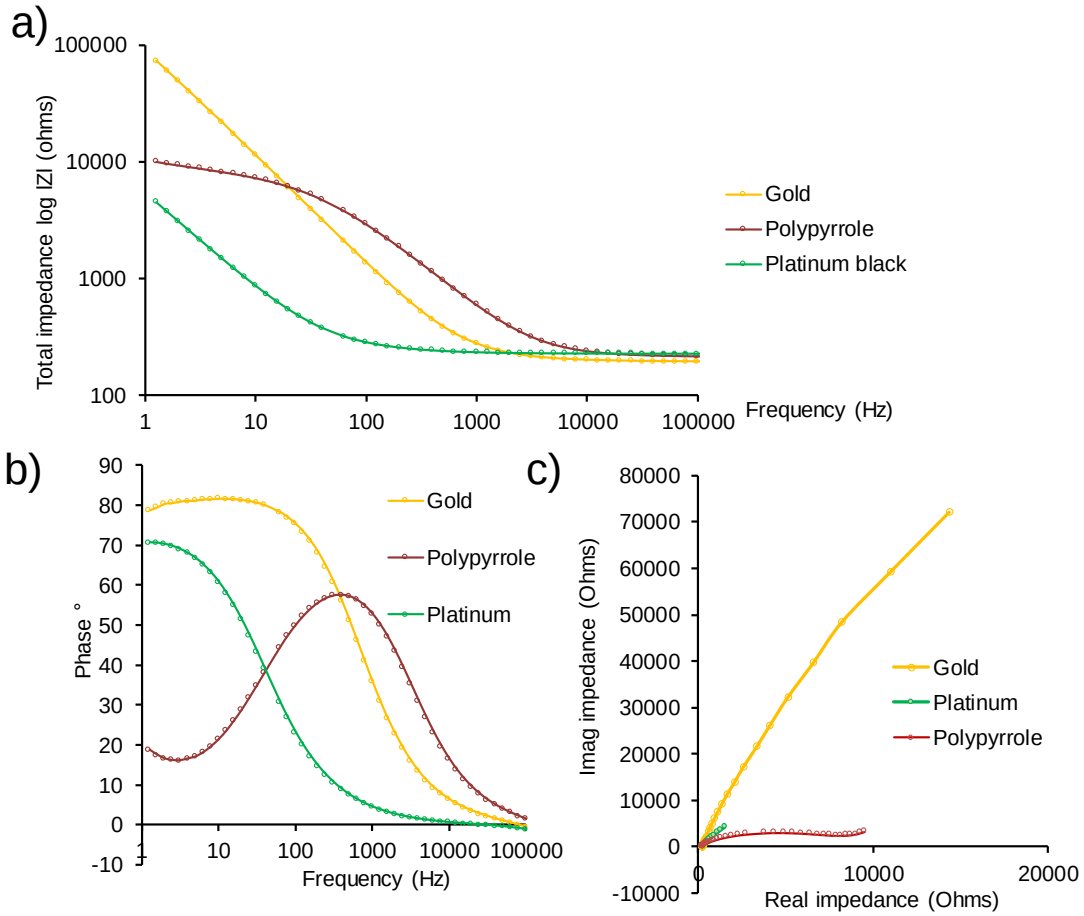

Figure 7.1 - Comparison of the measured impedance characteristics of bare polypyrrole, gold and platinum electrodes in endothelial cell media. a) Total impedance, b) Phase and c) Wessel plot.

7.2.2 Characterisation of porcine endothelial cells on polypyrrole coated electrodes

In total 2 polypyrrole experiments were carried out with details of these summarised in Table 7.1.

Expt no.	**Seeding density (x 10^4 cells/cm^2)**	**Passage no.**	**Duration (hours)**	**Chamber allocation**	**Cell growth observations**
1	6.2 to 8.1	2	96	4 cell seeded 4 control	Confluency attained in all cell seeded chambers.
2	5 to 6	2	96	4 cell seeded 4 control	Variable cell growth, confluency not attained over electrodes.

Table 7.1- Experimental summary of the endothelial cell characterisation experiments on polypyrrole electrodes.

Polypyrrole coated electrodes were sufficiently transparent to permit light microscopy imaging. Observations of seeded endothelial cells in experiment 1 showed settling and proliferation behaviour in the same manner as cells seeded onto platinum black electrodes previously presented in section 5.2.2 (Impedance based characterisation of endothelial cells). Confluency was attained in experiment 1 between 72 and 96 hours and representative images of cell seeded electrodes after 96 hours are shown in the light microscopy images in Figure 7.2 a and b. Cells seeded onto electrodes in experiment 2 displayed different behaviour and failed to adhere in large numbers with growth observed in patches only. Representative images of cell seeded electrodes from experiment 2 are shown in Figure 7.2 c and d, showing that these cells then did not attain confluence after 96 hours of culture, as would be expected for the given seeding density. In the case of 4 electrodes, endothelial cells were observed to have detached from the electrodes forming spheroid aggregates (Figure 7.2 c). The cells adhered to the plastic culture ware surface had a higher density and were not observed to have detached as depicted in the areas around the electrodes in Figure 7.2 c and d. The only experimental variations between the two experiments were a change of cell line and an increased seeding density in the failed

experiment 2, owing to a higher number of cells being available. Comparison of the initial impedance profiles immediately after cell seeding reveal no significant differences between the two experimental data sets. Besides experiment 1, the attainment of an endothelial cell monolayer on polypyrrole has been previously achieved in the same laboratory using primary porcine endothelial cells (Reay, 2012).

Due to the observed behaviour of the cells in experiment 2 being inconsistent with all other observations of endothelial cell settling and proliferation the impedance data for the purposes of cell characterisation and assessment of polypyrrole for impedance spectroscopy will only be presented from experiment 1. This will also permit a more reliable comparison with endothelial cell data from the previously presented experiments in section 5 (In vitro cell characterisation by impedance spectroscopy), which displayed similar settling and proliferation characteristics.

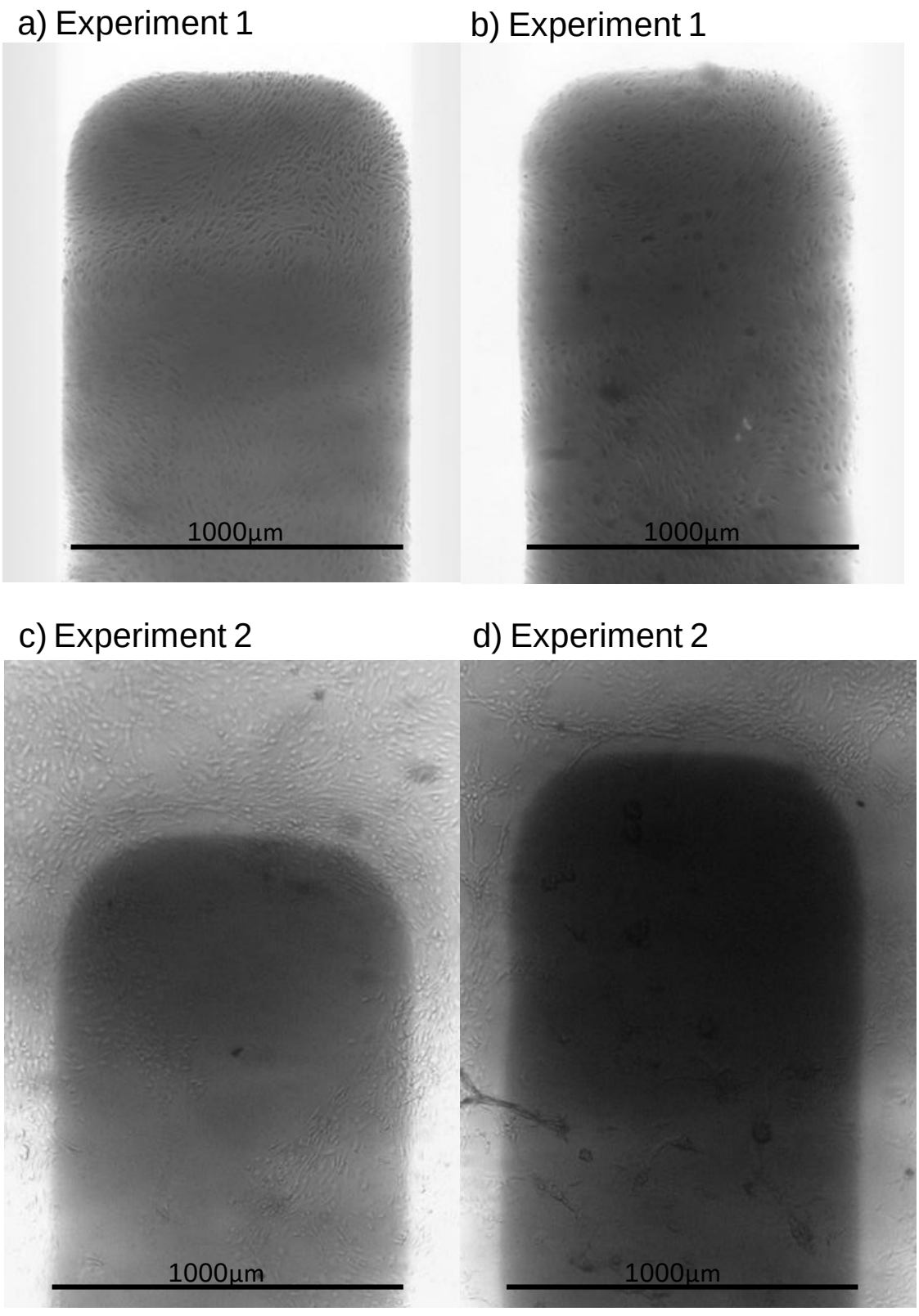

Figure 7.2 – Representative light microscopy images of endothelial cells 96 hours after seeding on polypyrrole coated electrode tips from experiment 1, a) and b) and experiment 2 c) and d). Scale bars are 1000µm provided by the known electrode width images representative of observations from 16 electrodes for each experiment.

The 3D reactance profiles for polypyrrole electrodes seeded with cells and media only control electrodes are shown in Figure 7.3. These figures show that reactance elevations are greatest at lower frequencies towards 1*kHz*. In comparing the two plots it can be seen that the cell seeded polypyrrole electrodes experienced a decline in reactance following confluence in the frequency range 1*kHz* to 10*kHz*. Post confluent reactance profiles have been previously observed for endothelial cells seeded onto platinum black electrodes and are shown in section 5.2.2 (Impedance based characterisation of endothelial cells). The similarity between the two 3D plots shows that control variation is likely to be obscuring any cellular reactance contribution.

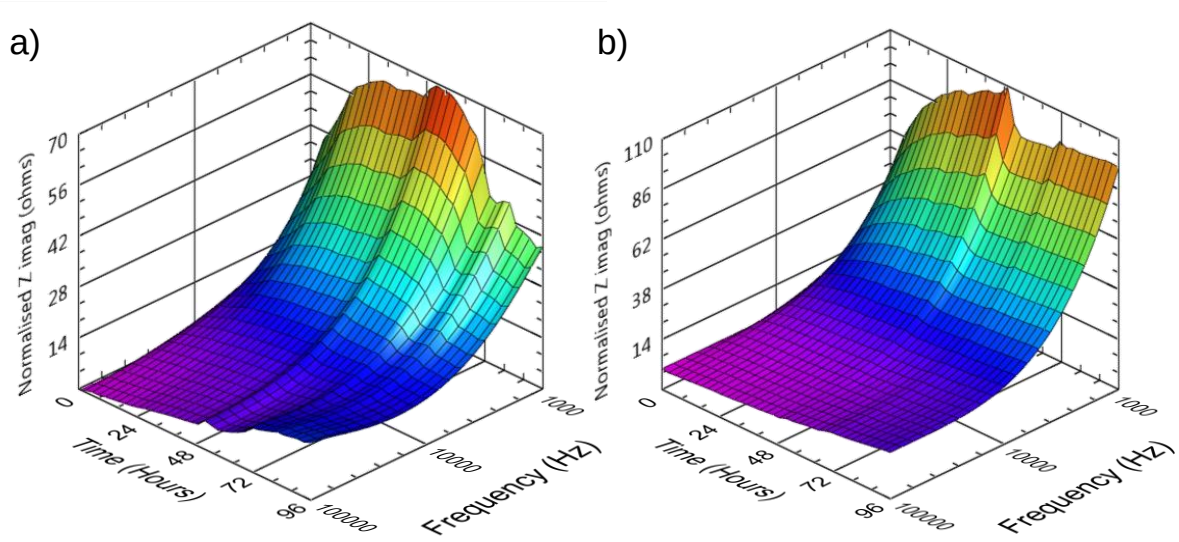

Figure 7.3 - Mean 3D reactance (z axis) variation over time (x axis) and across the frequency range1KHz to 100KHz (y axis). a) porcine endothelial cell seeded polypyrrole electrodes (n=10, max standard error mean 6.097) and b) control polypyrrole electrodes (n=10, max standard error mean 5.457).

To enable comparison between electrode substrates the 3D reactance profiles for porcine endothelial cells seeded onto polypyrrole electrodes (Figure 7.4a) and the previously presented platinum black electrodes (Figure 7.4b) are shown below. It can be seen that the magnitude of reactance variations over the course of the experiments are up to 7 times greater for polypyrrole coated electrodes than platinum black electrodes. The higher frequency reactance peak visible for platinum electrodes maybe evident in the polypyrrole data with a slight elevation after 72 hours at frequencies towards 100*kHz*.

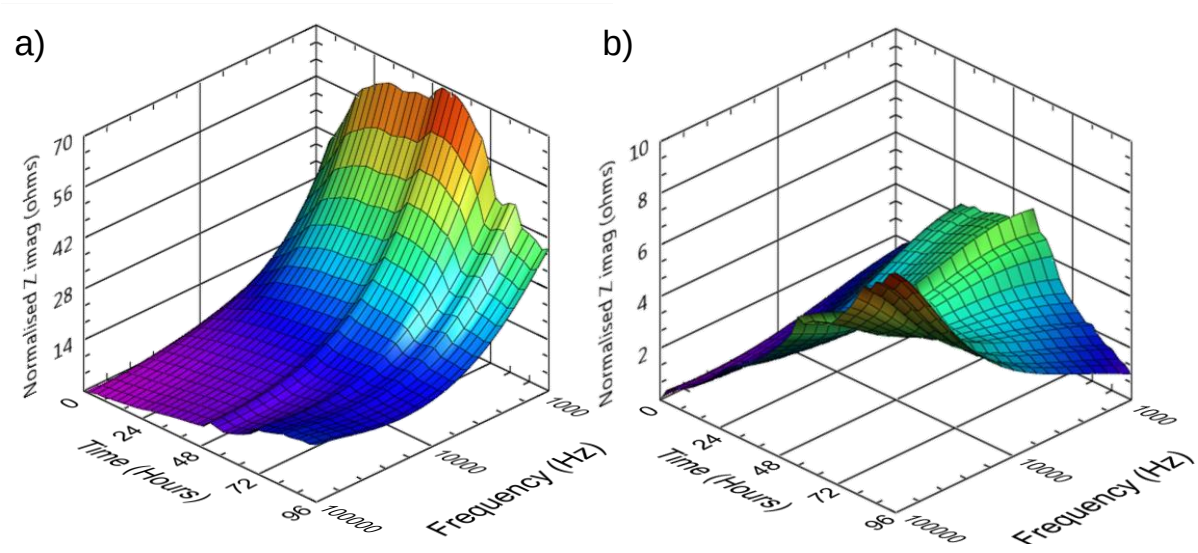

Figure 7.4 - Mean 3D reactance (z axis) variation over time (x axis) and across the frequency range1KHz to 100KHz (y axis). a) porcine endothelial cell seeded polypyrrole electrodes (n=10, max standard error mean 6.097) and b) porcine endothelial cell seeded platinum black electrodes (n=33, max standard error mean 0.40).

Experimental reactance data, at 10*kHz,* from experiment 1 are shown in Figure 7.5. 10*kHz* has been used in previous sections of this study to demonstrate cell proliferation. The cell seeded electrodes all demonstrated an initial increase in reactance within the first 24 hours that subsequently stabilised following confluence. Control electrodes demonstrated almost identical reactance variation in the first 72 hours of the experiment before diverging in the final 24 hours of the experiment.

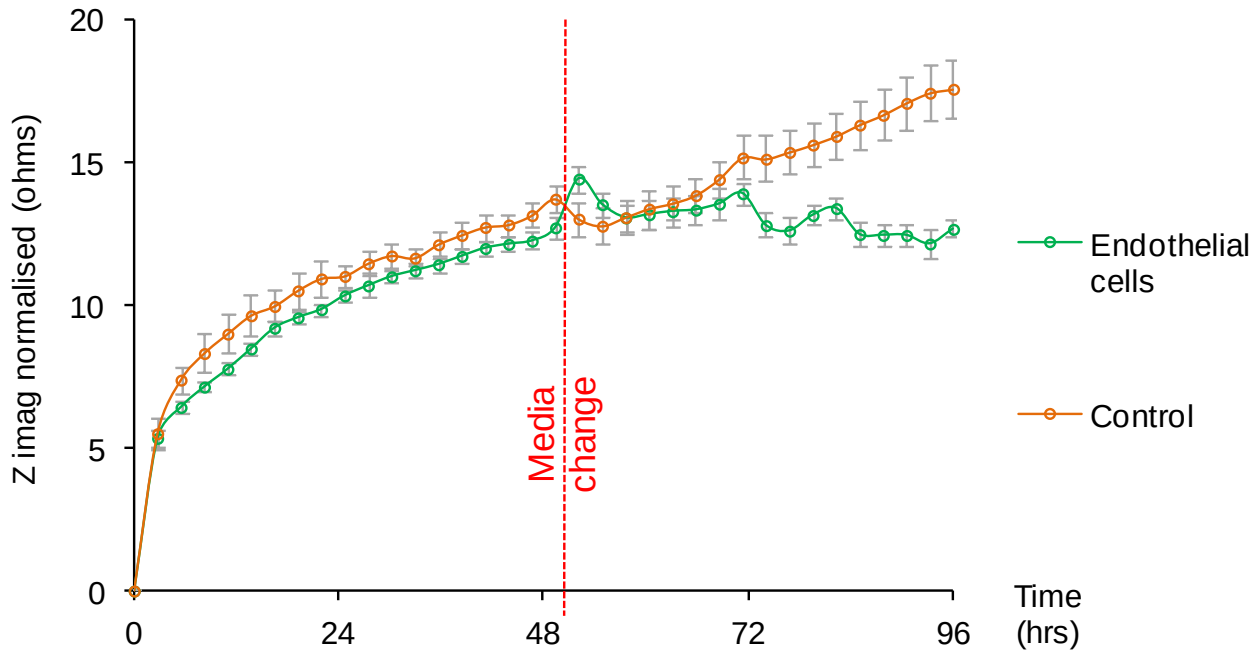

Figure 7.5 – Mean reactance profiles at 10kHz for endothelial cell seeded polypyrrole coated electrodes (red, n=10) and cell free control polypyrrole coated electrodes (orange, n=12) Error bars are ± SEM. Media change shown with red dashed line.

Following observation of the reactance elevations in polypyrrole control electrodes a test was conducted to ascertain if this could be due to the sodium salicylate dopant eluting out of the substrate. The elution of salicylate was therefore measured over time in order to generate a release profile. A detailed method can be found in section 3.1.2 (Electrode coating). In total 11 chambers were tested for sodium salicylate release ywith each measured amount representing the combined drug release from all 4 small working electrodes and 1 large reference electrode within each chamber. Salicylate elution into distilled water was measured using UV spectroscopy. The cumulative mass released over time is displayed in Figure 7.6. The results demonstrate that the dopant ion was released from the electrodes into the surrounding distilled water and that the majority of this release occurred in the first 24 hours. The time dependent profile of salicylate release correlates with the recorded increase in reactance recorded, of which the majority was also within the first 24 hours, as shown previously in Figure 7.5. These results indicate that the release of the sodium salicylate could be a contributing factor towards the instability of the electrode that may be obscuring any impedance contributions from the proliferation of cells over the electrodes.

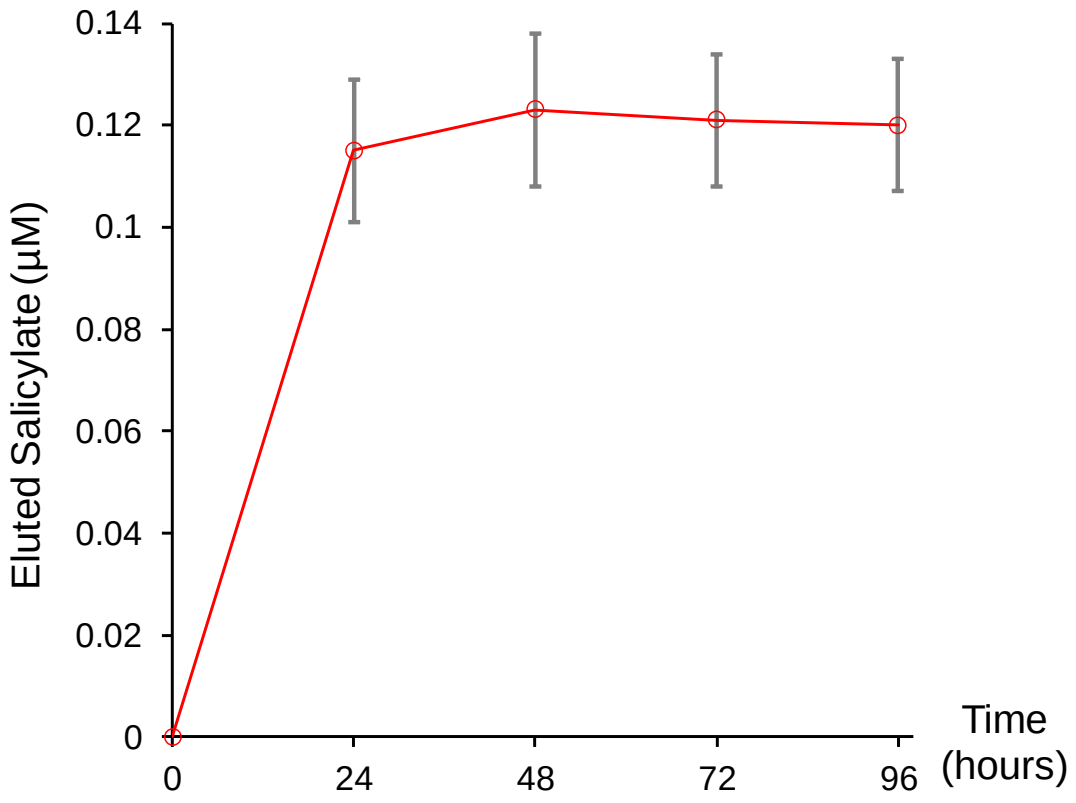

Figure 7.6 - Sodium salicylate release profile into distilled water from polypyrrole coated electrodes in chambers. Error bars are ± standard error mean, n = 11.

The total impedance ratio has previously been presented as a method for cell characterisation in the results in section 5 (In vitro cell characterisation by impedance spectroscopy). To allow comparison between different electrode surfaces the total impedance ratio for confluent porcine endothelial cells on platinum black and polypyrrole is shown in Figure 7.7. The plot shows a greater impedance ratio for cells seeded onto the polypyrrole electrodes in comparison to those seeded onto platinum black electrodes. Also shown are the frequencies where peak total impedance ratios occurred with a lower peak of 500*Hz* for polypyrrole electrodes compared to 1260*Hz* for platinum black electrodes. The data for cell-free polypyrrole control electrodes after 96 hours is also presented and demonstrates the magnitude of total impedance variation over the course of the experiment for these electrodes.

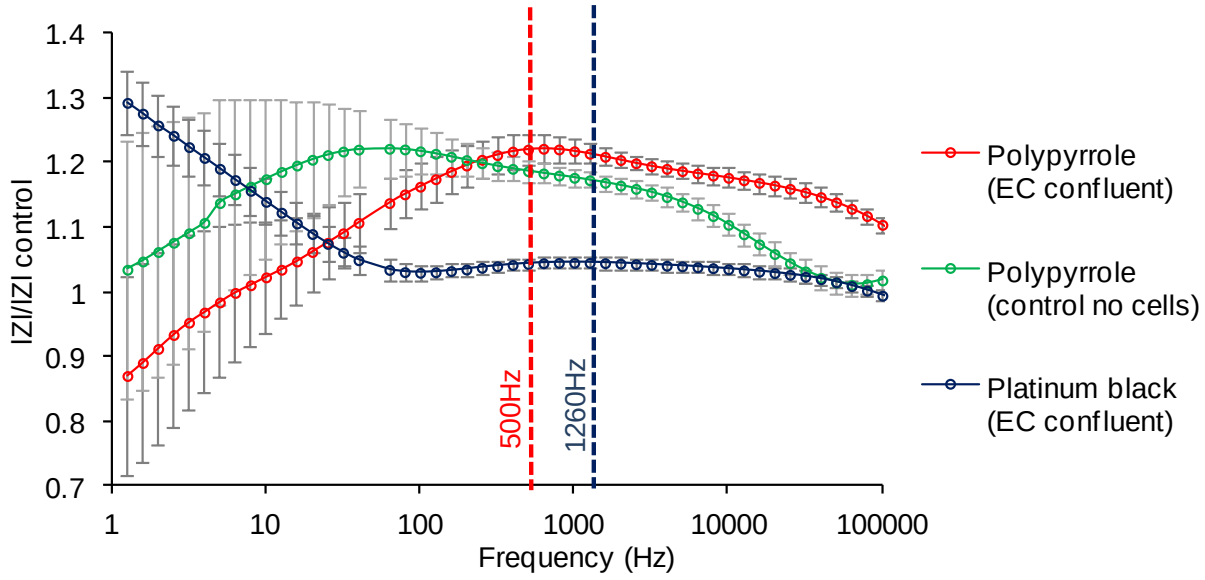

Figure 7.7 - Total impedance ratio for confluent porcine endothelial cells after 96 hours of culture on platinum black electrodes (n=39) and polypyrrole electrodes n= 10. Polypyrrole control electrodes with media only electrodes n=12. Peak ratios shown at 500Hz for polypyrrole and 1260Hz platinum black. Error bars are ± SEM.

7.3 Discussion

The objective of this component of the study was to investigate the feasibility of using conducting polymers as a substrate for a future self-reporting stent. The conducting polymer polpyrrole was successfully coated over gold electrodes using sodium salicylate as a representative dopant and drug.

The impedance properties of the cell free coated electrodes shown in Figure 7.1, were found to be similar to published galvanostatically coated examples in the literature. Several studies have shown reduced reactance and real impedance properties after coating thin film platinum electrodes with a polypyrrole - polystyrene sulphonate dopant ion combination (Pickup and Ren, 1995; Malleo *et al.*, 2010). Similar reductions from gold thin film electrodes after polpyrrole – salicylate coating used in this study are presented in Figure 7.1. No examples of impedance properties for the specific polypyrrole-salicylate dopant ion material combination were found in the literature.

The observations from experiment 2, where cells failed to proliferate to confluence could be interpreted as evidence of the limited biocompatibility of polypyrrole, particularly given that the cells on the surrounding plastic were of a higher density

and appeared to be healthy as observed through light microscopy. However evidence from the literature has consistently demonstrated the suitability of polypyrrole surfaces for cell adhesion (Wong, Langer and Ingber, 1994; Garner *et al.*, 1999; Wang *et al.*, 2004; Ateh, Navsaria and Vadgama, 2006; Reay, 2012). In addition, the evidence from another cell line used in experiment 1 showed no atypical observations in cell settling and proliferation on the polypyrrole surface. There were also no significant differences between the cell-free impedance profiles and the current density measured during the galvanostatic electropolymerisation, indicating consistency in the electrode surfaces. The presence of an unobserved bacterial or fungal infection in the cells used in experiment 2 cannot be discounted. Consequently no definitive reason for the cell behaviour in experiment 2 can be determined but it may be attributable to differences between the primary cell lines since each was isolated from a different source.

The in vitro results from electrodes coated with the conducting polymer, polypyrrole showed that impedance spectroscopy measurements can be made using such a material and that the coatings were sufficiently transparent to permit light microscopy observation of adherent cell behaviour. However analysis of the reactance profiles revealed that the bare electrodes not seeded with cells had an inherent instability. These control electrodes showed large mean reactance increases of 11.02Ω in the first 24 hours and the same reactance profile was also seen in the initial experimental stages for those electrodes seeded with cells, with mean elevations of 10.33Ω. Light microscopy clearly showed evidence of cellular adhesion to cell seeded electrodes. A potential conclusion is that the instability of the salycilate doped polypyrrole is dominating the reactance profile to such an extent that the influence of cellular proliferation is obscured. This hypothesis can be countered however by comparison with platinum black electrodes which showed a maximum elevation of 4.5Ω at 10*kHz* following seeding with endothelial cells (see Figure 5.8, section 5.2.2 Impedance based characterisation of endothelial cells). If a similar increase were to be expected for polypyrrole seeded electrodes then this should be appended onto the elevations seen in the control cell free electrodes and therefore at10*kHz* a total reactance elevation of approximately 18Ω would be expected. Inspection of Figure 7.5 reveals that at this frequency, cell proliferation does not cause such a rise but closely approximates to the control profile. This effect is present across a wider frequency range as evidenced by the similarity between the

3D reactance profiles, shown in Figure 7.3. A cause may be that cell proliferation over polypyrrole substrates induces smaller reactance changes than those grown on platinum black. With the available data a firm conclusion as to why endothelial cell proliferation cannot be discerned through reactance inspection in polypyrrole electrodes is not possible.

A possible cause for the polypyrrole instability may be found in the time dependent measurements of the dopant salicylate ion release from the polypyrrole electrodes. These measurements showed a similar profile to that of the reactance measurements, best observed by comparing Figure 7.5 and Figure 7.6, with rapid release of the salicylate in the first 24 hrs corresponding to the sharpest rise in the reactance. The salicylate release results presented here are in agreement with those observed previously by Arbizzani et al, 2007, who also measured salicylate elution from thin film polypyrrole coatings. They observed a similar elution profile of rapid 24 hour drug release into saline solution, using the same UV absorption methodology as used in the present study. Arbizzani et al did not investigate if the time dependent profile of drug elution had any impact on the electrical properties of the polypyrrole coatings. A decay in conductivity upon dopant ion release from polypyrrole films has however been previously reported by Fonner et al, 2008, although salicylate was not one of the dopants used so caution is urged in drawing direct comparisons with the present study findings. An additional interesting observation by Fonner's group was that two of the dopants tested, tosylate and polystyrene sulphonate, had demonstrably faster release profiles in PBS when compared to water. These variable elution rates into water and PBS correlated with measurements showing rapid conductivity decay, and the authors postulated that ions in the PBS solution were displacing the dopant ions in the polypyrrole. The salicylate release profile presented here was carried out in distilled water and it is possible that its elution may too be accelerated in more physiologically relevant conditions. Further experimentation in PBS or cell culture media as part of a future work program would be able to provide greater certainty on the relationship between salicylate release and conductivity we have observed.

The data demonstrates that the developed impedance spectroscopy system, with salicylate doped polypyrrole electrodes was not capable of detecting cellular proliferation. The instability of the electrode and the elution of the dopant drug are a potential cause. This finding is important in the context of considering future

coatings for a self-reporting stent. As previously stated conducting polymers are a potential coating for such a device due to their conductivity and drug encapsulation capability. However if the elution of the drug from the device is hindering detection of the cellular regrowth scenario then the specific material variant of salicylate doped polypyrrole is not feasible for monitoring post-stenting cellular regrowth. Time-dependent impedance spectroscopy measurements of cell monolayers on polypyrrole electrodes has previously been achieved by Sun et al, 2010. The group demonstrated impedance reductions following the introduction of the barrier function disruptor EGTA to confluent human epithelial bronchial cells. Cell proliferation to confluence was not presented however, although for the time periods shown cell free electrodes remained stable. Sun et al, used polystyrene sulphonate as a dopant which is considered a large dopant that is thought to be entangled with the polymer backbone and consequently slowly elutes from polymer electrodes, increasing their stability. Smaller dopants such as chlorine have been shown to rapidly release from conducting polymers and a relationship between conducting polymer dopant size and elution rates has been established by several research groups (Garner *et al.*, 1999; Balint, Cassidy and Cartmell, 2014). This published research can be used to suggest that increasing the size of the drug dopant in a self-reporting stent coating would extend the release profile. A further method of extending the release may reside in increasing the depth of the conducting polymer coating. Unpublished results from salicylate doped polypyrrole, carried out in the same laboratory as the present study have provided an indication that increasing the coating thickness can indeed attenuate the rate of drug release (Morgan, 2016).

In order to further improve conducting polymer suitability for use in a self-reporting stent, greater stability throughout the drug elution process is required. It should also be considered that conducting polymers other than polypyrrole may prove to be more suitable in this regard with cell growth having been shown on a range of types, including polyaniline (PANI) (Thrivikraman, Madras and Basu, 2014), Poly 3,4-ethylenedioxythiophene (PEDOT) (Ostrakhovitch *et al.*, 2012) and poly 3,4-ethylenedioxypyrrole (PEDOP) (Forcelli *et al.*, 2012). A key study that investigated the potential of PEDOT as an electrode substrate for impedance spectroscopy measurements was published by Karimullah et al, 2013. This group used PEDOT to detect total impedance increases arising from the proliferation of MCDK monolayers. In contrast to the results presented here they observed with no

significant elevations in cell free control PEDOT electrodes and the materials stability was cited as a factor in their selection. Direct comparison of the stability of polypyrrole and PEDOT in PBS with the same polystyrene sulphonate dopant was carried out by Yamato et al, 1995. This research group were able to show that PEDOT exhibited increased electrical stability when compared against polypyrrole as assessed through cyclic voltammetry, although dopant release was not investigated. PEDOT is therefore a potential material for use as a coating in a self-reporting stent that may have superior characteristics to polypyrrole.

Despite the challenges that drug elution from the electrode surface presents to the use of impedance for measurement of cell proliferation, there may nonetheless be opportunities to exploit this as a method for determining drug release following implantation. Drug release profiles from stents are relatively short, with drug release being normally complete within weeks (Acharya and Park, 2006), in comparison to anticipated rates of re-endothelialisation or restenosis, which typically occur over months and sometimes years (Finn, Nakazawa, *et al.*, 2007). Published data showing 80% of drug release in the first 10 days (Seidlitz *et al.*, 2015) compares to a reported 10 months for restenosis (Dangas *et al.*, 2010) with uncertainty regarding re-endothelialisation rates in humans (Joner *et al.*, 2008). Therefore a conducting polymer coated, self-reporting stent could be able to record and confirm the release of the drug. Having reached a stable state further measurement of impedance data could measure cellular regrowth over the stent struts. In addition frequency dependencies may be discovered whereby one frequency is sensitive to the measurement of drug release and another is sensitive to cellular regrowth, allowing a dual monitoring scenario. Besides passively monitoring elution the controlled release of drugs from conducting polymers has also been explored in several studies with voltage stimulation causing step changes in elution profiles (Kontturi, Pentti and Sundholm, 1998; Abidian, Kim and Martin, 2006; Wadhwa, Lagenaur and Cui, 2006). Such a material capability could be exploited in a self-reporting coronary stent environment by releasing appropriate therapeutic drugs when certain disease pathologies are detected.

Comparison of the results obtained using porcine endothelial cells on polypyrrole electrodes with those from platinum black electrodes reveals differences in the reactance profiles and in the total impedance ratio. The 3D reactance profiles, best

compared in Figure 7.4, show that the dual reactance peaks detailed previously using platinum black electrodes were not evident in polypyrrole electrode profiles. A polypyrrole reactance decline is evident at lower frequencies and the previously discussed polypyrrole electrode instabilities may be obscuring a higher frequency cell induced reactance variability. Additional consideration should be given to comparison of the total impedance ratio from Shedden, 2008, who advocated the use of the total impedance ratio as a method of cell characterisation. These experiments were performed using the same cell type, on electrodes of the same dimensions but with gold substrates. Shedden recorded a peak total impedance ratio of 1.15 at a frequency of 22387*Hz*, a far greater frequency than those measured for platinum black (1.09, 1260*Hz*) and polypyrrole (1.24, 500*Hz*) electrodes. With the key experimental variation between the results presented here and Shedden's being the electrode material this provides evidence that the cell characterisation profiles are likely to be substrate specific as previously suggested when comparing results from platinum black and gold electrodes, discussed previously in section 5.3 (Discussion). This finding has implications for both the development of a self-reporting stent and for the future use of the technology for in vitro cell culture characterisation. Comparison of substrate has been studied previously but with a focus on protein adherence to the electrode before cell attachment, rather than the specific conducting material (Wegener, Keese and Giaever, 2000; Bouafsoun, Helali, Othmane, *et al.*, 2007; Newbold *et al.*, 2010a). The influence of electrode substrate on impedance spectroscopy for cell type characterisation purposes has not been investigated.

Our results suggest that caution should be exercised in drawing direct comparisons in the impedance profiles between studies, where different conducting substrates are used. The standardisation of electrodes between experiments should be a focus for researchers engaged in non-invasive cell characterisation impedance spectroscopy studies, with efforts made to ensure that the only experimental variable is the cells themselves. With regards to the development of a self-reporting stent the study provides guidance that any material under consideration as a substrate for use in an in vivo device will require extensive in vitro cellular scenario regrowth characterisation.

7.4 Limitations

A limitation of the present study is that additional dopant ions were not tested. Polypyrrole was electropolymerised onto the electrodes in presence of only one dopant ion, salicylate. Data on the instability of polypyrrole electrodes and the elution of the salicylate ion from electrodes was therefore limited to one material type. It is not known if other polypyrrole - dopant combinations would be similarly unstable and unable to detect the proliferation of endothelial cells.

Only endothelial cells were investigated during the experimentation presented in this section. Other cell types would have enabled a more comprehensive analysis of the suitability of conducting polymers for cell characterisation purposes.

7.5 Future work

Further work could be undertaken aimed at developing a stable conducting polymer that is able to act as an electrode substrate for cell characterisation whilst eluting a therapeutically relevant drug. This program of research would aim to build on the results presented in this section where the stability of the electrode was determined to be a key factor in measuring the establishment of an endothelial cell monolayer. The results also demonstrated that a salicylate dopant ion rapidly elutes from the conducting polymer polypyrrole, far in excess of the progression rates of restenosis and reendothelialisation. These findings provide guidance that future research should aim to develop a material that remains electrically stable with an extended drug elution profile and that a potential interdependent relationship between these properties should be a focus of the investigation. Such a phase of work should not be constrained to the conducting polymer polypyrrole used in the experimentation presented in this study. Analysis of the literature described in section 7.3 (Discussion) suggests that other conducting polymers such as PEDOT may be more suitable materials in this regard.

7.6 Summary

This section has investigated one aspect involved in the translation of a self-reporting stent from the laboratory to the clinical environment. The conducting polymer polypyrrole with salicylate as the dopant ion was investigated through the proliferation of endothelial cells to confluence in populations clinically relevant for stents. Analysis of the data revealed that the cell-seeded and cell-free electrodes both exhibited similar elevations in reactance that hindered identification of a cell growth profile. Such a finding is in contrast to the previously presented results obtained using the same setup with platinum black electrodes where cell-free electrodes remained stable throughout the experiment duration. A potential cause of polypyrrole-salicylate electrode instability was the measured rapid elution of the dopant from the electrode coating in the first 24 hours and evidence from other conducting polymer-dopant combinations in the literature supports this assumption. Further development will be required to develop a suitable coating that can fulfil the dual properties of conductivity and drug encapsulation that are required for a drug-eluting, self-reporting stent.

8 General discussion

8.1 Introduction

The advent and extensive clinical use of coronary artery stents has revolutionised the treatment of coronary heart disease, with these devices being used in around 100,000 procedures each year in the United Kingdom (Ludman and Gavalova, 2014). However despite multiple design improvements the occurrence rate of in stent restenosis 2 years after implantation for the latest generation of stents is 4%, requiring patients to return to hospital for repeat revascularisation (Sarno *et al.*, 2012). Stent thrombosis also remains a persistent risk, with the use of prolonged dual anti-platelet therapy necessary until recovery of a functional endothelial cell layer is complete. The nature of post procedure cell proliferation around the deployed stent struts is therefore critical to the success of the intervention. Despite this, current methods of both in vivo clinical diagnosis and in vitro research are limited in terms of their capability to continuously monitor the process of cell regrowth. Clinically this places patients at risk from undiagnosed disease progression and in the research domain it hinders efforts to develop enhanced stent designs and improved clinical treatment strategies. The concept of a self-reporting stent has been proposed as means of addressing these limitations. Shedden, 2008, has previously demonstrated that a stent itself could be used as an electrode to monitor arterial tissue growth and that vascular cell types can be characterised through impedance spectroscopy. However these results were carried out on gold electrodes using measurements taken every 24 hours in an environment outside of the physiological conditions recreated in an incubator. The study aimed to address these limitations by developing a more advanced in vitro system for in situ vascular cell characterisation. Additionally the use of separate mono-cultures of the two vascular cell types does not reflect the complexity of the healing taking place around stent struts in vivo, where both endothelial and smooth muscle cell types will be present and so this thesis has also focused on addressing this. The extent to which the impedance based technology could be used to identify endothelial dysfunction also remained to be determined. Finally, the impact of local drug elution from the stent surface on the utility of the approach had not been investigated. The current study set out to address these challenges.

8.2 Results – System development

The previous work by Shedden, 2008, indicated that cell characterisation requires the measurement of impedance parameters over a wide frequency range; however her system was limited to measurements every 24 hours, restricting further characterisation of cell proliferation. Whilst commercial impedance spectroscopy systems can provide high resolution measurements over time they are limited in terms of their frequency range and also by the available size of electrodes (Bischoff *et al.*, 2016a). It was therefore necessary to develop a more advanced system that had the capability to carry out regular impedance measurements across a wide frequency range.

The system developed in the current study has successfully addressed the limitations summarised above. It was found to be capable of monitoring up to 32 electrode pairs, with impedance measurements taken from each one every 120 minutes over a frequency range of 1*Hz* to 100*kHz*. The system was shown to be capable of collecting impedance data automatically in a repeatable and reliable manner, best evidenced by the use of the system in capturing data from a range of cell types over multiple experiments. The final specifications compared favourably with commercial and bespoke systems used in published studies as summarised in Table 4.5 in section 4.10 (Discussion – System development). The present study however differed in the key aspect of the $7mm^2$ working electrode area. Analysis of stent manufacturer's data confirmed that this electrode area was of a comparable surface area to the in vivo exposed area of a coronary stent after expansion. The inclusion of this aspect into the system design permitted cellular impedance experimentation measurements on cell populations that are likely to proliferate over the exposed area of an implanted stent. Leaks and electrode disconnections did cause the data from a proportion of the electrodes to be removed, although this became less of a problem as slight modifications to the chamber manufacturing process were made as the study progressed, thereby minimising any impact on the final experimental results. Also integrated was a time-lapse microscopy system that permitted real-time observation of cell behaviour for comparison with the corresponding impedance data.

8.3 Results – Cell characterisation

Three in vitro models of cell regrowth over stent struts were proposed comprising, porcine endothelial cells, smooth muscle cells and a direct co-culture of both of these cell types. Human Umbilical Vein Endothelial Cells (HUVECs) were also included to provide a human cell type and to allow comparison against examples in the literature. These simplified models aimed to recreate, in vitro, the early stages of cell regrowth over the stent struts during re-endothelialisation and restenosis.

The establishment of a monolayer of primary porcine endothelial cells was successfully monitored by the developed system. Analysis of the reactance component of impedance revealed that the proliferation of endothelial cells gave rise to distinct frequency dependent peaks best visualised using 3D data presentation methods. These characteristic endothelial cell reactance profiles could be utilised to non-invasively characterise the cell types. The falls in reactance were only observed after cells attained confluency and have not been previously reported in the literature. Amongst the possible reasons was the rearrangement of internal cellular structures as the monolayer transitions into a mature endothelium.

The proliferation of a monolayer of smooth muscle cells over the electrodes to a confluent monolayer was non-invasively measured over a 240 hour time period using the developed impedance spectroscopy system. The reactance profile revealed a higher rate of increase at low frequencies towards 1*kHz* and a reduced rate towards 100*kHz*. 3D presentation of this data enabled visualisation of a distinct smooth muscle cell profile that could in the same manner as the endothelial cell data be used to characterise the cell type.

HUVECs were seeded and grown to confluence over the electrodes. Reactance data revealed a central post-confluence peak that was unique to the cell type enabling its characterisation. The magnitude of the reactance increases was also observed to be a maximal 5 times greater for HUVECs in comparison to porcine endothelial cells.

A period of literature analysis and experimental development preceded the establishment of a smooth muscle and endothelial cell co-culture. The final embodiment of the in vitro model consisted of a quiescent, sub-confluent layer of smooth muscle cells underneath a confluent layer of endothelial cells. The developed system was able to non-invasively capture impedance data of each successive stage

of the co-culture. Analysis revealed that the reactance was dominated by the endothelial cells, with a characteristic peak as discerned in previous experimentation on cell monolayers. The 3D presentation of the reactance revealed a unique 3D profile in comparison to other cell types tested.

Key achievements and findings from this phase of experimentation are stated below.

- Endothelial cells have an impedance signature that is distinct from smooth muscle cells and this provides a means of non-invasively characterising between the two cell types.
- HUVECs demonstrated a distinct impedance signature to porcine arterial endothelial cells indicating that impedance spectroscopy could be able to characterise endothelial cell heterogeneity.
- The establishment of a direct co-culture of smooth muscle and endothelial cells for the purposes of impedance spectroscopy measurements.
- Endothelial cells dominant the impedance signature of a co-culture model.

A wider objective of this phase of work was to determine if impedance spectroscopy could identify vascular cell regrowth that characterises re-endothelialisation and in-stent restenosis with a final view to using such techniques in an in vivo self-reporting stent. The results indicate that in vitro impedance spectroscopy testing on clinically relevant cell populations can be used to characterise vascular cell types. It is not known if these impedance profiles will be repeated when captured by a self-reporting stent in an in vivo environment however; the in vitro results suggest that such a concept remains possible. Furthermore the existence of several patents (Shedden *et al.*, 2009; Barakat *et al.*, 2016) and ongoing commercial development by the medical device company Sensome also indicates that such a device remains a clinically feasible objective.

Besides the development of a self-reporting stent and taken holistically the results from this section indicate that as a research tool impedance spectroscopy is capable of non-invasively determining cell type. During experiments to develop a co-culture model the switching of smooth muscle cells from a proliferative to a quiescent phenotype was non-invasively measured using the developed system. This result highlights that impedance spectroscopy can be a useful tool for researchers

investigating the phenotypic switching of smooth muscle cells, a mechanism known to play a key role in atherosclerosis.

The results also strongly indicate that the use of a wide frequency range is important in attempting to determine cell characteristic impedance signatures, and in the case of the vascular cell types that feature in this study the reactance component of impedance is of particular importance. These findings will be of relevance to researchers who wish to use impedance spectroscopy to non-invasively characterise cells. The findings also present a cautionary warning that careful consideration should be given to the frequency at which researchers select for their experiments. The data presented here has shown that in the case of endothelial cells their seeding, settling, proliferation and maturation, without the addition of agonists, will cause frequency dependent elevations and declines in reactance. Should researchers select only a narrow range or singular frequency, impedance variations arising from this normal cell growth process could be misinterpreted.

8.4 Results – Endothelial functionality

Whilst post-stenting rapid re-endothelialisation is considered as the optimal clinical outcome, the functionality of the new endothelium is of importance in preventing the occurrence of future disease states of thrombosis, in stent restenosis and neoatherosclerosis (Caramori *et al.*, 1999; Thanyasiri *et al.*, 2007; Celik *et al.*, 2008; Kubo *et al.*, 2015; Tesfamariam, 2016). A self-reporting stent with the capability to provide data on an endothelial layer's functionality would be of great use to clinicians monitoring the post procedure recovery phase. The developed system was therefore applied to determine if impedance spectroscopy measurements could be used to indicate the endothelial functionality in vitro. Confluent endothelial cell monolayers were transitioned from a functional to a dysfunctional state through the addition of gap junction inhibitors. Gap junctions allow the transfer of metabolites and signalling molecules between cells and are considered important in the maintenance of a functional endothelium (Yeh *et al.*, 2006; Brisset, Isakson and Kwak, 2009).

Endothelial cells were induced into a dysfunctional state through the addition of two drugs, carbenoxolone and heptanol, both widely reported in the literature as inhibitors of gap junctions (Salameh and Dhein, 2005). Cells were also dosed with dipyridamole, a drug reported to enhance gap junction formation (Begandt *et al.*,

2010). The inhibitory and enhancing effect of these drugs was confirmed throughout the experimentation using analysis of fluorescent microscopy images from dye transfer scratch assays. Inspection of the impedance data captured by the developed system revealed that both inhibitors precipitated a decline in total impedance in a dose dependent manner. Such an impedance response in impedance monolayers is typically associated with a reduction in endothelial cell monolayer barrier function. Conversely the gap junction enhancer dipyridamole caused an increase in total impedance. Key findings from this phase of experimentation are stated below.

- Gap junction inhibition causes a decrease in endothelial cell monolayer total impedance that can be associated with a fall in endothelium barrier function.
- Gap junction enhancement causes an increase in endothelial cell monolayer total impedance that can be associated with an elevation in endothelium barrier function.
- Gap junction expression and barrier function reduction is dose dependent when induced by the gap junction inhibitors carbenoxolone and heptanol.
- Gap junction inhibited cells exhibited variable magnitudes of recovery in their barrier function 24 hours after dose administration.
- Barrier function reduction as induced by gap junction inhibition is independent of the expression of the tight junction protein ZO-1.

These results confirmed for the first time that impedance spectroscopy is a suitable tool for discerning a dysfunctional endothelium with inhibited gap junctions. In the context of a self-reporting stent they provide an indication that such a device could have the capability to determine the functionality of a newly reformed endothelial layer. The results have also shown that impedance spectroscopy can be a valuable tool in cardiovascular disease research. A particular advantage of using impedance spectroscopy is the ability to carry out measurements non-invasively on cells over extended time periods. Cardiovascular disease, the associated cellular mechanisms and the remedial drug interventions will all themselves have time dependency and a technique that can provide temporal information is of use to investigative researchers. An example of this can be seen where the rapid inhibition and long term recovery of barrier function as caused by gap junction mediation was measured.

8.5 Results – Conducting polymer substrate

The platinum black electrode substrate was replaced with the conducting polymer polypyrrole with the drug salicylate as the dopant ion. The measurement of impedance parameters revealed a time dependent elevation in electrode reactance that was found to hinder measurement of impedance variation arising from the proliferation of endothelial cells. Only a 6.6% difference between control and cell electrodes was observed after 24 hours of culture. The elution of salicylate from the polypyrrole electrode was profiled and identified as a potential cause for this electrode instability, showing 93% of drug release in 24 hours. Polypyrrole will require further work to be developed into a material that is suitable for use in a self-reporting stent. The aspirational objectives for such a coating are the capability to elute a therapeutically relevant drug whilst remaining sufficiently electrically stable to permit non-invasive measurement of cell proliferation. Key findings from this phase of experimentation are stated below.

- The instability of thin film polypyrrole electrodes doped with salicylate hindered the measurement of cell proliferation using impedance spectroscopy measurements.
- Salicylate eluted rapidly from the polypyrole and may be a contributory cause of electrode instability.
- Comparison of polypyrrole total impedance ratio results from other experiments in this thesis and elsewhere in the literature revealed that cell type impedance signatures are likely to be substrate specific.

8.6 Clinical translation

8.6.1 Challenges

The results presented in this thesis provide an indication that impedance spectroscopy has the potential to monitor cellular regrowth as part of a self-reporting stent. However the clinical translation of this technology into a functional medical device faces significant technical, regulatory and commercial challenges.

Previous to this study it was envisaged that the final embodiment of the device would comprise a stent with fully integrated circuitry all within the artery. This device would carry out the impedance sweeps and then transmit the data through at least

5cm of tissue (Shedden, 2008). This design has been perceived as the final arrangement in patents proposed by both Shedden et al, and the commercial company Sensome (Shedden *et al.*, 2009; Barakat *et al.*, 2016). The miniaturisation of the required impedance and data transmission circuits to the scale whereby they were able to fit inside an artery with a lower diameter limit of approximately 2.25mm, without occluding the blood flow is a major design challenge and this level of scale reduction would represent a considerable step change in implanted electrical device design. Current miniaturisation of impedance devices for implantation is best represented in the device developed by Rodriguez et al, 2016, which has a diameter of 13mm. A further design concern is that if placed inside the artery the container for the circuitry would itself be a potential site for thrombus development or inflammatory induced restenosis.

Consideration should be given to how the struts in a self-reporting stent are modified into electrodes that allow impedance spectroscopy measurements to be performed. The arrangement and design of stent struts has been continually developed by manufacturers to create structures capable of delivery and deployment whilst minimising arterial wall damage (Duckers, Nabel and Serruys, 2007). Stents are manufactured using laser cutting from a cylindrical tube to create a single metallic construction. This process creates a structure that mechanically is made of a series of hoops arranged in a zig-zag pattern. These hoops are then connected together by a limited number of bridges to create the overall tubular structure that has a high resistance to hoop stresses yet remains sufficiently longitudinally flexible to match artery anatomies. In converting these struts into impedance monitoring electrodes for a self-reporting stent these structural design arrangements should be compromised as little as possible. The capability of the device to be deployed via catherization is also an important consideration. An example of a device where such design features were compromised is the Stentenna device which modified the struts into a coil arrangement to allow arterial pressure sensing (Takahata, DeHennis and Wise, 2003). Sensome propose to integrate thin film microelectrodes onto the stent surface, which appears to maintain the original stent structure. These electrodes are then connected into, as yet undefined, measurement circuitry (Barakat *et al.*, 2016). An alternative approach that maintains a larger area for surface measurement would be to replace the connecting bridges between hoops with a non-conducting material. By electrically isolating sections of the stent from one another in this way, individual

electrodes can be created whilst maintaining the architecture the overall device. The interconnection of several hoops could create a larger counter electrode that can be used to measure against smaller, single hoop working electrodes, mimicking in vitro impedance measurement systems such as the one presented in this study. To treat complex or large lesions clinicians are often required to deploy more than one stent in series, such a scenario would be a significant clinical challenge for a self-reporting stent concept. Two or more overlapping stents may cause uncontrolled current paths between adjacent electrodes. This would create erroneous measurements, in a similar manner to the impedance data seen in the present study when media leakages outside of the culture area connected adjacent electrodes. Further development of the concept will need to address such a clinical objective.

8.6.2 Self-reporting stent concept

A conceptual design is proposed here that attempts to address the major design challenge of integrating measurement circuitry into the device and is shown in Figure 8.1. This version of the design places the impedance and transmission circuitry outside of the artery permitting a far greater volume for the electronic design bringing it into the range of the current state of the art. The fragmentary arrangement of the device exploits the proximity of coronary arteries to the outer surface of the heart allowing connectors to interface with the stent without adding additional components into the artery. The use of inductive coupling to power the device would be simplified by the subcutaneous placement of the impedance circuitry, as would the transmission of data. The challenge of transmitting power and data through larger tissue depths was identified by Shedden as a further design challenge. The positioning and placement of devices on the heart in this manner is very similar to the use of pacemakers, a mature medical device technology and a common surgical procedure. The key challenge for the concept is in the connection of the stent through the vessel wall and into the connectors without causing excessive damage to the artery. This represents a more surmountable technological challenge than integration of the whole circuitry into the artery. Over such small distances non-contact current inducement from the wires to the stent may be possible. Wireless impedance measurement of cells adhered to electrodes has been achieved in vitro and the translation of this technique to an in vivo environment would form part of the development process for the concept (Wissenwasser *et al.*, 2011).

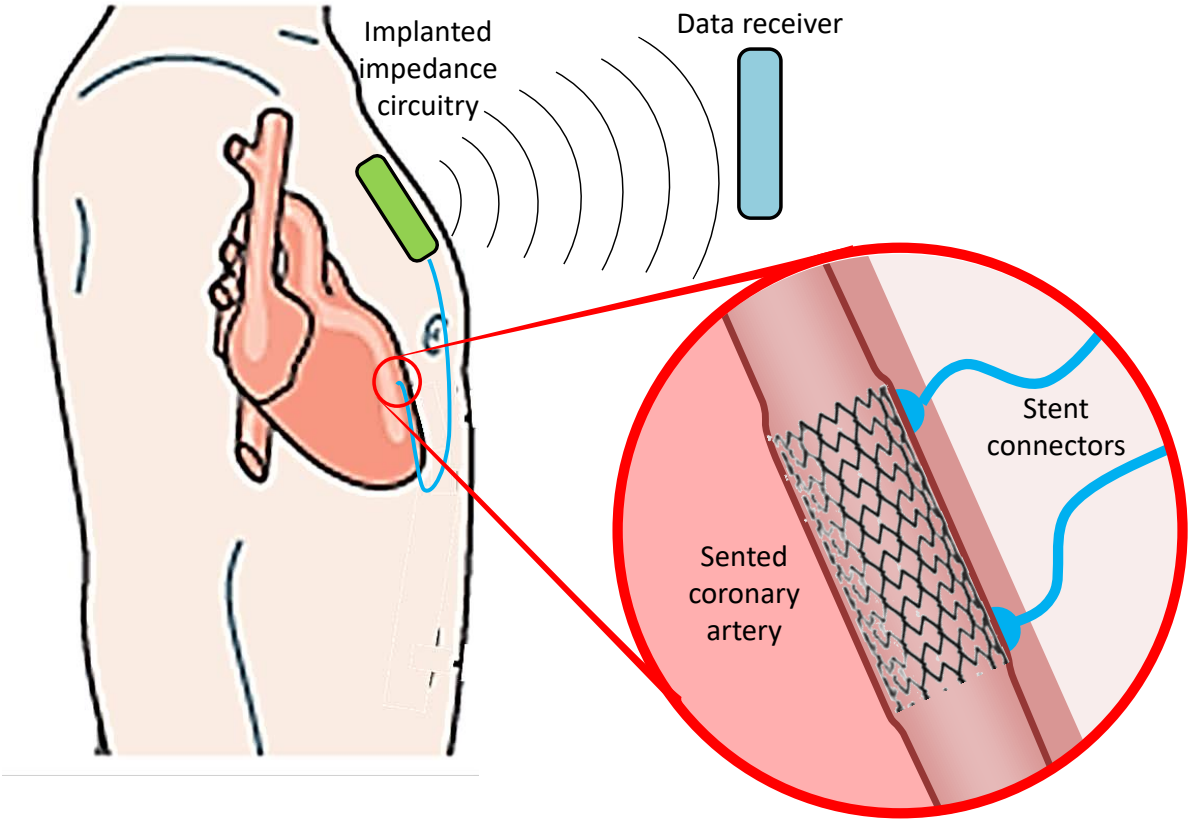

Figure 8.1 - Self-reporting stent concept schematic with remote subcutaneous impedance and transmission circuitry placement.

Although this concept addresses some of the previously highlighted design challenges that a self-reporting stent will face there are several disadvantages that should be acknowledged. Pertinent amongst these is that the attachment of the connectors and placement of the electronic circuitry is an additional surgical procedure on top of the implantation of the stent via catheterisation. A clinical assessment may determine that the benefits of non-invasively monitoring re-endothelialisation and in stent restenosis are not great enough to warrant use of the device or may only be deemed justifiable for those patients who are considered at high risk of developing in stent restenosis. Diabetic patients are one example of such a patient group where increased rates of in stent restenosis occurrence have been documented (Garg and Serruys, 2010). However, the most likely use of the described concept in the near future would be as an in vivo research tool for use in research studies investigating arterial disease states. This envisaged application of a self-reporting stent is further detailed in the later section 8.9.1 (In vivo experimental tool).

8.6.3 Long term clinical translation risks

There also exists a risk that the during the time taken to develop a clinically applicable self-reporting stent the clinical need for non-invasive in stent restenosis and re-endothelialisation detection will have diminished. The development time for a self-reporting stent from its current laboratory development state to a fully functioning regulatory approved medical device will be considerable. Undoubtedly over the same time period the development of current stent designs will progress with improvements targeted at reducing the occurrence of in stent restenosis and promoting re-endothelialisation. The COMBO stent (Orbusneich) which aims to promote adhesion of circulating endothelial progenitor cells in combination with siroloimus elution is one example of such technological advancement in the field (Jaguszewski *et al.,* 2017). Emerging results from clinical trials of the Cre8 (Alvimedica), BioFreedom (Biosensors Int.), and Medtronic's Drug Filled Stent, look particularly promising and may allow significantly reduced anti-platelet regimes to be used (O'Brien *et al.,* 2016; Rozemeijer *et al.,* 2016; Worthley *et al.,* 2017). Further drug-eluting stents developments in terms of the therapeutic compounds used and elution profiles are also likely. An additional similar consideration in the field is the advent and continued development of the new class of bioabsorbable stents. These devices have been termed as the fourth revolution in interventional cardiology and are designed to dissolve over time leaving a fully re-endothelialised open artery (Onuma and Serruys, 2011; Rajendra, Wrigley and Gershlick, 2012). Although in their current state they have been shown to exhibit some level of thrombogenicity in the early stages after deployment (Koppara *et al.,* 2015), and recent clinical data on the industry leading Absorb Stent (Abbott Vascular) has led to removal of this product from the market (Sorrentino *et al.,* 2017). However, further development and improvements are anticipated with an estimated 24 separate companies pursuing device development (Tenekecioglu *et al.,* 2016). The development of bioabsorbable stents that demonstrate minimal occurrence rates of re-stenosis and thrombosis would further reduce the clinical requirement for a self-reporting stent. The combined result of these future developments over the coming years is likely to be a fall in in stent restenosis rates. It is therefore possible that in the time it would take to clinically translate an impedance based self-reporting stent the perceived clinical need for such a device would have been reduced by other technological developments.

8.7 General study limitations

Limitations specific to the experimentation in the results sections have been previously presented. Beyond these there are limitations that are general to the whole study and they will be presented and discussed here.

8.7.1 In vitro study

The present study is an entirely in vitro study and therefore does not include any results from more clinically relevant in vivo animal models. Whilst in vitro models of disease states are reported extensively throughout the literature in vivo results are considered to be more clinically relevant. Within an in vivo environment smooth muscles cells exist in 3D constructs unlike the planar 2 dimensional cultures used in this study. The in vitro scenarios used in this study that modelled in stent restenosis were either a monolayer of smooth muscle cells or a co-culture incorporating endothelial cells. More certainty can be attached to clinical relevance of the re-endothelialistation scenario as endothelial cells in vivo exist in monolayers on the arterial wall. The same 2D to 3D limitation can be applied to the arrangement of the electrodes in this study. The planar arrangement of the thin film platinum black electrodes does not accurately represent the envisages 3D tubular configuration of the electrodes in a self-reporting stent.

8.7.2 Porcine cells

The majority of the work presented uses primary porcine cells which although utilised in a large array of in vitro cardiovascular studies are of less clinical relevance than human primary cells. The observed differences between the impedance profiles of porcine endothelial cells and human umbilical vein endothelial cells could be attributable to a species difference. Further in vitro testing using primary human cells would enable the relevance of porcine cell models to be established. In vitro data from porcine cells is of relevance in the developmental process for a self-reporting stent. Pigs are widely used during in vivo studies involving stents and are considered as the gold standard of coronary artery stent animal models (McKittrick *et al.*, 2016). In vivo experimentation using pigs is a potential future step in the development of a self-reporting stent and the in vitro data presented here using cells from the same species will be useful for future experimental guidance.

8.7.3 Endothelial cell heterogeneity

The post-stenting cell regrowth scenarios investigated in this study occur in the coronary regions of the vasculature. The primary porcine endothelial cells used in the study were harvested from a section of pulmonary artery and not from a coronary artery, where the smooth muscle cells were isolated from, and in this regard can be considered a limitation of the present study. Although the difference between these cells in terms of their distance in the vascular tree is short there is a variation in the diameter and function of their source arteries. As a result there is expected to be some level of heterogeneity between the two, as found in studies on endothelial cells from other areas of the vasculature (Aird, 2007a). Attempts were made to address this limitation by isolating endothelial cells from the coronary artery using the same scraping procedure. However this was not successful on enough occasions to make cells available in sufficient quantities for seeding into chambers. The results presented in section 5 (In vitro cell characterisation by impedance spectroscopy) showing differences between HUVECs and porcine pulmonary artery endothelial cells suggest that impedance spectroscopy measurements have the potential to characterise endothelial heterogeneity. They therefore provide guidance that cardiovascular research should aim to match the cell type from the same region as the disease states being investigated.

8.7.4 Zero flow conditions

All of the cell culture work reported was carried out on in zero flow conditions. The disease states of restenosis, in stent thrombosis and the preferable re-endothelialisation process take place in an environment of pulsatile blood flow through the coronary artery. The final embodiment of the envisaged self-reporting stent will need to operate in pulsatile flow conditions and serious consideration will need to be given to the effect that this has on the measured impedance parameters. Intriguingly, experimentation on endothelial cells in flow conditions has revealed increases in transendothelial resistance and total impedance (DePaola *et al.*, 2001; Seebach *et al.*, 2007), suggesting that the in vivo impedance signature from re-endothelialisation would be even greater than those reported here.

8.8 Future work

8.8.1 Human coronary vascular cell experimentation

A first step towards the realisation of a functional self-reporting stent would be to confirm that the cell characterisation results shown here are repeated in human vascular cells isolated from coronary arteries. As outlined in sections 8.7.2 (Porcine cells) and 8.7.3 (Endothelial cell heterogeneity) the work has thus far been carried out on primary porcine and human umbilical vein source cells. Repeating the experimentation using human coronary cells would provide further confidence that the concept of using impedance spectroscopy to determine post stenting cell regrowth scenarios is feasible. Comparing these results with the porcine data presented in this study would also provide a useful indication on the impedance property differences that can be expected between cells from different mammalian species. This information would be of interest to researchers using impedance spectroscopy in other applications.

8.8.2 In vitro stent electrode experimentation

A further method of obtaining clinically relevant in vitro results would be to modify the chambers by replacing the thin film platinum black electrodes with stent sections. These sections would be cut from an expanded stent and flattened out, as depicted below in Figure 8.2. The seeding of cells onto the stent sections and the measurement of impedance variation over time would provide a close approximation to the post-stenting cellular regrowth scenarios. Characterisation of these scenarios would provide additional confidence in the feasibility of an in vivo device.

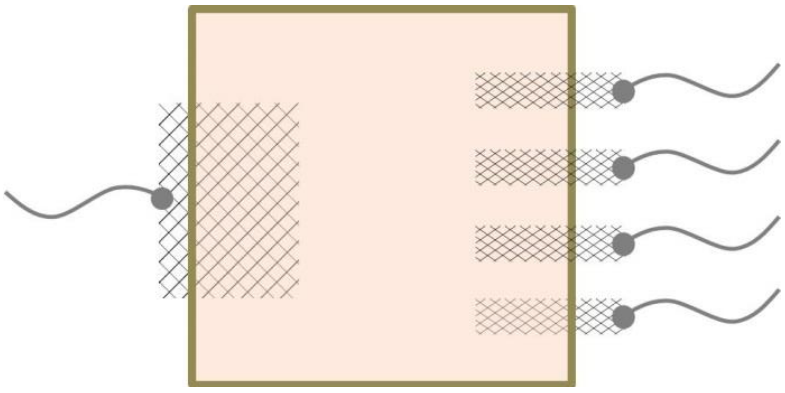

Figure 8.2 - Schematic image of a proposed chamber modification, replacing thin film platinum electrodes with planar stent sections.

8.8.3 Technological device development

Technological device development could also be instigated with an intermediate developmental objective being the aforementioned large vessel self-reporting stent for use in animal models (see section 8.9.1 In vivo experimental tool). Pertinent amongst the device development tasks is the design and testing of circuitry arrangement that is capable of performing impedance sweeps in desired frequency range of $1kHz$ to $100kHz$ whilst meeting the space requirements outlined in the proposed concept in section 8.6.2 (Self-reporting stent design concept). Furthermore the design should aim to transmit the data through the required distance of tissue.

8.8.4 In vitro model of in stent thrombosis,

Whilst this study has focussed on the identification of the re-endothelialisation and in stent restenosis scenarios there is an additional in vivo scenario of thrombosis. Independent research groups, Sapkota et al, 2014, and Hayashi et al, 2010, have demonstrated that thrombotic blood has a discernible impedance signature suggesting that the coagulation cascade could be detected in-vivo. A future study could analyse the impedance signature of thrombus development on the electrodes, adding a fourth in vitro scenario to those used in this study. Should this data provide a different impedance signature to any form of cell growth all of the potential clinical outcomes for stent implantation would be detectable. The early identification of thrombus development would allow clinicians to intervene before the lesion becomes dangerously occluded or the thrombus becomes detached. Such a phase of work would also provide a new in vitro method of investigating thrombus development. In the context of the previously proposed prototype self-reporting stent for use in animal studies, real time in vivo data of thrombus initiation, growth and detachment could be provided. This clinically relevant experimental data would be greatly beneficial to researchers developing anti-thrombotic drugs and medical devices. This could reduce the need for current invasive techniques such as intravital microscopy where windows are implanted into animals to allow direct observation of thrombus development (Furie and Furie, 2005).

8.9 Future applications

The experimentation presented in the present study was carried out with the objective of determining the feasibility of using impedance spectroscopy as a method for an in vivo self-reporting stent. The study findings can however, also be used to postulate a role for the technology in other biomedical applications.

8.9.1 In vivo experimental tool

Should a self-reporting stent be developed to the point whereby it is a functional, in vivo device that can monitor the functionality of a reformed endothelium it would provide a hugely valuable tool for testing drugs in animal studies. The implantation of this research device into a healthy animal and the establishment of an endothelial layer over the measuring surfaces would provide a representative baseline for a functional endothelium. The subsequent dosing of the animal with various drugs and the simultaneous real time monitoring of the functionality of the endothelial layer would add a temporal dimension to the in vivo study of drugs not currently achievable. Such a device could also extend beyond the study of drugs and be used to examine the effect of other inventions such as variations in diet, exercise regimens and other environmental factors linked to cardiovascular disease. Potentially such a device could open up a new method for in vivo cardiovascular research. The ability to gather data in real time would also negate the requirement to euthanise the animal to extract cardiovascular devices, which is current practice and also only able to provide a single temporal data point. For the purposes of animal studies the device need not be miniaturised to the point whereby it fits into a coronary artery but could be designed to fit into a larger vessel such as a pulmonary artery. The design and implementation of a larger self-reporting stent targeted at in vivo experimentation in animals would also provide a useful technological stepping stone towards the development of a fully functional device for use in human coronary arteries. By following this technological development procedure the final goal of a self-reporting stent for clinical use in human coronary arteries would be broken down into surmountable scientific and technological steps whilst also providing beneficial research output.

8.9.2 In vitro monitoring of long term cellular responses to drugs

The existence of a recovery mechanism in the barrier properties measured in the endothelial functionality experiments suggests that cellular responses to drugs may

be temporally dependant and it is possible that similar effects may be evident in other drugs. The non-invasive nature of impedance spectroscopy measurement makes it an excellent tool for the in vitro monitoring of such responses. The study of temporal cell response to agonists would be of relevance to pharmacists and those involved in drug development and specifically pharmacokinetics. Drugs are required to pass through one or more barriers before they can attain a concentration whereby they can become effective at the targeted tissue (Michaelis *et al.*, 2012). Additional experimentation aided at discovering a cause for the measured barrier function recovery would aid researchers seeking to target drugs at specific tissues.

8.9.3 Stem cell expansion and differentiation monitoring

The non-invasive characterisation of cells presented here has a potential application in the domain of regenerative medicine. This emerging field aims to use laboratory grown cells in combination with scaffolds to create functional, tissue engineered constructs that can replace or augment a patient's dysfunctional tissue. In utilising somatic cells differentiated from the patient's own stems cells the chance of an autoimmune response to these implanted devices is mitigated. Consequently the future therapeutic application of such artificial 3D constructs will require a large number of cells, representing a step change in the scale of current laboratory culture practices (Ratcliffe, Thomas and Williams, 2011). As an example of only one therapeutic target, it has been estimated that that to supply an annual demand of 250,000 patients with cellular therapy for heart infarction, 10^{16} stem cells will be required (Want *et al.*, 2012). It is as a monitoring technology in the expansion and differentiation of these high volume cell lines where impedance spectroscopy may have a role to play in the future. Current methods of cell characterisation following stem cell differentiation involve the invasive attachment of specific cell markers and are considered laborious for use in high volume manufacturing environments. The labelling of a cell in this manner also renders it unusable as a product and label free methods of determining stem cell differentiation are therefore predicted to play a pivotal role in the future of regenerative medicine (Hay *et al.*, 2010). Impedance spectroscopy using microelectrodes has previously been used as an in vitro laboratory based technique for monitoring stem cell differentiation into adipogenic, osteogenic, neural and astroglial lineages (Angstmann *et al.*, 2011; Bagnaninchi and Drummond, 2011; Lee *et al.*, 2014) and the results in the present study add further confidence in the vascular characterisation capabilities of the technology.

Furthermore by performing measurements on clinically relevant populations the results also demonstrate that impedance based cell analysis is possible in larger cell populations. It is predicted that to meet this demand the future regenerative medicine industry will require a high level of automation, mimicking current pharmaceutical manufacturing processes (Abbasalizadeh and Baharvand, 2012; Serra *et al.*, 2012). The automated nature of impedance spectroscopy measurement shown in this and other studies demonstrates its suitability for use as an industrial monitoring technology.

8.9.4 Impedance monitoring for other medical implants

The monitoring of cellular regrowth over implanted surfaces is not restricted to coronary stents alone. The success of a variety of implanted devices is dependent on integration with the local cell population. The sensitivity of the system developed in the work described in this thesis highlights the potential of impedance spectroscopy as a non-invasive method that could be incorporated into implanted devices. Relevant examples include orthopaedic implants, replacement heart valves and artificial vascular grafts. The larger dimensions of the aforementioned implants when compared to coronary stents would make them more suitable candidates for the integration of implanted impedance measurement circuitry.

8.9.5 In vitro cell characterisation platform technology

The frequency dependent peak observed in the impedance profiles of porcine endothelial cells is of relevance to research carried out using the available commercial impedance spectroscopy systems. Studies using these systems often compromise the application of a range of frequencies in preference to achieving a high time resolution and in the case of the xcelligence system the frequency at which measurements are made is not always published (Peper *et al.*, 2014; Bischoff *et al.*, 2016a). The presence of frequency dependent variable peaks in the porcine endothelial data suggests that careful consideration should made as to which frequencies are used to analyse cell behaviour. Therefore the results gathered and presented in this study can be used as a basis for a proposal to standardise cell characterisation between studies. As previously stated in section 1.15 (Commercially available impedance spectroscopy systems) commercial impedance systems, using standardised gold electrodes, are ubiquitous throughout laboratories, and predominate in published cellular impedance spectroscopy studies. However they are

restricted to perform measurements across a small number of frequencies in order to allow measurement at a high temporal resolution. Through a simple modification to include slower measurements over a wider, high resolution, frequency range, these systems would be able to capture and present reactance data in 3D, as presented here. The specificity of cell characterisation results to the electrode substrates shown in the results presented here from platinum black and polypyrrole electrodes would be negated through the use of the standard gold electrodes that commercial systems are configured to use. With access to impedance measurements over a wide, high resolution frequency range carried out on standardised electrodes researchers would be able to compare characterisation results from different cell types for experiments performed in different laboratories. Such a method of measurement could form a new benchmark of cell characterisation for in vitro studies on cell monolayers and allow greater confidence when comparing results between studies from different research groups.

8.9.6 Recommended future direction

Considerable barriers remain in translating impedance spectroscopy into the clinical environment and it is not certain that a functioning device is feasible with the currently available technology. The most immediate use for the technology is therefore likely to be in the research domain rather than a self-reporting stent for clinical usage in humans and this should be the focus of future developmental research. A target objective should be the realisation of the previously detailed in vivo research tool. Such a device could reveal new insights in cardiovascular diseases that could be exploited by stent and therapeutic drug manufacturers alike, ultimately improving clinical outcomes for patients.

The end

9 Appendix

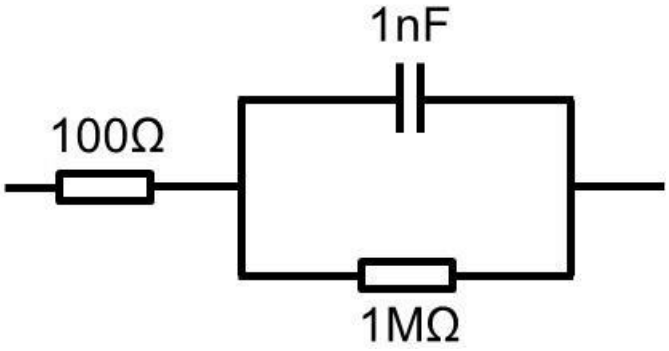

Figure 9.1 - Dummy cell circuit used in system testing and characterisation phases.

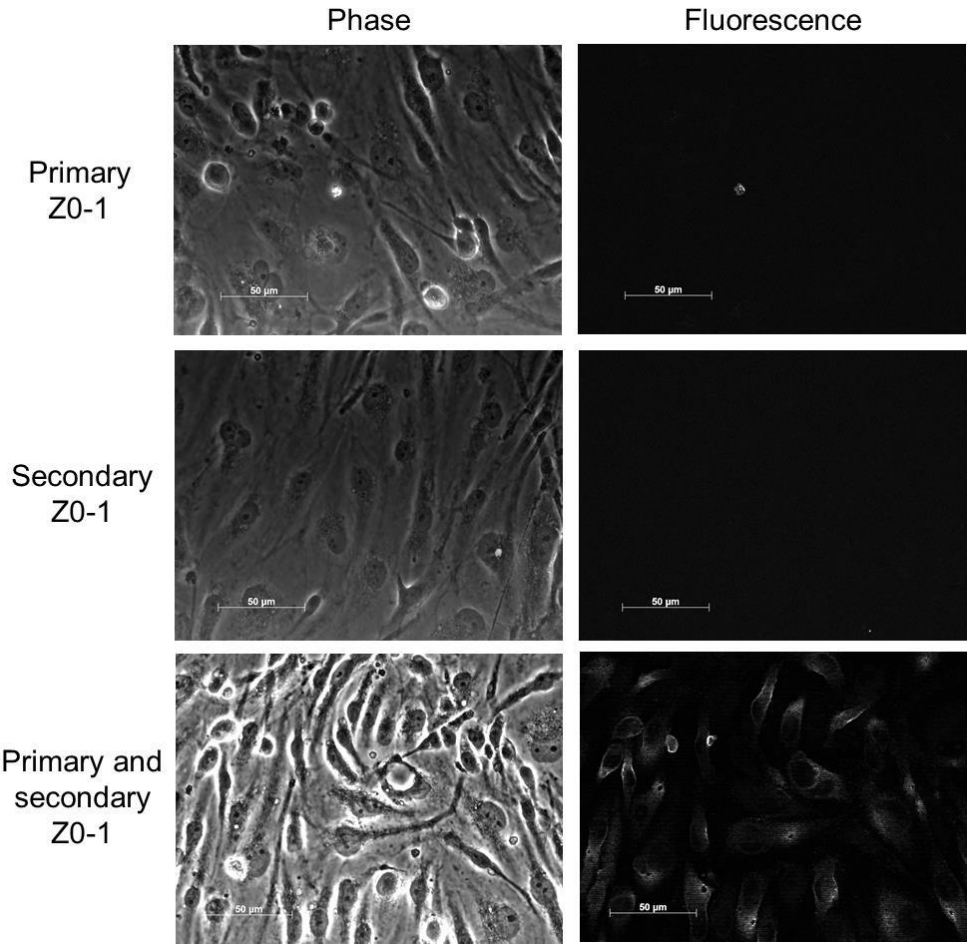

Figure 9.2 - Grey scaled positive and negative control images for ZO-1 expression in porcine endothelial cells. Negative controls - exposure to primary and secondary antibodies alone as per protocol. Positive control exposure to primary and secondary antibodies as per protocol. Phase microscopy images provide evidence of cells. Scale bars are 50µm.

Sputter coating thickness calculations, per coating operation.

$$d = mA \times kV \times t \times K$$

Where, mA is the milliamps applied, kV is the kilovolt setting, t is the discharge time in minutes, K is a gas constant (5 for Argon in the case presented here) and d is the thickness in Angstroms. 5 coating operations were used.

In the case for the gold coatings used throughout this thesis this calculates to as thickness of 1250 Angstroms or 125 nanometres.

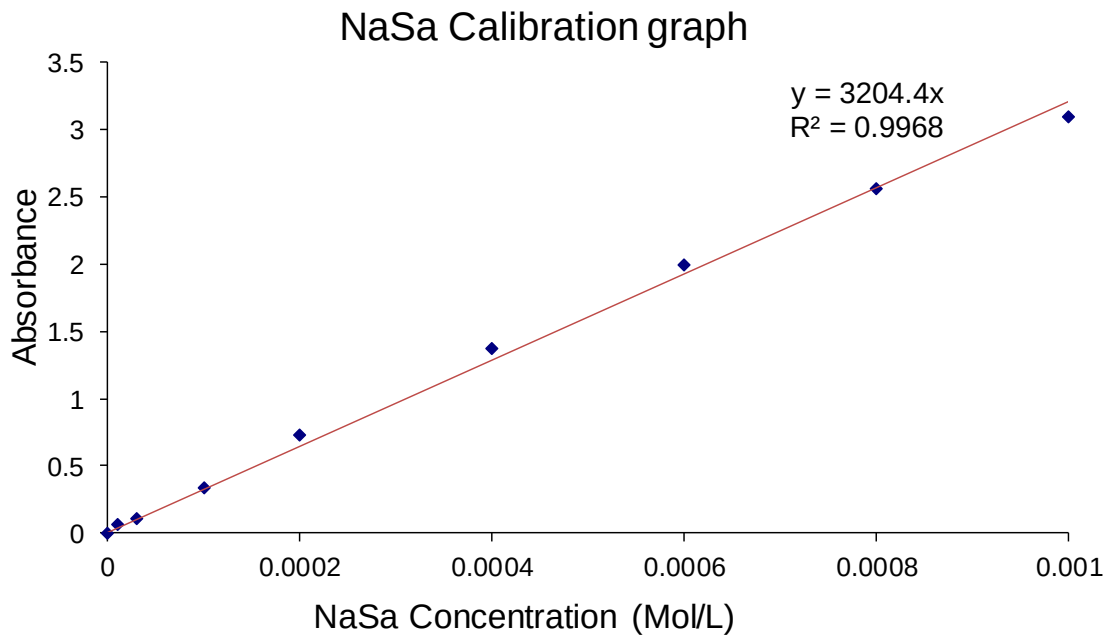

Figure 9.3 - Sodium Salicylate concentration – UV absorbance calibration graph.

10 References

Abbaci, M. et al., 2008. Advantages and limitations of commonly used methods to assay the molecular permeability of gap junctional intercellular communication. BioTechniques, 45(1), pp.33–62. Available at: http://www.biotechniques.com/article/000112810.

Abbasalizadeh, S. & Baharvand, H., 2012. Technological progress and challenges towards cGMP manufacturing of human pluripotent stem cells. Biotechnology Advances, 31(8), pp.1600–23.

Abidian, M.R., Kim, D.H. & Martin, D.C., 2006. Conducting-polymer nanotubes for controlled drug release. Advanced Materials, 18(4), pp.405–409.

Acharya, G. & Park, K., 2006. Mechanisms of controlled drug release from drug-eluting stents. Advanced Drug Delivery Reviews, 58(3), pp.387–401.

Aird, W.C., 2007a. Phenotypic Heterogeneity of the Endothelium. Circulation Research, 100(2), pp.158–173. Available at: http://circres.ahajournals.org/content/100/2/158.abstract [Accessed November 7, 2013].

Aird, W.C., 2007b. Phenotypic heterogeneity of the endothelium: II. Representative vascular beds. Circulation research, 100(2), pp.174–90. Available at: http://www.ncbi.nlm.nih.gov/pubmed/17272819 [Accessed November 8, 2013].

Alfonso, F. et al., 2014. Current treatment of in-stent restenosis. Journal of the American College of Cardiology, 63(24), pp.2659–2673.

Alfonso, F. et al., 2015. Mechanisms of balloon angioplasty and repeat stenting in patients with drug-eluting in-stent restenosis. International Journal of Cardiology, 178, pp.213–220. Available at: http://dx.doi.org/10.1016/j.ijcard.2014.10.139.

Álvarez-Romero, G. et al., 2006. Electrochemical and AFM characterization of the electropolimerization of pyrrole over a graphite–epoxy resin solid composite electrode, in the presence of different anions. Applied Surface Science, 252(16), pp.5783–5792. Available at: http://linkinghub.elsevier.com/retrieve/pii/S0169433205010718 [Accessed November 10, 2013].

Anagnostopoulou, A. et al., 2007. Examination of gap junctional, intercellular communication by in situ electroporation on two co-planar indium-tin oxide electrodes. Molecular Oncology, 1(2), pp.226–231.

Andreini, D. et al., 2012. Coronary in-stent restenosis: assessment with CT coronary angiography. Radiology, 265(2), pp.410–7. Available at: http://www.ncbi.nlm.nih.gov/pubmed/22966068.

Angstmann, M. et al., 2011. Monitoring human mesenchymal stromal cell differentiation by electrochemical impedance sensing. Cytotherapy, 13(9), pp.1074–89. Available at: http://www.ncbi.nlm.nih.gov/pubmed/21619493 [Accessed November 8, 2013].

Antonetti, D.A. et al., 1999. Vascular Endothelial Growth Factor Induces Rapid Phosphorylation of Tight Junction Proteins Occludin and Zonula Occluden 1. Journal of Biological Chemistry, 274(33), pp.23463–23467. Available at: http://www.ncbi.nlm.nih.gov/pubmed/10438525%5Cnhttp://www.jbc.org/cgi/doi/10.1074/jbc.274.33.23463.

Arbizzani, C. et al., 2007. Polypyrrole: A drug-eluting membrane for coronary stents. Electrochimica Acta, 52(9), pp.3274–3279.

Arndt, S. et al., 2004. Bioelectrical impedance assay to monitor changes in cell shape during apoptosis. Biosensors and Bioelectronics, 19(6), pp.583–594.

Asami, K., 2007. Dielectric properties of biological tissues in which cells are connected by communicating junctions. Journal of Physics D: Applied Physics, 40, pp.3718–3727.

Asfour, H. et al., 2010. Low frequency impedance spectroscopy of cell monolayers using the four-electrode method. Journal of Physics: Conference Series, 224, p.12085.

Ashrafi, A., Golozar, M. a. & Mallakpour, S., 2006. Morphological investigations of polypyrrole coatings on stainless steel. Synthetic Metals, 156(18–20), pp.1280–1285. Available at: http://linkinghub.elsevier.com/retrieve/pii/S0379677906002244 [Accessed November 9, 2013].

Ateh, D.D., Navsaria, H. a & Vadgama, P., 2006. Polypyrrole-based conducting polymers and interactions with biological tissues. Journal of the Royal Society, Interface / the Royal Society, 3(11), pp.741–52. Available at: http://www.pubmedcentral.nih.gov/articlerender.fcgi?artid=1885362&tool=pmcentrez&rendertype=abstract [Accessed January 10, 2014].

Azarbal, B. & Currier, J.W., 2006. Allergic reactions after the implantation of drug-eluting stents: Is it the pill or the polymer? Journal of the American College of Cardiology, 47(1), pp.182–183. Available at: http://dx.doi.org/10.1016/j.jacc.2005.09.045.

Bachetti, T. & Morbidelli, L., 2000. Endothelial cells in culture: a model for studying vascular functions. Pharmacological research : the official journal of the Italian Pharmacological Society, 42(1), pp.9–19.

Bagnaninchi, P.O. & Drummond, N., 2011. Real-time label-free monitoring of adipose-derived stem cell differentiation with electric cell-substrate impedance sensing. Proceedings of the National Academy of Sciences of the United States of America, 108(16), pp.6462–6467. Available at: http://www.pubmedcentral.nih.gov/articlerender.fcgi?artid=3080969&tool=pmcentrez&rendertype=abstract [Accessed November 8, 2013].

Balasubramanian, L. et al., 2008. Impedance analysis of renal vascular smooth muscle cells. American journal of physiology. Cell physiology, 295(4), pp.954–965.

Balda & Matter, K., 1998. Tight junctions. Journal of cell science, 111 (Pt 5, pp.541–547.

Balint, R. & Cartmell, S.H., 2013. Electrical Stimulation : A Novel Tool for Tissue Engineering. Tissue engineering. Part B,, 19(1), pp.48–57.

Balint, R., Cassidy, N.J. & Cartmell, S.H., 2014. Conductive polymers: Towards a smart biomaterial for tissue engineering. Acta biomaterialia, 10(6), pp.2341–2353. Available at: http://www.ncbi.nlm.nih.gov/pubmed/24556448 [Accessed May 7, 2014].

Barakat, A. et al., 2016. Medical device provided with sensors having variable impedance. , p.5.

Bard, A.J. & Faulkner, L.R., 2001. Electrochemical methods: Fundamentals and Applications 2nd ed., New York: John Wiley & Sons.

Barlis, P. et al. (2010) ‘An optical coherence tomography study of a biodegradable vs. durable polymer-coated limus-eluting stent: A LEADERS trial sub-study’, European Heart Journal, 31(2), pp. 165–176. doi: 10.1093/eurheartj/ehp480.

Bazzoni, G. & Dejana, E., 2004. Endothelial cell-to-cell junctions: molecular organization and role in vascular homeostasis. Physiol Rev., 84(0031–9333 (Print)), pp.869–901.

Becker, P.M. et al., 2001. Differential regulation of diverse physiological responses to VEGF in pulmonary endothelial cells. American journal of physiology. Lung cellular and molecular physiology, 281(6), pp.L1500-11. Available at: http://www.ncbi.nlm.nih.gov/pubmed/11704547.

Beckmann, A. et al., 2015. Pannexin-1 channels show distinct morphology and no gap junction characteristics in mammalian cells. Cell and Tissue Research, pp.751–763.

Begandt, D. et al., 2013. Dipyridamole-related enhancement of gap junction coupling in the GM-7373 aortic endothelial cells correlates with an increase in the amount of connexin 43 mRNA and protein as well as gap junction plaques. Journal of bioenergetics and biomembranes, 45(4), pp.409–19. Available at: http://www.ncbi.nlm.nih.gov/pubmed/23800832.

Begandt, D. et al., 2010. Dipyridamole increases gap junction coupling in bovine GM-7373 aortic endothelial cells by a cAMP-protein kinase A dependent pathway. Journal of bioenergetics and biomembranes, 42(1), pp.79–84. Available at: http://www.ncbi.nlm.nih.gov/pubmed/20054624.

Begandt, D. et al., 2015. Gold nanoparticle-mediated (GNOME) laser perforation: a new method for a high-throughput analysis of gap junction intercellular coupling. Journal of bioenergetics and biomembranes, pp.441–449. Available at: http://www.ncbi.nlm.nih.gov/pubmed/26310434.

Behringer, E.J. et al., 2012. Electrical conduction along endothelial cell tubes from mouse feed arteries: confounding actions of glycyrrhetinic acid derivatives. British journal of pharmacology, 166(2), pp.774–87. Available at: http://doi.wiley.com/10.1111/j.1476-5381.2011.01814.x.

Bennett, M.R., 2003. In-stent stenosis: pathology and implications for the development of drug eluting stents. Heart, 89(2), pp.218–224.

Benson, K., Cramer, S. & Galla, H.-J., 2013. Impedance-based cell monitoring: barrier properties and beyond. Fluids and barriers of the CNS, 10(1), p.5. Available at: http://www.pubmedcentral.nih.gov/articlerender.fcgi?artid=3560213&tool=pmcentrez&rendertype=abstract.

Bischoff, I. et al., 2016. Pitfalls in assessing microvascular endothelial barrier function: impedance-based devices versus the classic macromolecular tracer assay. Scientific reports, 6(March), p.23671. Available at: http://www.ncbi.nlm.nih.gov/pubmed/27025965%5Cnhttp://www.pubmedcentral.nih.gov/articlerender.fcgi?artid=PMC4877919.

Bouafsoun, A., Helali, S., Mebarek, S., et al., 2007. Electrical probing of endothelial cell behaviour on a fibronectin/polystyrene/thiol/gold electrode by Faradaic electrochemical impedance spectroscopy (EIS). Bioelectrochemistry (Amsterdam, Netherlands), 70(2), pp.401–7. Available at: http://www.ncbi.nlm.nih.gov/pubmed/16844428 [Accessed November 8, 2013].

Bouafsoun, A., Helali, S., Othmane, A., et al., 2007. Evaluation of endothelial cell adhesion onto different protein/gold electrodes by EIS. Macromolecular bioscience, 7(5), pp.599–610. Available at: http://www.ncbi.nlm.nih.gov/pubmed/17477444 [Accessed November 8, 2013].

Bouiss, D. et al., 2001. Endothelium in vitro: A review of human vascular endothelial cell lines for blood vessel-related research. Angiogenesis, 4(2), pp.91–102.

Brischwein, M. et al., 2006. Electric cell-substrate impedance sensing with screen printed electrode structures. Lab on a Chip, 6(6), p.819. Available at: http://www.ncbi.nlm.nih.gov/pubmed/16738736%5Cnhttp://pubs.rsc.org/en/content/articlepdf/2006/lc/b602987f.

Brisset, A.C., Isakson, B.E. & Kwak, B.R., 2009. Connexins in vascular physiology and pathology. Antioxidants & redox signaling, 11(2), pp.267–282.

British Heart Foundation, 2017. BHF CVD STATISTICS COMPENDIUM 2017 -,

Busch, M. et al., 2005. On the heating of inductively coupled resonators (stents) during MRI examinations. Magnetic Resonance in Medicine, 54(4), pp.775–782.

Callies, C. et al., 2011. Membrane potential depolarization decreases the stiffness of vascular endothelial cells. Journal of cell science, 124(11), pp.1936–42. Available at: http://www.ncbi.nlm.nih.gov/pubmed/21558418.

Campbell, C.E. et al., 2007. Monitoring viral-induced cell death using electric cell-substrate impedance sensing. Biosensors & bioelectronics, 23(4), pp.536–42. Available at: http://www.ncbi.nlm.nih.gov/pubmed/17826975 [Accessed January 30, 2014].

Caramori, P.R. et al., 1999. Long-term endothelial dysfunction after coronary artery stenting [see comments]. J.Am.Coll.Cardiol., 34(6), pp.1675–1679.

Cascalheira, A.C. et al., 2003. Electrochemical synthesis and redox behaviour of polypyrrole coatings on copper in salicylate aqueous solution. Electrochimica Acta, 48(17), pp.2523–2529.

Castano, H. et al., 2004. Polypyrrole thin films formed by admicellar polymerization support the osteogenic differentiation of mesenchymal stem cells. Macromolecular bioscience, 4(8), pp.785–94. Available at: http://www.ncbi.nlm.nih.gov/pubmed/15468272 [Accessed November 21, 2013].

Celik, T. et al., 2008. The forgotten player of in-stent restenosis: Endothelial dysfunction. International Journal of Cardiology, 126(3), pp.443–444.

Ceriotti, L. et al., 2007. Real-time assessment of cytotoxicity by impedance measurement on a 96-well plate. Sensors and Actuators B: Chemical, 123(2), pp.769–778. Available at: http://linkinghub.elsevier.com/retrieve/pii/S0925400506007015 [Accessed March 12, 2014].

Chiu, J.-J., 2003. Shear stress inhibits adhesion molecule expression in vascular endothelial cells induced by coculture with smooth muscle cells. Blood, 101(7), pp.2667–2674. Available at: http://www.bloodjournal.org/cgi/doi/10.1182/blood-2002-08-2560.

Cho, S. & Thielecke, H., 2008. Electrical characterization of human mesenchymal stem cell growth on microelectrode. Microelectronic Engineering, 85(5–6), pp.1272–1274. Available at: http://linkinghub.elsevier.com/retrieve/pii/S0167931708000142 [Accessed November 8, 2013].

Chung, I.M. et al., 2002. Enhanced extracellular matrix accumulation in restenosis of coronary arteries after stent deployment. Journal of the American College of Cardiology, 40(12), pp.2072–2081.

Clark, P., 2009. Biology of Vascular Permeability. Allergy and Allergic Diseases, Second Edition, 1, pp.857–873.

Contractor, H., Mamas, M. & Fraser, D.G., 2008. Angiographic time course of in-stent restenosis with zotarolimus drug-eluting stents. Can J Cardiol, 24(7), p.e45. Available at: http://www.ncbi.nlm.nih.gov/pubmed/18612508.

Cote, K.R. & Gill, R.C., 1987. Development of a platinized platinum/iridium electrode for use in vitro. Annals of biomedical engineering, 15(5), pp.419–26. Available at: http://www.ncbi.nlm.nih.gov/pubmed/3688577.

Curcio, A., Torella, D. & Indolfi, C., 2011. Mechanisms of smooth muscle cell proliferation and endothelial regeneration after vascular injury and stenting: approach to therapy. Circulation journal : official journal of the Japanese Circulation Society, 75(6), pp.1287–1296.

D'hondt, C. et al., 2009. Pannexins, distant relatives of the connexin family with specific cellular functions? BioEssays, 31(9), pp.953–974.

Dangas, G.D. et al., 2010. In-stent restenosis in the drug-eluting stent era. Journal of the American College of Cardiology, 56(23), pp.1897–1907. Available at: http://dx.doi.org/10.1016/j.jacc.2010.07.028.

Dejana, E., Corada, M. & Lampugnani, M.G., 1995. Endothelial cell-to-cell junctions. The FASEB journal : official publication of the Federation of American Societies for Experimental Biology, 9(10), pp.910–918.

DePaola, N. et al., 2001. Electrical Impedance of Cultured Endothelium Under Fluid Flow. Annals of Biomedical Engineering, 29(8), pp.648–656. Available at: http://link.springer.com/10.1114/1.1385811 [Accessed November 8, 2013].

Desai, S.A. et al., 2010. Improving impedance of implantable microwire multi-electrode arrays by ultrasonic electroplating of durable platinum black. Frontiers in neuroengineering, 3(May), p.5. Available at: http://www.pubmedcentral.nih.gov/articlerender.fcgi?artid=2871717&tool=pmcentrez&rendertype=abstract [Accessed January 21, 2014].

Dhein, S., 2004. Pharmacology of gap junctions in the cardiovascular system. Cardiovascular Research, 62(2), pp.287–298.

Dixon, B.S. et al., 2009. Effect of Dipyridamole plus Aspirin on Hemodialysis Graft Patency. New England Journal of Medicine, 360(21), pp.2191–2201. Available at: http://dx.doi.org/10.1056/NEJMoa0805840.

Duckers, H.J., Nabel, E.G. & Serruys, P.W., 2007. Essentials of Restenosis, Towta, New Jersey: Humana Press. Available at: http://link.springer.com/10.1007/978-1-59745-001-0.

Ebong, E.E. & Depaola, N., 2013. Specificity in the participation of connexin proteins in flow-induced endothelial gap junction communication. Pflugers Archiv European Journal of Physiology, 465(9), pp.1293–1302.

Ehret, R. et al., 1997. Monitoring of cellular behaviour by impedance measurements on interdigitated electrode structures. Biosensors & bioelectronics, 12(1), pp.29–41.

Van Eijnatten, M.A.J.M. et al., 2014. Comparison of cardiac time intervals between echocardiography and impedance cardiography at various heart rates. Journal of Electrical Bioimpedance, 5(1), pp.2–8. Available at: https://www.journals.uio.no/index.php/bioimpedance/article/view/690.

El-Fouly, M.H., Trosko, J.E. & Chang, C.-C., 1987. Scrape-loading and dye transfer. Experimental Cell Research, 168(2), pp.422–430. Available at: http://linkinghub.elsevier.com/retrieve/pii/0014482787900140.

El-Sabban, M., Martin, C. & Homaidan, F., 1998. Signalling between immune cells and epithelial cells in vitro. In R. Werner, ed. Gap Junctions: Proceedings of the 8th International Gap Junction Conference.

Evensen, L. et al., 2009. Mural cell associated VEGF is required for organotypic vessel formation. PLoS ONE, 4(6).

Fakhry, , Cachet, H. & Debiemme-Chouvy, C., 2013. Electrochemical Characterisations of Ultra Thin Overoxidized Polypyrrole Films Obtained by One-Step Electrosynthesis. Journal of the Electrochemical Society, 160(10), pp.D465–D470. Available at: http://jes.ecsdl.org/cgi/doi/10.1149/2.070310jes [Accessed November 14, 2013].

Fanning, a S., Mitic, L.L. & Anderson, J.M., 1999. Transmembrane proteins in the tight junction barrier. Journal of the American Society of Nephrology : JASN, 10(6), pp.1337–45. Available at: http://www.ncbi.nlm.nih.gov/pubmed/10361874.

Farooq, V., Gogas, B.D. & Serruys, P.W., 2011. Restenosis: Delineating the numerous causes of drug-eluting stent restenosis. Circulation: Cardiovascular Interventions, 4(2), pp.195–205.

Figueroa, X.F., Isakson, B.E. & Duling, B.R., 2004. Connexins: gaps in our knowledge of vascular function. Physiology (Bethesda, Md.), 19(13), pp.277–284.

Finn, A. V., Joner, M., et al., 2007. Pathological correlates of late drug-eluting stent thrombosis: Strut coverage as a marker of endothelialization. Circulation, 115(18), pp.2435–2441.

Finn, A. V., Nakazawa, G., et al., 2007. Vascular responses to drug eluting stents: Importance of delayed healing. Arteriosclerosis, Thrombosis, and Vascular Biology, 27(7), pp.1500–1510.

Finn, A. V. & Otsuka, F., 2012. Neoatherosclerosis a culprit in very late stent thrombosis. Circulation: Cardiovascular Interventions, 5(1), pp.6–9.

Fonner, J.M. et al., 2008. Biocompatibility implications of polypyrrole synthesis techniques. Biomedical materials (Bristol, England), 3(3), p.34124. Available at: http://www.pubmedcentral.nih.gov/articlerender.fcgi?artid=2562301&tool=pmcentrez&rendertype=abstract [Accessed November 21, 2013].

Forcelli, P. a et al., 2012. Histocompatibility and in vivo signal throughput for PEDOT, PEDOP, P3MT, and polycarbazole electrodes. Journal of biomedical materials research. Part A, 100(12), pp.3455–62. Available at: http://www.pubmedcentral.nih.gov/articlerender.fcgi?artid=3479360&tool=pmcentrez&rendertype=abstract [Accessed December 18, 2013].

Forciniti, L. et al., 2010. Unique electrochemically synthesized polypyrrole:poly(lactic-co-glycolic acid) blends for biomedical applications. Journal of Materials Chemistry, 20(40), p.8865. Available at: http://xlink.rsc.org/?DOI=c0jm01015d [Accessed March 14, 2014].

Fox, C.S. et al., 2015. Total Artificial Hearts-Past, Current, and Future. Journal of Cardiac Surgery, 30(11), pp.856–864. Available at: http://doi.wiley.com/10.1111/jocs.12644.

Franks, W. et al., 2005. Impedance characterization and modeling of electrodes for biomedical applications. IEEE transactions on bio-medical engineering, 52(7), pp.1295–302. Available at: http://www.ncbi.nlm.nih.gov/pubmed/16041993.

Fricke, H., 1925. The electric capacity of suspensions with special reference to blood. The journal of general physiology, 9, pp.137–152.

Furie, B.B.C. & Furie, B.B.C., 2005. Review series Thrombus formation in vivo. The Journal of Clincial Investigation, 115(12), pp.3355–3362. Available at: http://www.ncbi.nlm.nih.gov/entrez/query.fcgi?cmd=Retrieve&db=PubMed&dopt=Citation&list_uids=16322780.

Furlan, M., 1996. Von Willebrand factor: Molecular size and functional activity. Annals of Hematology, 72(6), pp.341–348.

Gabriel, C. et al., 1996. The dielectric properties of biological tissues: I. Literature survey. Physics in medicine and biology, 41(11), pp.2231–49. Available at: http://www.ncbi.nlm.nih.gov/pubmed/8938024.

Garg, S. & Serruys, P.W., 2010. Coronary stents: Current status. Journal of the American College of Cardiology, 56(10 SUPPL.), pp.S1–S42. Available at: http://dx.doi.org/10.1016/j.jacc.2010.06.007.

Garner, B. et al., 1999. Human endothelial cell attachment to and growth on polypyrrole-heparin is vitronectin dependent. Journal of materials science. Materials in medicine, 10(1), pp.19–27. Available at: http://www.ncbi.nlm.nih.gov/pubmed/15347990.

Geddes, L., 1972. Electrodes and the measurement of bioelectric events 1st ed., New York: John Wiley & Sons.

van Geuns, R.J. & Baks, T., 2007. Magnetic Resonance Imaging for Restenosis. In Essentials of restenosis for intervential cardiologists. Towta, New Jersey: Humana Press.

Gheorghiu, E., Balut, C. & Gheorghiu, M., 2002. Dielectric behaviour of gap junction connected cells: a microscopic approach. Physics in medicine and biology, 47(2), pp.341–8. Available at: http://www.ncbi.nlm.nih.gov/pubmed/11837622.

Giaever, I., 2016. Keynote address, 16th International conference on Electrical Bioimpedance. In Karolinska Institutet, Stockholm, Sweden.

Giaever, I. & Keese, C.R., 1993. A morphological biosensor for mammalian cells. Nature, 366, pp.591–592.

Giaever, I. & Keese, C.R., 1991. Micromotion of mammalian cells measured electrically. Proceedings of the National Academy of Sciences of the United States of America, 88(17), pp.7896–900. Available at: http://www.pubmedcentral.nih.gov/articlerender.fcgi?artid=52411&tool=pmcentrez&rendertype=abstract.

Giaever, I. & Keese, C.R., 1986. Use of Electric Fields to Monitor the Dynamical Aspect of Cell Behavior in Tissue Culture. Biomedical Engineering, IEEE Transactions on, BME-33(2), pp.242–247.

Goldberg, G.S., Valiunas, V. & Brink, P.R., 2004. Selective permeability of gap junction channels. Biochimica et biophysica acta, 1662(1–2), pp.96–101. Available at: http://www.ncbi.nlm.nih.gov/pubmed/15033581.

Gorelik, J. et al., 2008. Non-invasive Imaging of Stem Cells by Scanning Ion Conductance Microscopy : Future Perspective. Tissue Engineering Part C: Methods, 14(4).

Grimnes, S. et al., 2015. Chapter 8 – Instrumentation and Measurements. In Bioimpedance and Bioelectricity Basics. pp. 255–328.

Guimard, N.K., Gomez, N. & Schmidt, C.E., 2007. Conducting polymers in biomedical engineering. Progress in Polymer Science, 32(8–9), pp.876–921. Available at: http://linkinghub.elsevier.com/retrieve/pii/S0079670007000676 [Accessed November 8, 2013].

Guo, R. et al., 2007. Endothelial cell motility is compatible with junctional integrity. Journal of cellular physiology, 211(1), pp.327–335.

Haas, S. et al., 2010. Real-time monitoring of relaxation and contractility of smooth muscle cells on a novel biohybrid chip. Lab on a chip, 10(21), pp.2965–2971.

Hanani, M., 2012. Lucifer yellow - an angel rather than the devil. Journal of Cellular and Molecular Medicine, 16(1), pp.22–31.

Hansson, G.K., 2014. Inflammation, atherosclerosis, and coronary artery disease. The New England Journal of Medicine, 352, pp.1685–1695.

Hartmann, C. et al., 2007. The impact of glia-derived extracellular matrices on the barrier function of cerebral endothelial cells: an in vitro study. Experimental cell research, 313(7), pp.1318–1325. Available at: http://www.ncbi.nlm.nih.gov/pubmed/17346702.

Hay, D.C. et al., 2010. The complexities of engineering human stem cell-derived therapeutics. Journal of biomedicine & biotechnology, 2010, p.654964. Available at: http://www.pubmedcentral.nih.gov/articlerender.fcgi?artid=3070168&tool=pmcentrez&rendertype=abstract [Accessed December 22, 2014].

Hayashi, Y. et al., 2010. Dielectric coagulometry: A new approach to estimate venous thrombosis risk. Analytical Chemistry, 82(23), pp.9769–9774.

Heydarkhan-Hagvall, S. et al., 2003. Co-culture of endothelial cells and smooth muscle cells affects gene expression of angiogenic factors. Journal of Cellular Biochemistry, 89(6), pp.1250–1259.

Hildebrandt, C. et al., 2010. Detection of the osteogenic differentiation of mesenchymal stem cells in 2D and 3D cultures by electrochemical impedance spectroscopy. Journal of Biotechnology, 148, pp.83–90.

Hill, C.E. et al., 2002. Heterogeneity in the distribution of vascular gap junctions and connexins: implications for function. Clincal and experimental pharmacology & physiology, 29(7), pp.620–625.

Hobbie, R.K. & Roth, B., 2007. Intermediate Physics for Medicine and Biology Fourth Edi., New York: Springer Science.

Holmes, D.R. et al., 2004. Analysis of 1-Year Clinical Outcomes in the SIRIUS Trial: A Randomized Trial of a Sirolimus-Eluting Stent Versus a Standard Stent in Patients at High Risk for Coronary Restenosis. Circulation, 109(5), pp.634–640.

Hyun Jo, D. et al., 2015. Real-time estimation of paracellular permeability of cerebral endothelial cells by capacitance sensor array. Scientific Reports, 5(1), p.11014. Available at: http://www.nature.com/articles/srep11014.

Ianeselli, L. et al., 2013. Development of stable and reproducible biosensors based on electrochemical impedance spectroscopy: Three-electrode versus two-electrode setup. Biosensors & bioelectronics, 55C, pp.1–6. Available at: http://www.ncbi.nlm.nih.gov/pubmed/24355458 [Accessed January 10, 2014].

Imberti, B. et al., 2002. The Response of Endothelial Cells to Fluid Shear Stress Using a Co-Culture Model of the Arterial Wall. Endothelium, 9(1), pp.11–23. Available at: http://www.tandfonline.com/doi/full/10.1080/10623320210714.

Inoue, T. et al., 2011. Vascular inflammation and repair: Implications for re-endothelialization, restenosis, and stent thrombosis. JACC: Cardiovascular Interventions, 4(10), pp.1057–1066. Available at: http://dx.doi.org/10.1016/j.jcin.2011.05.025.

Inzelt, G., 2008. Conducting Polymers - A New Era in Electrochemistry, Heidelberg: Springer Berlin Heidelberg.

Jaguszewski, M. et al. (2017) 'The REMEDEE-OCT Study', JACC: Cardiovascular Interventions, 10(5), pp. 489–499. doi: 10.1016/j.jcin.2016.11.040.

Ji, G. et al., 2002. Stretch-induced calcium release in smooth muscle. The Journal of General Physiology, 119(6), pp.533–544. Available at: http://eutils.ncbi.nlm.nih.gov/entrez/eutils/elink.fcgi?dbfrom=pubmed&id=12034761&retmode=ref&cmd=prlinks%5Cnpapers3://publication/uuid/B7ECC8AE-6BD4-48BD-BF16-328A658180E3.

Joner, M. et al., 2008. Endothelial Cell Recovery Between Comparator Polymer-Based Drug-Eluting Stents. Journal of the American College of Cardiology, 52(5), pp.333–342.

Joner, M. et al., 2007. Pioglitazone inhibits in-stent restenosis in atherosclerotic rabbits by targeting transforming growth factor-β and MCP-1. Arteriosclerosis, Thrombosis, and Vascular Biology, 27(1), pp.182–189.

Jorcin, J.-B. et al., 2006. CPE analysis by local electrochemical impedance spectroscopy. Electrochimica Acta, 51(8–9), pp.1473–1479.

Jun, H.-S. et al., 2013. Effect of cell senescence on the impedance measurement of adipose tissue-derived stem cells. Enzyme and microbial technology, 53(5), pp.302–6. Available at: http://www.ncbi.nlm.nih.gov/pubmed/24034428 [Accessed November 8, 2013].

Juszczak, G.R. & Swiergiel, A.H., 2009. Properties of gap junction blockers and their behavioural, cognitive and electrophysiological effects: Animal and human studies. Progress in Neuro-Psychopharmacology and Biological Psychiatry, 33(2), pp.181–198. Available at: http://linkinghub.elsevier.com/retrieve/pii/S0278584608003989.

Karimullah, A.S. et al., 2013. Development of a conducting polymer cell impedance sensor. Sensors and Actuators B: Chemical, 176, pp.667–674. Available at: http://linkinghub.elsevier.com/retrieve/pii/S0925400512009884 [Accessed November 8, 2013].

Kauffmann, C., Motreff, P. & Sarry, L., 2010. In vivo supervised analysis of stent reendothelialization from optical coherence tomography. IEEE Transactions on Medical Imaging, 29(3), pp.807–818.

Kayinamura, Y.P., Roberts, J.H. & Rubinson, J.F., 2012. Near-ohmic behavior for conducting polymers: extension beyond PEDOT on gold-plated platinum to other polymer-counterion/substrate combinations. ACS applied materials & interfaces, 4(3), pp.1601–7. Available at: http://www.ncbi.nlm.nih.gov/pubmed/22356825.

Kim, M.S. & Dean, L.S., 2011. In-Stent Restenosis. Cardiovascular Therapeutics, 29(3), pp.190–198.

Kinard, F. et al., 1997. Compartmentalized coculture of porcine arterial endothelial and smooth muscle cells on a microporous membrane. In vitro cellular & developmental biology. Animal, 33(2), pp.92–103.

Klauss, V. & Pijls, N., 2007. The Use of Pressure Gradient in the Diagnosis of Restenosis. In Essentials of restenosis for intervential cardiologists. Towta, New Jersey: Humana Press.

Kontturi, K., Pentti, P. & Sundholm, G., 1998. Polypyrrole as a model membrane for drug delivery. Journal of Electroanalytical Chemistry, 453(1–2), pp.231–238.

Koppara, T. et al., 2015. Thrombogenicity and Early Vascular Healing Response in Metallic Biodegradable Polymer-Based and Fully Bioabsorbable Drug-Eluting Stents. Circulation: Cardiovascular Interventions, 8(6), pp.e002427–e002427. Available at: http://circinterventions.ahajournals.org/cgi/doi/10.1161/CIRCINTERVENTIONS.115.002427.

Kubo, M. et al., 2015. Prognostic significance of endothelial dysfunction in patients undergoing percutaneous coronary intervention in the era of drug-eluting stents. BMC Cardiovascular Disorders, 15(1), p.102. Available at: http://bmccardiovascdisord.biomedcentral.com/articles/10.1186/s12872-015-0096-z.

Lacorre, D.A. et al., 2004. Plasticity of endothelial cells: Rapid dedifferentiation of freshly isolated high endothelial venule endothelial cells outside the lymphoid tissue microenvironment. Blood, 103(11), pp.4164–4172.

LaFlamme, S. & Kowalczyk, A., 2008. Cell Junctions. Adhesion, Development and Disease. 1st ed., Weinheim: Wiley-VCH Verlag GmbH& Co.

Larsen, K. et al., 2012. Capture of circulatory endothelial progenitor cells and accelerated re-endothelialization of a bio-engineered stent in human ex vivo shunt and rabbit denudation model. European Heart Journal, 33(1), pp.120–128.

Lavender, M.D. et al., 2005. A system for the direct co-culture of endothelium on smooth muscle cells. Biomaterials, 26(22), pp.4642–4653.

Lee, R. et al., 2014. Real-time discrimination between proliferation and neuronal and astroglial differentiation of human neural stem cells. Scientific reports, 4, p.6319. Available at: http://www.pubmedcentral.nih.gov/articlerender.fcgi?artid=4159634&tool=pmcentrez&rendertype=abstract [Accessed January 7, 2015].

Lee, S.E. et al., 2009. Clinical outcomes and optimal treatment for stent fracture after drug-eluting stent implantation. Journal of Cardiology, 53(3), pp.422–428.

Li, C. et al., 2012. Regulatory effect of connexin 43 on basal ca2+ signaling in rat ventricular myocytes. PLoS ONE, 7(4), pp.13–16.

Libby, P., Ridker, P.M. & Hansson, G.K., 2011. Progress and challenges in translating the biology of atherosclerosis. Nature, 473(7347), pp.317–25. Available at: http://www.ncbi.nlm.nih.gov/pubmed/21593864.

Lind, R. et al., 1991. Single cell mobility and adhesion monitoring using extracellular electrodes. Biosensors and Bioelectronics, 6(4), pp.359–367.

Liu, X. et al., 2009. Electrical stimulation promotes nerve cell differentiation on polypyrrole/poly (2-methoxy-5 aniline sulfonic acid) composites. Journal of neural engineering, 6(6), p.65002. Available at: http://www.ncbi.nlm.nih.gov/pubmed/19850977 [Accessed March 3, 2014].

Lo, C.M., Keese, C.R. & Giaever, I., 1995. Impedance analysis of MDCK cells measured by electric cell-substrate impedance sensing. Biophysical journal, 69(6), pp.2800–2807. Available at: http://dx.doi.org/10.1016/S0006-3495(95)80153-0.

Löffler, S. & Richter-Dahlfors, A., 2015. Phase angle spectroscopy on transparent conducting polymer electrodes for real-time measurement of epithelial barrier integrity. J. Mater. Chem. B, 3(25), pp.4997–5000. Available at: http://dx.doi.org/10.1039/C5TB00381D.

Lohman, A.W. & Isakson, B.E., 2014. Differentiating connexin hemichannels and pannexin channels in cellular ATP release. FEBS Letters, 588(8), pp.1379–1388. Available at: http://doi.wiley.com/10.1016/j.febslet.2014.02.004.

Looser, P.M., Kim, L.K. & Feldman, D.N., 2016. In-Stent Restenosis: Pathophysiology and Treatment. Current Treatment Options in Cardiovascular Medicine, 18(2), p.10. Available at: http://www.ncbi.nlm.nih.gov/pubmed/26781658%0Ahttp://link.springer.com/10.1007/s11936-015-0433-7.

Lowe, H.C., Oesterle, S.N. & Khachigian, L.M., 2002. Coronary in-stent restenosis: Current status and future strategies. Journal of the American College of Cardiology, 39(2), pp.183–193.

Ludman, P. & Gavalova, L., 2014. National audit of percutaneous coronary interventional procedures,

Lundin, V. et al., 2011. Control of neural stem cell survival by electroactive polymer substrates. PloS one, 6(4), p.e18624. Available at: http://www.pubmedcentral.nih.gov/articlerender.fcgi?artid=3073951&tool=pmcentrez&rendertype=abstract [Accessed November 8, 2013].

Lüscher, T.F. et al., 2007. Drug-eluting stent and coronary thrombosis: Biological mechanisms and clinical implications. Circulation, 115(8), pp.1051–1058.

Lynch, A.E., Triajianto, J. & Routledge, E., 2014. Low-Cost Motility Tracking System (LOCOMOTIS) for Time-Lapse Microscopy Applications and Cell Visualisation. PLoS ONE, 9(8), p.e103547. Available at: http://dx.plos.org/10.1371/journal.pone.0103547.

Macdonald, J.R., 1992. Impedance Spectroscopy. Annals of Biomedical Engineering, 20, pp.289–305.

Malleo, D. et al., 2010. Note: Characterization of electrode materials for dielectric spectroscopy. The Review of scientific instruments, 81(1), p.16104. Available at: http://www.ncbi.nlm.nih.gov/pubmed/20113135 [Accessed December 16, 2013].

Manoharan, G., Davidavicius, G. & Wijns, W., 2007. Clinical Presentation of Restenosis. In Essentials of restenosis for intervential cardiologists. Towta, New Jersey: Humana Press.

Marx, S.O., Totary-Jain, H. & Marks, A.R., 2011. Vascular smooth muscle cell proliferation in restenosis. Circulation: Cardiovascular Interventions, 4(1), pp.104–111.

McAdams, E.T. & Jossinet, J., 1996. Problems in equivalent circuit modelling of the electrical properties of biological tissues. Bioelectrochemistry and Bioenergetics, 40(2), pp.147–152.

Mcadams, E.T. et al., 1995. The linear and non-linear electrical properties of the electrode-electrolyte interface. Biosensors & Bioelectronics, 10, pp.67–74.

McKittrick, C.M. et al., 2016. Modelling the Impact of Atherosclerosis on Drug Release and Distribution from Coronary Stents. Annals of Biomedical Engineering, 44(2), pp.477–487.

Meier, T. et al., 2008. Assessment of regional lung recruitment and derecruitment during a PEEP trial based on electrical impedance tomography. Intensive Care Medicine, 34(3), pp.543–550.

Michaelis, S. et al., 2012. Macroporous silicon chips for laterally resolved, multi-parametric analysis of epithelial barrier function. Lab on a chip, 12(13), pp.2329–36. Available at: http://www.ncbi.nlm.nih.gov/pubmed/22522671.

Michaelis, S., Wegener, J. & Robelek, R., 2013. Label-free monitoring of cell-based assays: Combining impedance analysis with SPR for multiparametric cell profiling. Biosensors & Bioelectronics, 49(15), pp.63–70. Available at: http://www.sciencedirect.com/science/article/pii/S0956566313003084.

Mintz, G.S., 2007. Features and Parameters of Drug-Eluting Stent Deployment Discoverable by Intravascular Ultrasound. The American Journal of Cardiology, 100(8), pp.S26–S35. Available at: http://linkinghub.elsevier.com/retrieve/pii/S0002914907016578.

Mitra, a K. & Agrawal, D.K., 2006. In stent restenosis: bane of the stent era. Journal of clinical pathology, 59, pp.232–239.

Morgan, S., 2016. Bioactive surfaces for improved coronary stent performance,

Morice, M.-C. et al., 2002. A Randomized Comparison of a Sirolimus-Eluting Stent with a Standard Stent for Coronary Revascularization. New England Journal of Medicine, 346(23), pp.1773–1780. Available at: http://www.ncbi.nlm.nih.gov/pubmed/12050336.

Nagasawa, K. et al., 2006. Possible involvement of gap junctions in the barrier function of tight junctions of brain and lung endothelial cells. Journal of cellular physiology, 208(1), pp.12–22.

Nakano, M. et al., 2013. Human autopsy study of drug-eluting stents restenosis: Histomorphological predictors and neointimal characteristics. European Heart Journal, 34(42), pp.3304–3313.

Nayak, A.K. et al., 2006. Myocardial infarction as a presentation of clinical in-stent restenosis. Circulation journal : official journal of the Japanese Circulation Society, 70(8), pp.1026–9. Available at: http://www.ncbi.nlm.nih.gov/pubmed/16864936.

Newbold, C. et al., 2010. Changes in biphasic electrode impedance with protein adsorption and cell growth. Journal of Neural Engineering, 7(5), p.56011. Available at: http://www.pubmedcentral.nih.gov/articlerender.fcgi?artid=3543851&tool=pmcentrez&rendertype=abstract [Accessed November 8, 2013].

Nichols, M. et al., 2012. European cardiovascular disease statistics 2012,

O'Brien, B. et al., 2016. Coronary Stent Materials and Coatings: A Technology and Performance Update. Annals of Biomedical Engineering, 44(2), pp.523–535.

Okner, R. et al., 2009. Electrocoating of stainless steel coronary stents for extended release of paclitaxel. Journal of Biomedical Materials Research - Part A, 88(2), pp.427–436.

Onuma, Y. & Serruys, P.W., 2011. Bioresorbable scaffold: The advent of a new era in percutaneous coronary and peripheral revascularization? Circulation, 123(7), pp.779–797.

Opp, D. et al., 2009. Use of electric cell-substrate impedance sensing to assess in vitro cytotoxicity. Biosensors & bioelectronics, 24(8), pp.2625–9. Available at: http://www.pubmedcentral.nih.gov/articlerender.fcgi?artid=2668605&tool=pmcentrez&rendertype=abstract [Accessed January 20, 2014].

Orazem, M.E. et al., 2013. Dielectric Properties of Materials Showing Constant-Phase-Element (CPE) Impedance Response. Journal of the Electrochemical Society, 160(6), pp.C215–C225.

Ostrakhovitch, E. a et al., 2012. Directed differentiation of embryonic P19 cells and neural stem cells into neural lineage on conducting PEDOT-PEG and ITO glass substrates. Archives of biochemistry and biophysics, 528(1), pp.21–31. Available at: http://www.ncbi.nlm.nih.gov/pubmed/22944870 [Accessed November 11, 2013].

Öz, S., Maercker, C. & Breiling, A., 2013. Embryonic carcinoma cells show specific dielectric resistance profiles during induced differentiation. PloS one, 8(3), p.e59895. Available at: http://www.pubmedcentral.nih.gov/articlerender.fcgi?artid=3606267&tool=pmcentrez&rendertype=abstract [Accessed November 8, 2013].

Packard, R.R.S. et al., 2016. Two-Point Stretchable Electrode Array for Endoluminal Electrochemical Impedance Spectroscopy Measurements of Lipid-Laden Atherosclerotic Plaques. Annals of Biomedical Engineering. Available at: http://link.springer.com/10.1007/s10439-016-1559-9.

Park, H.E. et al., 2011. Real-time monitoring of neural differentiation of human mesenchymal stem cells by electric cell-substrate impedance sensing. J Biomed Biotechnol, 2011, p.485173. Available at: http://www.ncbi.nlm.nih.gov/pubmed/21716652 [Accessed November 8, 2013].

Park, S.J. et al., 2012. In-stent neoatherosclerosis: A final common pathway of late stent failure. Journal of the American College of Cardiology, 59(23), pp.2051–2057. Available at: http://dx.doi.org/10.1016/j.jacc.2011.10.909.

Patra, S., Barai, K. & Munichandraiah, N., 2008. Scanning electron microscopy studies of PEDOT prepared by various electrochemical routes. Synthetic Metals, 158(10), pp.430–435. Available at: http://linkinghub.elsevier.com/retrieve/pii/S0379677908000660 [Accessed November 20, 2013].

Patsch, C. et al., 2015. Generation of vascular endothelial and smooth muscle cells from human pluripotent stem cells. Nature cell biology, 17(8), pp.994–1003.

Pelegrin, P. & Surprenant, A., 2006. Pannexin-1 mediates large pore formation and interleukin-1beta release by the ATP-gated P2X7 receptor. The EMBO journal, 25(21), pp.5071–82. Available at: http://www.pubmedcentral.nih.gov/articlerender.fcgi?artid=1630421&tool=pmcentrez&rendertype=abstract.

Pelto, J. et al., 2013. Novel Polypyrrole-Coated Polylactide Scaffolds. Tissue Engineering Part A, 19, pp.882–893.

Penuela, S., Gehi, R. & Laird, D.W., 2013. The biochemistry and function of pannexin channels. Biochimica et Biophysica Acta - Biomembranes, 1828(1), pp.15–22. Available at: http://dx.doi.org/10.1016/j.bbamem.2012.01.017.

Peper, J.K. et al., 2014. An impedance-based cytotoxicity assay for real-time and label-free assessment of T-cell-mediated killing of adherent cells. Journal of Immunological Methods, 405, pp.192–198.

Perk, J. et al., 2012. European Guidelines on cardiovascular disease prevention in clinical practice (version 2012). European Heart Journal, 33(13), pp.1635–1701.

Pethig, R. & Kell, D.B., 1987. The passive electrical properties of biological systems: their significance in physiology, biophysics and biotechnology. Physics in medicine and biology, 32(8), pp.933–70. Available at: http://www.ncbi.nlm.nih.gov/pubmed/3306721.

Pickup, P.G. & Ren, X., 1995. Impedance measurements of ionic conductivity as a probe of structure in electrochemically deposited polypyrrole films. Journal of electroanalytical chemistry, 396, pp.359–364.

Piraino, D. et al., 2017. Recurrent in-stent restenosis, certainty of its origin, uncertainty about treatment. International Journal of Cardiology, 230, pp.91–96. Available at: http://linkinghub.elsevier.com/retrieve/pii/S0167527316345624.

de Prado, a P. et al., 2011. Time course of reendothelialization of stents in a normal coronary swine model: characterization and quantification. Veterinary pathology, 48(6), pp.1109–17. Available at: http://www.ncbi.nlm.nih.gov/pubmed/21393629.

Prasad, C.K. et al., 2005. Survival of endothelial cells in vitro on Paclitaxel-loaded coronary stents. Journal of biomaterials applications, 19(4), pp.271–86. Available at: http://www.ncbi.nlm.nih.gov/pubmed/15788425.

Qiao, G. et al., 2012. Bioimpedance analysis for the characterization of breast cancer cells in suspension. IEEE transactions on bio-medical engineering, 59(8), pp.2321–9. Available at: http://www.ncbi.nlm.nih.gov/pubmed/22692870.

Qin, F. et al., 2003. Overexpression of von Willebrand factor is an independent risk factor for pathogenesis of intimal hyperplasia: Preliminary studies. Journal of Vascular Surgery, 37(2), pp.433–439.

Rabiet, M.J. et al., 1996. Thrombin-induced increase in endothelial permeability is associated with changes in cell-to-cell junction organization. Arteriosclerosis, thrombosis, and vascular biology, 16(3), pp.488–96. Available at: http://www.ncbi.nlm.nih.gov/pubmed/8630677.

Rahman, A., Price, D. & Bhansali, S., 2007. Effect of electrode geometry on the impedance evaluation of tissue and cell culture. Sensors and Actuators B: Chemical, 127(1), pp.89–96. Available at: http://linkinghub.elsevier.com/retrieve/pii/S0925400507004625 [Accessed January 13, 2014].

Rahman, A.R.A., Lo, C.-M. & Bhansali, S., 2006. A micro-electrode array biosensor for impedance spectroscopy of human umbilical vein endothelial cells. Sensors and Actuators B: Chemical, 118(1–2), pp.115–120. Available at: http://linkinghub.elsevier.com/retrieve/pii/S0925400506002784 [Accessed November 6, 2013].

Rajendra, N.S., Wrigley, B.J. & Gershlick, A.H., 2012. Bioabsorbable stents: Nothing from something. Clinical Investigation, 2(12), pp.1185–1189. Available at: http://www.embase.com/search/results?subaction=viewrecord&from=export&id=L366270261%5Cnhttp://dx.doi.org/10.4155/cli.12.126%5Cnhttp://sfx.library.uu.nl/utrecht?sid=EMBASE&issn=20416792&id=doi:10.4155%2Fcli.12.126&atitle=Bioabsorbable+stents%3A+Nothing+fro.

Ratcliffe, E., Thomas, R.J. & Williams, D.J., 2011. Current understanding and challenges in bioprocessing of stem cell-based therapies for regenerative medicine. British medical bulletin, 100, pp.137–55. Available at: http://www.ncbi.nlm.nih.gov/pubmed/21852279 [Accessed November 8, 2013].

Reay, R.V., 2012. Novel polymers to encourage rapid recovery of arterial function following coronary stenting. University of Strathclyde.

Reitinger, S. et al., 2012. Electric impedance sensing in cell-substrates for rapid and selective multipotential differentiation capacity monitoring of human mesenchymal stem cells. Biosensors and Bioelectronics, 34(1), pp.63–69.

Rezaei Niya, S.M. & Hoorfar, M., 2013. Study of proton exchange membrane fuel cells using electrochemical impedance spectroscopy technique – A review. Journal of Power Sources, 240, pp.281–293. Available at: http://dx.doi.org/10.1016/j.jpowsour.2013.04.011.

Rodriguez, S. et al., 2016. A Batteryless Sensor ASIC for Implantable Bio-Impedance Applications. IEEE Transactions on Biomedical Circuits and Systems, 10(3), pp.533–544.

Ron, A. et al., 2010. Dielectric screening of early differentiation patterns in mesenchymal stem cells induced by steroid hormones. Bioelectrochemistry (Amsterdam, Netherlands), 78(2), pp.161–72. Available at: http://www.ncbi.nlm.nih.gov/pubmed/19837013 [Accessed November 8, 2013].

Rossen, J.D. et al., 1991. Comparison of Coronary Vasodilation with Intravenous Dipyridamile and Adenosine. Journal of the American College of Cardiology, 18(2), pp.485–491.

Rowlands, A.S. & Cooper-White, J.J., 2008. Directing phenotype of vascular smooth muscle cells using electrically stimulated conducting polymer. Biomaterials, 29(34), pp.4510–20. Available at: http://www.ncbi.nlm.nih.gov/pubmed/18789820 [Accessed February 27, 2014].

Rozemeijer, R. et al., 2016. TCT-267 Clinical outcomes of diabetic patients treated with an amphilimus-eluting stent and a short duration of dual antiplatelet therapy in routine clinical practice: first results of the Utrecht Cre8 (U-Cre8) Registry. Journal of the American College of Cardiology, 68(18), p.B109. Available at: http://dx.doi.org/10.1016/j.jacc.2016.09.396.

Rubinson, J.F. & Kayinamura, Y.P., 2009. Charge transport in conducting polymers: insights from impedance spectroscopy. Chemical Society reviews, 38(12), pp.3339–47. Available at: http://www.ncbi.nlm.nih.gov/pubmed/20449053 [Accessed December 17, 2013].

Rümenapp, C. et al., 2009. Improved method for impedance measurements of mammalian cells. Biosensors & bioelectronics, 24(9), pp.2915–9. Available at: http://www.ncbi.nlm.nih.gov/pubmed/19321331 [Accessed November 8, 2013].

Sacco, R.L. et al., 2008. Aspirin and extended-release dipyridamole versus clopidogrel for recurrent stroke. The New England journal of medicine, 359(12), pp.1238–51. Available at: http://www.pubmedcentral.nih.gov/articlerender.fcgi?artid=2772657&tool=pmcentrez&rendertype=abstract.

Sagar, G.D.V. & Larson, D.M., 2006. Carbenoxolone inhibits junctional transfer and upregulates Connexin43 expression by a protein kinase A-dependent pathway. Journal of Cellular Biochemistry, 98(6), pp.1543–1551.

Sahu, G., Sukumaran, S. & Bera, A.K., 2014. Pannexins form gap junctions with electrophysiological and pharmacological properties distinct from connexins. Scientific reports, 4, p.4955. Available at: http://www.nature.com/srep/2014/140514/srep04955/full/srep04955.html.

Sakamoto, N., Kiuchi, T. & Sato, M., 2011. Development of an endothelial-smooth muscle cell coculture model using phenotype-controlled smooth muscle cells. Annals of Biomedical Engineering, 39(11), pp.2750–2758.

Salameh, A. & Dhein, S., 2005. Pharmacology of Gap junctions. New pharmacological targets for treatment of arrhythmia, seizure and cancer? Biochimica et Biophysica Acta - Biomembranes, 1719(1–2), pp.36–58.

Sandison, M.E., Dempster, J. & McCarron, J.G., 2016. The Transition of Smooth Muscle Cells from a Contractile to a Migratory , Phagocytic Phenotype : Direct Demonstration of Phenotypic Modulation. The Journal of physiology, epub befor, pp.6189–6209.

Sapkota, A. et al., 2014. Analysis of electrical properties of thrombogenic blood using electrical impedance spectroscopy. Transactions of Japanese Society for Medical and Biological Engineering, 52, pp.3–4.

Sarno, G. et al. (2012) 'Lower risk of stent thrombosis and restenosis with unrestricted use of "new-generation" drug-eluting stents: A report from the nationwide Swedish Coronary Angiography and Angioplasty Registry (SCAAR)', European Heart Journal, 33(5), pp. 606–613. doi: 10.1093/eurheartj/ehr479.

Sarró, E. et al., 2012. Electrical impedance spectroscopy measurements using a four-electrode configuration improve on-line monitoring of cell concentration in adherent animal cell cultures. Biosensors & bioelectronics, 31(1), pp.257–63. Available at: http://www.ncbi.nlm.nih.gov/pubmed/22061268 [Accessed November 11, 2013].

Seebach, J. et al., 2000. Endothelial Barrier Function under Laminar Fluid Shear Stress. Laboratory Investigation, 80(12), pp.1819–1831.

Seebach, J. et al., 2007. Regulation of endothelial barrier function during flow-induced conversion to an arterial phenotype. Cardiovascular Research, 75(3), pp.596–607.

Seidlitz, A. et al., 2015. In vitro study of sirolimus release from a drug-eluting stent: Comparison of the release profiles obtained using different test setups. European Journal of Pharmaceutics and Biopharmaceutics, 93, pp.328–338. Available at: http://dx.doi.org/10.1016/j.ejpb.2015.04.016.

Serra, M. et al., 2012. Process engineering of human pluripotent stem cells for clinical application. Trends in biotechnology, 30(6), pp.350–9. Available at: http://www.ncbi.nlm.nih.gov/pubmed/22541338 [Accessed November 8, 2013].

Shedden, L. et al., 2009. Intelligent Stent. World intellectual property organisation, p.26.

Shedden, L., 2008. The intelligent stent. University of Strathclyde.

Shedden, L. et al., 2010. Towards a self-reporting coronary artery stent--measuring neointimal growth associated with in-stent restenosis using electrical impedance techniques. Biosensors & bioelectronics, 26(2), pp.661–6. Available at: http://www.ncbi.nlm.nih.gov/pubmed/20667708 [Accessed November 18, 2013].

Shelley, M., 1818. Frankenstein or, the modern prometheus, London: Penguin Books.

Shen, L. et al., 2011. Tight junction pore and leak pathways: a dynamic duo. Annual review of physiology, 73, pp.283–309. Available at: http://www.pubmedcentral.nih.gov/articlerender.fcgi?artid=4655434&tool=pmcentrez&rendertype=abstract.

Shirakawa, H. et al., 1977. Synthesis of Electrically Conducting Organic Polymers : Halogen Derivatives. Chemical Communications, pp.578–580.

Sigwart, U. et al., 1987. Intravascular Stents to Prevent Occlusion and Re-Stenosis after Transluminal Angioplasty. New England Journal of Medicine, 316(12), pp.701–706. Available at: http://www.nejm.org/doi/abs/10.1056/NEJM198703193161201.

Singh, J.P.S. et al., 1994. Dipyridamole directly inhibits vascular smooth muscle cell proliferation in vitro and in vivo: Implications in the treatment of restenosis after angioplasty. J.Am.Coll.Cardiol., 23(11).

Smith, J.G., Thomas, B.J. & Cornish, B.H., 2007. A Pilot Study For Tissue Characterisation Using Bioimpedance Mapping. In Proceedings 13th International Conference on Electrical Bioimpedance and the 8th Conference on Electrical Impedance Tomography. pp. 146–149.

Song, H. et al., 2013. A microfluidic impedance flow cytometer for identification of differentiation state of stem cells. Lab on a chip, 13(12), pp.2300–10. Available at: http://www.ncbi.nlm.nih.gov/pubmed/23636706 [Accessed November 8, 2013].

Sorrentino, S. et al., 2017. Everolimus-Eluting Bioresorbable Scaffolds versus Metallic Everolimus-Eluting Stents: Meta-Analysis of Randomized Controlled Trials. Journal of the American College of Cardiology. Available at: http://linkinghub.elsevier.com/retrieve/pii/S0735109717370134.

Spray, D., Ye, Z. & Ransom, B., 2006. Functional Connexin "'Hemichannels'": A Critical approach. Glia, 54(7), pp.758–73.

Spuentrup, E. et al., 2005. Artifact-free coronary magnetic resonance angiography and coronary vessel wall imaging in the presence of a new, metallic, coronary magnetic resonance imaging stent. Circulation, 111(8), pp.1019–1026.

Stefanini, G.G. & Holmes, D.R., 2013. Drug-Eluting Coronary-Artery Stents. New England Journal of Medicine, 368(3), pp.254–265. Available at: http://www.nejm.org/doi/abs/10.1056/NEJMra1210816.

Stolwijk, J.A. et al., 2015. Impedance analysis of GPCR-mediated changes in endothelial barrier function: overview and fundamental considerations for stable and reproducible measurements. Pflügers Archiv - European Journal of Physiology, 467(10), pp.2193–2218. Available at: http://link.springer.com/10.1007/s00424-014-1674-0.

Stone, J.D. et al., 2013. AMP-activated protein kinase inhibits vascular smooth muscle cell proliferation and migration and vascular remodeling following injury. Am J Physiol Heart Circ Physiol, 304(3), pp.H369-81. Available at: http://www.ncbi.nlm.nih.gov/pubmed/23203966%5Cnhttp://ajpheart.physiology.org/content/ajpheart/304/3/H369.full.pdf.

Straub, A.C., Zeigler, A.C. & Isakson, B.E., 2014. The Myoendothelial Junction: Connections That Deliver the Message. Physiology (Bethesda, Md.), 29(4), pp.242–249. Available at: http://www.ncbi.nlm.nih.gov/pubmed/24985328.

Streitner, I. et al., 2012. Cellular imaging of human atherosclerotic lesions by intravascular electric impedance spectroscopy. PLoS ONE, 7(4), pp.2–6.

Sun, T. et al., 2010. On-chip epithelial barrier function assays using electrical impedance spectroscopy. Lab on a chip, 10(12), pp.1611–7. Available at: http://www.ncbi.nlm.nih.gov/pubmed/20379587 [Accessed November 28, 2013].

Süselbeck, T., Thielecke, H., Weinschenk, I., et al., 2005. In vivo intravascular electric impedance spectroscopy using a new catheter with integrated microelectrodes. Basic Research in Cardiology, 100(1), pp.28–34.

Süselbeck, T., Thielecke, H., Köchlin, J., et al., 2005. Intravascular electric impedance spectroscopy of atherosclerotic lesions using a new impedance catheter system. Basic Research in Cardiology, 100(5), pp.446–452.

Szulcek, R., Bogaard, H.J. & van Nieuw Amerongen, G.P., 2014. Electric Cell-substrate Impedance Sensing for the Quantification of Endothelial Proliferation, Barrier Function, and Motility. Journal of Visualized Experiments, (85), pp.1–12. Available at: http://www.jove.com/video/51300/electric-cell-substrate-impedance-sensing-for-quantification.

Takahata, K., DeHennis, A. & Wise, K.D., 2003. Stentenna: a micromachined antenna stent for wireless monitoring of implantable microsensors. In Proceedings of the 25th Annual International Conference of the IEEE. pp. 0–5.

Takens-Kwak, B.R. et al., 1992. Mechanism of heptanol-induced uncoupling of cardiac gap junctions: a perforated patch-clamp study. The American journal of physiology, 262(6 Pt 1), pp.C1531–C1538. Available at: http://www.ncbi.nlm.nih.gov/pubmed/1616013.

Taylor, S.L. et al., 2013. Endothelial Cell Permeability during Hantavirus Infection Involves Factor XII-Dependent Increased Activation of the Kallikrein-Kinin System. PLoS Pathogens, 9(7).

Tenekecioglu, E. et al., 2016. Bioresorbable scaffolds: a new paradigm in percutaneous coronary intervention. BMC cardiovascular disorders, 16(1), p.38. Available at: http://www.pubmedcentral.nih.gov/articlerender.fcgi?artid=4751731&tool=pmcentrez&rendertype=abstract.

Tesfamariam, B., 2016. Endothelial Repair and Regeneration Following Intimal Injury. Journal of Cardiovascular Translational Research, 9(2), pp.91–101. Available at: http://link.springer.com/10.1007/s12265-016-9677-1.

Tesfamariam, B., 2007. Local vascular toxicokinetics of stent-based drug delivery. Toxicology Letters, 168(2), pp.93–102.

Thanyasiri, P. et al., 2007. Endothelial dysfunction and restenosis following percutaneous coronary intervention. International Journal of Cardiology, 119(3), pp.362–367.

Thompson, R.C. et al., 2013. Atherosclerosis across 4000 years of human history: The Horus study of four ancient populations. The Lancet, 381(9873), pp.1211–1222. Available at: http://dx.doi.org/10.1016/S0140-6736(13)60598-X.

Thrivikraman, G., Madras, G. & Basu, B., 2014. Intermittent electrical stimuli for guidance of human mesenchymal stem cell lineage commitment towards neural-like cells on electroconductive substrates. Biomaterials, 35(24), pp.6219–35. Available at: http://www.ncbi.nlm.nih.gov/pubmed/24816362 [Accessed July 11, 2014].

Thuringer, D., 2004. The vascular endothelial growth factor-induced disruption of gap junctions is relayed by an autocrine communication via ATP release in coronary capillary endothelium. Annals of the New York Academy of Sciences, 1030, pp.14–27.

Triantafyllou, K.D., Frangoulis, S. & Kolettis, T.M., 2006. Coronary endarterectomy and stent removal with off-pump coronary artery bypass surgery. Heart (British Cardiac Society), 92(7), p.885. Available at: http://www.pubmedcentral.nih.gov/articlerender.fcgi?artid=1860711&tool=pmcentrez&rendertype=abstract.

Truskey, G. a, 2011. Endothelial Cell Vascular Smooth Muscle Cell Co-Culture Assay For High Throughput Screening Assays For Discovery of Anti-Angiogenesis Agents and Other Therapeutic Molecules. international journal of high throughput screening, 2010(1), pp.171–181.

Urban, P. et al., 2015. Polymer-free Drug-Coated Coronary Stents in Patients at High Bleeding Risk. New England Journal of Medicine, 373(21), pp.2038–2047. Available at: http://www.nejm.org/doi/10.1056/NEJMoa1503943.

Urdapilleta, E., Bellotti, M. & Bonetto, F., 2006. Impedance analysis of cultured cells: A mean-field electrical response model for electric cell-substrate impedance sensing technique. Physical Review E, 74(4), p.41908. Available at: http://link.aps.org/doi/10.1103/PhysRevE.74.041908 [Accessed June 27, 2014].

Venkatanarayanan, A., Keyes, T.E. & Forster, R.J., 2013. Label-free impedance detection of cancer cells. Analytical chemistry, 85(4), pp.2216–22. Available at: http://www.ncbi.nlm.nih.gov/pubmed/23331159.

Venkatraman, S. & Boey, F., 2007. Release profiles in drug-eluting stents: Issues and uncertainties. Journal of Controlled Release, 120(3), pp.149–160.

Voets, T., Droogmans, G. & Nilius, B., 1996. Membrane currents and the resting membrane potential in cultured bovine pulmonary artery endothelial cells. The Journal of Physiology, 497(1), pp.95–107. Available at: papers://d8e9569c-3053-4f4e-bfb0-c8b1b3194e73/Paper/p4650%5Cnhttp://doi.wiley.com/10.1113/jphysiol.1996.sp021752.

Wadhwa, R., Lagenaur, C.F. & Cui, X.T., 2006. Electrochemically controlled release of dexamethasone from conducting polymer polypyrrole coated electrode. Journal of Controlled Release, 110(3), pp.531–541.

Wallace, C.S., Strike, S. a & Truskey, G. a, 2007. Smooth muscle cell rigidity and extracellular matrix organization influence endothelial cell spreading and adhesion formation in coculture. American journal of physiology. Heart and circulatory physiology, 293(3), pp.H1978–H1986.

Wallace, C.S. & Truskey, G. a., 2010. Direct-contact co-culture between smooth muscle and endothelial cells inhibits TNF- -mediated endothelial cell activation. AJP: Heart and Circulatory Physiology, 299(2), pp.H338–H346.

Wallace, G. & Spinks, G., 2007. Conducting polymers ? bridging the bionic interface. Soft Matter, 3(6), p.665. Available at: http://xlink.rsc.org/?DOI=b618204f [Accessed November 20, 2013].

Wang, W., Dentler, W.L. & Borchardt, R.T., 2001. VEGF increases BMEC monolayer permeability by affecting occludin expression and tight junction assembly. American journal of physiology. Heart and circulatory physiology, 280(1), pp.H434-40. Available at: http://www.ncbi.nlm.nih.gov/pubmed/11123261.

Wang, X. et al., 2004. Evaluation of biocompatibility of polypyrrole in vitro and in vivo. Journal of biomedical materials research. Part A, 68(3), pp.411–22. Available at: http://www.ncbi.nlm.nih.gov/pubmed/14762920.

Wang, X. et al., 2015. Nano-Biomechanical Study of Spatio-Temporal Cytoskeleton Rearrangements that Determine Subcellular Mechanical Properties and Endothelial Permeability. Scientific Reports, 5(February), p.11097. Available at: http://www.nature.com/doifinder/10.1038/srep11097.

Want, A. et al., 2012. Large-scale expansion and exploitation of pluripotent stem cells for regenerative medicine purposes: beyond the t flask. Regenerative medicine, 7(1), pp.71–84.

Webb, R.C., 2003. Smooth muscle contraction and relaxation. Advances in physiology education, 27(1–4), pp.201–6. Available at: http://advan.physiology.org/content/27/4/201.abstract.

Weber, P. a et al., 2004. The permeability of gap junction channels to probes of different size is dependent on connexin composition and permeant-pore affinities. Biophysical journal, 87(2), pp.958–973. Available at: http://dx.doi.org/10.1529/biophysj.103.036350.

Wegener, J., 2008. Impedance analysis of cell junctions. In G. M. Schmid, ed. Nanotechnology2. Wiley-VCH Verlag GmbH& Co., pp. 325–357.

Wegener, J., Keese, C.R. & Giaever, I., 2000. Electric cell-substrate impedance sensing (ECIS) as a noninvasive means to monitor the kinetics of cell spreading to artificial surfaces. Experimental cell research, 259(1), pp.158–166.

Wegener, J. & Seebach, J., 2014. Experimental tools to monitor the dynamics of endothelial barrier function: A survey of in vitro approaches. Cell and Tissue Research, 355(3), pp.485–514.

Wegener, J. & Sieber, M., 1996. Impedance analysis of epithelial and endothelial cell monolayers cultured on gold surfaces. Journal of biochemical and biophysical methods, 32(96), pp.151–170.

Weiss, Z. et al., 2003. Pyrrole Derivatives for Electrochemical Coating of Metallic. Journal of Polymer Science: Part A: Polymer Chemistry, 42, pp.1658–1667

Wilson, S. J. et al. (2017) 'Duration of dual antiplatelet therapy in acute coronary syndrome', Heart, 103(8), pp. 573–580. doi: 10.1136/heartjnl-2016-309871.

Wissenwasser, J. et al., 2011. Multifrequency impedance measurement technique for wireless characterization of microbiological cell cultures. The Review of scientific instruments, 82(11), p.115110. Available at: http://www.ncbi.nlm.nih.gov/pubmed/22129016 [Accessed November 8, 2013].

Wong, J.Y., Langer, R. & Ingber, D.E., 1994. Electrically conducting polymers can noninvasively control the shape and growth of mammalian cells. Proceedings of the National Academy of Sciences of the United States of America, 91(8), pp.3201–4. Available at: http://www.pubmedcentral.nih.gov/articlerender.fcgi?artid=43543&tool=pmcentrez&rendertype=abstract.

Worthley, S.G. et al., 2017. First-in-Human Evaluation of a Novel Polymer-Free Drug-Filled Stent. JACC: Cardiovascular Interventions, 10(2), pp.147–156. Available at: http://linkinghub.elsevier.com/retrieve/pii/S193687981631843X.

Xiao, Y. et al., 2004. Electrochemical polymerization of poly(hydroxymethylated-3,4-ethylenedioxythiophene) (PEDOT-MeOH) on multichannel neural probes. Sensors and Actuators B: Chemical, 99(2–3), pp.437–443. Available at: http://linkinghub.elsevier.com/retrieve/pii/S0925400503009006 [Accessed November 12, 2013].

Xu, Y. et al., 2016. A review of impedance measurements of whole cells. Biosensors and Bioelectronics, 77, pp.824–836. Available at: http://dx.doi.org/10.1016/j.bios.2015.10.027.

Yamada, M. et al., 2007. Electrical stimulation modulates fate determination of differentiating embryonic stem cells. Stem cells, 25(3), pp.562–570. Available at: http://www.ncbi.nlm.nih.gov/pubmed/17110622 [Accessed November 8, 2013].

Yamato, H., Ohwa, M. & Wernet, W., 1995. Stability of polyp yrrole and poly (3 , 4 _ ethylenedioxythiophene) for biosensor application. Journal of Electroanalytical Chemistry, 397(1–2), pp.163–170.

Yeh, H.I. et al., 2006. Comparison of endothelial cells grown on different stent materials. Journal of Biomedical Materials Research - Part A, 76(4), pp.835–841.

Young, E.F. & Smilenov, L.B., 2011. Impedance-Based Surveillance of Transient Permeability Changes in Coronary Endothelial Monolayers after Exposure to Ionizing Radiation. Radiation Research, 424, pp.415–424.

Yu, F. et al., 2011. Electrochemical impedance spectroscopy to characterize inflammatory atherosclerotic plaques. Biosensors and Bioelectronics, 30(1), pp.165–173. Available at: http://dx.doi.org/10.1016/j.bios.2011.09.007.

Zhang, X. et al., 2012. Von Willebrand Factor permeates small vessels in CADASIL and inhibits smooth muscle gene expression. Translational stroke research, 3(1), pp.138–45. Available at: http://www.pubmedcentral.nih.gov/articlerender.fcgi?artid=3358806&tool=pmcentrez&rendertype=abstract.

Zhao, M. et al., 2000. Alignment of endothelial cells in a physiological electric field: involvement of MAP kinase and PI3 kinase signalling. Journal of physiology, 528P(SI), p.85P–85P.

Zhou, M. & Heinze, J., 1999. Electropolymerization of pyrrole and electrochemical study of polypyrrole: 1. Evidence for structural diversity of polypyrrole. Electrochimica Acta, 44(11), pp.1733–1748. Available at: http://linkinghub.elsevier.com/retrieve/pii/S001346869800293X.

Zhu, Z. et al., 2015. Time-lapse electrical impedance spectroscopy for monitoring the cell cycle of single immobilized S. pombe cells. Scientific Reports, 5(1), p.17180. Available at: http://dx.doi.org/10.1038/srep17180.

Zobel, K., Hansen, U. & Galla, H.J., 2016. Blood-brain barrier properties in vitro depend on composition and assembly of endogenous extracellular matrices. Cell and Tissue Research, pp.1–13. Available at: http://dx.doi.org/10.1007/s00441-016-2397-7.